

VIRAL TOOL DEVELOPMENT FOR INVESTIGATIONS OF
LEARNING AND MEMORY

by

Christopher Andrew de Solis



APPROVED BY SUPERVISORY COMMITTEE:

Dr. Jonathan E. Ploski, Chair

Dr. Sven Kroener

Dr. Christa K. McIntyre

Dr. Gregory Dussor

Copyright 2018

Christopher Andrew de Solis

All Rights Reserved

I dedicate this work to all those who played a role in my academic development and allowed me to pursue a career in science.

VIRAL TOOL DEVELOPMENT FOR INVESTIGATIONS OF
LEARNING AND MEMORY

by

CHRISTOPHER ANDREW DE SOLIS, BS

DISSERTATION

Presented to the Faculty of
The University of Texas at Dallas
in Partial Fulfillment
of the Requirements
for the Degree of

DOCTOR OF PHILOSOPHY IN
COGNITION AND NEUROSCIENCE

THE UNIVERSITY OF TEXAS AT DALLAS

August 2018

ACKNOWLEDGMENTS

I would like to thank both of my parents, Arthur de Solis and Mimi de Solis, for their support throughout my education. I thank my old friend Hughie Mckinnley for improving my critical thinking and research skills. Diana S. Woodruff-Pak was my primary undergraduate mentor who first opened the doors for me to pursue science. I will be forever grateful for the 2 years I was allowed to spend in her lab. Another instrumental person in my career development was Meagan McManus, who served as a mentor to me during my 2 post graduate years in the Center for Mitochondrial and Epigenomic Medicine at The Children's Hospital of Philadelphia. She taught me to always be confident in myself and still serves as an inspiration to persevere with your experiments. One of my fellow students, Lindsey Noble, was instrumental in "dragging" me through my Ph.D. and being a constant support line and shoulder to cry on. In addition to being an outstanding academic colleague, she also served as my landlord for my last 2 years in the program, allowing me to live in her home gym. Robert and Susan Barraza were also instrumental in keeping me off the streets, allowing me to live in their home during the remaining six months in the program. I thank my girlfriend, Cora Barraza, for providing emotional and financial support thought the last half of my Ph.D. I wish to thank all the faculty and staff of the Cognition and Neuroscience program, as their service exceeded my expectations. I would like to thank my Ph.D. advisor, Jonathan Ploski, to whom I owe most of my academic successes and scientific skills. Finally, endless thanks to all my undergraduate and masters students-- I could not have done all this without your help.

June 2018

VIRAL TOOL DEVELOPMENT FOR INVESTIGATIONS OF
LEARNING AND MEMORY

Christopher Andrew de Solis, PhD
The University of Texas at Dallas, 2018

Supervising Professor: Jonathan E. Ploski

Developing new viral tools to investigate biological and behavioral phenomena is important to push neuroscience research to new avenues that were once limited by expensive and time consuming transgenic and knockout rodent models. This dissertation is a collection of experiments that outline the development and optimization of several viral vector systems for application of studying a gene's function in the brain and the role it plays in behavioral phenomena. First, I show that knockdown of a gene's transcript using short hairpin RNAs (shRNAs) delivered to neurons using adeno associated virus (AAV), is toxic to neurons and results in an impairment of Pavlovian auditory fear conditioning. Next, I outline the development of a doxycycline dependent CRISPR/Cas genome editing system for knockdown of genes in the brain using AAV as an alternative to gene knockdown with shRNAs. I then examine the efficiency of several AAV serotypes for their ability to function in a specific cell type, inhibitory neurons. Next, I sought to look for important genes that might be potentially important for memory consolidation in the hippocampus, with respect to transport of mRNA transcripts to the distal ends of dendrites of dentate gyrus granule cells following the induction of long-term

potentiation (LTP). I found that Arc (Activity related cytoskeletal protein) mRNA was the most present in the dendrites following neuronal activation compared to all other known transcripts in the rat genome. Interestingly, another gene that was highly upregulated was an unprocessed microRNA (pri-miRNA), pri-miRNA-132. Finally, I use lentiviral vectors to investigate the role of GluN2B, an NMDA receptor subunit, in the updating of strong memories and found that increasing the level of GluN2B within the mouse basal and lateral complex of the amygdala (BLA) allows for the modification of an existing strong fear memory via reconsolidation, a process typically not initiated in stronger memories.

TABLE OF CONTENTS

ACKNOWLEDGMENTS	v
ABSTRACT.....	vi
LIST OF FIGURES	x
CHAPTER 1 INTRODUCTION	1
References.....	8
CHAPTER 2 VIRAL DELIVERY OF SHRNA TO AMYGDALA NEURONS LEADS TO NEUROTOXICITY AND DEFICITS IN PAVLOVIAN FEAR CONDITIONING.....	11
Abstract.....	12
Introduction.....	13
Methods and Materials.....	15
Results.....	26
Discussion.....	49
References.....	55
CHAPTER 3 A VIRAL MEDIATED CRISPR/CAS9 SYSTEM WITH DOXYCYCLINE DEPENDENT GRNA EXPRESSION FOR INDUCIBLE IN VITRO AND IN VIVO GENOME EDITING.....	59
Abstract.....	60
Introduction.....	60
Materials and Methods.....	63
Results.....	71
Discussion.....	88
References.....	92
CHAPTER 4 ADENO-ASSOCIATED VIRAL SEROTYPES DIFFERENTIALLY TRANSDUCE INHIBITORY NEURONS WITHIN THE RAT AMYGDALA.....	96
Abstract.....	97
Introduction.....	98
Materials and Methods.....	100

Results.....	111
Discussion.....	130
References.....	136
CHAPTER 5 IS ARC MRNA LOCALIZATION UNIQUE: A SEARCH FOR MRNAS THAT LOCALIZE TO THE DISTAL DENDRITES OF DENTATE GYRUS GRANULE CELLS FOLLOWING NEURAL ACTIVITY	141
Abstract.....	142
Introduction.....	142
Materials and Methods.....	144
Results.....	152
Discussion.....	175
References.....	183
CHAPTER 6 INCREASING GLUN2B VIA GLUN2B(E1479Q) ENABLES MODIFICATION OF A STRONG FEAR MEMORY TRACE VIA RECONSOLIDATION UPDATING.....	189
Abstract.....	190
Introduction.....	191
Material and Methods.....	194
Results.....	198
Discussion.....	211
References.....	213
CHAPTER 7 CONCLUSIONS.....	216
References.....	225
BIOGRAPHICAL SKETCH	229
CURRICULUM VITAE.....	230

LIST OF FIGURES

Figure 2.1 Viral delivery of RNAi to the rat amygdala results in relatively weak fear conditioning.	30
Figure 2.2 Viral mediated shRNA expression within the BLA interferes with fear conditioning and leads to dysregulation of gene expression.....	35
Figure 2.3 Viral mediated expression of shLuc within the BLA dose dependently interferes with Pavlovian fear conditioning and increases microglia activation.....	38
Figure 2.5 Viral mediated expression of shCntrl in BLA neurons induces deficits in fear conditioning and increases in microglia activation compared to GFP only, and Sham control groups	42
Figure 2.6 Virally mediated RNAi induced depletion of GluN2A within BLA neurons impairs Pavlovian fear conditioning, as compared to the GFP only, shLuc, shArc and shEgr1 groups.....	47
Figure 2.7 Lowering the titer of AAV virus infused, will result in less neurons transduced and an overall decrease in GFP expression.	49
Figure 3.1 Demonstration of genome editing with spCas9.....	74
Figure 3.2 The TRE3G promoter is leaky within AAV viral plasmids and leads leaky genome editing	77
Figure 3.3 Modification of TRE3G-spCas9 plasmid in an attempt to decrease leakiness	80
Figure 3.4 The development of inducible gRNA genome editing system.....	84
Figure 3.5 Inducible genome editing <i>in vivo</i> via regulation of gRNA.....	86
Figure 3.6 Inducible genome editing can be achieved in as little as 1 day on Dox	88
Figure 4.1 Western blot detection of VP1, VP2 and VP3.	103
Figure 4.2 AAV VP1 capsid proteins exhibit divergent sequences.....	112
Figure 4.3 Representative images of BLA viral transduction of AAV serotypes using AAV-Gad65-GFP and AAV-PAG-RFP.....	117

Figure 4.4 AAV serotypes exhibit differential transduction of BLA neurons.....	118
Figure 4.5 Magnified merged images depicting BLA cells positive for GFP (AAV-Gad65-GFP) and cells that are positive for RFP (AAV-PAG-RFP).....	119
Figure 4.6 Representative images indicate that AAV5 serotype displays poor transduction efficiency at a low and high titer, compared to AAV7.....	119
Figure 4.7 Representative images depicting differential neuronal transduction of AAV serotypes within the CeA.....	123
Figure 4.8 AAV serotypes exhibit differential transduction of CeA neurons.....	124
Figure 4.9 Double FISH was performed to determine the specificity of AAV-Gad65-GFP expression for Gad65 positive cells.....	127
Figure 4.10 NeuN immunohistochemistry within CeA neurons transduced with either AAV-PAG-RFP or AAV-Gad65-GFP.....	130
Figure 5.1 The dendrites of dentate gyrus granule neurons are suitable to screen to RNA transcripts in distal dendrites.....	157
Figure 5.2 Microarray of distal dendrites of granule cell 2hr and 4hr post stimulation.....	159
Figure 5.3 Confirmation of microarray via qRTPCR.....	159
Figure 5.4 Unpossessed miR132 present in the dendrites.....	162
Figure 5.5 FISH for genes upregulated 4hr post induction of LTP.....	163
Figure 5.6 Signal intensity from FISH plotted across granule cells and dendrites.....	165
Figure 5.7 qRTPCR of sample from the ML and GCL 2 hr and 4 hr post induction of LTP.....	167
Figure 5.8 Standard curves for qRTPCR primers.....	168
Figure 5.9 qRTPCR Primer Sequences.....	169
Figure 5.10 Statistics for qRTPCR experiments.....	171
Figure 5.11 qRTPCR results normalized to Arc.....	174
Figure 5.12 qRTPCR result comparison of ML and GCL levels.....	175

Figure 6.1 Strong fear memories are resistant to typical extinction and reconsolidation.....	199
Figure 6.2 Lentiviral maps.....	201
Figure 6.3 Functionality of GFP and GluN2B lentiviruses in vitro and in vivo.....	202
Figure 6.4 Increasing GluN2B levels with GluN2B(E1479Q) leads to enhanced consolidation of a fear memory.	204
Figure 6.5 Increasing GluN2B at the time of extinction learning does not lead to enhanced extinction.....	206
Figure 6.6 Overexpression of GluN2B(E1479Q) enables reconsolidation of a strong fear memory.	209
Figure 6.7 Enabling of initiation of reconsolidation of strong fear memories enabled by overexpression of GluN2B(E1479Q) is retrieval dependent.	210
Figure 6.8 Increasing the GluN2B/GluN2A ratio does not interfere with the reconsolidation of a weak fear memory.....	211

CHAPTER 1

INTRODUCTION

Better understanding of the molecular correlates of fear learning and memory is crucial to development of superior treatments for fear-related anxiety disorders. There are currently over 20 million individuals in the United States suffering with post-traumatic stress disorder (PTSD) and other fear related anxiety disorders (Olszewski & Varrasse, 2005), making research on fear and anxiety a priority for labs studying mental health. Using ever-evolving molecular biology techniques to make new discoveries of mechanisms underlying these disorders is key to understanding them, particularly in the brain. The use of recombinant viral technology to study the mammalian brain in the past several decades (Kootstra & Verma, 2003) has played an enormous role in accelerating neuroscience research, as these tools give neuroscientists the ability to make genetic manipulations in specific regions of the brain (Chao et al., 2000; Rabinowitz et al., 2002). This dissertation consists of a series of studies that seek to improve upon and apply viral vector technology for the study of learning and memory research.

The development of transgenic and knock-in models are currently at the center of analysis for individual genes (Capecchi, 2005). As an alternative to using expensive, time consuming transgenic or knock-in rodent lines, adeno associated virus (AAV) has been altered for efficient use in the mammalian brain to express a transgene from its viral genome and deliver it to neurons. Short hairpin RNA (shRNA) are RNAs designed to target a particular mRNA and target it for degradation via the RNAi pathway (Hommel et al., 2003). This technology has been used to investigate many topics in neuroscience for over a decade, however, there have been

multiple reports that shRNAs are toxic to neurons (McBride et al., 2008; Martin et al., 2011). Despite published data on this issue, many labs are still using the technology (Cruz et al., 2015; Mews et al., 2017). In chapter 2, I outline my attempt to use the technology to knockdown genes involved in learning and memory processes. We found that it caused an impairment in a fear-based memory task, Pavlovian auditory fear conditioning. Auditory fear consists of pairing an unconditioned stimulus (US; a shock) with a conditioned stimulus (CS; a tone) to form an associative memory (Johansen et al., 2011). This particular task is dependent on the basolateral complex of the amygdala (BLA) (Wilensky et al., 2006), where we made our manipulations using virus designed to express shRNAs. I was able to determine that the degree of impairment on this task is dependent on the concentration of virus used and this correlated with an increased amount of microglia activation, which is indicative of toxicity (de Solis et al., 2015). Although severely lowering the concentration of the virus alleviated some of the memory impairing effects, the knockdown of the targeted genes was not efficient and viral transduction efficacy was low. This chapter makes the argument that shRNAs may not be the best choice for studying role of gene in neurons.

As an alternative to the neurotoxic viral technology described in chapter 2, I explored using AAV to create gene editing in neurons. The CRISPR(Clustered regulatory Interspersed Palindromic Repeats)/Cas9 (Cas9 endonuclease) system is a recently developed genome editing system that has been developed to target a specific area on the genome for editing, effectively knocking down a gene (Ran et al., 2015). This technology has been shown to effectively knockdown a gene in vitro (Hsu et al., 2014)(via plasmid) and in vivo (Ran et al., 2015)(via AAV). This technology could be very useful in learning and memory research, however, the

inability for the gene editing to be activated at the time a specific mnemonic process hinders this tools usefulness for behavioral neuroscientists. In chapter 3, I demonstrate the technology can be effective editing in the mouse brain and present the development of a doxycycline inducible CRISPR/Cas9 system (de Solis et al., 2016). Initially, we attempted to drive expression of the Cas9 nuclease from a TRE3G (Tetracycline Responsive Element 3rd Generation) promoter for in vivo genome editing to induce editing only in the presence of Dox, however, it was shown that the promoter allowed for expression of Cas9 in the absence of Dox, making this system not suitable for inducible genome editing. We then regulated the gRNA (guideRNA) using a truncated H1/TO promoter so that the gRNA expresses in the presence of Dox. This system was shown to be tightly regulated in vitro and in vivo in the brain and just as efficient as a system that is not inducible. In addition, we showed this system can induce genome editing of a target locus in the mammalian brain in as little as 1 day on Dox.

One of the many benefits of using AAV to investigate neuronal phenomena is not only the control over where in the brain the transgene is delivered, but one could also control what specific cell type the virus will express the transgene (Wu et al., 2006; Van Vliet et al., 2008). In chapter 4, I categorize which of the AAV serotypes function more efficiently in inhibitory neurons (de Solis et al., 2017). To accomplish this, AAVs were generated with several of the AAV serotypes, AAV1, AAV4, AAV5, AAV6, AAV7, AAV8, AAV9, AAVrh10, AAVDJ and AAVDJ8 that express GFP (green fluorescent protein) under the control of a Gad65 promoter. Gad65 is involved in synthesis of GABA (gamma-aminobutyric acid), thus, the GFP should only be expressed in inhibitory neurons. We infused these viruses into either the BLA or the CeA (the central nucleus of the amygdala). We found that the expression was not restricted to inhibitory

neurons in the BLA, however, the expression in the CeA was transducing nearly 100% of inhibitory neurons, allowing the interpretation of AAV serotype efficiencies in inhibitory neurons. It was found that AAV1, AAV7, AAV9 and AAVDJ8 functioned best in this cell type, compared to the other AAV serotypes. Surprisingly, AAV4 and AAV5 showed very little expression; these results are consistent with previous reports where expression was attempted to be restricted to excitatory neurons (Holehonnur et al. 2014). It was also shown in these experiments that all serotypes were primarily restricted to neurons.

After developing viral tools to study gene function, I sought to find target genes that might be involved in memory formation in the hippocampus, particularly, genes that might be locally translated within the dendrites of granule cells of the dentate gyrus. Local translation of proteins is an intriguing topic because it seeks to answer the question of how an individual neuron forms and maintains connections with 1000s of other neurons (Steward et al., 2001). We chose to look in the dentate gyrus because its dense population of dendrites are able to be seen easily and we were able to extract RNA from the dendrites for analysis. It has been shown that induction of long term potentiation (LTP) via high frequency stimulation of the perforant pathway in rats stimulates transcription of RNA for many hours after the initial stimulation (Ramirez-Amaya et al., 2013), and some of these RNAs are transported to the distal ends of the dendrites for local translation by polyribosomes (Steward et al., 1998). Activity related cytoskeletal protein (Arc) is an example of one of these transcripts that has been well categorized for abundant translation in the distal dendrites of neurons (Steward, 1997), which plays a large role in the consolidation of memories (Ploski et al., 2008). Before the experiments I outline in chapter 5, there were no experiments that unbiasedly screened for all RNAs are present in the

dendrites following the induction of LTP. To do this, we induced LTP within the dentate gyrus of rats, then 2 hr or 4 hr later we extracted the brains and dissected out the distal dendrites of the dentate gyrus granule cells via laser microdissection. After processing the samples for a microarray, we found that out of all known mRNA transcripts from the rat genome, Arc mRNA was the most upregulated at both time points. Surprisingly, the next highest transcript was an unprocessed miRNA (pri-miRNA) containing miRNA-132, a microRNA that has been shown to also be involved in the consolidation of memories (Wang et al., 2013). There were several other transcripts that were highly upregulated that are also known to be involved in memory formation, however, they were much less abundant compared to Arc mRNA.

Protein synthesis has been known to be a crucial component of learning and memory process for decades (Agranoff & Klinger, 1964). It is a requirement for both the consolidation and reconsolidation process of memory formation (Nader et al., 2000). If protein synthesis is inhibited with drugs within the BLA before an animal undergoes the consolidation or reconsolidation process of a Pavlovian auditory fear memory, the animal will have an attenuated fear response, or another way of putting it, the animal will display characteristics of amnesia of the associative memory. However, this is only in the case of relatively weak fear memories (Wang et al., 2009). In stronger, more “pathological” memories, this method of attenuating a fear response is ineffective (Nader & Hardt, 2009). Since these stronger memories are resistant to treatment with amnestic agents, this rules out the possibility of using any such treatment for traumatic memories (i.e. PTSD) and other severe fear and anxiety related disorders in which a patient has an inflated physiological and behavioral response to a fear cue (Wood et al., 2015). In chapter 6, I show how increasing the ratio of GluN2B to GluN2A, can allow for a strong

memory to undergo reconsolidation, thus, rendering it susceptible to the effects of pharmacologically induced amnesia.

Reconsolidation is a well-studied phenomenon that serves as a mechanism to update an existing memory trace following retrieval of a consolidated memory. There are two phases of reconsolidation. The first is the initiation of reconsolidation phase, which occurs within seconds to minutes after a memory is retrieved (Lee et al., 2017), and serves to ‘destabilize’ neurons involved in the memory trace. Since the memory is now labile, it is subject to updating and goes through the second phase, the destabilization phase, before the newly updated memory can be solidified/stabilized. The restabilization phase involves synthesis of new proteins to update connections at the synapse, and if this phase is interrupted due to exposure to protein synthesis inhibitors, the memory will be lost. Recently, a molecular marker for strong memories was identified. It was found that the NMDA receptor subunit content changes its ratio of GluN2A to GluN2B as a result strong fear memory formation (Holehonnur et al., 2015). More specifically, animals trained on auditory fear conditioning using many tone-shock pairings (TSP) (10 TSP) show a high GluN2A/GluN2B ratio compared to weakly trained animals (1 or 3 TSP). Using double transgenic animals, it was possible to take weakly trained animals and increase the GluN2A levels specifically at the time of the initiation of the reconsolidation phase. What they found was the artificially created increase in GluN2A (normally a characteristic of a strong fear memory) made the animals resistant to the effects of pharmacologically induced amnesia (infusion of a protein synthesis inhibitor, anisomycin, into the BLA). This was a clear identification of a molecular marker of a strong memory that blocks the initiation phase of reconsolidation, thus making the memory resistant to amnestic agents. In chapter 6, I

demonstrate my work on the role of GluN2B in the initiation of reconsolidation of strong fear memories. We used lentivirus, due to its ability to package large transgenes. To render the virus inducible, we used a TRE3G promoter to drive expression of a mouse GluN2B (GluN2B(WT)) transgene. Infusing this virus into α CamkII-tTA mice, we were able to restrict expression to excitatory neurons within the BLA. Our goal was to increase the GluN2B/GluN2A ratio, so we also used a GluN2B transgene that harbors a mutation in the c-terminal tail (GluN2B(E1479Q)) preventing it to be endocytosed, as a method to further increase the GluN2B/GluN2A ratio. Using these lentiviruses to increase GluN2B levels in the BLA we tested how this shift affects consolidation, extinction and reconsolidation of a strong and weak auditory fear memories.

References

- Agranoff, B.W. & Klinger, P.D. (1964) Puromycin Effect on Memory Fixation in the Goldfish. *Science*, 146, 952-953.
- Capecchi, M.R. (2005) Gene targeting in mice: functional analysis of the mammalian genome for the twenty-first century. *Nature reviews. Genetics*, 6, 507-512.
- Chao, H., Liu, Y., Rabinowitz, J., Li, C., Samulski, R.J. & Walsh, C.E. (2000) Several log increase in therapeutic transgene delivery by distinct adeno-associated viral serotype vectors. *Molecular therapy : the journal of the American Society of Gene Therapy*, 2, 619-623.
- Cruz, E., Soler-Cedeno, O., Negron, G., Criado-Marrero, M., Chompre, G. & Porter, J.T. (2015) Infralimbic EphB2 Modulates Fear Extinction in Adolescent Rats. *The Journal of neuroscience : the official journal of the Society for Neuroscience*, 35, 12394-12403.
- de Solis, C.A., Ho, A., Holehonnur, R. & Ploski, J.E. (2016) The Development of a Viral Mediated CRISPR/Cas9 System with Doxycycline Dependent gRNA Expression for Inducible In vitro and In vivo Genome Editing. *Front Mol Neurosci*, 9, 70.
- de Solis, C.A., Holehonnur, R., Banerjee, A., Luong, J.A., Lella, S.K., Ho, A., Pahlavan, B. & Ploski, J.E. (2015) Viral delivery of shRNA to amygdala neurons leads to neurotoxicity and deficits in Pavlovian fear conditioning. *Neurobiol Learn Mem*, 124, 34-47.
- de Solis, C.A., Hosek, M.P., Holehonnur, R., Ho, A., Banerjee, A., Luong, J.A., Jones, L.E., Chaturvedi, D. & Ploski, J.E. (2017) Adeno-associated viral serotypes differentially transduce inhibitory neurons within the rat amygdala. *Brain research*, 1672, 148-162.
- Holehonnur, R., Kim, L.J., Jones, L.E., Daison, D.K., Vuong, D.T., Khakoo, S.F. & Ploski, J.E. (2015) Overexpression of GluN2A or GluN2B within neurons of the mouse basal and lateral amygdala alters amygdala dependent mnemonic processing. *Society for Neuroscience Abstract - Chicago*.
- Hommel, J.D., Sears, R.M., Georgescu, D., Simmons, D.L. & DiLeone, R.J. (2003) Local gene knockdown in the brain using viral-mediated RNA interference. *Nat Med*, 9, 1539-1544.
- Hsu, P.D., Lander, E.S. & Zhang, F. (2014) Development and Applications of CRISPR-Cas9 for Genome Engineering. *Cell*, 157, 1262-1278.
- Johansen, J.P., Cain, C.K., Ostroff, L.E. & LeDoux, J.E. (2011) Molecular mechanisms of fear learning and memory. *Cell*, 147, 509-524.

- Kootstra, N.A. & Verma, I.M. (2003) Gene therapy with viral vectors. *Annual review of pharmacology and toxicology*, 43, 413-439.
- Lee, J.L.C., Nader, K. & Schiller, D. (2017) An Update on Memory Reconsolidation Updating. *Trends in cognitive sciences*, 21, 531-545.
- Martin, J., Wolken, N., Brown, T., Dauer, W., Ehrlich, M. & Gonzalez-Alegre, P. (2011) Lethal toxicity caused by expression of shRNA in the mouse striatum: implications for therapeutic design. *Gene Ther*, 18, 666 - 673.
- McBride, J.L., Boudreau, R.L., Harper, S.Q., Staber, P.D., Monteys, A.M., Martins, I., Gilmore, B.L., Burstein, H., Peluso, R.W., Polisky, B., Carter, B.J. & Davidson, B.L. (2008) Artificial miRNAs mitigate shRNA-mediated toxicity in the brain: Implications for the therapeutic development of RNAi. *Proceedings of the National Academy of Sciences*, 105, 5868-5873.
- Mews, P., Donahue, G., Drake, A.M., Luczak, V., Abel, T. & Berger, S.L. (2017) Acetyl-CoA synthetase regulates histone acetylation and hippocampal memory. *Nature*, 546, 381-386.
- Nader, K. & Hardt, O. (2009) A single standard for memory: the case for reconsolidation. *Nat Rev Neurosci*, 10, 224-234.
- Nader, K., Schafe, G.E. & Le Doux, J.E. (2000) Fear memories require protein synthesis in the amygdala for reconsolidation after retrieval. *Nature*, 406, 722-726.
- Olszewski, T.M. & Varrasse, J.F. (2005) The neurobiology of PTSD: implications for nurses. *Journal of psychosocial nursing and mental health services*, 43, 40-47.
- Ploski, J.E., Pierre, V.J., Smucny, J., Park, K., Monsey, M.S., Overeem, K.A. & Schafe, G.E. (2008) The activity-regulated cytoskeletal-associated protein (Arc/Arg3.1) is required for memory consolidation of pavlovian fear conditioning in the lateral amygdala. *The Journal of neuroscience : the official journal of the Society for Neuroscience*, 28, 12383-12395.
- Rabinowitz, J.E., Rolling, F., Li, C., Conrath, H., Xiao, W., Xiao, X. & Samulski, R.J. (2002) Cross-packaging of a single adeno-associated virus (AAV) type 2 vector genome into multiple AAV serotypes enables transduction with broad specificity. *Journal of virology*, 76, 791-801.
- Ramirez-Amaya, V., Angulo-Perkins, A., Chawla, M.K., Barnes, C.A. & Rosi, S. (2013) Sustained transcription of the immediate early gene Arc in the dentate gyrus after spatial exploration. *The Journal of neuroscience: the official journal of the Society for Neuroscience*, 33, 1631-1639.
- Ran, F.A., Cong, L., Yan, W.X., Scott, D.A., Gootenberg, J.S., Kriz, A.J., Zetsche, B., Shalem, O., Wu, X., Makarova, K.S., Koonin, E.V., Sharp, P.A. & Zhang, F. (2015) In vivo genome editing using *Staphylococcus aureus* Cas9. *Nature*, 520, 186-191.

- Steward, O. (1997) mRNA localization in neurons: a multipurpose mechanism? *Neuron*, 18, 9-12.
- Steward, O., Wallace, C.S., Lyford, G.L. & Worley, P.F. (1998) Synaptic activation causes the mRNA for the IEG Arc to localize selectively near activated postsynaptic sites on dendrites. *Neuron*, 21, 741-751.
- Steward, O., Wallace, C.S. & Worley, P.F. (2001) Synaptic plasticity in epileptogenesis: cellular mechanisms underlying long-lasting synaptic modifications that require new gene expression. *Int Rev Neurobiol*, 45, 269-292.
- Van Vliet, K.M., Blouin, V., Brument, N., Agbandje-McKenna, M. & Snyder, R.O. (2008) The Role of the Adeno-Associated Virus Capsid in Gene Transfer. In Jain, K.K. (ed) *Drug Delivery Systems*. Humana Press, Totowa, NJ, pp. 51-91.
- Wang, R.Y., Phang, R.Z., Hsu, P.H., Wang, W.H., Huang, H.T. & Liu, I.Y. (2013) In vivo knockdown of hippocampal miR-132 expression impairs memory acquisition of trace fear conditioning. *Hippocampus*, 23, 625-633.
- Wang, S.H., de Oliveira Alvares, L. & Nader, K. (2009) Cellular and systems mechanisms of memory strength as a constraint on auditory fear reconsolidation. *Nat Neurosci*, 12, 905-912.
- Wilensky, A.E., Schafe, G.E., Kristensen, M.P. & LeDoux, J.E. (2006) Rethinking the fear circuit: the central nucleus of the amygdala is required for the acquisition, consolidation, and expression of Pavlovian fear conditioning. *The Journal of neuroscience : the official journal of the Society for Neuroscience*, 26, 12387-12396.
- Wood, N.E., Rosasco, M.L., Suris, A.M., Spring, J.D., Marin, M.F., Lasko, N.B., Goetz, J.M., Fischer, A.M., Orr, S.P. & Pitman, R.K. (2015) Pharmacological blockade of memory reconsolidation in posttraumatic stress disorder: three negative psychophysiological studies. *Psychiatry Res*, 225, 31-39.
- Wu, Z., Asokan, A. & Samulski, R.J. (2006) Adeno-associated virus serotypes: vector toolkit for human gene therapy. *Molecular therapy : the journal of the American Society of Gene Therapy*, 14, 316-327.

CHAPTER 2

VIRAL DELIVERY OF SHRNA TO AMYGDALA NEURONS LEADS TO NEUROTOXICITY AND DEFICITS IN PAVLOVIAN FEAR CONDITIONING

Authors: Christopher A. de Solis, Roopashri Holehonnur, Anwasha Banerjee, Jonathan A. Luong, Srihari K. Lella, Anthony Ho, Bahram Pahlavan, Jonathan E. Ploski

School of Behavioral and Brain Sciences

The University of Texas at Dallas

800 West Campbell Road

Richardson, TX 75080-3021, USA

*Reprinted with permission from Elsevier: *Neurobiology of Learning and Memory*, Volume 124, Issue 2, October – July 2017

Viral delivery of shRNA to amygdala neurons leads to neurotoxicity and deficits in Pavlovian fear conditioning

Christopher A. de Solis, Roopashri Holehonnur, Anwasha Banerjee, Jonathan A. Luong, Srihari K. Lella, Anthony Ho, Bahram Pahlavan, Jonathan E. Ploski

Neurobiology of Learning and Memory, 2015; <https://doi.org/10.1016/j.nlm.2015.07.005>

Abstract

The use of viral vector technology to deliver short hairpin RNAs (shRNAs) to cells of the nervous system of many model organisms has been widely utilized by neuroscientists to study the influence of genes on behavior. However, there have been numerous reports that delivering shRNAs to the nervous system can lead to neurotoxicity. Here we report the results of a series of experiments where adeno-associated viruses (AAV), that were engineered to express shRNAs designed to target known plasticity associated genes (i.e. Arc, Egr1 and GluN2A) or control shRNAs that were designed not to target any rat gene product for depletion, were delivered to the rat basal and lateral nuclei of the amygdala (BLA), and auditory Pavlovian fear conditioning was examined. In our first set of experiments we found that animals that received AAV ($3.16E13 - 1E13$ GC/mL; 1ul/side), designed to knockdown Arc (shArc), or control shRNAs targeting either luciferase (shLuc), or nothing (shCntrl), exhibited impaired fear conditioning compared to animals that received viruses that did not express shRNAs. Notably, animals that received shArc did not exhibit differences in fear conditioning compared to animals that received control shRNAs despite gene knockdown of Arc. Viruses designed to harbor shRNAs did not induce obvious morphological changes to the cells/tissue of the BLA at any dose of virus tested, but at the highest dose of shRNA virus examined ($3.16E13$ GC/mL; 1ul/side), a significant increase in microglia activation occurred as measured by an increase in IBA1 immunoreactivity. In our final set of experiments we infused viruses into the BLA at a titer of ($1.60E+12$ GC/mL; 1ul/side), designed to express shRNAs designed to target Egr1 (shEgr1), GluN2A (shGluN2A), shArc, shLuc, shCntrl, or a virus which did not express an shRNA, and found that all groups exhibited impaired fear conditioning compared to the group which received a virus that did not express an shRNA. The shEgr1 and shGluN2A groups exhibited gene knockdown of Egr1 and GluN2A compared to the other groups examined respectively, but Arc was not knocked down in the shArc group under these conditions. Differences in fear conditioning among the shLuc, shCntrl, shArc and shEgr1 groups were not detected under these circumstances, however the shGluN2A group exhibited significantly impaired fear conditioning compared to most of the groups, indicating that gene specific deficits in fear conditioning could be observed utilizing viral mediated delivery of shRNA. Collectively, these data indicate that viral mediated shRNA

expression was toxic to neurons *in vivo*, under all viral titers examined and this toxicity in some cases may be masking gene specific changes in learning. Therefore, the use of this technology in behavioral neuroscience warrants a heightened level of careful consideration and study design and potential methods to alleviate shRNA induced toxicity are discussed.

Introduction

The ability to genetically modify organisms provides the means to determine how individual genes contribute to the functioning of the nervous system. Currently, mouse and rat gene “knockouts/ins” and transgenics are the main systems used to investigate the role and function of individual mammalian genes in behavioral neuroscience (Capecchi, 2005). One technology to study gene function that offers alternatives to the above mentioned technology is to use viruses to deliver transgenes of interest to specific cells or regions of the nervous system. If the virus is designed to contain a gene that codes for a short hairpin RNA (shRNA), specific gene products (i.e. mRNAs) can be targeted for degradation via the RNA interference (RNAi) pathway (Hommel *et al.*, 2003). This technology can essentially be used to knockout genes in particular tissues/cells quickly, before or after behavioral training and relatively easily.

Intriguingly, there are numerous reports that *in vivo* use of shRNAs can be problematic. For example, there have been studies that report that viral delivery of shRNAs to the mouse and rat brain is associated with neural toxicity. For example, AAV mediated delivery of shRNA to the striatum of mice has been reported to induce neural toxicity, neuronal cell loss, increased inflammation as measured by an increase in microglia activation, motor disturbances and early demise (McBride *et al.*, 2008; Martin *et al.*, 2011). These findings were caused by the expression of all shRNAs examined, even shRNAs that were not designed to target any gene product for depletion. Similar neurotoxicity has been reported to be induced by viral delivery of shRNA to

the rat substantia nigra (Ulusoy *et al.*, 2009; Khodr *et al.*, 2011), cerebellum (Boudreau *et al.*, 2009), and red nucleus (Ehlert *et al.*, 2010). However, despite these previous findings that viral mediated delivery of shRNA may cause neural toxicity when administered to the central nervous system of mice and rats, it remains a common tool to examine the role of genes in behavior.

In this series of experiments, we were specifically interested in determining if robust learning and memory deficits could be created when viral mediated delivery of shRNA technology was used to target the mRNAs for the Activity regulated cytoskeletal (Arc) gene, Early Growth Response 1 (Egr1) gene, and the GluN2A gene - a subunit of the *N*-Methyl-D-aspartate receptor (NMDAR). Because these genes have previously been shown to be critical for amygdala dependent Pavlovian fear conditioning (Jones *et al.*, 2001; Plath *et al.*, 2006; Ploski *et al.*, 2008; Walker & Davis, 2008; Maddox *et al.*, 2011), we reasoned that if this technology was effective, it should be able to knockdown these genes within the amygdala and impair Pavlovian fear conditioning. Therefore, we designed adeno-associated viruses that harbored short-hairpin RNAs (shRNA) designed to target the mRNAs for each of these genes. These viruses, along with control viruses which harbor shRNA genes that are not designed to target any rat mRNA for degradation, were bilaterally infused into the rat basal and lateral amygdala and subsequently these animals were auditory fear conditioned and fear memory was assessed. We found that the viruses designed to express control shRNAs and shRNAs designed to target known plasticity associated genes (i.e. Arc, Egr1 and GluN2A) were toxic and auditory Pavlovian fear conditioning was significantly impaired. Our results indicate that the impairments in Pavlovian fear conditioning were due to the viruses harboring shRNA genes and were not due to surgery, the virus itself or viral mediated GFP expression and these results were dose dependent.

Unfortunately, even when significantly lower doses of shRNA harboring viruses were infused into the amygdala, impairments in fear conditioning were observed, which likely prevented the detection of gene specific deficits in fear learning. Here we report our findings and discuss the implications of these results.

Methods and Materials

Subjects: 3-4 month male Sprague Dawley rats (Harlan) were individually housed in polycarbonate cages on a 12 hour light/dark cycle. Food and water were provided *ad libitum*. Animal use procedures were in accordance with the National Institutes of Health Guide for the Care and Use of laboratory animals and were approved by the University of Texas at Dallas Animal Care and Use Committee.

Plasmid Constructs Plasmids used within this study have been developed using standard recombinant cloning procedures. Short hairpin RNAs (shRNAs) previously described for targeting Arc (Rial Verde *et al.*, 2006) were cloned into pSuper (Oligoengine). Specifically, the following oligos (shARC-TOP GATCcccGCTGATGGCTACGACTACAttcaagagaTGTAGTCGTAGCCATCAGCttttt, shARC-BOT AGCTaaaaaGCTGATGGCTACGACTACAtctctttaaTGTAGTCGTAGCCATCAGCggg) were annealed and ligated to the BglII and HindIII restriction enzyme sites of the pSUPER vector (Oligoengine) to create the pSuper-shARC plasmid. The plasmid (pSuper) containing the shRNA designed to target Luciferase (shLuc) and GluN2A (shGluN2A), were kindly provided by Dr. Morgan Sheng (Foster *et al.*, 2010; Hung *et al.*, 2010). To create the pAAV-GFP-shArc(1) and pAAV-GFP-shLuc(1) plasmids, the shArc and shLuc expression cassettes, which

include the 226 base pair H1 RNA polymerase III promoter, were PCR amplified using the following DNA primers, (Super FP Acc65I aaaggtaccGAATTCGAACGCTGACGTCATC, Super RP AscI CAAGGCGCGCCTACCGGGCCCCCCTCG), and these DNA products were ligated to the Acc65I and AscI restriction enzymes sites of the pNEB193 plasmid (New England Biolabs), creating pNEB193-shArc1 and pNEB193-shLuc, respectively. Subsequently, the entire shRNA expression cassette was PCR amplified from pNEB193 using the following DNA primers, (pNeb193 FP GGCGAAAGGGGGATGTGCTG, pNeb193 RP BlnI cacGctcagCACCTCTGACTTGAGCGTCG), and these PCR products were ligated to the Acc65I and BlnI sites of the AAV2 viral genome plasmid, pAAV-GFP-shRNA, (Hommel *et al.*, 2003) to create pAAV-GFP-shArc(1) and pAAV-GFP-shLuc(1) plasmids, respectively. The pAAV-GFP-shArc(4) and pAAV-GFP-shLuc(4) plasmids that contain 4 shRNA expression cassettes in tandem were created in a similar manner as to pAAV-GFP-shArc(1) and pAAV-GFP-shLuc(1) plasmids but the 2nd, 3rd and 4th shRNA expression cassettes were sequentially cloned into the pNEB193-shArc1 and pNEB193-shLuc plasmids via the AscI/BamHI, BamHI/SphI, and the SphI/AflIII restriction enzymes sites, respectively, using the following DNA primers, (Super FP AscI aaaGGCGCGCCGAATTCGAACGCTGACGTCATC, Super RP BamHICAAGGATCCTACCGGGCCCCCCTCG; Super FP BamHI CAAGGATCCGAATTCGAACGCTGACGTCATC, Super RP SphI CAAGCATGCTACCGGGCCCCCCTCG; Super FP SphI CAAGCATGCGAATTCGAACGCTGACGTCATC, Super RP AflIII CAAACATGTTACCGGGCCCCCCTCG). Subsequently, the entire region containing the 4 shRNA expression cassettes was PCR amplified from pNEB193 using the following DNA

primers, (pNeb193 FP GGCGAAAGGGGGATGTGCTG, pNeb193 RP BlnI cacGctcagcCACCTCTGACTTGAGCGTCG), and this PCR product was ligated to the Acc65I and BlnI sites of the pAAV-GFP-shRNA vector to create pAAV-GFP-shArc(4) and pAAV-GFP-shLuc(4) plasmids, respectively. The pAAV-GFP vector was created by digesting the pAAV-GFP-shRNA plasmid with AscI and XbaI and re-ligating it to remove the existing U6 promoter/shRNA Expression cassette to create a GFP transgene only pAAV vector. To create AAV vectors that contain HI promoter mutants, shArc and shLuc expression cassettes were PCR amplified from pSuper-shArc and pSuper-shLuc, respectively, using the following primers, (Super FP AscI mutant AAAGGCGCGCCAATATTTGCATGTCGCTATGTGTTTCg_{ttt}AAATCACCATAAACGTG, Super RP XbaI CAATCTAGATACCGGGCCCCCCTCG), and these DNA products were ligated to the AscI and XbaI restriction enzymes sites of the pAAV-GFP-shRNA vector. These ~100 bps H1 promoter mutants contain a truncated promoter with a TGGG > GTTT mutation occurring at position -72. This mutation is indicated in the forward primer with lower case letters. pAAV-GFP-shGluN2A was created by PCR amplifying the shGluN2A expression cassette from pSuper-shGluN2A using the following DNA primers, (Super FP Acc65I aaagtaccGAATTCGAACGCTGACGTCATC, Super RP AscI CAAGGCGCGCCTACCGGGCCCCCCTCG), and ligating the DNA product to the Acc65I and AscI sites of pAAV-GFP-shRNA vector (Hommel *et al.*, 2003). To create pAAV-GFP-shControl, the pAAV-GFP-shArc (Asc-XbaI) plasmid was first digested with BglII and HindIII and religated to destroy the intervening XhoI sites and the BglII sites. Then this new plasmid was digested with AscI and XbaI and the empty shRNA expression cassette from pSuper was PCR

amplified using the following DNA primers, (Super FP AscI
aaaGGCGCGCCGAATTCGAACGCTGACGTCATC, Super RP XbaI
CAATCTAGATACCGGGCCCCCCTCG), and this DNA product was ligated to the AscI and
XbaI

sites to create pAAV-GFP-(H1)shRNA (empty) plasmid. Subsequently, the control shRNA
oligonucleotides (Top:

GATCCCCGCGCGCTTTGTAGGATTCGTTCAAGAGACGAATCCTACAAAGCGCGCTTT
TTA, Bottom:

TCGATAAAAAGCGCGCTTTGTAGGATTCGTCTCTTGAACGAATCCTACAAAGCGCGC
GGG) were annealed and ligated to the BglII and XhoI sites of pAAV-GFP-H1shRNA (empty)

plasmid to create pAAV-GFP-shControl. To create pAAV-GFP-shEgr1, the following
oligonucleotides (Top:

tttGATGAGTTGGGACTGGTAGGTGTTCTTCCTGTCAAACACCTACCAGTCCCAACTCA
TaTTTTT, Bottom:

ctagAAAAAtATGAGTTGGGACTGGTAGGTGTTTGACAGGAAGAACACCTACCAGTCC
CAACTCATC), were annealed and ligated to the SapI and XbaI sites of the pAAV-GFP-

shRNA vector, (Hommel *et al.*, 2003). The AAV genome plasmids created in this study all
consisted of a viral genome that was ~3-3.5 kb, except for the shArc4/Luc4 viral genomes which

were ~4 kb in length. To create plasmids that were designed to express Arc and Egr1 coding
regions fused with red fluorescent protein (RFP) at the c-terminus, the Arc and Egr1 rat coding

regions were PCR amplified from rat brain cDNA using the following primers (Arc: FP Xho
AAACTCGAGcagatggagctggaccatgatgac, RP BamHI

TTTTGGATCCCGTTCAGGCTGGGTCCTGTCAC; Egr1: FP X1
cCTCGAGatggacaactaccccaaactg, RP R1

CAGAATTCGGCAAATTTCAATTGTCC) and these DNA products were ligated into the XhoI and BamHI sites or XhoI and EcoR1 sites of pdsRedN-1 plasmid (Clontech), to create pdsRedN-1-Arc and pdsRedN-1-Egr1, respectively. The pCI-GFP-GluN2A plasmid designed to express GluN2A as a GFP fusion protein was generously provided by Andreas Barria (Barria & Malinow, 2002; 2005). All constructs were confirmed through sequencing. Plasmids and plasmid sequences will be provided upon request.

In vitro Knockdown Experiments *In vitro* knockdown experiments were performed as previously described [13]. For *in vitro* knockdown of Arc-RFP, Egr1-RFP and GFP-GluN2A, 293FT cells (Invitrogen, Cat# R700-07) were grown in a 24 well plate to 30-50% confluency. Cells were then co-transfected with a pdsRedN-1-Arc, pdsRedN-1-Egr1 or pCI-GFP-GluN2A, and the appropriate shRNA expression cassette containing plasmids in a 1:1 ratio using lipofectamine 2000 (Invitrogen) following the manufacturer's instructions. RFP or GFP intensity was observed 96 hours post transfection to visually/qualitatively observe knockdown of the Arc-RFP or Egr1-RFP fusion proteins using an Olympus IX51 inverted fluorescent microscope under RFP and GFP filters and the images were acquired using an Olympus DP72 Digital Camera and Cellsens software (Olympus). To quantitatively measure shRNA mediated gene knockdown of Arc, Egr1, or GluN2A, cells were treated as above, but the cells were harvested forty eight hours post transfection and the RNA was extracted with Trizol reagent (Invitrogen) following the manufacturer's instructions. RNA was precipitated with PelletPaint (Novagen) and converted to

cDNA with Superscript Reverse Transcriptase II (Invitrogen) following the manufacturer's instruction, respectively, and cDNA levels were measured with qRT-PCR in a standard 20 μ L Taqman PCR assay (Applied Biosystems) using a CFX96 Real-time PCR system (BioRad). One μ l of a 20X Taqman custom RFP Primer/Probe to measure RFP levels was used (RFP FP: AGCGCGTGATGAACTTCGA, RFP RP: GCCGATGAACTTCACCTTG TAGAT, RFP Probe: 6FAM-ACCCAGGACTCCTCC) (as previously described (Althage *et al.*, 2008)). One μ l of a 20X Taqman GluN2A Primer/Probe was used to measure GluN2A levels (Life Technologies, Cat#Rn00561341_m1) Complementary DNA input was normalized to GAPDH using GAPDH specific primers/Vic labeled probe (ID# Hs02758991_g1, Invitrogen). Quantitative RT-PCR was performed using the $\Delta\Delta$ Ct method as described previously (Ploski *et al.*, 2006; Ploski *et al.*, 2010; Ploski *et al.*, 2011) and these data are represented as the average threshold cycle (Ct) difference values for each group after normalization to GAPDH, with the error bars representing the standard error of the mean for each group, (average fold change = $2^{(\text{average Ct difference value})}$). Wells were seeded in triplicate and qRT-PCR data was compared via 2 tailed t-test assuming equal variances or One-Way ANOVA, where appropriate.

Viral Production, Purification, and Titering Viral production, purification, and titering were performed as previously described (Holehonnur *et al.*, 2014). Briefly, AAV2 genome plasmids were pseudotyped as AAV2/DJ8. Pseudotyped viruses were produced using a triple-transfection, helper-free method using 293FT cells, and the resultant viruses were purified on an iodixanol step gradient and further concentrated using Amicon Ultra-15 centrifugal filter units

(Millipore). Purified AAV viruses were titered using a quantitative-PCR based titering method with the following DNA primers (GFP Primer/Probe (ID# Mr04329676_mr, Invitrogen)), to calculate DNase resistant viral particles. The titers were reported as genome copies GC/ml.

Viral infusions to the Basolateral complex (BLA) Viral infusions targeting the BLA were performed as previously described (Holehonnur *et al.*, 2014). Briefly, rats were rendered unconscious with an intra-peritoneal injection of ketamine (100mg/kg) and xylazine (10mg/kg) prior to stereotaxic surgery. Thirty-three gauge custom infusion cannulas (C315G, PlasticsOne) were inserted into polyethylene tubing (I.D. 0.0150 in, O.D. 0.043 in, wall thickness 0.0140 in)(A-M systems, Inc.) that were ~50 cm in length. These tubes were first backfilled with 1 x phosphate buffered saline, pH 7.4 (PBS), followed by sesame oil so that the ~5 cm closest to the infusion needle contained PBS and the rest of the infusion line was filled with sesame oil. These lines were then connected to 2 μ L, 23-gauge (88500) stainless steel Hamilton syringes (Hamilton Company). Rats were bilaterally infused into the BLA [AP -2.9, ML \pm 4.7, DV -8.6], with 1 μ L/side at a rate of 0.07 μ L/min for 15 minutes. The titers used were as follows: high (3.16 E + 13 GC/mL), medium (1.0 E + 13 GC/mL), low (3.16 E + 12 GC/mL), and extra-low (1.6E + 12 GC/mL). Behavioral and molecular experiments were performed 21 days post viral infusion.

Fear Conditioning: Fear conditioning training and testing was essentially completed as previously performed (Ploski *et al.*, 2011; Banerjee *et al.*, 2014). Twenty one days post-viral infusion the rats were fear conditioned. *Training* consisted of a 2 min acclimation period, followed by exposure to a single tone (30 sec, 5 kHz, 75 dB), which co-terminated with a 1.5 sec, 1.5 mA foot shock. Animals remained in the training chamber for an additional minute

following the delivery of the foot shock and subsequently the animals were placed back into their home cages. Short-term memory (STM) was examined 3 hours after training by exposing the rats to 3 tones (2 min intertrial interval; 30 sec, 5 kHz, 75 dB) in an altered context (a modified chamber and the absence of light, with distinct olfactory and tactile cues). Long-term memory, (LTM) was examined 24 hours post-training in a similar context as the STM test. Freezing behavior of each animal was measured during the exposure to each of the three tones presenting during STM an LTM testing. A Coulbourn Instruments fear conditioning system with computer controlled shockers, USB cameras for video monitoring / video capture and FreezeFrame Software (Actimetrics) for unbiased behavioral analysis was used to auditory fear condition rats and to test for conditioned fear responses. 154 animals were used for pavlovian fear conditioning experiments. Data was analyzed using a One-Way ANOVA for repeated measures or 2 tailed t-test assuming equal variances where appropriate. The individual that scored the freezing behavior and analyzed the data was blind to the experimental conditions. Rats were perfused the day following LTM, their brains were sectioned, and evaluated for placement analysis. Animals with poor viral placement within the BLA were excluded from the experiment.

Measurement of in vivo knockdown via qRT-PCR The effectiveness of viral delivered shRNAs to knockdown gene expression was examined by qRT-PCR. Animals were sacrificed 21 days post infusion. Rats were anesthetized lightly with CO² and quickly decapitated. Brains were immediately removed and placed on dry ice and stored at -80 C°. Ten micron coronal sections containing viral transduction within the amygdala were obtained and placed on MMI Laser Microdissection (LMD) slides (product #50102) and were dissected via laser

microdissection on a SmartCut Laser Microdissection System configured on an Olympus CKX41 inverted microscope. Section preparation, dehydration and laser microdissection were performed as previously described (Partin *et al.*, 2013). Viral transduced BLA tissue was microdissected from approximately 10 sections and these microdissected tissue pieces were collected in 25 μ L of cell lysis buffer (RNAqueous-Micro Kit; Ambion) and the RNA was purified according to the manufacturer's instructions. The RNA was precipitated using Pellet Paint NF (Novagen) and converted to cDNA with Superscript Reverse Transcriptase II (Invitrogen) following the manufacturer's instructions. Quantitative RT-PCR was performed in a similar manner as for the *in vitro* knockdown experiments, using RNA prepared from at least 5 individual amygdala, per group (i.e. $n > 5$). ANOVA or 2 tailed t-test assuming equal variances, where appropriate, were used for statistical analysis.

Measurement of shArc levels 293FT cells were seeded in a 12 well plate. Twenty four hours later the cells were co-transfected in triplicate with 0.08 μ gs of shArc or shArc(4) plasmids and 1.5 μ gs of pNEB193 plasmid following the standard lipofectamine 2000 protocol (Invitrogen). Forty eight hours post transfection, the cells were harvested and the RNA was purified using the mirVana miRNA Isolation Kit, (Ambion, Cat #AM1560) following the manufacturer's instructions. Specific qRT-PCR primers and reverse transcription primers were designed against the antisense portion of the Arc shRNA (5' TGTAGTCGTAGCCATCAGC 3') utilizing the Custom TaqMan Small RNA Assay Design Tool (Invitrogen; Batch ID: w1211234309000; Assay ID# CS0IWAH). The purified RNA samples were reverse transcribed with the custom stem loop primer provided in the Custom TaqMan Small RNA Assay, using the TaqMan

MicroRNA Reverse Transcription Kit, (Ambion, cat # 4366596), and these samples were subjected to Taqman qRT-PCR. RNA from the same samples was also reverse transcribed with the stem loop primer for the U6 snRNA (Invitrogen, TaqMan MicroRNA Assay; U6 snRNA Assay, ID# 001973) using the TaqMan MicroRNA Reverse Transcription Kit and these samples were subjected to Taqman qRT-PCR. Quantitative RT-PCR was performed using the $\Delta\Delta C_t$ method as described previously (Ploski *et al.*, 2006; Ploski *et al.*, 2010; Ploski *et al.*, 2011) and these data are represented as the average threshold cycle (Ct) difference values for each group after normalization to U6 snRNA levels, with the error bars representing the standard error of the mean for each group, (average fold change = $2^{(\text{average Ct difference value})}$).

Immunohistochemistry and Quantification

Immunohistochemistry (IHC) for IBA1 was carried out to detect microglia activation. Animals were perfused through the heart with 4% paraformaldehyde in PBS and cryoprotected with a 30% sucrose solution in PBS. Tissue was sectioned coronally using a cryostat sectioner. Slices containing amygdala that were transduced with virus were collected in PBS with 0.1% sodium azide. Free-floating sections were washed in PBS and quenched in a solution containing 3% H₂O₂ in H₂O for 5 min. Following quenching, the tissue was rinsed in PBS once, and then subsequently placed in blocking solution (1.5% normal goat serum and 0.3% Triton X-100 in PBS-A (NaCl 150mM, NaOH 96mM, NaH₂PO₄ 106mM)) for one hour, followed by an overnight incubation in blocking solution containing anti-IBA1 antibody (anti-IBA1 rabbit polyclonal; 1:1000; Wako 019-19741). Tissue was washed in PBS-B (NaCl, 150mM, NaOH 10mM, NaH₂PO₄ 11mM) 3 times for 10 min each, following by processing using VectaStain

ABC kit (Vector Laboratories PK-6801) following the manufacturer's instructions. The tissue was developed in DAB peroxidase substrate and H₂O₂ (Sigma) for 7 min. The tissue was then mounted on Fisher Super Frost glass slides with DPX mountant media (Sigma). The IBAI signal was quantified by calculating the integrated density of the IBAI signal using ImageJ software from no less than 6 amygdala per group.

Immunohistochemistry for NeuN was performed to determine if virus was localized to neurons. Animals received viral infusions to the BLA and were perfused twenty one days post infusion with 4% PFA in PBS. Free floating sections were washed 3 times for 10 min in PBS at RT. Tissue was then transferred to blocking solution (5% normal goat serum and 0.3% triton-100 in PBS) for 30 min. Sections were then placed in blocking solution with a NeuN Antibody (anti-NeuN mouse monoclonal ; 1:500; Millipore MAB377) and incubated overnight at 4C°. Sections were washed 3 times for 10 min at RT before being transferred to blocking solution containing secondary antibody (anti-mouse Texas Red-X conjugate; 1:1000 ; Invitrogen T6390) for two hours. Sections were then washed 3 times for 10 min and then mounted on VectaShield mounting medium(H-1000). Localization of virus to neurons was quantified using Adobe Photoshop across 3 40uM slices that were a considerable distance apart from each other.

Statistical Analysis Data presented in graphs is displayed as the mean \pm standard error of the mean (SEM). A One-Way ANOVA or two-tailed t-test assuming equal variances was used to compare group means for qRT-PCR analysis. A One-Way ANOVA for repeated measures was

used for STM and LTM fear conditioning experiments. All post hoc analysis was done using Fischer's LSD.

Results

Viral delivery of shRNA to the rat amygdala results in relatively weak fear conditioning

In our first set of experiments we aimed to knockdown Arc gene expression within neurons of the rat basal and lateral amygdala (BLA) utilizing viral mediated delivery of shRNA, and then we wanted to determine how viral mediated knockdown of Arc influenced learning and memory utilizing Pavlovian auditory fear conditioning. We developed AAV2 viral genome vectors that contain a gene expression cassette designed to express GFP from a CMV promoter, and an shRNA expression cassette designed to express the shRNA from an H1 RNA polymerase III promoter. To target Arc for depletion, we utilized an shRNA sequence (shARC), that has previously been shown to be effective at lowering Arc levels within neurons (Rial Verde *et al.*, 2006; Waung *et al.*, 2008). As a control, we developed a similar viral vector that contained an shRNA sequence (shLuc), that was designed to target and deplete luciferase gene products and this shRNA has been widely utilized within many *in vitro* studies as a control, since it is not designed to target any rat gene product for depletion (Hung *et al.*, 2010).

To measure the effectiveness of the shArc viral plasmid *in vitro*, the AAV-shArc and AAV-shLuc plasmids were co-transfected into 293FT cells with a plasmid that was designed to express Arc protein fused to red fluorescent protein (RFP). Ninety-six hours post transfection, the levels of RFP and GFP were examined via fluorescence microscopy. Each well contained similar levels of GFP indicating that the transfection efficiency for each plasmid was similar

among samples. However, the levels of Arc-RFP were lower in the cells that received shArc compared to the cells that received shLuc, indicating that the shArc was effective at depleting Arc-RFP levels, as intended. To quantitatively assess shArc effectiveness, cells were treated in a similar manner as above, but they were harvested at forty-eight hours post transfection, and Arc mRNA levels were assessed by qRT-PCR. Arc mRNA levels were found to be significantly lower in cells that received shArc versus cells that received shLuc [$t_{(4)} = 4.3812$, $p = 0.0006$] (Figure 2.1C).

Next, we created adeno-associated viruses with the viral shArc and shLuc plasmids, pseudotyped as AAV2/DJ8 and infused these viruses bilaterally into the rat BLA at a titer of $3.16E+13$ GC/mL DNase resistant viral particles. Twenty-one days later, the animals were sacrificed, and the brains were removed and processed so the viral transduced areas of the BLA could be laser microdissected (LMD) and Arc mRNA levels could be subsequently examined via qRT-PCR. The LMD/qRT-PCR approach was used to examine gene expression levels, because it provides the most accurate means possible to assess gene expression changes within such a relatively small region of the brain and provides the means to specifically dissect areas of tissue that are transduced by virus. More traditional approaches, such as using punch tools to dissect the amygdala, would inevitably dissect out tissue that was not entirely of BLA origin and areas of tissue that were not transduced by virus. The qRT-PCR results revealed a significant decrease in Arc mRNA in animals that received an infusion of shArc compared to animals infused with a virus expressing shLuc [$t_{(9)} = -5.07$, $p = 0.0007$; (shArc, $n = 6$; shLuc, $n = 5$)](Figure 2.1F). Collectively, these data indicate that these shRNA vectors are effective at depleting Arc mRNA levels *in vivo* and *in vitro*.

To examine how viral mediated delivery of shRNA may influence learning in a Pavlovian auditory fear conditioning paradigm, shArc and shLuc viruses were infused bilaterally into the BLA at a titer of 3.16×10^{13} GC/mL. Twenty-one days later, the animals were auditory fear conditioned to a 30 sec, 5 kHz, 75 dB tone that co-terminated with a 1.5 mA foot shock. Three hours following fear conditioning training, retention of short term memory (STM) was assessed by exposing the rats to three 5 kHz, 75 dB tones within a novel context. The tone induced freezing behavior was determined for each rat and an ANOVA revealed there was not a significant difference in freezing levels between the groups [$F_{(1,17)} = 0.3560$, $p = 0.5585$] (Figure 2.1G). Long-term memory (LTM) was assessed 24 hours post-training, in a similar manner as to STM, and freezing levels did not differ between the groups [$F_{(1,17)} = 0.020$, $p = 0.8883$] (Figure 2.1H). Despite the fact that freezing levels did not differ between the shArc and shLuc groups across STM and LTM measures within these experiments, the most striking observation was the extremely low levels of freezing observed in these experiments.

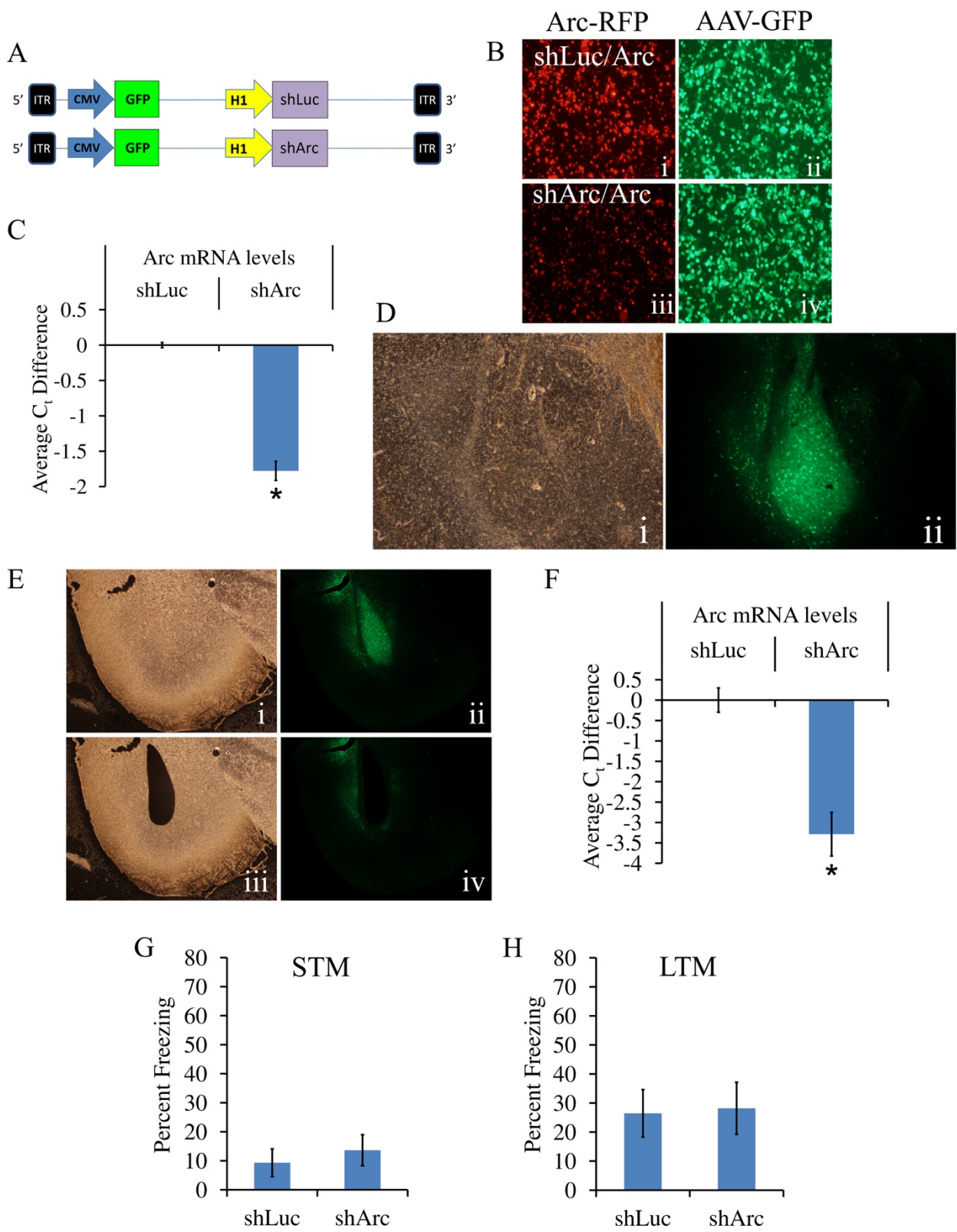


Figure 2.1 Viral delivery of RNAi to the rat amygdala results in relatively weak fear conditioning

(A) AAV genome maps for AAV-shLuc and AAV-shArc. ITR = inverted terminal repeats (B) 293FT cells were co-transfected with plasmids designed to express Arc-RFP and AAV-shLuc (i, ii) or Arc-RFP and AAV-shArc (iii, iv) and were imaged for GFP(ii, iv) and Arc-RFP(i, iii) 96 hrs post-transfection. AAV-shArc causes an observable decrease in Arc RFP signal compared to AAV-shLuc (i vs. iii). (C) 293FT cells were treated in a similar manner as in B, but they were harvested 48 hrs post-transfection and used to assess Arc mRNA levels via qRT-PCR. Cells transfected with AAV-shARC exhibited a decrease in Arc mRNA levels compared to cells that received AAV-shLuc ($p = 0.0006$). (D) Images of the BLA that received AAV2/DJ8 virus designed to express GFP; brightfield image (i), GFP fluorescence (ii). (E) Similar images as described in D, at different stages of laser microdissection of viral transduced BLA tissue. Brightfield and GFP images before LMD (i, ii) and after LMD (iii, iv). (F) AAV-shLuc and AAV-shArc viruses were infused into the BLA and 21 days post infusion the brains were extracted and processed via LMD/qRT-PCR to examine Arc mRNA levels (shArc, $n = 6$; shLuc, $n = 5$). Quantitative RT-PCR revealed a significant decrease of Arc mRNA in tissue transduced with the shArc virus compared to tissue transduced with shLuc virus ($p = 0.0007$). (G-H) Animals infused with either shLuc virus or shArc virus (shLuc $n = 9$, shArc $n = 10$) did not exhibit significant differences in freezing during STM (G) and LTM (H). Error bars represent standard error of the mean (SEM) (***) ($p < 0.001$).

Viral mediated shRNA expression within the BLA interferes with fear conditioning and leads to dysregulation of gene expression

In our first series of experiments, we observed very low levels of cue induced freezing in animals that received bilateral BLA infusions of viruses designed to deliver RNAi. We reasoned that the low freezing levels may have been caused by the viruses that were designed to express the shRNA genes. To test this hypothesis, we developed a series of AAV2 viral genome plasmids that differed in their ability to express shRNA. Viral plasmids were developed that did not contain an shRNA expression cassette (GFP only), or that contained an shArc and shLuc expression cassette that contained a mutated/truncated H1 promoter (shArc(H1 Δ), shLuc(H1 Δ)). This particular H1 promoter mutation has previously been shown to virtually abolish

transcription from this promoter (Myslinski *et al.*, 2001). Viral plasmids were also constructed to contain 4 shRNA expression cassettes in tandem (shArc(4) and shLuc(4)).

To confirm that the shArc(4) viral plasmids indeed expressed more shRNA, shArc and shArc(4) plasmids were transfected into 293FT cells and forty eight hours later, small RNAs were harvested from these cells and qRT-PCR was performed to specifically measure shARC levels, utilizing PCR primers specific for the shARC short hairpin RNAs these constructs were designed to express. Quantitative RT-PCR revealed that cells which received shArc(4) plasmids expressed higher levels of shRNAs, as compared to cells that received shArc plasmids which contain only one shArc expression cassette [$t_{(4)} = 3.98$, $p = 0.00164$] (Figure 2.2B). Next, each of the viral plasmids, (GFP, shArc(H1 Δ), shLuc(H1 Δ), shArc, shLuc, shArc(4) and shLuc(4)), were co-transfected into 293FT cells with the Arc-RFP plasmid. Ninety six hours post transfection, the levels of RFP and GFP were examined via fluorescence microscopy. Each well contained similar levels of GFP, indicating that the transfection efficiency for each plasmid was similar among samples (Figure 2.2C ii, iv, vi, viii, x, xii, xiv). However, the levels of Arc-RFP were lower in the cells that received shArc and shArc(4), compared to all other groups, indicating that the shArc and shArc(4) plasmids were effective at depleting Arc-RFP levels and the H1 promoter mutant plasmids were indeed impaired in their ability to knockdown Arc, as expected. To quantitatively assess the effectiveness of these plasmids for knocking down Arc, cells were treated in a similar manner as above, but they were harvested at forty eight hours post transfection, and Arc mRNA levels were assessed by qRT-PCR. An ANOVA revealed an overall significant effect [$F_{(3,8)} = 73.492$, $p < 0.0001$], where Arc mRNA was significantly reduced in cells transfected with shArc and shArc(4), compared to cells transfected with shLuc

and shLuc(4) ($p < 0.0001$) (Figure 2.2D), and Arc mRNA was significantly lower in the shArc group ($p = 0.002$), as compared to the shLuc and promoter mutants groups (shArc(H1 Δ), shLuc(H1 Δ)) [$F_{(3,8)} = 20.525, p = 0.0004$] (Figure 2.2E).

Next, adeno-associated viruses pseudotyped as AAV2/DJ8 were produced using these 7 different viral genome plasmids and these viruses were bilaterally infused into the BLA at a titer of $1.0E+13$ GC/mL – a half log lower titer of virus than what was used for our first experiment. Twenty one days later, the animals were sacrificed, the brains were removed, and processed via LMD/qRT-PCR to examine Arc mRNA levels within the BLA (Figure 2.2F). There was an overall significant effect across groups [$F_{(6,32)} = 4.385, p = 0.0024$; GFP $n = 5$, shLuc(H1 Δ) $n = 5$, shArc(H1 Δ) $n = 5$, shLuc $n = 6$, shArc $n = 6$, shLuc(4) $n = 6$, shArc(4) $n = 6$]. Post hoc analysis revealed that the shArc and shArc(4) groups did not differ significantly ($p = 0.4833$), but both of these groups exhibited significantly lower Arc mRNA levels compared to the shLuc and shLuc(4) groups ($p < 0.0056$). The GFP, shArc(H1 Δ) and shLuc(H1 Δ) groups did not differ significantly ($p > 0.2383$). Strikingly, the GFP and shArc(H1 Δ) groups exhibited significantly lower levels of Arc mRNA compared to the shLuc and shLuc(4) groups, ($p < 0.0413$), indicating that shLuc expression was dysregulating Arc levels, leading to higher than normal levels of Arc mRNA.

These 7 viruses were infused into the BLA as described above and twenty one days later, the animals were auditory fear conditioned to a 30 sec, 5 kHz, 75 dB tone that co-terminated with a 1.5 mA foot shock. Three and twenty four hours following fear conditioning training, STM and LTM were assessed as described above, respectively. A significant overall effect was observed across groups in STM [$F_{(6,37)} = 7.841, p < 0.0001$; (GFP $n = 6$, shLuc(H1 Δ) $n = 6$, shArc(H1 Δ) n

= 7, shLuc n = 6, shArc n = 7, shLuc(4) n = 6, shArc(4) n = 6)](Figure 2.2G) and LTM [$F_{(6,37)} = 7.611, p < 0.0001$] (Figure 2.2H). For STM and LTM, animals that received viruses designed to express shRNAs (shArc, shArc(4), shLuc, and shLuc(4)) did not exhibit significantly different freezing levels, indicating that abnormalities in fear learning due to Arc gene knockdown could not be detected ($p > 0.1829$), but these groups exhibited significantly lower freezing levels as compared to the shArc(H1 Δ), shLuc(H1 Δ) and GFP groups ($p < 0.0034$). During STM, the shLuc(H1 Δ) group displayed significantly lower freezing to the tone, compared to the GFP and shArc(H1 Δ) groups ($p < 0.0463$), while, during LTM, the three groups did not differ among each other ($p > 0.5524$). Collectively, these experiments indicate that viral mediated shLuc expression interferes with fear conditioning and shLuc expression can lead to a dysregulation of Arc gene expression.

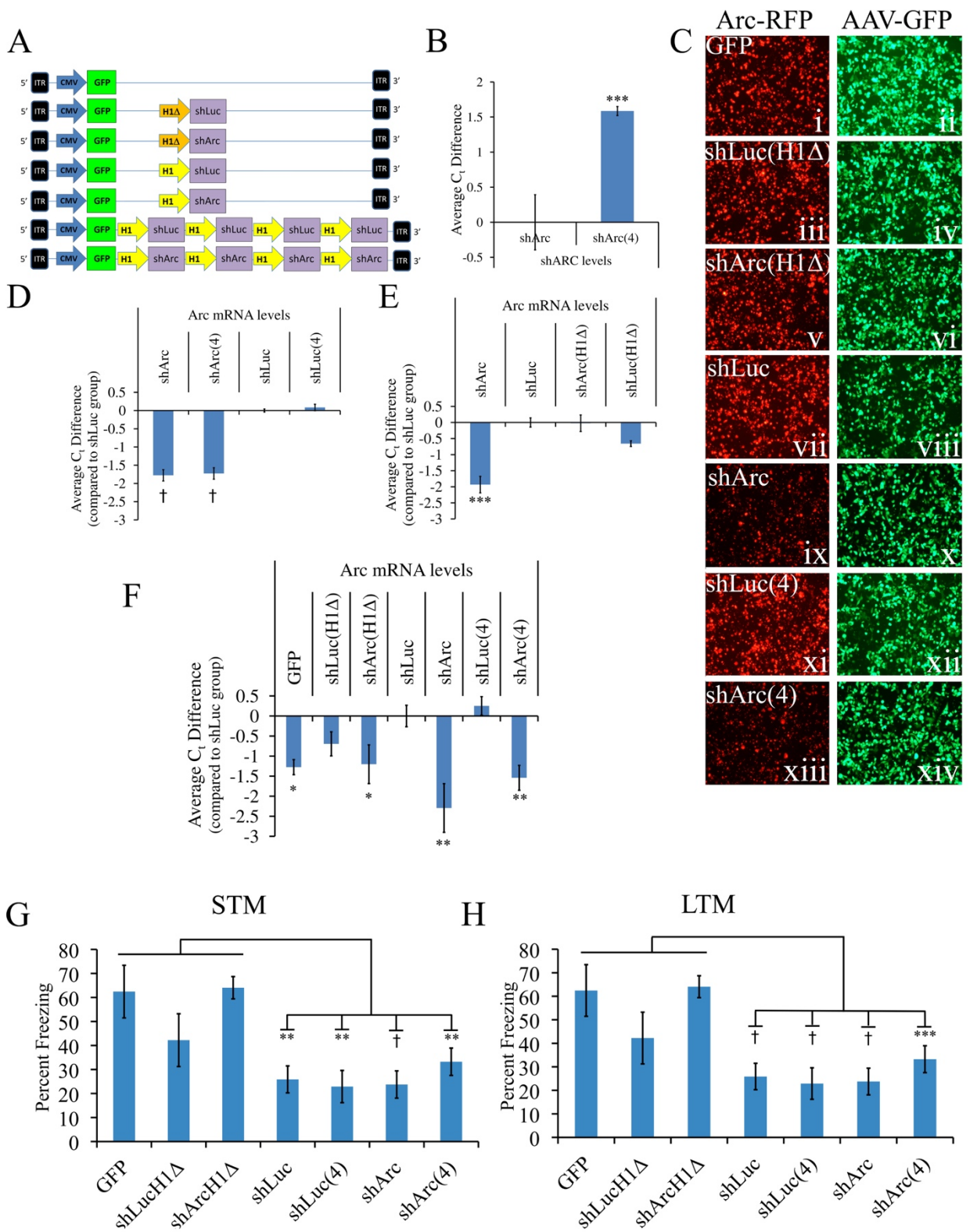


Figure 2.2 Viral mediated shRNA expression within the BLA interferes with fear conditioning and leads to dysregulation of gene expression

(A) AAV genome maps depicting viral genomes for viruses designed to: not express an shRNA (GFP only), contain shLuc or shArc with H1 promoter mutations (shArc(H1Δ), shLuc(H1Δ)), contain one copy of shLuc or shArc, or contain 4 copies of shLuc and shArc (shLuc(4), shArc(4)). (B) 293FT cells were transfected with plasmids designed to express AAV-shArc or AAV-shArc(4) and were harvested 48 hrs post-transfection to examine shArc RNA levels via qRT-PCR. AAV-shArc displayed less shRNA expression compared to shArc(4) ($p = 0.00164$). (C) 293FT cells were co-transfected with a plasmid designed to express Arc-RFP and the AAV viral plasmids depicted in A and these were imaged for GFP(ii, iv, vi, viii, x, xii, xiv) and Arc-RFP(i, iii, v, vii, ix, xi, xiii) 96 hrs post-transfection. An observable decrease in Arc-RFP signal is only observed in cells transfected with either shArc or shArc(4), as compared to all other groups. (D) 293FT cells were transfected with a plasmid designed to express Arc-RFP and either shArc, shArc(4), shLuc or shLuc(4) plasmids. Forty eight hrs post-transfection, the cells were harvested and Arc mRNA levels were assessed via qRT-PCR. ShArc and shArc(4) exhibited lower Arc mRNA levels compared to the shLuc and shLuc(4) groups ($p < 0.0001$). (E) A similar experiment was performed as described in D to compare Arc mRNA levels among the shArc, shLuc, shArc(H1Δ) and shLuc(H1Δ) groups. shArc displayed significantly lower levels of Arc mRNA compared to all other groups ($p < 0.002$). (F) Viruses for the above mentioned plasmids were generated and infused bilaterally into the BLA. Twenty one days post infusion, the brains were extracted and processed via LMD/qRT-PCR to examine Arc mRNA levels. (GFP $n = 5$, shLuc(H1Δ) $n = 5$, shArc(H1Δ) $n = 5$, shLuc $n = 6$, shArc $n = 6$, shLuc(4) $n = 6$, shArc(4) $n = 6$). A post hoc analysis revealed that the shArc and shArc(4) groups had lower levels of Arc mRNA, compared to the shLuc and shLuc(4) groups ($p < 0.0056$). The GFP, shArc(H1Δ) and shLuc(H1Δ) groups did not differ significantly from each other ($p > 0.2383$). The GFP and shArc(H1Δ) groups exhibited significantly lower levels of Arc mRNA compared to the shLuc and shLuc(4) groups, ($p < 0.0413$). *, ** indicates significance compared to shLuc group. (G) These viruses were again infused bilaterally into the BLA and animals were tested in Pavlovian fear containing 21 days post infusion (GFP $n = 6$, shLuc(H1Δ) $n = 6$, shArc(H1Δ) $n = 7$, shLuc $n = 6$, shArc $n = 7$, shLuc(4) $n = 6$, shArc(4) $n = 6$). Animals that received viral infusions of virus designed to express an shRNA (shLuc, shArc, shLuc(4) and shARC(4)) exhibited lower freezing levels during STM (G) and LTM testing (H) as compared to animals that received infusion of viruses not designed to express shRNAs (GFP only, shLuc(H1Δ), shArc(H1Δ)) ($p < 0.0031$). Error bars represent standard error of the mean (SEM) (* $p < 0.05$; ** $p < 0.01$; *** $p < 0.001$; † $p < 0.0001$).

Viral mediated delivery of shRNA to the BLA, dose dependently induces neurotoxicity and deficits in fear conditioning

In this next experiment, we aimed to determine if viral mediated delivery of shRNA to BLA neurons dose dependently interferes with fear conditioning. Animals were bilaterally infused

with differing doses of the shLuc virus, which spanned an order of magnitude (Low, 3.16E+12 GC/mL, Medium 1.0E+13 GC/mL, High 3.16E+13 GC/mL) or GFP virus (High 3.16E+13 GC/mL). Twenty one days post infusion, the animals were trained and tested in Pavlovian fear conditioning for STM and LTM as described above. An ANOVA revealed an overall significant effect for STM [$F_{(3,29)} = 3.981$, $p = 0.0172$; (GFP $n = 10$, shLuc-High $n = 6$, shLuc-Med $n = 8$, shLuc-Low $n = 9$)] (Figure 2.3B) and LTM [$F_{(3,29)} = 5.846$, $p = 0.0030$] (Figure 2.3C). Post-hoc analysis revealed that freezing levels between the Low, Medium and High dose groups, were significantly different compared to the GFP only group during the STM test ($p < 0.002$). Animals in the Medium and High dose groups froze significantly less, as compared to the GFP only group during LTM ($p < 0.0012$). Animals in the Low and Medium dose groups froze significantly more than the animals in the High groups during both the STM and LTM tests ($p < 0.0325$). Collectively, these data indicate viral mediated overexpression of shLuc, within neurons of the BLA, dose dependently interferes with fear conditioning. Notably, even the lowest dose of virus interfered with fear conditioning and this dose was 10 fold lower than the high dose.

Next, we examined coronal tissue slices within the area of viral infusion/transduction from animals that received the shLuc (Low, Med, High) and GFP only (High) viruses. There was no evidence that the infusion of viruses through the stereotaxically placed infusion needle or the virus itself created gross morphological damage or abnormalities within the BLA. In most cases, detecting where the infusion needle itself was placed was impossible and this is likely due to the fact that the needle itself is very small and it was only inserted into the BLA for a very short time. Because there was no evidence of gross abnormalities, we reasoned that there might be other anomalies that could be detected using immunohistochemistry (IHC). We performed IHC

for the microglia protein IBA1. An increase in IBA1 signal is an indication of microglia activation, which is routinely used as a marker to infer an ongoing inflammatory response. Coronal tissue slices containing the BLA transduced with either of the shLuc (Low, Med, High) and GFP only (High) groups were subjected to IBA1 IHC. The shLuc-High dose group exhibited an increase in the amount of IBA1 signal that was noticeably different compared to the shLuc-Medium, shLuc-Low and GFP only groups (Figure 2.3Ei-iv). Quantification of IHC for IBA1 revealed a significant difference of IBA1 staining [$F_{(3,20)} = 195.665$, $p < 0.0001$, (GFP n = 6, shLuc-High n = 6, shLuc-Med n = 6, shLuc-Low n = 6)], where the shLuc-High group exhibited significantly more IBA1 signal compared to the other groups ($p < 0.0001$). IBA1 staining for the shLuc-Low and shLuc-Medium groups was not different compared to the GFP only groups, despite the fact that the shLuc-Low and shLuc-Medium groups exhibited impairments in Pavlovian fear conditioning. These findings indicate that expression of shLuc can cause cellular dysfunction that is not necessarily associated with an inflammatory response.

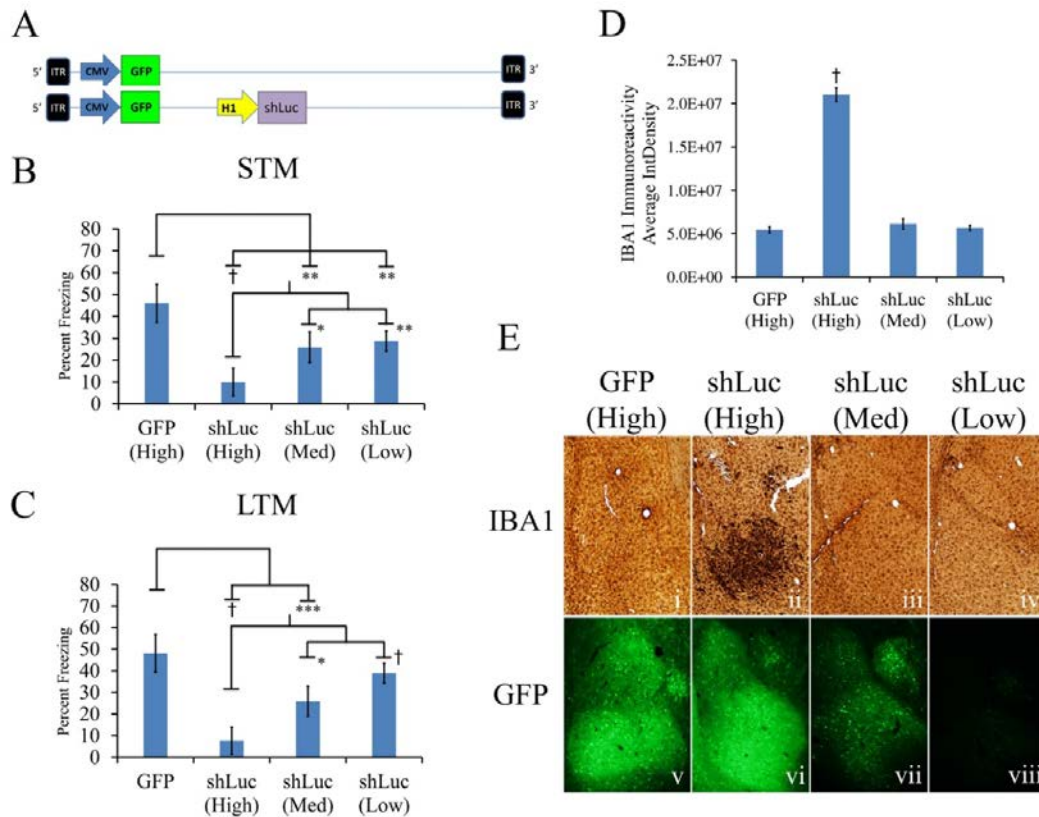


Figure 2.3 Viral mediated expression of shLuc within the BLA dose dependently interferes with Pavlovian fear conditioning and increases microglia activation

(A) AAV-shLuc virus was infused into the BLA at 3 different titers (High 3.16×10^{13} GC/mL; Med 1.0×10^{13} GC/mL; Low 3.16×10^{12} GC/mL) along with a group that was infused with a GFP only virus (High 3.16×10^{13} GC/mL) (GFP n = 10, shLuc-High n = 6, shLuc-Med n = 8, shLuc-Low n = 9). Twenty one days post infusion, animals were tested in Pavlovian fear conditioning. (B) During STM, lower freezing levels were observed in the High, Med and Low groups, as compared to the GFP group ($p < 0.002$). (C) During LTM, the High and Medium groups displayed lower freezing compared to the GFP group during LTM ($p < 0.0012$). (D) Animals were infused with the different doses of shLuc expressing virus and GFP only virus as described in A, and twenty one days later, the transduced tissue was subjected to IHC for IBA1 immunoreactivity to assess microglia activation (GFP n = 6, shLuc-High n = 6, shLuc-Med n = 6, shLuc-Low n = 6). Image analysis revealed tissue transduced with the high dose of shLuc virus exhibited increased IBA1 immunoreactivity as compared to all other groups ($p < 0.0001$). (E i-iv) Representative images for IBA1 IHC and GFP (E v-viii) for the experiment described in D. The shLuc High dose exhibits an obvious increase in IBA1 staining compared to the other doses and GFP only virus. Corresponding GFP reporter, exhibits dose dependent GFP fluorescence across the different doses of virus. Error bars represent standard error of the mean (SEM) (* $p < 0.05$; ** $p < 0.01$; *** $p < 0.001$; † $p < 0.0001$).

AAV naturally transduces neurons preferentially *in vivo*. To confirm that our viruses are predominantly transducing neurons *in vivo*, we performed IHC on BLA containing tissue that was transduced with the GFP only virus at the High titer, with the neuronal specific marker, NeuN (Figure 2.4Bi-iii). Quantification of the IHC revealed that 93.3% of the GFP expressing cells were also positive for NeuN expression (Figure 2.4A), indicating that, as expected, these viruses were predominantly transducing neurons. Collectively, because these viruses are predominately targeting neurons, and viruses that harbor shLuc, impair fear conditioning, these findings support the notion that viral mediated shLuc expression is causing damage to neurons and therefore it would be accurate to state that neuronal shLuc expression is causing neural toxicity. However there is no indication that shLuc expression is causing cell death, given that the gross tissue morphology appears normal.

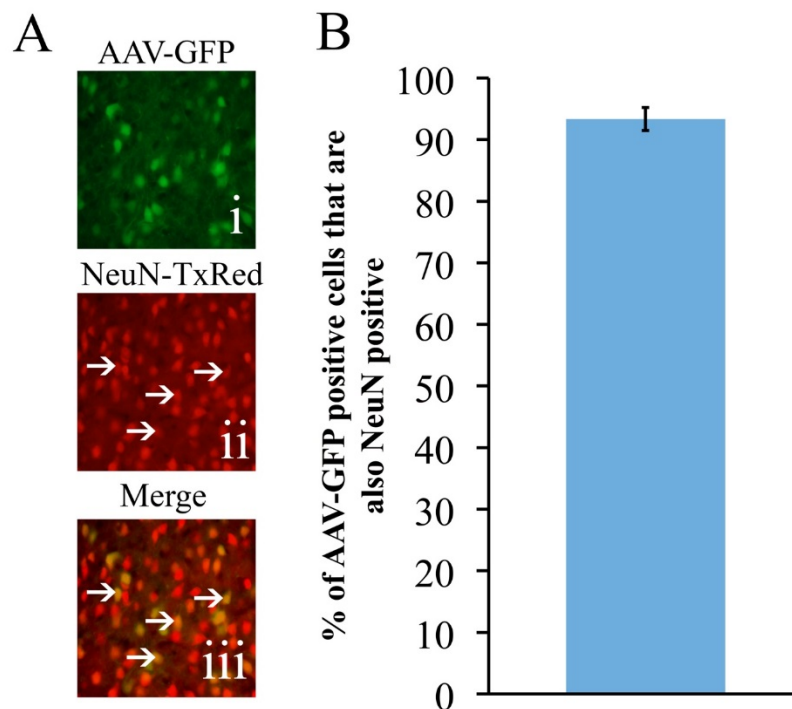


Figure 2.4 AAV2/DJ8 viruses predominantly transduce neurons when infused into the BLA
In this experiment, animals were infused with the GFP only virus into the BLA at a titer of $3.16E+13$ GC/mL. Twenty-one days post infusion, animals were sacrificed and tissue sections containing transduced amygdala were examined for NeuN IHC. (A i) Image depicting GFP expressing, virally transduced cells (A ii). Same field as depicted in (A i), but depicting NeuN IHC using a TxRed secondary antibody. (A iii) Depicts the merge of the AAV-GFP image and the NeuN-TxRed image. Arrows point to a subset of NeuN positive neurons that are also AAV-GFP positive. (B) Quantification revealed that 93.3% NeuN positive neurons were also AAV-GFP positive neurons ($n = 3$).

The experiments described thus far all utilized shLuc as a control. This control shRNA is designed to express an shRNA that is designed to not target any mRNA for degradation. However, it remains possible that there is something about the shLuc shRNA that is inherently toxic. Therefore, in our next experiment we examined another control shRNA that is not designed to target any mRNA for degradation and it is referred to here as shCntrl. In this experiment we bilaterally infused, into the BLA, the GFP only virus or the shCntrl virus at a titer of $3.16E+13$ GC/mL. We also included a third group of animals in this experiment that were subjected to stereotaxic surgery and had the infusion needle lowered into the BLA, but nothing was infused. This group is referred to as the Sham group and it serves as a control for how the GFP only virus may influence Pavlovian fear conditioning. Twenty-one days post infusion, the animals were fear conditioned and examined for cue induced freezing behavior during STM and LTM tests as described above. An ANOVA revealed an overall effect for STM [$F_{(2,20)} = 15.172$, $p = < 0.0001$; (Sham $n = 6$, GFP $n = 9$, shCntrl $n = 8$)], where the shCntrl group was freezing significantly less than the GFP only and Sham groups ($p < 0.0001$) (Figure 2.5C). An overall effect was observed for LTM [$F_{(2,20)} = 19.388$, $p < 0.0001$], where the shCntrl group was freezing significantly less than the GFP only and Sham groups ($p < 0.0001$) (Figure 2.5D). Freezing

levels did not differ between the Sham and GFP only groups during STM or LTM ($p > 0.1071$), indicating that the presence of the virus and the fluorescent protein expressed in BLA neurons does not influence Pavlovian fear conditioning.

Next, animals were bilaterally infused with the GFP only virus or the shCntrl virus at a titer of $3.16E+13$ GC/mL. In addition, a group of animals that received a sham surgery were also included. Twenty-one days post infusion, the animals were sacrificed and IHC for IBA1 was performed on coronal tissue slices that contained transduced BLA. BLA transduced with the shCntrl virus exhibited obvious IBA1 staining in comparison to the Sham and GFP groups, indicative that the shCntrl virus is neurotoxic and leads to microglia activation (Figure 2.5B). Collectively, these data indicate that shRNA overexpression induces neurotoxicity and leads to deficits in Pavlovian fear conditioning.

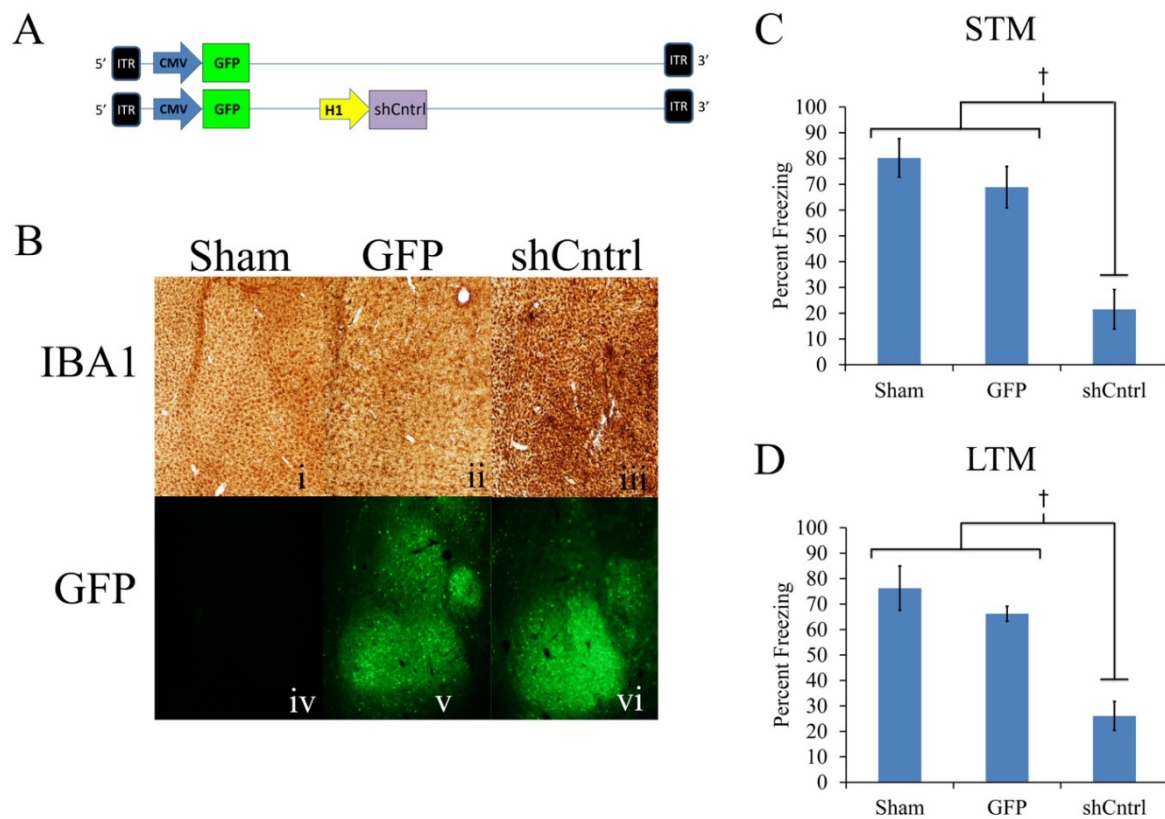


Figure 2.5 Viral mediated expression of shCntrl in BLA neurons induces deficits in fear conditioning and increases in microglia activation compared to GFP only, and Sham control groups

(A) An adeno-associated virus was designed to express a control shRNA (shCntrl) that was designed not to target any rat mRNA for degradation. This virus and the GFP only virus were bilaterally infused into the rat BLA at a titer of $3.16E+13$ GC/mL. A third group of animals was included that underwent surgery and the infusion needle was lowered into the BLA, but nothing was infused into the BLA (Sham). (B i-iii) Twenty one days post-surgery/infusion, the animals were perfused and BLA transduced tissue was examined for IBA1 IHC. An obvious increase in IBA1 immunoreactivity is apparent in the group that received the virus designed to express the shCntrl, but not in the GFP only or Sham groups. (B iv-vi) GFP reporter expression was similar between the GFP and shCntrl group, as expected. (C, D) Animals received either infusions of shCntrl, GFP only virus, or a sham surgery and were fear conditioned twenty one days post-surgery/infusion (Sham $n = 6$, GFP $n = 9$, shCntrl $n = 8$). Animals that received infusion of shCntrl virus exhibited significantly lower freezing levels during STM(C) and LTM (D), as compared to the GFP and Sham groups ($p < 0.0001$). Error bars represent standard error of the mean (SEM) ($\dagger p < 0.0001$).

Virally mediated shRNA induced depletion of GluN2A within BLA neurons impairs Pavlovian fear conditioning, as compared to the GFP only, shLuc, shArc and shEgr1 groups.

In the experiments depicted thus far, a significant difference in learning between the shLuc and shArc groups was not observed, and this is likely due to the fact that the toxicity induced by shRNA overexpression is masking the influence of gene specific knockdown on Pavlovian fear conditioning. Therefore, in our last set of experiments, we examined whether lowering the dose of virus further might result in decreased shRNA induced toxicity, so gene specific deficits in Pavlovian fear conditioning could be detected. We also examined how gene knockdown of Egr1 and GluN2A within BLA neurons might influence Pavlovian fear conditioning.

Viral plasmids were created to express shRNAs designed to target Egr1 and GluN2A. The shEgr1 was designed based on a previously reported algorithm (Reynolds *et al.*, 2004). To target GluN2A for depletion, we utilized an shRNA sequence (shGluN2A), that has previously been shown to be effective at lowering GluN2A levels within neurons (Kim *et al.*, 2005; Foster *et al.*, 2010). To measure the effectiveness of the shEgr1 viral plasmid *in vitro*, the AAV-shEgr1 and a control shRNA plasmid (AAV-shScram, previously described (Hommel *et al.*, 2003)), were co-transfected into 293FT cells with a plasmid that was designed to express Egr1 protein fused to RFP. Ninety six hours post transfection, the levels of RFP and GFP were examined via fluorescence microscopy. Each well contained similar levels of GFP, indicating that the transfection efficiency for each plasmid was similar among the samples (Figure 2.6Bii, iv). However, the levels of Egr1-RFP were lower in the cells that received shEgr1, compared to the cells that received shScram (Figure 2.6Bi, iii,) indicating that the shEgr1 was effective at

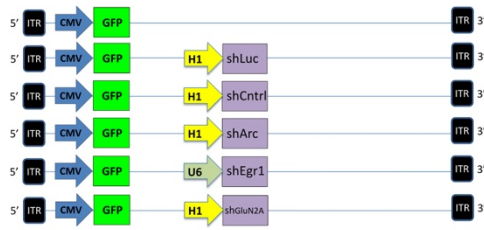
depleting Egr1-RFP levels, as intended. To quantitatively assess shEgr1 effectiveness, cells were treated in a similar manner as above, but they were harvested at forty eight hours post transfection, and Egr1 mRNA levels were assessed by qRT-PCR. Egr1 mRNA levels were found to be lower in cells that received shEgr1, versus cells that received shScram (Figure 2.6C). To measure the effectiveness of the shGluN2A viral plasmid *in vitro*, the AAV-shGluN2A and shLuc were co-transfected into 293FT cells with a plasmid that was designed to express GluN2A protein fused to a GFP. Forty eight hours post transfection, and GluN2A mRNA levels were assessed by qRT-PCR. GluN2A mRNA levels were found to be lower in cells that received shGluN2A versus cells that received shLuc [$t_{(4)} =$, $p = 0.0107$] (Figure 2.6D).

Next, we created adeno-associated viruses with the viral shEgr1 and shGluN2A plasmids, pseudotyped as AAV2/DJ8, and infused these viruses, along with GFP only, shLuc, shCntrl, and shArc viruses bilaterally into the BLA at a titer of $1.60E+12$ GC/mL. This dose of virus is ~20 times lower than the High dose of virus used in previous experiments. Twenty one days post infusion, the animals were sacrificed, and the brains were removed and processed via LMD/qRT-PCR to examine Arc, Egr1 and GluN2A mRNA levels within the BLA (GFP n = 6, shLuc n = 6, shCntrl n = 6, shArc n = 6, shEgr1 n = 8, shGluN2A n = 6). Surprisingly, there was no significant difference in Arc mRNA levels among the groups [$F_{(5,31)} = 1.317$, $p = 0.2828$] (Figure 2.6E). There was, however, a significant difference among the groups for Egr1 mRNA levels [$F_{(5,31)} = 3.282$, $p = 0.0171$] (Figure 2.6F). A post hoc analysis revealed Egr1 mRNA levels were significantly lower in the shEgr1 group compared to the GFP, shLuc, shArc, and shGluN2A groups ($p < 0.0087$), however, Egr1 mRNA levels in the shEgr1 group were not significantly lowered, as compared to the shCntrl group, however, there was a trend ($p = 0.0511$). When we

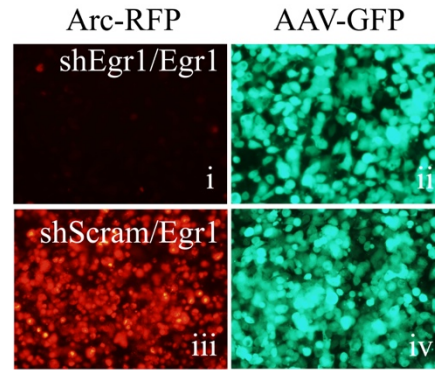
examined GluN2A mRNA levels, we found a significant difference among the groups [$F_{(5,31)} = 6.650$, $p = 0.0003$](Figure 2.6G). A post hoc analysis revealed that GluN2A mRNA levels were significantly different among the shGluN2A group as compared all other groups ($p < 0.0029$).

Next, these 6 viruses were infused into the BLA and twenty one days post infusion, animals were auditory fear conditioned, and cue induced freezing was examined during STM and LTM tests, as described above. A significant difference was not observed among the groups for STM [$F_{(5,34)} = 2.162$, $p = 0.0816$; (GFP $n = 6$, shLuc $n = 7$, shCntrl $n = 7$, shArc $n = 7$, Egr1 $n = 7$, shGluN2A $n = 6$)](Figure 2.6H). However, for LTM, there was a significant difference among the groups [$F_{(5,34)} = 2.573$, $p = 0.0445$] (Figure 2.6I). For LTM, a post hoc analysis revealed that each group that received virus designed to express shRNA exhibited significantly lower freezing levels as compared to the group that received virus that was not designed to express shRNA, (GFP only) ($p < 0.0021$). The shArc, shEgr1, shLuc and shCntrl groups did not differ significantly indicating that gene specific influences on learning and memory could not be detected, under these circumstances for Egr1 or Arc ($p > 0.4235$). The shGluN2A group froze significantly less than the GFP only, shLuc, shArc, and shEgr1 groups ($p < 0.0195$). The shCntrl and shGluN2A group did not significantly differ from each other, however there was a trend ($p = 0.0890$). Collectively, these data indicate that it is possible to detect learning deficits induced by targeting specific mRNAs utilizing viral mediated shRNA delivery, but this may be restricted to situations when highly potent shRNAs are utilized.

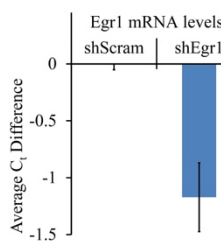
A



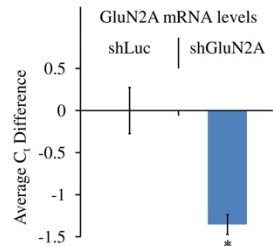
B



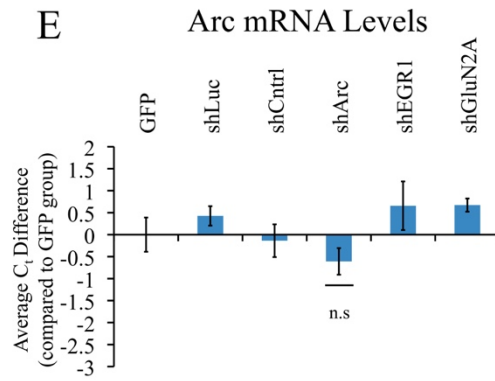
C



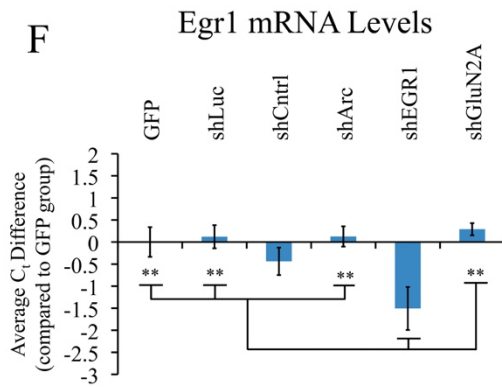
D



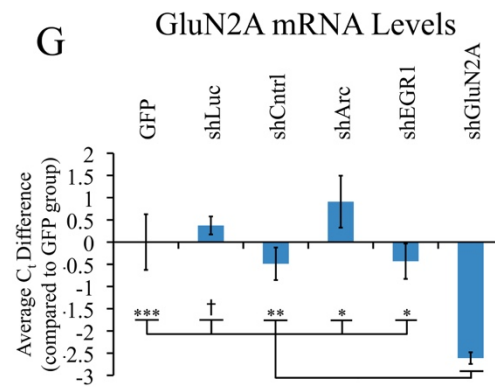
E



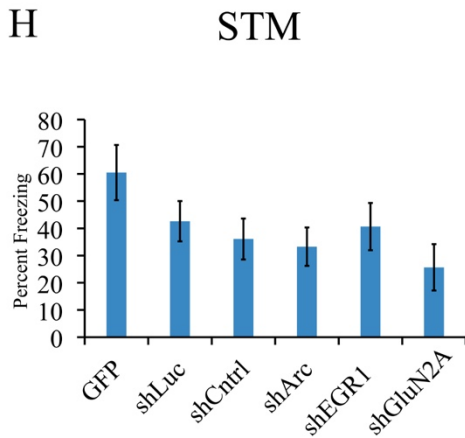
F



G



H



I

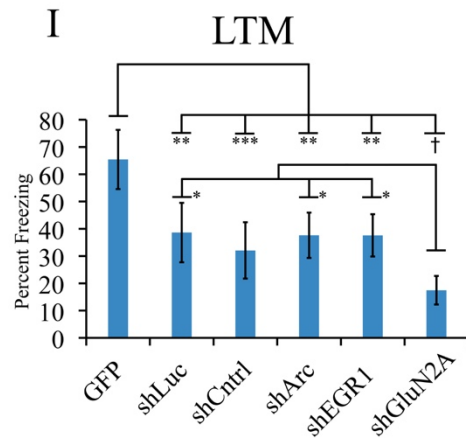


Figure 2.6 Virally mediated RNAi induced depletion of GluN2A within BLA neurons impairs Pavlovian fear conditioning, as compared to the GFP only, shLuc, shArc and shEgr1 groups

(A) AAV genome maps depicting viral genomes for viruses designed to express GFP only, or in addition, one of the following shRNAs expression cassettes: shLuc, shCntrl, shArc, shEgr1, shGluN2A. (B i-iv) 293FT cells were co-transfected with plasmids designed to express Egr1-RFP and shEgr1 (i, ii) or Egr1-RFP and shScram (iii, iv) and were imaged for GFP(ii, iv) and Egr1-RFP(i, iii) 96 hrs post-transfection. AAV-shEgr1 causes an observable decrease in Egr1-RFP signal compared to AAV-shScram (i vs. iii). (C) 293FT cells were treated in a similar manner as in B, but they were harvested 48 hrs post-transfection and used to assess Egr1 mRNA levels via qRT-PCR. Cells transfected with AAV-shEgr1 exhibited a decrease in Egr1 mRNA levels compared to cells that received AAV-shScram. (D) 293FT cells were co-transfected with plasmids designed to express GluN2A and shGluN2A or GluN2A and shLuc. Forty eight hours later, cells were harvested and GluN2A mRNA levels were measured by qRT-PCR. GluN2A mRNA levels were significantly lower in cells transfected with AAV-shGluN2A as compared to cells transfected with AAV-shLuc ($p = 0.0107$). (E-G) Viruses from the above mentioned AAV plasmids were generated and infused bilaterally into the BLA at a titer of $1.60E+12$ GC/mL. Twenty one days post infusion, the brains were extracted and processed via LMD/qRT-PCR to examine Arc, Egr1 and GluN2A mRNA levels. (GFP $n = 6$, shLuc $n = 6$, shCntrl $n = 6$, shArc $n = 6$, shEgr1 $n = 8$, shGluN2A $n = 6$). (E) Arc mRNA levels were relatively the same across all groups and were not significant across groups. (F) Egr1 mRNA levels were significantly lower in the shEgr1 group, compared to the GFP, shLuc, shArc, and shGluN2A groups ($p < 0.0087$), however, Egr1 levels were not significantly different from levels in the shCntrl group, there was a trend ($p = 0.0511$). (G) GluN2A mRNA levels were significantly lower compared to all other shRNA groups ($p < 0.0029$). Interestingly, GluN2A mRNA levels were significantly higher in the shArc group, compared to the shCntrl and shEgr1 group ($p < 0.0329$). (H-I) These viruses were infused into the BLA as described above and animals were fear conditioned twenty one days post infusion (GFP $n = 6$, shLuc $n = 7$, shCntrl $n = 7$, shArc $n = 7$, Egr1 $n = 7$, shGluN2A $n = 6$). (H) For STM, an ANOVA indicated there was not a significant difference in freezing levels between the groups. (I) For LTM, freezing levels were significantly lower in all shRNA groups compared to the GFP group ($p < 0.0021$). The shArc, shEgr1, shLuc and shCntrl groups did not differ significantly ($p > 0.4235$). The shGluN2A group froze significantly less than the GFP only, shLuc, shArc, and shEgr1 groups ($p < 0.0195$). The shCntrl and shGluN2A group did not significantly differ from each other, however there was a trend ($p = 0.0890$). Error bars represent standard error of the mean (SEM)(* $p < 0.05$; ** $p < 0.01$; *** $p < 0.001$; † $p < 0.0001$).

To determine if there was an observable difference in the intensity of GFP reporter signal and number of neurons fluorescing across the different doses of AAV virus used in these experiments, we imaged brain tissue sections that were transduced with shLuc virus at various titers. We infused shLuc virus bilaterally into the BLA at 4 different titers (High $3.16E+13$

GC/mL, Medium $1.0E+13$ GC/mL, Low $3.16E+12$ GC/mL, and Extra Low ($1.6E+12$ GC/mL). Twenty one days post infusion, the animals were perfused and the brains were sectioned within the coronal plane. In addition, tissue sections that contained no virus (naïve) were used as a comparison. Imaging of GFP fluorescence in the BLA was performed at 4 different exposure times, in which each exposure time is optimal for one of the specific viral titers (Figure 2.7A). These images were used to evaluate cellular detail by magnifying the existing image (Figure 2.7B). There was an observable decrease in amount of cells fluorescing and overall GFP fluorescence as the dose of virus is decreased. These data demonstrate that lowering the titer of AAV virus infused will result in less neurons transduced and an overall decrease in GFP, thus, indicating that this technology may be less effective at lower titers.

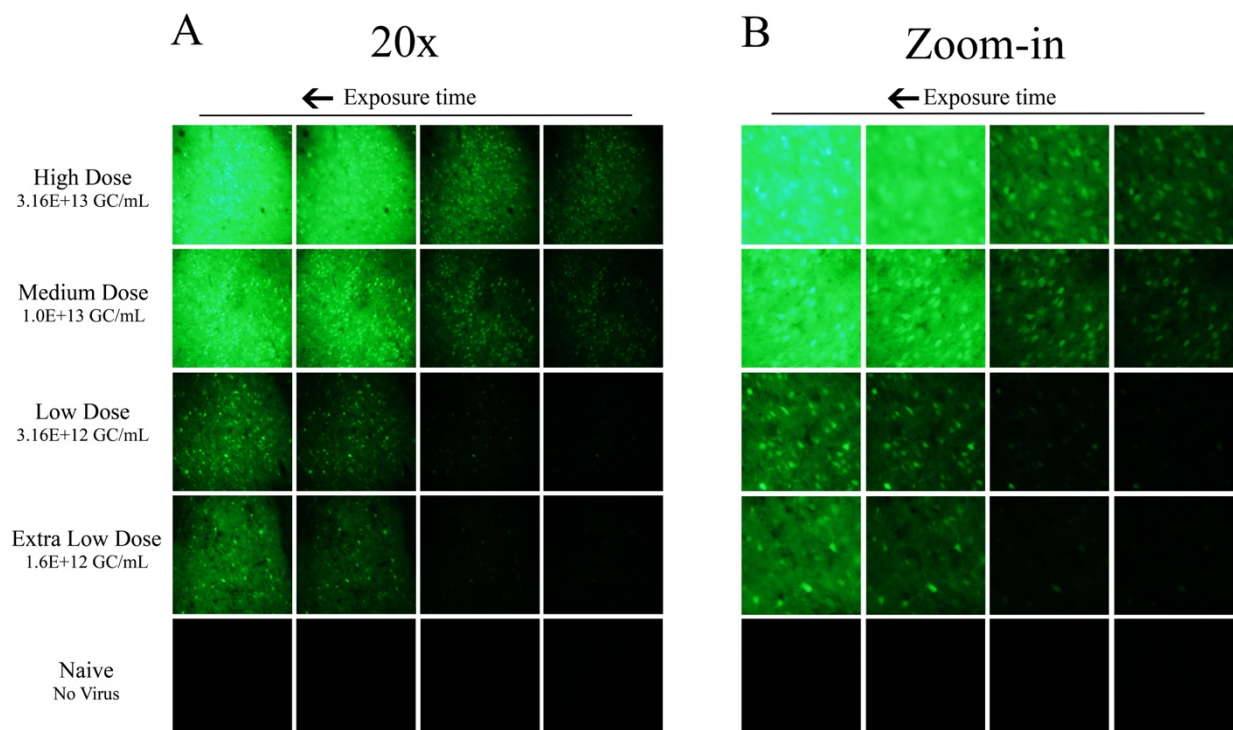


Figure 2.7 Lowering the titer of AAV virus infused, will result in less neurons transduced and an overall decrease in GFP expression.

We imaged tissue sections containing transduced BLA that were infused with virus at either of the 4 titers used in these experiments (High $3.16E+13$ GC/mL, Medium $1.0E+13$ GC/mL, Low $3.16E+12$ GC/mL, and Extra Low $1.6E+12$ GC/mL). Each group was imaged at 4 different exposure times; each exposure time is optimal for one of the 4 titers. Tissue sections were imaged at (A) 20x, in addition, we include a (B) magnified view of this image to visualize cellular detail of the transduced neurons.

Discussion

Here we report that viral mediated delivery of shRNA to rat neurons *in vivo* is toxic and impairs auditory Pavlovian fear conditioning. These findings were not due to surgery, the virus or GFP expression, but rather they were due to shRNA expression. ShRNAs delivered to BLA neurons, using varying doses of virus, induced highly reproducible deficits in Pavlovian fear conditioning, even at the lowest dose tested, which was ~20 times lower than the highest dose we examined. These findings were surprising, considering the widespread *in vivo* use of viral mediated delivery of shRNA in the behavioral neuroscience field. However, despite its consistent use, it is well established that viral mediated delivery of shRNA can be toxic to cells (Grimm, 2011), including neurons (McBride *et al.*, 2008; Boudreau *et al.*, 2009; Ulusoy *et al.*, 2009; Ehlert *et al.*, 2010; Khodr *et al.*, 2011; Martin *et al.*, 2011). This is the first report that a common learning and memory paradigm was adversely influenced by viral mediated delivery of shRNA.

Gene knockdown approaches that utilize viral mediated delivery of shRNA are attractive because they can be implemented quickly and delivered in a spatially and temporally restricted manner to the CNS of numerous model organisms. However, unlike conventional mouse and rat knockouts that are designed to have every cell or cell type genetically manipulated within the organism, viral mediated delivery of shRNA does not necessarily target every cell or neuron

within a brain region. This is because the number of cells the virus transduces is dependent on how efficiently the virus transduces the cell type/brain region, and the concentration and volume of the virus administered. In practice, not every cell is transduced by virus and some cells are transduced by multiple viruses, thus, delivering many copies of the viral transgene to the cell, and as the dose of virus is lowered, fewer cells are transduced. It would be ideal to be able to target every neuron within a specific brain region since the odds of targeting neurons relevant to the behavior would increase as the number of genetically modified neurons increased within the targeted brain region. This is because not every neuron within a brain region would likely contribute to a specific behavior. As a greater number of neurons within a brain region are targeted and genetically manipulated, a greater augmentation of behavior would be expected, and this could lead to more robust and reproducible findings. Unfortunately, our findings and findings from others indicate that viral mediated delivery of shRNA can be toxic to neurons, which of course can limit one's ability to use this technology in a manner that would allow the targeting of every neuron within the target region. For example, McBride and colleagues previously raised the concern that using doses of virus that transduced most of the neurons within a brain region resulted in shRNA induced toxicity, and doses of virus that did not exhibit shRNA induced toxicity transduced significantly less neurons within the target region, therefore limiting its utility (McBride *et al.*, 2008). However, this prior study solely utilized microglia activation as a marker of toxicity. We found that there was likely neuronal toxicity induced at viral doses that did not necessarily lead to microglia activation, since deficits in Pavlovian conditioning were detected when these lower doses were used. Therefore, lowering the dose of virus may not only lead to transducing less cells, but it also may not completely alleviate the

shRNA induced toxicity. But our data clearly indicate that the amount of virus infused into the CNS needs to be chosen wisely, because infusing too much of a virus that harbors an shRNA expression cassette can cause toxicity and too little may not be effective at knocking down the gene of interest or producing a gene specific behavioral impairment.

All shRNAs are not equally effective at depleting the gene products that they are intended to. Because of this, we specifically chose to work with shArc and shGluN2A, because these shRNAs have been previously reported to very effective at knocking down these gene products in neurons. Across experiments that utilized shLuc and shArc, we found Arc knockdown was dependent on the dose of virus used. For example, the greatest difference in Arc levels between the shLuc and shArc groups occurred when the High dose was utilized. We observed a moderate degree of Arc knockdown at the Medium dose. At the lowest dose of virus, we did not detect a significant difference in Arc levels between the shLuc and shArc groups. However, the fact that shLuc expression alone led to increases in levels of Arc as compared to the GFP only group, complicates these findings. Short-hairpins designed to target Egr1 and GluN2A were effective at knocking down these gene products at the lowest dose of virus utilized. Despite gene knockdown across numerous experiments that utilized differing doses of virus, we were never able to detect a difference in fear conditioning among the shLuc, shCntrl, shArc and shEgr1 groups. We suspect that this might be due the fact that shRNA induced toxicity may be masking a subtle impairment in fear conditioning that might be due to gene specific knockdown. For example, mouse knockouts of both Arc and Egr1 exhibit deficits in Pavlovian fear conditioning, but in both of these cases, these deficits are small (Jones *et al.*, 2001; Plath *et al.*, 2006). We found that knockdown of GluN2A exhibited significantly lower freezing levels during the LTM

test, as compared to all the groups examined, except shCntrl (trend $p = 0.0890$), indicating that, despite shRNA induced toxicity, gene specific deficits in fear conditioning could be observed utilizing viral mediated delivery of shRNA.

Considering that shRNA overexpression can induce neuronal toxicity, potential “gene specific” findings obtained using this technology might not be physiologically relevant, since they may be a byproduct of, or in response to, ongoing neuronal dysfunction. Also, shRNA induced neuronal toxicity is not isolated to the viral delivery approach. A recent study reported that shRNA delivered to cortical neurons via *in vivo* electroporation resulted in a non-specific deficit in neural migration (Baek *et al.*, 2014). Collectively, these results also raise concerns regarding the use of shRNA in primary neurons grown in culture or in organotypic slice cultures. ShRNA is frequently delivered to primary neurons grown in culture or in organotypic slice cultures using a variety of approaches, (i.e. lipofection, viral transduction, gene guns, and electroporation) and, therefore, observations made from such studies need to be carefully interpreted with proper controls, especially since it is difficult to accurately titrate the amount of shRNA that is delivered to each neuron.

It is currently believed that shRNA induced cellular toxicity is due at least in part, to the shRNAs interfering with the endogenous cellular microRNA (miRNA) pathways (Grimm *et al.*, 2006; Grimm *et al.*, 2010; Grimm, 2011; Baek *et al.*, 2014). For example when highly potent AAVs harboring shRNAs were intravenously administered to mice, they were found to cause hepatocellular toxicity and in some cases, caused death. AAV mediated shRNA over-expression was found to interfere with the processing of endogenous miRNAs, leading to lower levels of mature miRNAs, and this was believed to occur in part due to a saturation of exportin-5

mediated nuclear export of the shRNA/miRNAs (Grimm *et al.*, 2006). More recently similar findings that endogenous miRNA levels are dysregulated by AAV mediated shRNA overexpression within the rat brain were found, and the severity of the miRNA dysregulation increased over time (van Gestel *et al.*, 2014). Notably the use of siRNAs, which are frequently used in cell culture systems, do not interfere with miRNA export, since they begin their cellular processing at a later stage of this pathway; however, off target effects can still be a problem with siRNAs (Fedorov *et al.*, 2006).

Despite the fact that the *in vivo* use of shRNAs can be toxic, there may be possible ways to mitigate these issues and successfully use this technology *in vivo*. For example embedding the sense and antisense portions of the shRNA into a miRNA scaffold creating an artificial miRNA can alleviate some of the toxicity associated with conventional shRNAs (McBride *et al.*, 2008). Additionally reducing the overall expression of shRNAs within the cell could significantly reduce the shRNA induced toxicity, by preventing the oversaturation of the endogenous miRNA pathways. This could be achieved using weaker promoters to drive shRNA expression by opting to use RNA polymerase II based promoters instead of the strong U6 and H1 RNA polymerase III promoters that are typically used or by mutating the existing U6 and H1 promoters to reduce their ability to drive transcription (Giering *et al.*, 2008). Alternatively administering less viral particles or opting to use a viral serotype with reduced cellular transduction ability, could reduce the shRNA induced toxicity; however, as stated above, these two methods would sacrifice the number of cells likely transduced *in vivo*. Lastly performing behavioral analysis at early time points following viral infusion could limit the adverse influence of shRNA induced toxicity, since miRNA dysregulation appears to get worse with increasing duration of shRNA

overexpression (van Gestel *et al.*, 2014). Since there can be large differences in viral transduction efficiency that exist across types of viruses and serotypes of viruses (Holehonnur *et al.*, 2014), differences in potency of the shRNA or artificial miRNA used (Knott *et al.*, 2014), and differences in the half-life of protein products that are intended to be depleted, the exact experimental conditions for viral based shRNA delivery that will achieve the best results likely need to be empirically determined for individual cases.

In conclusion, we believe that the use of shRNAs in behavioral neuroscience warrants careful consideration and careful study design. Unfortunately there are a large number of variables that will influence the success of these types of experiments since ectopic expression of shRNAs can induce neurotoxicity.

References

- Althage, M.C., Ford, E.L., Wang, S., Tso, P., Polonsky, K.S. & Wice, B.M. (2008) Targeted ablation of glucose-dependent insulintropic polypeptide-producing cells in transgenic mice reduces obesity and insulin resistance induced by a high fat diet. *J Biol Chem*, 283, 18365-18376.
- Baek, S.T., Kerjan, G., Bielas, S.L., Lee, J.E., Fenstermaker, A.G., Novarino, G. & Gleeson, J.G. (2014) Off-target effect of doublecortin family shRNA on neuronal migration associated with endogenous microRNA dysregulation. *Neuron*, 82, 1255-1262.
- Banerjee, A., Engineer, C.T., Sauls, B.L., Morales, A.A., Kilgard, M.P. & Ploski, J.E. (2014) Abnormal emotional learning in a rat model of autism exposed to valproic acid in utero. *Front Behav Neurosci*, 8, 387.
- Barria, A. & Malinow, R. (2002) Subunit-specific NMDA receptor trafficking to synapses. *Neuron*, 35, 345-353.
- Barria, A. & Malinow, R. (2005) NMDA receptor subunit composition controls synaptic plasticity by regulating binding to CaMKII. *Neuron*, 48, 289-301.
- Boudreau, R., Martins, I. & Davidson, B. (2009) Artificial microRNAs as siRNA shuttles: improved safety as compared to shRNAs in vitro and in vivo. *Mol Ther*, 17, 169 - 175.
- Capecchi, M.R. (2005) Gene targeting in mice: functional analysis of the mammalian genome for the twenty-first century. *Nat Rev Genet*, 6, 507-512.
- Ehlert, E.M., Eggers, R., Niclou, S.P. & Verhaagen, J. (2010) Cellular toxicity following application of adeno-associated viral vector-mediated RNA interference in the nervous system. *BMC Neurosci*, 11, 20.
- Fedorov, Y., Anderson, E.M., Birmingham, A., Reynolds, A., Karpilow, J., Robinson, K., Leake, D., Marshall, W.S. & Khvorova, A. (2006) Off-target effects by siRNA can induce toxic phenotype. *RNA*, 12, 1188-1196.
- Foster, K.A., McLaughlin, N., Edbauer, D., Phillips, M., Bolton, A., Constantine-Paton, M. & Sheng, M. (2010) Distinct roles of NR2A and NR2B cytoplasmic tails in long-term potentiation. *J Neurosci*, 30, 2676-2685.
- Giering, J.C., Grimm, D., Storm, T.A. & Kay, M.A. (2008) Expression of shRNA from a tissue-specific pol II promoter is an effective and safe RNAi therapeutic. *Mol Ther*, 16, 1630-1636.

- Grimm, D. (2011) The dose can make the poison: lessons learned from adverse in vivo toxicities caused by RNAi overexpression. *Silence*, 2, 8.
- Grimm, D., Streetz, K., Jopling, C., Storm, T., Pandey, K., Davis, C., Marion, P., Salazar, F. & Kay, M. (2006) Fatality in mice due to oversaturation of cellular microRNA/short hairpin RNA pathways. *Nature*, 441, 537 - 541.
- Grimm, D., Wang, L., Lee, J., Schurmann, N., Gu, S., Borner, K., Storm, T. & Kay, M. (2010) Argonaute proteins are key determinants of RNAi efficacy, toxicity, and persistence in the adult mouse liver. *J Clin Invest*, 120, 3106 - 3119.
- Holehonnur, R., Luong, J.A., Chaturvedi, D., Ho, A., Lella, S.K., Hosek, M.P. & Ploski, J.E. (2014) Adeno-associated viral serotypes produce differing titers and differentially transduce neurons within the rat basal and lateral amygdala. *BMC Neurosci*, 15, 28.
- Hommel, J.D., Sears, R.M., Georgescu, D., Simmons, D.L. & DiLeone, R.J. (2003) Local gene knockdown in the brain using viral-mediated RNA interference. *Nat Med*, 9, 1539-1544.
- Hung, A.Y., Sung, C.C., Brito, I.L. & Sheng, M. (2010) Degradation of postsynaptic scaffold GKAP and regulation of dendritic spine morphology by the TRIM3 ubiquitin ligase in rat hippocampal neurons. *PLoS One*, 5, e9842.
- Jones, M.W., Errington, M.L., French, P.J., Fine, A., Bliss, T.V., Garel, S., Charnay, P., Bozon, B., Laroche, S. & Davis, S. (2001) A requirement for the immediate early gene *Zif268* in the expression of late LTP and long-term memories. *Nat Neurosci*, 4, 289-296.
- Khodr, C., Sapru, M., Pedapati, J., Han, Y., West, N., Kells, A., Bankiewicz, K. & Bohn, M. (2011) An alpha-synuclein AAV gene silencing vector ameliorates a behavioral deficit in a rat model of Parkinson's disease, but displays toxicity in dopamine neurons. *Brain Res*, 1395, 94 - 107.
- Kim, M.J., Dunah, A.W., Wang, Y.T. & Sheng, M. (2005) Differential roles of NR2A- and NR2B-containing NMDA receptors in Ras-ERK signaling and AMPA receptor trafficking. *Neuron*, 46, 745-760.
- Knott, S.R., Maceli, A.R., Erard, N., Chang, K., Marran, K., Zhou, X., Gordon, A., El Demerdash, O., Wagenblast, E., Kim, S., Fellmann, C. & Hannon, G.J. (2014) A computational algorithm to predict shRNA potency. *Molecular cell*, 56, 796-807.
- Maddox, S.A., Monsey, M.S. & Schafe, G.E. (2011) Early growth response gene 1 (Egr-1) is required for new and reactivated fear memories in the lateral amygdala. *Learn Mem*, 18, 24-38.

Martin, J., Wolken, N., Brown, T., Dauer, W., Ehrlich, M. & Gonzalez-Alegre, P. (2011) Lethal toxicity caused by expression of shRNA in the mouse striatum: implications for therapeutic design. *Gene Ther*, 18, 666 - 673.

McBride, J., Boudreau, R., Harper, S., Staber, P., Monteys, A., Martins, I., Gilmore, B., Burstein, H., Peluso, R., Polisky, B., Carter, B. & Davidson, B. (2008) Artificial miRNAs mitigate shRNA-mediated toxicity in the brain: implications for the therapeutic development of RNAi. *Proc Natl Acad Sci USA*, 105, 5868 - 5873.

Myslinski, E., Ame, J.C., Krol, A. & Carbon, P. (2001) An unusually compact external promoter for RNA polymerase III transcription of the human H1RNA gene. *Nucleic Acids Res*, 29, 2502-2509.

Partin, A.C., Hosek, M.P., Luong, J.A., Lella, S.K., Sharma, S.A. & Ploski, J.E. (2013) Amygdala nuclei critical for emotional learning exhibit unique gene expression patterns. *Neurobiol Learn Mem*, 104, 110-121.

Plath, N., Ohana, O., Dammermann, B., Errington, M.L., Schmitz, D., Gross, C., Mao, X., Engelsberg, A., Mahlke, C., Welzl, H., Kobalz, U., Stawrakakis, A., Fernandez, E., Waltereit, R., Bick-Sander, A., Therstappen, E., Cooke, S.F., Blanquet, V., Wurst, W., Salmen, B., Bosl, M.R., Lipp, H.P., Grant, S.G., Bliss, T.V., Wolfer, D.P. & Kuhl, D. (2006) Arc/Arg3.1 is essential for the consolidation of synaptic plasticity and memories. *Neuron*, 52, 437-444.

Ploski, J.E., Monsey, M.S., Nguyen, T., DiLeone, R.J. & Schafe, G.E. (2011) The neuronal PAS domain protein 4 (Npas4) is required for new and reactivated fear memories. *PLoS One*, 6, e23760.

Ploski, J.E., Newton, S.S. & Duman, R.S. (2006) Electroconvulsive seizure-induced gene expression profile of the hippocampus dentate gyrus granule cell layer. *J Neurochem*, 99, 1122-1132.

Ploski, J.E., Park, K.W., Ping, J., Monsey, M.S. & Schafe, G.E. (2010) Identification of plasticity-associated genes regulated by Pavlovian fear conditioning in the lateral amygdala. *J Neurochem*, 112, 636-650.

Ploski, J.E., Pierre, V.J., Smucny, J., Park, K., Monsey, M.S., Overeem, K.A. & Schafe, G.E. (2008) The activity-regulated cytoskeletal-associated protein (Arc/Arg3.1) is required for memory consolidation of pavlovian fear conditioning in the lateral amygdala. *J Neurosci*, 28, 12383-12395.

Reynolds, A., Leake, D., Boese, Q., Scaringe, S., Marshall, W.S. & Khvorova, A. (2004) Rational siRNA design for RNA interference. *Nat Biotechnol*, 22, 326-330.

Rial Verde, E.M., Lee-Osbourne, J., Worley, P.F., Malinow, R. & Cline, H.T. (2006) Increased expression of the immediate-early gene *arc/arg3.1* reduces AMPA receptor-mediated synaptic transmission. *Neuron*, 52, 461-474.

Ulusoy, A., Sahin, G., Bjorklund, T., Aebischer, P. & Kirik, D. (2009) Dose optimization for long-term rAAV-mediated RNA interference in the nigrostriatal projection neurons. *Mol Ther*, 17, 1574 - 1584.

van Gestel, M.A., van Erp, S., Sanders, L.E., Brans, M.A., Luijendijk, M.C., Merkestein, M., Pasterkamp, R.J. & Adan, R.A. (2014) shRNA-induced saturation of the microRNA pathway in the rat brain. *Gene Ther*, 21, 205-211.

Walker, D.L. & Davis, M. (2008) Amygdala infusions of an NR2B-selective or an NR2A-preferring NMDA receptor antagonist differentially influence fear conditioning and expression in the fear-potentiated startle test. *Learn Mem*, 15, 67-74.

Waung, M.W., Pfeiffer, B.E., Nosyreva, E.D., Ronesi, J.A. & Huber, K.M. (2008) Rapid translation of *Arc/Arg3.1* selectively mediates mGluR-dependent LTD through persistent increases in AMPAR endocytosis rate. *Neuron*, 59, 84-97.

CHAPTER 3

A VIRAL MEDIATED CRISPR/CAS9 SYSTEM WITH DOXYCYCLINE DEPENDENT GRNA EXPRESSION FOR INDUCIBLE IN VITRO AND IN VIVO GENOME EDITING

Authors: Christopher A. de Solis, Anthony Ho, Roopashri Holehonnur, Jonathan E. Ploski

School of Behavioral and Brain Sciences

The University of Texas at Dallas

800 West Campbell Road

Richardson, TX 75080-3021, USA

*Reprinted with permission from *Frontiers: Frontiers in Molecular Neuroscience*, Volume 289, August 2016.

The Development of a Viral Mediated CRISPR/Cas9 System with Doxycycline Dependent gRNA Expression for Inducible In vitro and In vivo Genome Editing

Christopher A. de Solis, Anthony Ho, Roopashri Holehonnur, Jonathan E. Ploski

Frontiers in Molecular Neuroscience, 2016; doi: <https://doi.org/10.3389/fnmol.2016.00070>

Abstract

The RNA-guided Cas9 nuclease, from the type II prokaryotic Clustered Regularly Interspersed Short Palindromic Repeats (CRISPR) adaptive immune system, has been adapted and utilized by scientists to edit the genomes of eukaryotic cells. Here, we report the development of a viral mediated CRISPR/Cas9 system that can be rendered inducible utilizing doxycycline (Dox) and can be delivered to cells *in vitro* and *in vivo* utilizing adeno-associated virus (AAV). Specifically, we developed an inducible gRNA (gRNAi) AAV vector that is designed to express the gRNA from a H1/TO promoter. This AAV vector is also designed to express the Tet repressor (TetR) to regulate the expression of the gRNAi in a Dox dependent manner. We show that H1/TO promoters of varying length and a U6/TO promoter can edit DNA with similar efficiency *in vitro*, in a Dox dependent manner. We also demonstrate that our inducible gRNAi vector can be used to edit the genomes of neurons *in vivo* within the mouse brain in a Dox dependent manner. Genome editing can be induced *in vivo* with this system by supplying animals Dox containing food for as little as one day. This system might be cross compatible with many existing *S. pyogenes* Cas9 systems (i.e. Cas9 mouse, CRISPRi, etc.), and therefore it likely can be used to render these systems inducible as well.

Introduction

The CRISPR/Cas9 based genome editing system has proven to be an extremely powerful tool for scientists seeking to genetically manipulate cells and tissues *in vitro* and *in vivo* across multiple species. This genome editing system takes advantage of the RNA-guided Cas9 nuclease from the type II prokaryotic Clustered Regularly Interspersed Short Palindromic Repeats (CRISPR) adaptive immune system, where it has been adapted for the use of knocking out genes,

creating specific modifications to genes and for the activation and suppression of transcription in a gene specific manner (Jinek et al., 2012; Cong et al., 2013; Gilbert et al., 2013; Larson et al., 2013; Mali et al., 2013; Qi et al., 2013; Sander & Joung, 2014; Tanenbaum et al., 2014). CRISPR/Cas9 can be used to genetically manipulate embryonic stem cells quickly and relatively easily, which has enabled genetically modified mice to be created significantly faster than conventional methodologies and this is especially true in cases where multiple genes are modified (Wang et al., 2013). This system also offers a potentially better alternative to RNAi mediated gene knockdown which requires the constant overexpression of an shRNA to mediate gene knockdown and in some cases has proven to be toxic when utilized in vivo (Hommel et al., 2003; Grimm et al., 2006; McBride et al., 2008; de Solis et al., 2015).

The success of the CRISPR/Cas9 system can be explained, in part, by its simplicity. For example, this genome editing system can be reconstituted in eukaryotic cells simply by the presence of the Cas9 protein and guide RNA (gRNA) consisting of the fusion of a CRISPR RNA (crRNAs) and a fixed transactivating CRISPR RNA (tracrRNA) – just two genes are required. The first 20 nucleotides of the gRNA are custom designed to be complementary to the intended target site within the genome and consequently guide the Cas9 protein to this site, allowing Cas9 to create double strand breaks (DSB) of the targeted DNA. The DSB initiates the error prone nonhomologous end joining (NHEJ) DNA repair mechanism. Due to the error prone nature of this repair pathway, insertions and deletions (Indels) can be created at the DSB break/repair site. If the DSB occurs within the protein coding region of a gene, a loss of protein function can occur due to: the deletion of relevant codons, an insertion of inappropriate codons, or the creation of indels that lead to a shift in the reading frame – collectively, leading to a null allele/gene

knockout. Alternatively, if a donor DNA template is provided, Homology Directed Repair (HDR) can occur instead of NHEJ. This phenomenon can be harnessed to create precise modifications of the genome at specific loci (Cong et al., 2013; Mali et al., 2013; Wang et al., 2013).

Recently, the CRISPR/Cas9 system has been rendered amenable for delivery to cells in vivo via adeno-associated virus (AAV) (Swiech et al., 2014; Ran et al., 2015). Delivery of CRISPR/Cas9 via AAV could be useful for potential human gene therapy approaches that might intend to utilize CRISPR/Cas9 technology and it is also highly relevant for preclinical studies that could benefit from the delivery of CRISPR/Cas9 to tissues of living mammals. The field of behavioral neuroscience can greatly benefit from viral mediated genome editing because it can be used to knock out genes in discrete locations of the animal brain in a cell type specific manner to allow the interrogation of how a gene influences behavior and circuit function. However, in complex behavioral experiments it can be advantageous to induce the desired genetic manipulation at a specific time point during an ongoing experiment, but we are limited in our ability to temporally control when genome editing will occur utilizing existing technology.

Utilizing CRISPR/Cas9 systems in vivo, in mammals, may allow these systems to be active for days to weeks at a time. In cases where CRISPR/Cas9 might be virally delivered to humans for gene therapy, the CRISPR/Cas9 system could be active indefinitely. In these instances, where CRISPR/Cas9 is chronically active for extended durations, there might be an increase in the accumulation of off-target editing/mutations. Thus, for in vivo applications, it would likely be beneficial to minimize the duration of Cas9 mediated genome editing to the time necessary for Cas9 to edit its intended target site and this has been, in part, the motivation for

developing previously described inducible CRISPR/Cas9 genome editing systems (Davis et al., 2015; Nihongaki et al., 2015a; Zetsche et al., 2015). However, while some of CRISPR/Cas9 systems have been adapted for AAV delivery (Swiech et al., 2014; Karnan S., 2016; Yang et al., 2016), none of these AAV based systems, to date, have been adapted to allow the genome editing function to be temporally regulated.

Due to the benefits of possessing temporal control over the duration of Cas9 mediated genome editing, we sought to develop an inducible CRISPR/Cas9 system that could be virally delivered and regulated utilizing Doxycycline (Dox). In our first set of experiments, we attempted to regulate Cas9 expression from a tetracycline response element containing promoter, however, we determined that genome editing could not be regulated in a Dox dependent manner, due to the leakiness of Cas9 expression within this system. As an alternative, we developed a viral vector that could regulate gRNA expression in a Dox dependent manner, and we demonstrate that our two vector CRISPR/Cas9 system can be virally delivered in vivo to the mouse brain and genome editing can be induced in a Dox dependent manner. The inducible gRNA vector (gRNAi) we developed is cross compatible with many existing *S. pyogenes* Cas9 (SpCas9) systems and therefore coupling our gRNAi AAV vector with these systems may enable them to be inducible as well (i.e. Cas9 mouse, CRISPRi, etc.).

Materials and Methods

Plasmid constructs All viral plasmids generated for this study were produced utilizing standard recombinant DNA cloning techniques. The pAAV-pMecp2-SpCas9-spA plasmid (pX551) and was a gift from Feng Zhang's laboratory (Swiech *et al.*, 2014) (Addgene #60957)

and this vector served as the backbone for the inducible Cas9 vectors described in this study. The truncated P_{Tight} sequence was PCR amplified from pTRE-TIGHT-Cx43-eYFP (a gift from Robin Shaw (Smyth *et al.*, 2010) (Addgene plasmid # 31807)) and cloned into the AgeI-XbaI sites of pX551 to create the P_{Tight} -Cas9 vector. This truncated P_{Tight} sequence contained 3 Tet operators. This vector was subsequently modified by cloning into the BsmI-EcoR1 sites a new C-terminus region of Cas9 that lacked the C-term NLS and instead contained the following core PEST degron sequence (HGFPPAVAAQDDGTLPMSCAQESGMDRH) (Li *et al.*, 1998) utilizing an appropriately designed gBlock (Integrated DNA technologies) to create the P_{Tight} -Cas9PEST vector. This core PEST sequence is utilized in the destabilized eGFP variant, D1eGFP. To create the P_{TRE3G} -Cas9PEST vector, the truncated P_{TRE3G} sequence was PCR amplified from pLenti CMVTRE3G eGFP Neo (w821-1) (A gift from Eric Campeau) and cloned into the AgeI-KpnI sites of the P_{Tight} -Cas9PEST vector. The truncated TRE3G promoter contains 2 Tet operators. The P_{TRE3G} -Cas9PEST vector was subsequently modified by cloning in a new 5' UTR/N-terminus region into the AgeI-BstXI sites, utilizing an appropriately designed gBlock (Integrated DNA Technologies), that lacked a Kozak sequence and the N-Terminal NLS to create the P_{TRE3G} -Cas9-PEST viral vector. To create the gRNA/rtTA-GFP viral vector, the previously described AAV2 genome vector, pAAV-shRNA expression cassette vector, (Hommel *et al.*, 2003) was systematically gutted and the appropriate sequences were subsequently cloned into it. First, the CMV-rtTA-GFP-Blastocidin S Resistance-WPRE expression cassette was removed from the pMA2640 (Addgene, #25434) (Alexeyev *et al.*, 2010), and cloned into the XhoI-ClaI sites of the pAAV-shRNA vector. A short ~70 base pair 3'UTR sequence containing two polyadenylation signal sequences, which we've used previously (Holehonnur *et al.*, 2015), was

cloned into the ClaI-MluI sites. The Blastocidin S Resistance coding region was removed and the appropriate portion of GFP with a stop codon was cloned back into the BamHI-MroI sites. The gRNA expression cassette was PCR amplified from pX330 (Gift from Feng Zhang (Cong *et al.*, 2013) (Addgene, #42230)) using the following DNA primers, (gRNA RsrII FP ataCGGTCCGgagggcctatttcccatgattccttc, gRNA XhoI RP aacCTCGAGgccatttgtctgcagaattggcgcacg), and cloned into the RsrII-XhoI sites, to create the final AAV2-gRNA/rtTA-GFP viral vector. Because the BbsI sites used for cloning the gRNAs into the gRNA expression cassette were not unique to this AAV plasmid, the gRNAs were first cloned into the BbsI sites of the pX330 plasmid and then the entire gRNA expression cassette was transferred into the AAV plasmid via the RsrII-XhoI sites utilizing the above mentioned DNA primers. The DNA oligonucleotides coding for the Tet2 gRNAs compatible with the pX330 plasmid were previously described (Wang *et al.*, 2013) (Top: CACCGAAAGTGCCAACAGATATCC, Bot: AAACGGATATCTGTTGGCACTTTC). The AAV2-gRNAi-TetR viral vector was developed starting with the AAV:ITR-U6-sgRNA(backbone)-hSyn-Cre-2A-EGFP-KASH-WPRE-shortPA-ITR plasmid (Addgene, #60231)(Platt *et al.*, 2014) as a backbone. The CMV promoter driving the TetR coding region was PCR amplified from pQCXIN-TetR-mCherry plasmid (a gift from Tom Misteli (Roukos *et al.*, 2013) (Addgene, # 59417)) and it was inserted into this vector via the XbaI-NheI sites. This resulted in the removal of the hSyn-Cre region. Next, an inducible gRNA expression cassette containing an HI/TO promoter was created using an appropriately designed gBlock (Integrated DNA Technologies) and it was cloned into the MluI-XbaI sites, to create the AAV2-gRNAi-TetR viral vector. Guide RNA sequences can be cloned into this vector via the SapI sites, in a

similar manner as to how gRNA sequences are cloned into the AAV:ITR-U6-sgRNA(backbone)-hSyn-Cre-2A-EGFP-KASH-WPRE-shortPA-ITR plasmid (Addgene, #60231) (Platt *et al.*, 2014) or the similar pX552, pAAV-U6sgRNA-hSyn-GFP-KASH-bGH vector (Addgene, #60958). The Tet2 gRNA sequences used with this vector were (Top: ACCGAAAGTGCCAACAGATATCC, Bot: AACGGATATCTGTTGGCACTTTC). The entire HI/TO gRNAi expression cassette can be PCR amplified with the following DNA primers (H1TO gRNA FP (MluI) AGCTACGCGTAATATTTGCATGTC and H1TO gRNA RP (XbaI) ACGTTCTAGAACTAGTCCATGG). The entire U6/TO and H1-L/TO expression cassettes containing the Tet2 gRNA were PCR amplified from appropriately designed gBlocks (Integrated DNA Technologies) and inserted into the AAV2-gRNAi-TetR viral vector via the MluI-XbaI sites. The DNA sequences for these new plasmids will be made available upon request. All gRNA viral plasmids will be made available through Addgene.

Assessment of *in vitro* genome editing For *in vitro* genome editing experiments, Neuro-2a cells (N2A; ATCC) were grown to a confluency of 60-65% in a 24 well cell culture plate and transfected with a plasmid containing a Cas9 transgene and plasmid containing gRNA transgene in a 1:1 ratio with Lipofectamine 2000 (Invitrogen), following the manufacturer's instructions. In cases where pX330_{Tet2} or pX330_{Empty} were used, only one plasmid was transfected. For samples that required Doxycycline (Dox), the media was replaced with fresh media 6 hours post transfection that contained 10 µg/mL of Dox (Clontech). The cells were harvested 96 hours post-transfection and were collected by centrifugation (10 min @ 14,000 RPM). Genomic DNA was extracted using a the QIAamp DNA Mini Kit, (Qiagen, Cat #51304) following the

manufacturer's instructions. A 466 base pair region containing the Tet2 gRNA target site was PCR amplified from crude genomic DNA in a standard 25 µl PCR reaction (Platinum Taq; Invitrogen) using the following previously described DNA primers (Tet2 Surv FP CAGATGCTTAGGCCAATCAAG and Tet2 Surv RP AGAAGCAACACACATGAAGATG) (Wang *et al.*, 2013). 150ng of isolated genomic DNA (described above) was used as the DNA template, and the PCR was performed with the following cycling parameters [94 °C, 2 min; (94 °C, 30 sec; 54 °C, 30 sec; 72 °C, 30 sec) x 37 cycles, 72 °C, 45 sec]. Amplification was confirmed using gel electrophoresis on a 1.5 % agarose, 1 X TAE gel. Three µl of PCR product was digested with 5 units of EcoRV-HF (New England Biolabs) for 2 hr in a standard 10 µl restriction enzyme reaction following the manufacturer's instructions. Each 3 µL of digested PCR product was electrophoresed on a 2.0 % agarose, 0.5 X TBE gel to determine if genome editing had occurred. In some cases, the amount of genome editing was quantified using ImageJ (U. S. National Institutes of Health, Bethesda, Maryland, USA, <http://imagej.nih.gov/ij/>). This was accomplished by measuring the optical density peaks using the gel analysis feature. The peaks for the cut DNA and non-cut DNA were selected and the label peaks feature was used to determine the percentage of cut and non-cut DNA in each individual sample. Some *in vitro* samples were screened using resolvase-based mutation detection kit (Guide-it Mutation Detection Kit, Clontech, Cat #631443) following the manufacturer's instructions.

Immunocytochemistry (ICC) Glass coverslips were placed in 24 well cell culture plates and treated with poly-l-lysine (0.1 mg/mL; Sigma) overnight. The following day, the poly-l-lysine was removed and the coverslips were washed 3 x with phosphate buffered saline pH 7.4 (PBS).

N2A cells were seeded at 65% confluency on these glass coverslips. Twenty-four hours later, the cells were transfected with AAV viral plasmids designed to express Cas9 and rtTA/gRNA plasmids using Lipofetamine 2000 (Invitrogen), following the manufacturer's instructions. Six hours post transfection, media was replaced with fresh media and in some cases the media contained 10 $\mu\text{g}/\text{mL}$ of Dox. The ICC procedure was carried out 24 hr post addition of doxycycline as previously described (Holehonnur *et al.*, 2015) using an anti-Cas9 antibody (1:200; Diagenode, C15200203) and TxRed secondary antibody (1:000; Life Technologies). The ICCs were imaged at 200X magnification using a fluorescence microscope (Olympus, BX51). The on and off Dox pictures were taken at the same exposure conditions. An additional high exposure image was taken of the off Dox samples to reveal the low level Cas9 expression. For ICCs following viral transduction of 293FT cells, 1.6 μl of AAV2/DJ- P_{Tight} -Cas9 ($6\text{E}12$ GC/mL) and 1 μl of AAV2/DJ-gRNA/rtTA-GFP ($1\text{E}13$ GC/mL) were diluted in 200 μl of culture media containing 2% FBS and it was applied to cells for 2 hours, with gentle rocking every 30 minutes. Following the 2-hour incubation, 400 μl of culture media containing 18% FBS was added to the wells. Dox was added to the wells 6 hours later and the ICC was carried out 24 hours after the addition of Dox.

Viral production, purification, and titering Procedures were carried out as previously described (Holehonnur *et al.*, 2014). AAV2 genome plasmids were pseudotyped as either AAV2/DJ8 or AAV2/DJ as specified. Viruses were produced using a triple-transfection, helper-free method into 293FT cells (Invitrogen) using polyjet (Signagen Laboratories) following the manufacturer's instructions for AAV production. A total of 5 x 15 cm cell culture plates were

transfected per virus. Viruses were purified on an iodixanol step gradient and further concentrated and purified using Amicon Ultra-15 centrifugal filter units (Millipore). Purified AAV was titered using a quantitative-PCR based titering method as previously described (Holehonnur *et al.*, 2014). All Cas9 transgene containing viruses were titered utilizing custom Cas9 primers/probe (Custom Taqman gene expression assays, Invitrogen). All GFP transgene containing viruses were titered with (GFP Primer/Probe (ID# Mr04329676_mr; Invitrogen). The results were reported as the number of DNase resistant viral particles as genome copies per milliliter (GC/ml).

Viral infusion Viral infusions targeting the mouse BLA were performed similarly as described (Holehonnur *et al.*, 2014). Briefly, mice were rendered unconscious with an intra-peritoneal injection of ketamine (100 mg/kg) and xylazine (10 mg/kg) prior to stereotaxic surgery. Thirty-one-gauge custom infusion cannulas (C315G, PlasticsOne) were very securely inserted into polyethylene tubing (I.D. 0.0150in. O.D. 0.043 in., wall thickness 0.0140 in; A-M systems, Inc.) that were 50 cm in length. These tubes were first backfilled with 1 x phosphate buffered saline, pH 7.4 (PBS), followed by sesame oil, where only 1xPBS was present in the ~5 cm region closest to the infusers to avoid getting sesame oil in the brain. Syringes (2 μ L, 23-gauge (88500); Hamilton Company)) were used for the viral infusion. The viral cocktail was drawn up into the infusion cannula. Infusers were bilaterally lowered into the BLA of mice [AP +1.6, ML \pm 3.3, -DV \pm 4.97] and infused (1 μ L/side) at a rate of 0.07 μ L/min for 15 min using an infusion pump (New Era Pump Systems Inc., NE-300) The AAV2/DJ-P_{Tight}-Cas9 and AAV2/DJ-gRNA_{Tet2/Empty}/rtTA-GFP viruses were co-infused bilaterally into the BLA, each at a titer of

6E12 GC/mL (1µl/side). The AAV2/DJ8-P_{Mecp2}-Cas9 and AAV2/DJ8-gRNA_{iTet2/Empty} viruses were co-infused bilaterally into the BLA, each at a titer of 2.5E12 GC/mL (1µl/side). In cases when mice were provided Dox, it was supplied through their food (Dox 1 g/kg; Bio-Serv).

Assessment of *in vivo* genome editing At the appropriate time point, mice were euthanized via CO₂ euthanasia and the brain was rapidly removed and frozen with powdered dry ice and then stored at -80C. Tissue was then mounted and sliced using a cryostat sectioner (Thermo Scientific) to take coronal sections that contained the amygdala. When GFP reporter signal was present in the amygdala, 200 µm punches were taken within the amygdala with a 1 mm punch tool (Fine Science Tools) until the GFP signal ceased within the amygdala. Punched tissue was stored at -80C. Tissue was homogenized in a 1.7 mL centrifuge tube with pestle and extracted in the same manner as the *in vitro* experiments.

Sequencing of edited DNA N2A cells that were transfected with pX330_{Tet2} were prepared for DNA extraction and PCR amplification as described above. PCR product was digested with EcoRV and electrophoresed and the DNA band exhibiting editing was excised from the gel and purified using a gel purification kit (Qiagen). Gel purified DNA was cloned into the PCR4 Topo vector using a Topo cloning kit (Invitrogen) and transformed into Top10 cells (Invitrogen). Colonies were screened for the presence of the Tet2 sequence via PCR and PCR product was sent for DNA sequencing (Retrogen Inc.).

Subjects Adult C67B6 mice were used in this study. All animals were housed individually and maintained on a 12 hr light / dark cycle. Food and water were provided *ad libitum* throughout the

experiments. Animal use procedures were in accordance with the National Institutes of Health Guide for the Care and Use of Laboratory Animals and were approved by the University of Texas at Dallas Animal Care and Use Committee.

Statistical analysis Quantified genome editing data was analyzed using a non-parametric Kruskal–Wallis individual sample comparison or multiple sample comparison, with a probability threshold of 0.05. A one-way ANOVA, followed by a Fisher’s PSD post hoc analysis was used for compare the different inducible promoters. A two-tailed T-test assuming equal variances was used to compare samples analyzed with the mutation detection kit.

Results

Construction of a doxycycline regulated SpCas9 transgene within an AAV2 viral vector

Viral vectors are necessary to introduce the genetic components of the CRISPR/Cas9 system into specific mammalian cells *in vivo*. Adeno-associated virus (AAV) is the vector of choice to use within mammalian systems due to its high tolerability *in vivo*^(Daya & Berns, 2008) and because it is possible to produce high titer AAV relatively easily that is capable of transducing a large number of cells. In our first set of experiments, we focused on designing an inducible CRISPR/Cas9 system that was suitable for AAV delivery, where the SpCas9 transgene expression could be regulated. To accomplish this, it was necessary to fit the entire Cas9 transgene within AAV’s strict genome packaging limit which hovers somewhere between 4.7 and 5 kb. This packaging limit also includes the two inverted terminal repeats that are ~150 bases each, therefore limiting AAV’s ability to deliver transgenes that are no larger than ~4.4-4.7 kb. Since the coding region of SpCas9 is ~4.2 kb, this leaves very little room for the promoter

and 3' untranslated sequences (UTR). Because of this, we opted to design an AAV vector that harbored the Cas9 coding region under the control of a truncated 2nd generation tetracycline response element (TRE) promoter, P_{Tight} (Figure 3.1A). Of the three generations of TRE promoters (TRE2, Tight, TRE3G), the Tight promoter is the shortest of the three promoters. We also truncated the promoter at the 5' end so that it only included 3 Tet operators (TetO), creating a promoter that was ~175 bps. To regulate the P_{Tight}-Cas9 transgene and deliver the gRNA expression cassette, another AAV was developed, that harbored a gRNA transgene, utilizing a U6 promoter, and an additional transgene, containing a CMV promoter driving rtTA (Tet-On Advanced) transcription factor expression. This virus was also designed to express green fluorescent protein (GFP) from an internal ribosomal entry site (IRES), following the rtTA open reading frame (ORF) (Figure 3.1A). In cells that receive both the P_{Tight}-Cas9 virus and the gRNA/rtTA virus in the presence of Doxycycline (Dox), rtTA would become activated, allowing it to bind to the P_{Tight} promoter and drive Cas9 expression, inducing genome editing. When Dox is not present, the system theoretically should not be able to express Cas9 and therefore genome editing should not be possible. We produced both of these viral vectors pseudotyped as DJ serotype and transduced 293FT cells grown in culture in the presence or absence of Dox. Forty-eight hours post viral transduction, immunocytochemistry (ICC) was performed for Cas9 protein expression. The cells exhibited GFP fluorescence, indicating that they were efficiently transduced by the gRNA/rtTA-GFP virus. The ICC revealed a dramatic increase in Cas9 expression in the presence of Dox, indicating that our viral vectors appropriately expressed their intended transgenes and it appeared that Dox could regulate Cas9 expression (replicates of samples produced similar results) (Figure 3.1B).

Next, we wanted to determine if these viral vectors could edit the genome in an inducible manner. To do this we chose to utilize a previously described and validated gRNA targeting the mouse Tet2 genomic locus. Tet2 is a member of the Ten-eleven translocation (Tet) gene family, and is involved in the enzymatic conversion of 5-methylcytosine (5mC) to 5-hydroxymethylcytosine (5hmC) to promote DNA demethylation. In particular, this gRNA is designed to target a genomic sequence that contains an EcoRV restriction enzyme site that is directly adjacent to the Protospacer Adjacent Motif (PAM) sequence (Figure 3.1C). The PAM site is the DNA sequence immediately following the DNA sequence targeted by the Cas9 nuclease. The location of the restriction enzyme site, provides the ability to screen cells for genome editing, because Cas9 mediated genome editing utilizing this gRNA would likely destroy the enzyme site, and therefore genome editing can be accessed via restriction fragment length polymorphism (RFLP) analysis to assess the presence or absence of this restriction enzyme site. To demonstrate this and to validate that this Tet2 targeting gRNA indeed was capable of efficiently editing its intended target site, we transfected the mouse neuroblastoma cell line Neuro-2A (N2A), with the Cas9/gRNA expression plasmid pX330, that contained the Tet2 gRNA (pX330_{Tet2}). Ninety-six hours post transfection, the cells were harvested and genomic DNA was isolated, and the Tet2 locus was PCR amplified utilizing PCR primers that flank the intended Cas9 cut site. The full length uncut Tet2 PCR product is 466 bps. In cells that did not receive gRNAs targeting the Tet2 locus (pX330_{Empty}), genome editing did not occur, and the EcoRV digestion of the Tet2 PCR product yielded 2 bands at ~200bps as expected (Figure 3.1D. lane 2). However, in cells that were transfected with the pX330_{Tet2} plasmid, genome editing did occur, as demonstrated by the fact that the EcoRV digestion was not capable of

digesting the entire pool of PCR product. In this case, the digestion of the PCR product yielded fully digested DNA, creating 2 bands at ~200bps and one undigested band at ~440bps, indicating genome editing had occurred. In this case, the amount of editing was ~33% as determined by the ratio of the digested and undigested bands (Figure 3.1D, lane 3). We cloned and sequenced some of these edited PCR products to better characterize the nature of Cas9 mediated Indel formation. In the 6 independent clones we sequenced, Cas9 had created deletions spanning 1-15 nucleotides, therefore underscoring the utility of the RFLP screening (Figure 3.1E).

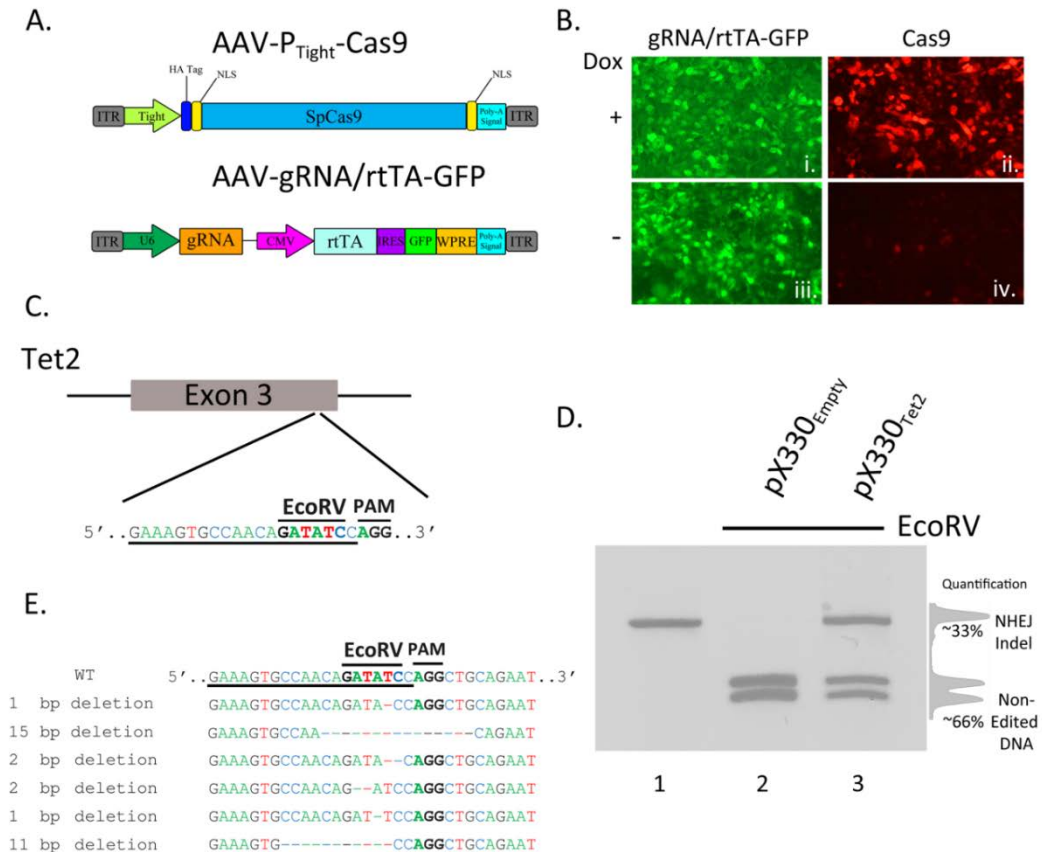


Figure 3.1. Demonstration of genome editing with spCas9

(A) AAV vector maps depicting AAV-P_{Tight}-Cas9 and AAV-gRNA/rtTA. AAV-P_{Tight}-Cas9 consists of a Cas9 transgene under the control the Dox inducible Tight promoter. AAV-

gRNA/rtTA consists of a gRNA expression cassette and a rtTA (Tet-On Advanced) transgene controlled by a CMV promoter. It also is designed to express GFP via an IRES element following the rtTA reading frame. **(B)** ICC for Cas9 and GFP was performed on 293FT cells transduced by AAV- P_{Tight} -Cas9 and AAV-gRNA/rtTA viruses in the presence or absence of Dox. Native GFP expression is visible in virtually all of the cells (i, iii). Cas9 expression is robustly induced in the presence of Dox (ii), compared to the no Dox condition (iv). Representative images are shown. The experiment was repeated twice with similar results. **(C)** Diagram depicting the approximate location of where the Tet2 gRNA targets the Tet2 locus. Underlined nucleotides indicate the sequence of the Tet2 gRNA. Location of the EcoRV site and PAM sequence are denoted. **(D)** An approximate 460 bps region of the Tet2 locus that includes the site targeted for editing via the gRNA_{Tet2}, was PCR amplified from N2A genomic DNA and electrophoresed on a standard agarose gel and stained with ethidium bromide (lane 1). N2A cells were transfected with the pX330_{Empty}, a plasmid designed to express spCas9 and no gRNA, and 96 hrs later, the genomic DNA was isolated and the Tet2 locus was PCR amplified and subjected to EcoRV digestion. The PCR product was cut into two pieces of DNA as expected (lane 2). However, when N2A cells were transfected with pX330_{Tet2} and similarly processed, the PCR product was incompletely digested resulting in a total of three bands on the gel - one uncut PCR product (~460 bps) and two smaller bands. In this case the genome editing was ~33%. **(E)** Edited DNA depicted in (D. Lane 3) was gel purified and TA cloned and 6 independent clones were sequenced. These 6 clones contained deletions which destroyed the EcoRV site.

A doxycycline regulated SpCas9, within AAV, exhibits leaky expression and genome editing in a doxycycline independent manner

To determine if our P_{Tight} -Cas9 and gRNA/rtTA-GFP viral plasmids could edit the Tet2 locus in a Dox dependent manner, we cotransfected the P_{Tight} -Cas9 plasmid with the gRNA_{Tet2}/rtTA-GFP plasmid containing the Tet2 gRNA into N2A cells in the presence and absence of Dox. As a control, we also cotransfected the P_{Tight} -Cas9 plasmid with the gRNA_{Empty}/rtTA-GFP plasmid that did not contain a gRNA into N2A cells in the presence or absence of Dox. Forty-eight hours post transfection, the cells were harvested and the genomic DNA was isolated and examined for genome editing at the Tet2 locus via PCR/RFLP analysis as described above. Cells that received the P_{Tight} -Cas9 and gRNA_{Empty}/rtTA-GFP plasmids, did not exhibit editing of the Tet2 locus, as expected. Cells that received the P_{Tight} -Cas9 and the gRNA_{Tet2}/rtTA-GFP plasmids did exhibit editing of the Tet2 locus, however, the editing

occurred in the presence and the absence of Dox (similar results obtained in 3 independent samples per group) (Figure 3.2A). Notably, there was no difference between the induced (i.e. Dox) samples, compared to the non-induced samples (i.e. no Dox), indicating that there might be a low level of Cas9 expression that is sufficient for genome editing in the non-induced samples. To determine if these viruses would function in an inducible manner *in vivo*, we infused these viruses into the basal and lateral amygdala (BLA) of mice. Specifically, AAV2/DJ-P_{Tight}-Cas9 and AAV2/DJ-gRNA_{Tet2}/rtTA-GFP were co-infused bilaterally into the BLA, each at a titer of 6E12 GC/mL (1µl/side). For a control, AAV2/DJ-P_{Tight}-Cas9 and AAV2/DJ-gRNA_{Empty}/rtTA-GFP were infused in a similar manner. Half of the animals in the Tet2 group and half of the animals in the Empty group were placed on a diet of 1 g/kg of Dox. Ten days following surgery, the animals were sacrificed, and their BLA were microdissected. The genomic DNA was isolated from the microdissected BLA tissue and subjected to PCR/RFLP analysis to assess genome editing at the Tet2 locus (Figure 3.2C). Animals that received the AAV2/DJ-P_{Tight}-Cas9 and AAV2/DJ-gRNA_{Empty}/rtTA-GFP viruses, did not exhibit editing of the Tet2 locus, as expected. Animals that received the AAV2/DJ-P_{Tight}-Cas9 and AAV2/DJ-gRNA_{Tet2}/rtTA-GFP viruses did exhibit editing at the Tet2 locus, but similarly to the *in vitro* experiments, the editing was not Dox dependent (similar results obtained in 3 independent samples per group) (Figure 3.2D). Since these viral plasmids cannot be tightly regulated using Dox, these vectors would not be suitable for inducible genome editing *in vitro* or *in vivo*.

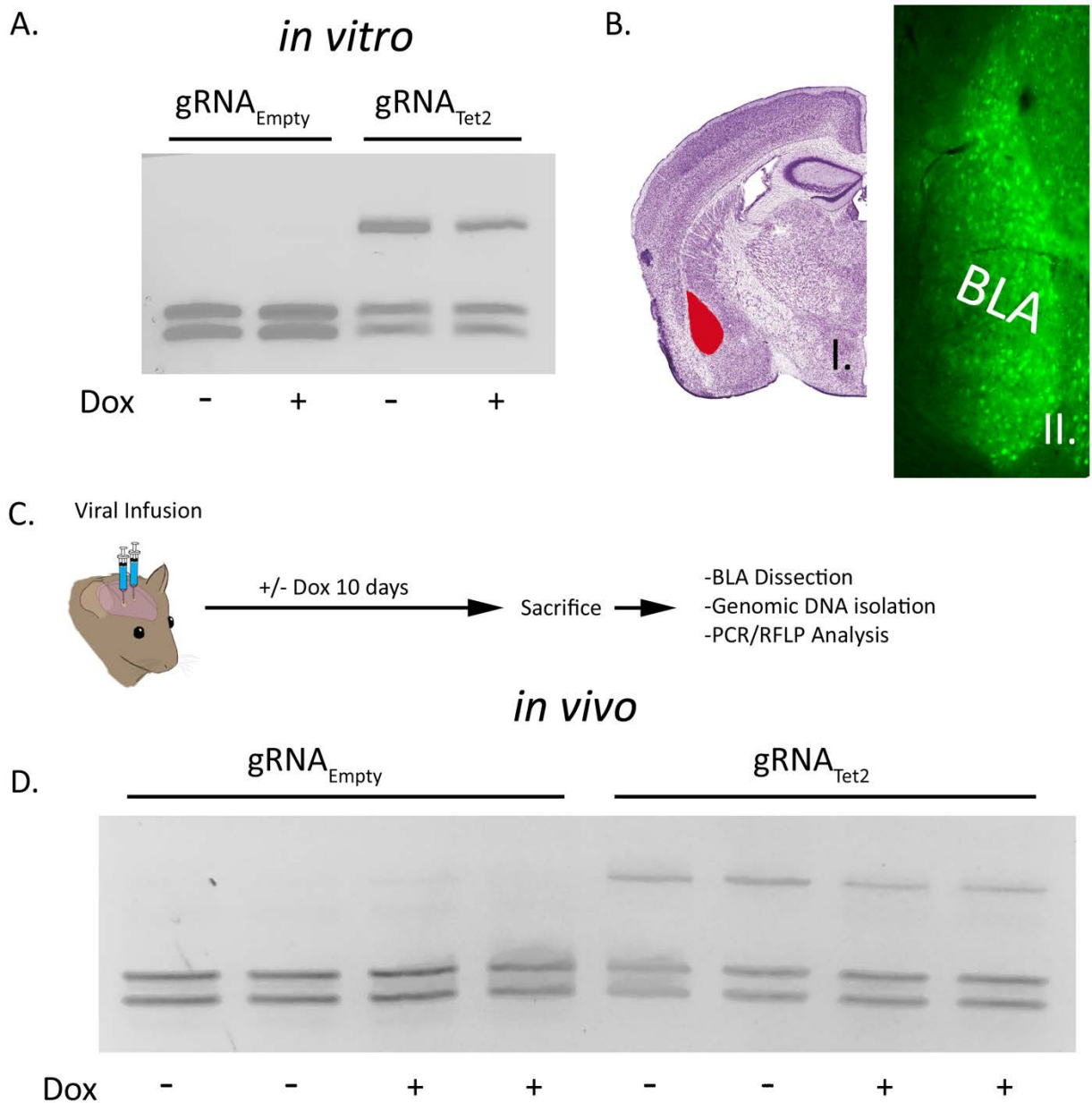


Figure 3.2 The TRE3G promoter is leaky within AAV viral plasmids and leads leaky genome editing

(A) The AAV-P_{Tight}-Cas9 plasmid and the AAV-gRNA_{Tet2}-rtTA plasmid were cotransfected into N2A cells in the presence or absence of Dox. As a control, the AAV-P_{Tight}-Cas9 plasmid and the AAV-gRNA_{Empty}-rtTA plasmid were co-transfected too. Ninety six hours post transfection, the cells were harvested, the genomic DNA was isolated and PCR and RFLP analysis was performed to assess if genome editing had occurred at the Tet2 locus. Genome editing was not observed in

cells that had received the gRNA_{Empty} plasmid either in the presence or absence of Dox as expected. Cells that were transfected with a plasmid containing the gRNA_{Tet2} plasmid, did exhibit editing, however the editing occurred in samples that were in the presence or absence of Dox, indicating that genome editing occurred independently of Dox. Similar results were observed in at least 3 independent samples per group. **(B)** Image of a Nissl stained coronal mouse brain section with the BLA highlighted in red (adapted from (K.B. & G, 2007))(i.) Image depicting GFP expression within BLA neurons in a similar anatomical coronal slice as in *i.*, taken 10 days following BLA infusion of both AAV-gRNA_{Tet2}-rtTA-GFP and AAV-P_{Tight}-Cas9 viruses (*ii.*). **(C)** Timeline from infusion of virus into the mouse amygdala to assessment of genome editing via RFLP analysis. **(D)** RFLP analysis of genome editing from BLA tissue transduced with AAV-P_{Tight}-Cas9 and AAV-gRNA_{Empty}-rtTA or AAV-P_{Tight}-Cas9 and AAV-gRNA_{Tet2}-rtTA from mice that were fed a diet that included Dox or a diet that did not include Dox. No genome editing occurred in samples that received gRNA_{Empty} as expected. Genome editing did occur in BLA samples that received gRNA_{Tet2} however, genome editing occurred independently of Dox administration. Two independent samples per group are shown. Similar results were observed in at least 3 independent samples per group.

We speculated that the inability to regulate genome editing with our P_{Tight}-Cas9 vector was due to low level Cas9 expression that was not rtTA dependent. Therefore, we created a number of other AAV vectors with modifications to attempt to reduce expression of Cas9 (Figure 3.3A). We first modified the P_{Tight}-Cas9 vector by removing the C-terminal NLS sequence at the end of the Cas9 ORF and adding a PEST sequence (P_{Tight}-Cas9PEST). The removal of the NLS should decrease the efficiency of Cas9 nuclear import which could reduce Cas9 activity and the addition of the PEST sequence could reduce the half-life of the Cas9 protein, thus reducing Cas9 levels. We subsequently modified P_{Tight}-Cas9PEST by exchanging the Tight promoter for a truncated 3rd generation TRE3G promoter which contained 2 TetOs in hopes that the TRE3G promoter might lead to lower background Cas9 expression (P_{TRE3G}-Cas9PEST). Finally, we modified the P_{TRE3G}-Cas9PEST vector by removing the Kozak sequence and the N-terminal NLS (P_{TRE3G}-ΔCas9PEST). The removal of the Kozak sequence, might lead to less efficient translation initiation, possibly lowering Cas9 protein levels, and the removal of

the N-Terminal NLS should reduce the efficiency of Cas9 nuclear import, leading to reduced Cas9 activity. These 4 viral vectors were transfected into N2A cells with the gRNA_{Tet2}/rtTA-GFP and gRNA_{Empty}/rtTA-GFP vectors in the presence or absence of Dox and genome editing of the Tet2 locus was assessed via PCR/RFLP analysis as described above (Figure 3.3B). Genome editing of the Tet2 locus did not occur in the gRNA_{Empty} groups as expected (Data not shown). Cells that received the Cas9 viral plasmids and the gRNA_{Tet2}/rtTA-GFP plasmid did exhibit editing of the Tet2 locus, however, there was virtually no differences in editing in the presence or the absence of Dox (similar results obtained in 3 independent samples per group). Next, we transfected N2A cells with the four Cas9 viral plasmids and the gRNA_{Tet2}/rtTA-GFP viral plasmid in the presence or absence of Dox. Twenty-eight hours post transfection, the cells were examined by immunocytochemistry (ICC), to observe Cas9 expression (Figure 3.3C). In all cases there was a clear induction of Cas9 expression due to the presence of Dox. Using exposure conditions that were optimal for visualizing Cas9 expression in the presence of Dox, there appeared to be very little, if any, Cas9 expression in the absence of Dox. However, at a much higher exposure time there was obvious Cas9 expression in the absence of Dox, which explains the genome editing we observed in the absence of Dox (samples performed in duplicate with similar results). Interestingly, these findings underscore that very little Cas9 protein is needed for efficient genome editing. We did not observe obvious differences in Cas9 expression across these four Cas9 viral constructs, indicating that the presence of the PEST sequence, the use of the TRE3G promoter and removal of the Kozak sequence had little influence over Cas9 steady state protein levels in the on or off Dox conditions. The removal of the N and C terminal Cas9 NLSs

did have a noticeable influence on the steady state Cas9 cellular localization, which became predominantly localized to the cytoplasm.

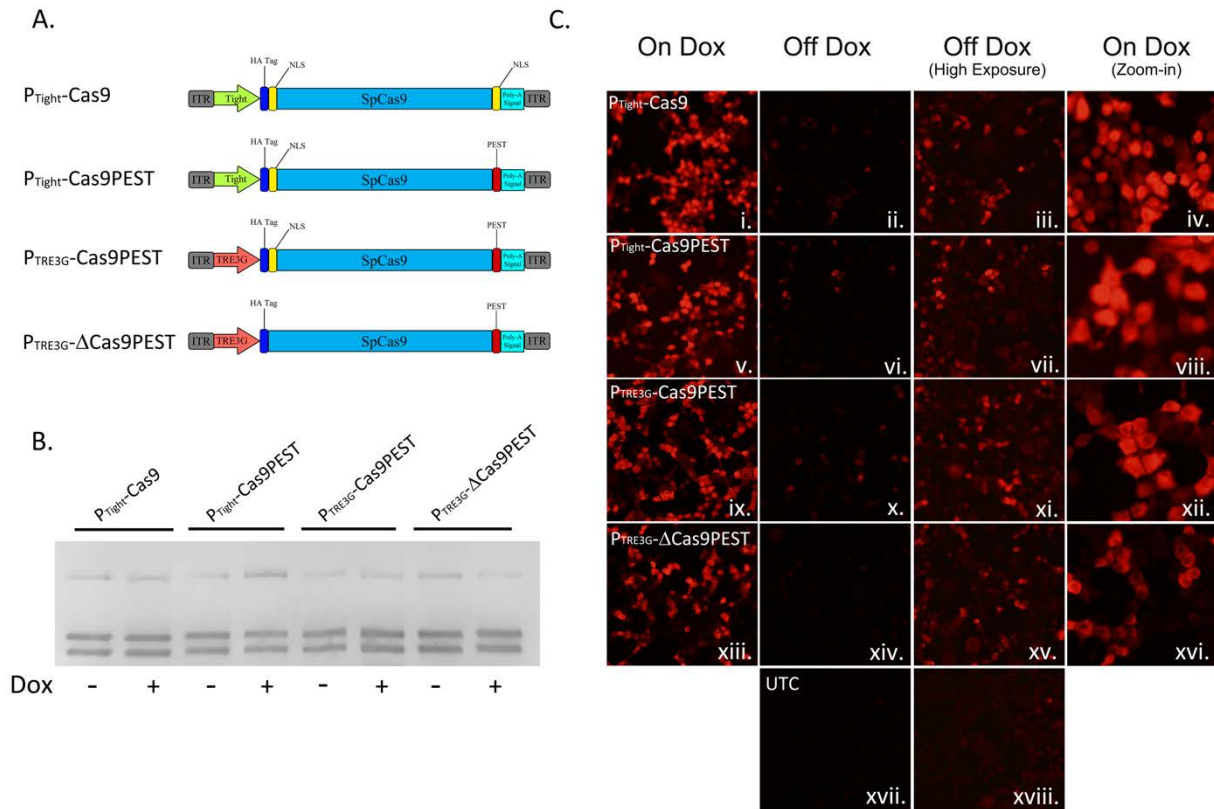


Figure 3.3 Modification of TRE3G-spCas9 plasmid in an attempt to decrease leakiness

(A) AAV vector maps depicting AAV-P^{Tight}-Cas9 and three new vectors derived from AAV-P^{Tight}-Cas9. The C-terminal NLS was removed from AAV-P^{Tight}-Cas9 and replaced with a PEST sequence to create AAV-P^{Tight}-Cas9PEST. Then the Tight promoter was exchanged for a TRE3G promoter to create P^{TRE3G}-Cas9PEST. Next, the kozak sequence and N-term NLS was removed to create P^{TRE3G}-ΔCas9PEST. (B) The plasmids described in (A), were co-transfected with AAV-gRNA_{Tet2}-rtTA into N2A cells in the presence or absence of Dox. Ninety six hours post transfection, the cells were harvested, the genomic DNA was isolated and PCR and RFLP analysis was performed to assess if genome editing had occurred at the Tet2 locus. None of the Cas9 plasmids exhibited genome editing that was Dox dependent. Similar results were observed in at least 3 independent samples per group. (C) These Cas9 plasmids were transfected into N2A cells in the presence or absence of Dox and an ICC for Cas9 was performed. Images depict cellular Cas9 expression from cells treated with Dox (i, v, ix and xiii) or off Dox (ii, vi, x, xiv and xvii).

xvii). These images were taken the same exposure. Images depicted in (*iii, vii, xi, xv* and *xviii*) are of the off Dox samples at a higher exposure, which reveal low amounts of Cas9 expression in the absence of Dox. Images depicted in (*iv, viii, xii* and *xvi*) are a zoom-in of the on Dox samples that shows a decreased nuclear localization of Cas9 protein for the PTRE3G- Δ Cas9PEST group. Samples were processed in duplicate with similar results. UTC = untransfected control.

AAV gRNAi vector exhibits doxycycline dependent genome editing *in vitro* and *in vivo*

Since we were not able to generate an AAV based Cas9 expression system where Cas9 expression could be regulated using a TRE containing promoter, due to the leakiness of Cas9 expression within this system, we chose an alternative approach. We reasoned that if we could regulate gRNA expression, we could still generate an inducible viral mediated genome editing system. We generated a gRNA AAV vector containing a gRNA transgene controlled by a hybrid H1/TO promoter (gRNAi) similar to the promoter used in the BLOCK-iT inducible H1 RNAi vectors (Invitrogen) (Figure 3.4A). This vector also contains a CMV promoter controlling the expression of TetR in frame with a self-cleaving P2A sequence followed by a GFP ORF fused to a KASH domain. Binding of TetR to the H1/TO promoter represses the gRNA transcription. The addition of Dox inhibits TetR binding and induces gRNA expression. The KASH domain will localize the GFP protein to the nuclear membrane, which will allow the nuclei of transduced neurons within the brain to be isolated away from non-transduced neurons using a combination of nuclei isolation via cellular fractionation and fluorescence-activated cell sorting (FACS). To test if the gRNA could regulate genome editing in a Dox dependent manner, we co-transfected the gRNAi_{Tet2}-TetR viral vector containing a gRNA designed to edit the Tet2 locus with a Cas9 expression plasmid that did not contain a gRNA (pX330_{Empty}) into N2A cells, in the presence or absence of Dox. As a control, we co-transfected the gRNAi_{Empty}-TetR viral

vector which did not contain a gRNA with pX330_{Empty} in the presence or absence of Dox. Ninety-six hours post transfection, the genome editing of the Tet2 locus was assessed via PCR/RFLP analysis as described above. Cells that received the gRNAi_{Empty}-TetR vector did not exhibit genome editing as anticipated. Cells that received the gRNAi_{Tet2}-TetR viral vector in the presence of Dox, exhibited genome editing, but in the absence of Dox, there was no editing (similar results obtained in 3 independent samples per group) (Figure 3.4B). These data indicated that the gRNAi-TetR vector could provide a plausible system for inducible viral mediated genome editing.

To test the efficiency of the H1/TO gRNA expression cassette, we compared its ability to mediate genome editing *in vitro* to two different inducible promoter based gRNA expression cassettes and a standard U6 based gRNA expression cassette (U6; pX552). We designed a gRNA expression cassette that included the full length sequence for the H1 promoter (H1-L/TO) and a U6/TO promoter based gRNA expression cassette, as described in (Henriksen *et al.*, 2007). These different vectors, were cotransfected with pX330_{Empty} into N2A cells, in the presence or absence of Dox for 96 hrs. PCR/RFLP analysis revealed that the U6 group exhibited moderately better editing compared to the U6/TO, H1/TO and H1-L/TO groups [$F(3,12) = 13.157$, $p = 0.0004$] ($p < 0.003$) (Figure 3.4C; 3.4D). We suspect that the presence of the Tet Operators, may slightly interfere with the efficiency of gRNA expression, however the inducible gRNA vectors do exhibit significant Dox dependent genome editing.

In order to determine if our restriction enzyme screening method to detect genome editing was comparable to other common methods that are designed to detect genome editing, we screened the same U6 and H1/TO samples from above utilizing the Resolvase based mutation

detection kit (Clontech). The PCR products were denatured, annealed and digested with Resolvase, an enzyme that makes a DSB at the site of mismatched DNA. The screening revealed a significant difference between the U6 and H1/TO groups [$t(6) = 4.332, p = 0.0049$], as expected. Additionally, similar levels of editing were detected utilizing this mutation detection method compared to the PCR/RFLP restriction enzyme analysis method (Figure 3.4F; 3.4G).

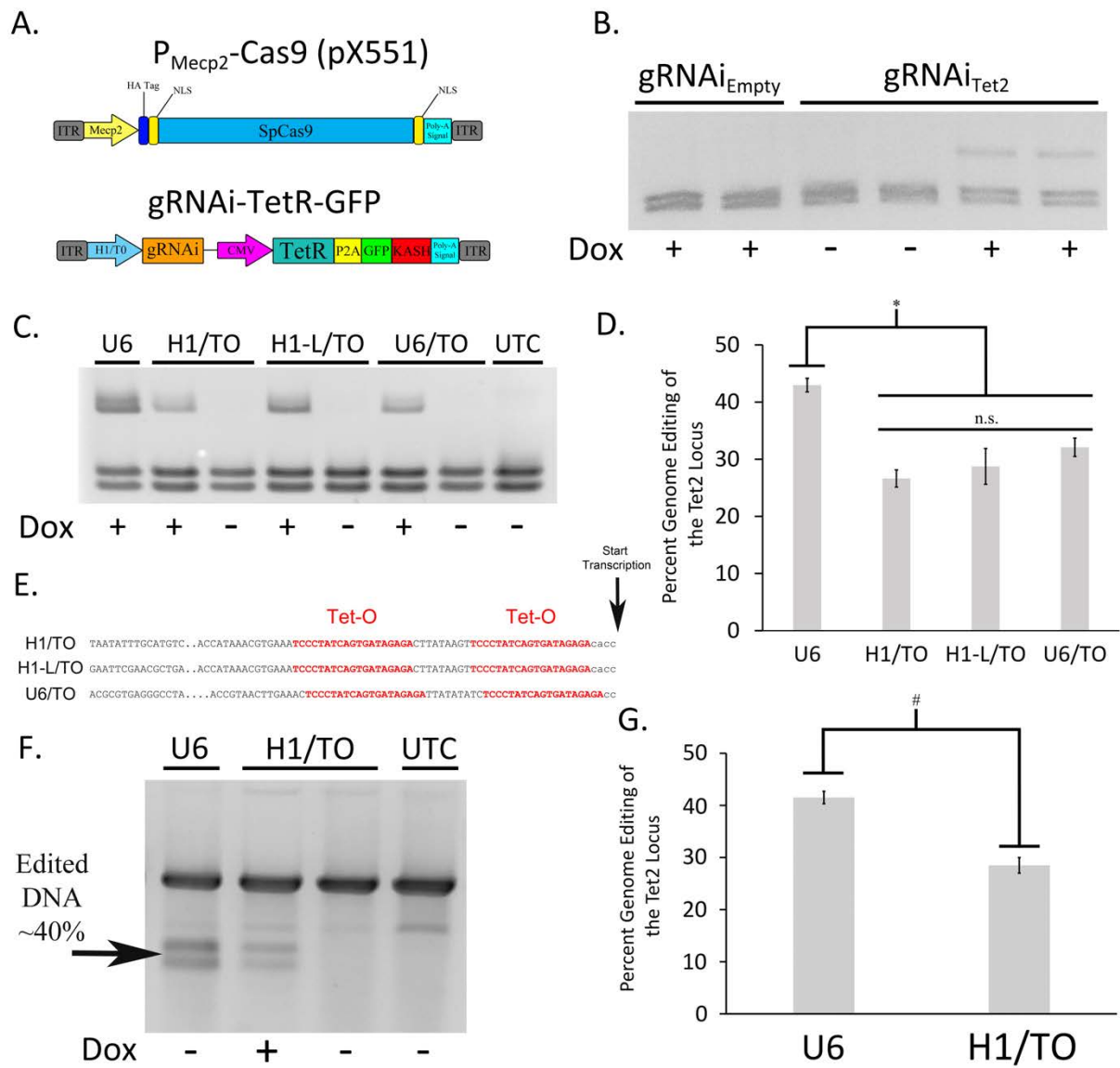


Figure 3.4 The development of inducible gRNA genome editing system

(A) AAV vector maps depicting the AAV- P_{Mecp2} -Cas9 vector and an inducible gRNA vector, AAV-gRNAi-TetR-GFP. (B) The gRNAi plasmid described in (A), containing either a Tet gRNA or no gRNA (Empty), were co-transfected with pX330_{Empty} into N2A cells in the presence or absence of Dox. Ninety six hours post transfection, the cells were harvested, the genomic DNA was isolated and PCR and RFLP analysis was performed to assess if genome editing had occurred at the Tet2 locus. Genome editing was not observed in cells that had received the gRNA_{Empty} plasmid either in the presence or absence of Dox as expected. Cells that were transfected with a plasmid containing the gRNA_{Tet2} plasmid, did exhibit editing in the presence of Dox, but not in the absence of Dox, indicating that genome editing could be regulated in a Dox dependent manner. Similar results were observed in at least 3 independent samples per group. (C) The H1/TO promoter gRNA expression cassette was compared to gRNA expression cassettes composed of either a full length H1/TO promoter (H1-L/TO), a U6/TO promoter or a non-inducible U6 promoter (U6) for their ability to edit the Tet2 locus. Cells were transfected with the respective vectors in the presence or absence of Dox and genome editing was assessed ninety-six hours post transfection (n = 4 per groups). (D) Quantification of genome editing revealed that the inducible promoter gRNA expression cassettes were not significantly different from each other (n.s. = $p = < 0.0778$, ANOVA) in their ability to edit the Tet2 locus and they were all slightly but significantly different from the non-inducible U6 promoter construct ($* = p = < 0.003$, ANOVA). Four independent samples were screened with similar results. (E) Partial sequences of the inducible promoters used, highlighting the tetracycline operators (Tet-O) and transcriptional start site. (F) Genomic DNA from the same U6, H1/TO and UTC samples used for (C and D) were subjected to a mutation detection kit (Clontech), in which the PCR amplified product was denatured, annealed and digested with Resolvase to directly detect genome edited DNA. (G) Levels of editing were comparable to those seen using the restriction digest PCR/RFLP analysis used for (C and D). Again, levels of editing were significantly higher in the U6 group, compared to the H1/TO group ($\# = p = < 0.005$, Two Tailed T-test).

Next, we wanted to assess if the gRNAi virus could be used *in vivo* to control genome editing in a Dox dependent manner. In these experiments we used a previously developed Cas9 AAV, where Cas9 expression is under the control of a neuronal specific truncated *Mecp2* promoter (AAV P_{Mecp2} -Cas9)(Swiech *et al.*, 2014). We produced AAV2/DJ8- P_{Mecp2} -Cas9 virus and the AAV2/DJ8-gRNAi_{Tet2} virus pseudotyped as DJ8 serotype. Specifically, AAV2/DJ8- P_{Mecp2} -Cas9 and AAV2/DJ8-gRNAi_{Tet2} were co-infused bilaterally into the BLA, each at a titer of $\sim 2.5E12$ GC/mL (1 μ l/side). For a control, AAV2/DJ8- P_{Mecp2} -Cas9 and AAV2/DJ8-gRNAi_{Empty} were infused in a similar manner. Half of the animals in the Tet2 group and half of

the animals in the Empty group were placed on a diet of 1 g/kg of Dox. Ten and 14 days following surgery, the animals were sacrificed, and their BLA were microdissected. The genomic DNA was isolated from the microdissected BLA tissue and subjected to PCR/RFLP analysis to assess genome editing at the Tet2 locus (Figure 3.5A). Animals that received the AAV2/DJ8-P_{Mecp2}-Cas9 and AAV2/DJ8-gRNAi_{Empty} viruses did not exhibit editing of the Tet2 locus as expected. Animals that received the AAV2/DJ8-P_{Mecp2}-Cas9 and AAV2/DJ8-gRNAi_{Tet2} viruses did exhibit editing at the Tet2 locus, but this time editing only occurred in cases where the animals received Dox, indicating that genome editing could be regulated in a Dox dependent manner (similar results obtained in 3 independent samples per group; $p = 0.04$) (Figure 3.5B and 5C). To compare our inducible system to a non-inducible system, we co-infused mice with an AAV designed to express a gRNA from a U6 promoter and AAV2/DJ8-P_{Mecp2}-Cas9 at the same viral titers as the above experiments and followed the same timeline as the above experiments. RFLP analysis revealed similar levels of genome editing at day 10 and 14 for the conventional non-inducible genome editing system(gRNA), compared to our inducible genome editing system (gRNAi) *in vivo* (similar results obtained in 3 independent samples per group; $p < 0.28$) (Figure 3.5D and 3.5E). In these *in vivo* experiments, we observed ~20% genome editing. This in part due to the fact that our viral vectors are targeting neurons selectively, due to AAV's natural tropism for neurons *in vivo* (de Solis *et al.*, 2015) and the fact that Cas9 expression is controlled from the Mecp2 promoter which restricts its expression to neurons (Swiech *et al.*, 2014). Within the brain, glia cells make up at least 50% of the cells (Azevedo *et al.*, 2009), so in this case we would at best only expect 50% of the cells within the microdissected brain tissue to exhibit editing and that is only if all the neurons within this microdissected tissue were transduced by

both viruses. Therefore the ~20% level of editing *in vivo* we are obtaining essentially means we are observing ~40% of the neurons undergo genome editing, and this is similar between our inducible system and the previously developed non-inducible system (Piechota *et al.*).

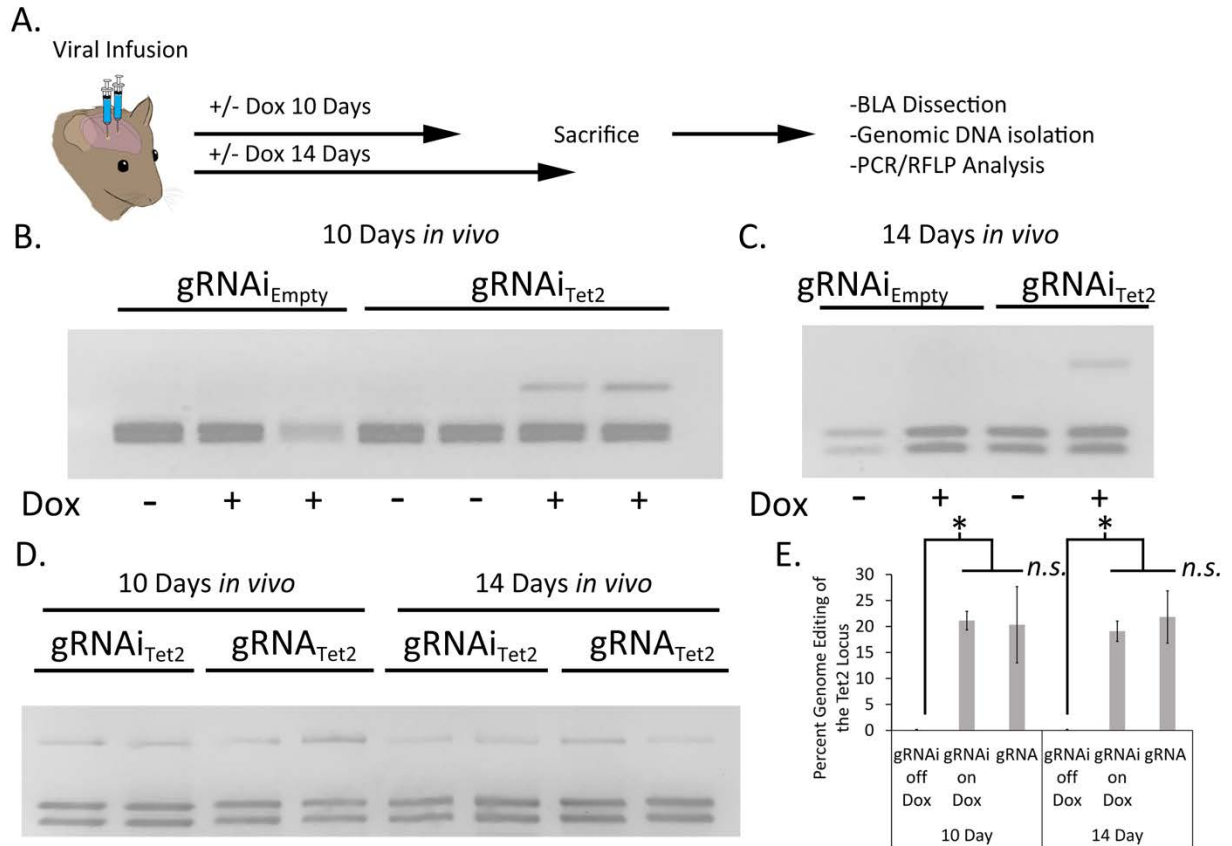


Figure 3.5 Inducible genome editing *in vivo* via regulation of gRNA

(A) Timeline from viral infusion to analysis of editing. Animals received either infusions of AAV-P_{Mecp2}-Cas9 and AAV-gRNAi_{Tet2}-TetR-GFP or AAV-P_{Mecp2}-Cas9 and AAV-gRNAi_{Empty}-TetR-GFP and were put on Dox or control (no Dox) food for 10 or 14 days post-infusion. Animals were then sacrificed and transduced cells within the amygdala were then microdissected and assessed for editing. (B) RFLP analysis of genome editing from BLA tissue transduced with AAV-P_{Mecp2}-Cas9 and AAV-gRNAi_{Tet2}-TetR-GFP or AAV-P_{Mecp2}-Cas9 and AAV-gRNAi_{Empty}-TetR-GFP from mice that were fed a diet that included Dox or a diet that did not include Dox and sacrificed 10 days post viral infusion. Genome editing did not occur in samples that received gRNA_{Empty} as expected. Genome editing did occur in BLA samples that received gRNA_{Tet2} and this genome editing was dependent on Dox administration. Two independent samples per group

are shown. Similar results were observed in at least 3 independent samples per group. (C) RFLP Analysis at day 14 post-infusion showed comparable amounts of editing as compared to the day 10 post-infusion experiments described in (B). One independent sample per group is shown. Similar results were observed in 3 independent samples per group. (D) A comparison of our inducible gRNAi virus was compared to a non-inducible system (gRNA) *in vivo*, following the same timeline for day 10 and 14 as described in (B and C). (E) Quantification of total edited DNA in RFLP experiments revealed a similar degree of editing between the inducible and non-inducible systems. Editing at both day 10 and 14 on Dox was significantly higher when compared to the no Dox group ($* = p = 0.04$, Kruskal–Wallis). Editing after 10 days on Dox with the gRNAi vector compared to the non-inducible vector (gRNA) was not significantly different between the two groups ($ns = p = 0.51$, Kruskal–Wallis). The same was found for the 14 day time point ($ns = p = 0.28$, Kruskal–Wallis).

In our last set of experiments, we wanted to determine the duration animals would need to receive Dox to induce genome editing. Therefore, in these experiments we infused AAV2/DJ8-P_{Mecp2}-Cas9 and AAV2/DJ8-gRNAi_{Tet2} virus into the mouse BLA as described above. In this case, we waited 10 days following the infusion of the virus to administer Dox to the animals. The animals were then taken off Dox 1, 5 or 7 days later. The animals were sacrificed 5 days after Dox was removed from their diet, and the transduced cells within the BLA were microdissected. The genomic DNA was isolated from the tissue and subjected to PCR/RFLP analysis to assess genome editing at the Tet2 locus (Figure 3.6A). PCR/RFLP analysis (Figure 3.6B) revealed that day 1, 5 and 7 time points demonstrated roughly similar levels of editing (3 independent samples per group) (Figure 3.6C). These data indicate that this system requires as little as 1 day on Dox to induce editing. The degree of genome editing within this experiment was roughly comparable to the degree of genome editing obtained with the inducible and non-inducible gRNA viruses utilized in the experiments described in Figure 3.5E.

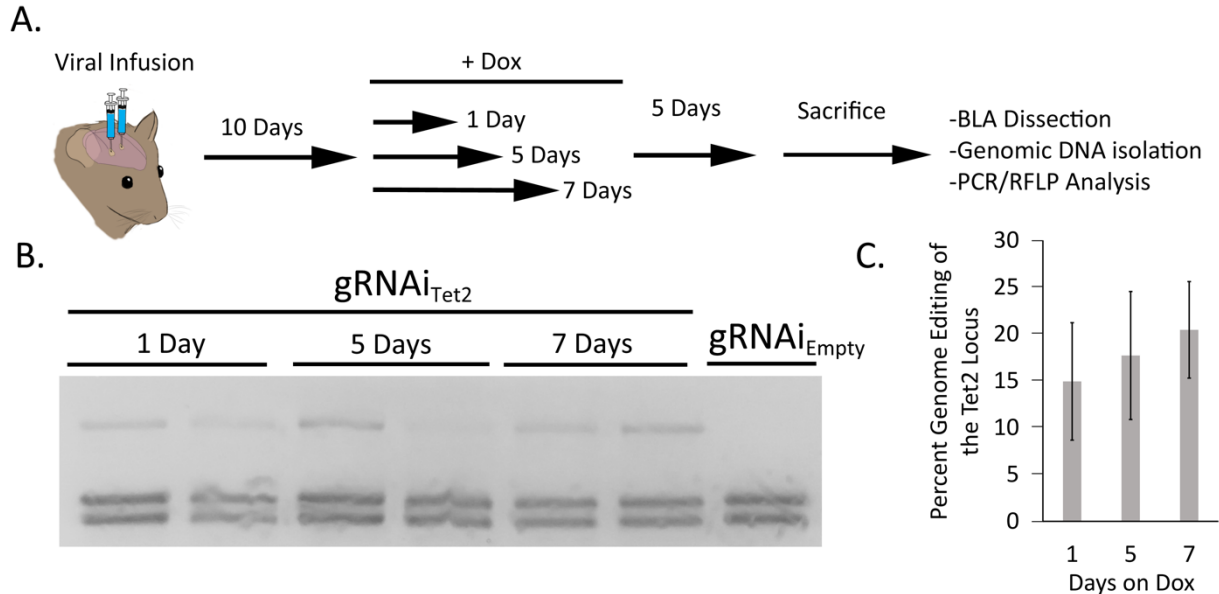


Figure 3.6 Inducible genome editing can be achieved in as little as 1 day on Dox

(A) Timeline from viral infusion to RFLP analysis of genome editing. Animals were infused into the BLA with AAV- P_{mecp2} -Cas9 and AAV-gRNA_{iTet2}-TetR-GFP. Ten days post-infusion animals were placed on Dox food and then Dox food was removed either 1 day, 3 days or 5 days later. Animals were sacrificed 5 days after removal of Dox and the BLA was microdissected and the genomic DNA was isolated and subjected to RFLP/ PCR analysis. (B) RFLP analysis of editing across 1, 5 and 7 days on Dox showed similar levels of editing and no editing in a gRNA_{iEmpty} no Dox control. (C) Quantification of total edited DNA revealed similar editing across days animals were on Dox. These levels of genome editing were very similar to the levels seen during the 10 and 14 day editing time course for the gRNA_i system and the non- inducible system. Percent genome editing was not significantly different between 1, 5 and 7 days on Dox ($p = 0.67$, Kruskal–Wallis).

Discussion

Here, we report the creation of an inducible CRISPR/Cas9 system that can be delivered to cells in vitro and in vivo via AAV. Genome editing in this system is regulated by a doxycycline inducible gRNA. We examined editing in vivo within the mouse brain at 10 days and 14 days post viral infusion and observed a similar level of editing between both time points and the amount of editing was very similar and comparable to a non-inducible system. We also

determined that this system is highly dependent on Dox to initiate genome editing in vitro and in vivo and therefore there does not appear to be any genome editing when Dox is not present. Administering animals Dox containing food for as little as one day (following 10 days post viral infusion) yielded roughly similar levels of genome editing to all other time points tested. We believe this system could be extremely useful for in vivo studies where regulating CRISPR/Cas9 genome editing in a temporally and spatially restricted manner would be beneficial. Certainly, behavioral neuroscience could benefit from this system because it would allow a gene to be knocked out at a specific time point during an ongoing behavioral assay that may span days to weeks.

Initially, we attempted to regulate the expression of Cas9 using a tetracycline response element (TRE) containing promoter; however, we determined that genome editing could not be regulated in a Dox dependent manner, due to the leakiness of Cas9 expression within this system. Some studies have described regulating Cas9 expression utilizing TRE containing promoters in other systems fairly successfully with limited leakiness (Gonzalez et al., 2014; Dow et al., 2015). In these cases, the TRE – Cas9 transgene was stably integrated into the genome, which might reduce the observed leakiness because the transgene copy number may be lower. In comparison, ectopic expression methods such as plasmid transfection and viral transduction, can deliver hundreds to thousands of copies of plasmid or virus, and this may lead to an increase in leakiness, as seen in our experiments since the transgene copy number is so high. It is also possible that the low level Cas9 expression we observed in the non-induced state is driven in part by low level promoter activity from the inverted terminal repeat (ITR), since it's well established that the AAV ITRs can serve as weak promoters for RNA polymerase II (Wang et al., 1999).

Several inducible systems have been developed for CRISPR/Cas9 based systems where either the expression of Cas9 or the gRNA are inducible; however, none of these systems, to date, have been adapted for AAV delivery. Kiani et al. demonstrated that gRNA expression could be regulated from a polymerase II, TRE3G promoter in CRISPRi experiments conducted in HEK293 cells (Kiani et al., 2014). More systems have been developed where Cas9 expression or activity is regulated. One such system is light inducible, in which Cas9 is present in cells in an inactive or incomplete form, and with the addition of light, Cas9 becomes active and is able to complex with the gRNA and edit the target gene in vitro (Nihongaki et al., 2015b). Qi and colleagues developed an anhydrotetracycline (aTc)-inducible Cas9 expression system for use in bacterial CRISPRi experiments (Qi et al., 2013). Davis and colleagues developed a system where inactive Cas9 becomes active in the presence of tamoxifen to enable genome editing (Davis et al., 2015) and Zetsche and colleagues developed an inducible system where Cas9 becomes active upon the addition of rapamycin (Zetsche et al., 2015). The tamoxifen inducible system in its current form would not be amenable to AAV delivery, due to AAV's genome packaging limits and the rapamycin inducible system would not be an ideal system to use in vivo, given rapamycin inhibits the mammalian target of rapamycin (mTOR), which is essential for many cellular processes (Ballou & Lin, 2008; Laplante & Sabatini, 2009) including those for memory formation (Nader et al., 2000).

To our knowledge, this is the first example of an inducible AAV mediated CRISPR/Cas9 system where the expression of the gRNA is regulated in vivo. One of the great features of this system is that the inducible gRNA vector (gRNAi) we developed might be cross compatible with

many existing *S. pyogenes* Cas9 (SpCas9) systems. Coupling our gRNAi AAV vector with these systems may enable them to be inducible as well (i.e. Cas9 mouse, CRISPRi, etc.).

References

- Alexeyev, M.F., Fayzulin, R., Shokolenko, I.N. & Pastukh, V. (2010) A retro-lentiviral system for doxycycline-inducible gene expression and gene knockdown in cells with limited proliferative capacity. *Molecular biology reports*, 37, 1987-1991.
- Azevedo, F.A., Carvalho, L.R., Grinberg, L.T., Farfel, J.M., Ferretti, R.E., Leite, R.E., Jacob Filho, W., Lent, R. & Herculano-Houzel, S. (2009) Equal numbers of neuronal and nonneuronal cells make the human brain an isometrically scaled-up primate brain. *The Journal of comparative neurology*, 513, 532-541.
- Ballou, L.M. & Lin, R.Z. (2008) Rapamycin and mTOR kinase inhibitors. *Journal of Chemical Biology*, 1, 27-36.
- Cong, L., Ran, F.A., Cox, D., Lin, S., Barretto, R., Habib, N., Hsu, P.D., Wu, X., Jiang, W., Marraffini, L.A. & Zhang, F. (2013) Multiplex genome engineering using CRISPR/Cas systems. *Science*, 339, 819-823.
- Davis, K.M., Pattanayak, V., Thompson, D.B., Zuris, J.A. & Liu, D.R. (2015) Small molecule-triggered Cas9 protein with improved genome-editing specificity. *Nature chemical biology*, 11, 316-318.
- Daya, S. & Berns, K.I. (2008) Gene therapy using adeno-associated virus vectors. *Clinical microbiology reviews*, 21, 583-593.
- de Solis, C.A., Holehonnur, R., Banerjee, A., Luong, J.A., Lella, S.K., Ho, A., Pahlavan, B. & Ploski, J.E. (2015) Viral delivery of shRNA to amygdala neurons leads to neurotoxicity and deficits in Pavlovian fear conditioning. *Neurobiology of learning and memory*, 124, 34-47.
- Dow, L.E., Fisher, J., O'Rourke, K.P., Muley, A., Kasthuber, E.R., Livshits, G., Tschaharganeh, D.F., Socci, N.D. & Lowe, S.W. (2015) Inducible in vivo genome editing with CRISPR-Cas9. *Nat Biotech*, 33, 390-394.
- Gilbert, L.A., Larson, M.H., Morsut, L., Liu, Z., Brar, G.A., Torres, S.E., Stern-Ginossar, N., Brandman, O., Whitehead, E.H., Doudna, J.A., Lim, W.A., Weissman, J.S. & Qi, L.S. (2013) CRISPR-mediated modular RNA-guided regulation of transcription in eukaryotes. *Cell*, 154, 442-451.
- Gonzalez, F., Zhu, Z., Shi, Z.D., Lelli, K., Verma, N., Li, Q.V. & Huangfu, D. (2014) An iCRISPR platform for rapid, multiplexable, and inducible genome editing in human pluripotent stem cells. *Cell stem cell*, 15, 215-226.

- Grimm, D., Streetz, K., Jopling, C., Storm, T., Pandey, K., Davis, C., Marion, P., Salazar, F. & Kay, M. (2006) Fatality in mice due to oversaturation of cellular microRNA/short hairpin RNA pathways. *Nature*, 441, 537 - 541.
- Henriksen, J.R., Løkke, C., Hammerø, M., Geerts, D., Versteeg, R., Flægstad, T. & Einvik, C. (2007) Comparison of RNAi efficiency mediated by tetracycline-responsive H1 and U6 promoter variants in mammalian cell lines. *Nucleic Acids Research*, 35, e67-e67.
- Holehonnur, R., Lella, S.K., Ho, A., Luong, J.A. & Ploski, J.E. (2015) The production of viral vectors designed to express large and difficult to express transgenes within neurons. *Molecular brain*, 8, 12.
- Holehonnur, R., Luong, J.A., Chaturvedi, D., Ho, A., Lella, S.K., Hosek, M.P. & Ploski, J.E. (2014) Adeno-associated viral serotypes produce differing titers and differentially transduce neurons within the rat basal and lateral amygdala. *BMC neuroscience*, 15, 28.
- Hommel, J.D., Sears, R.M., Georgescu, D., Simmons, D.L. & DiLeone, R.J. (2003) Local gene knockdown in the brain using viral-mediated RNA interference. *Nature medicine*, 9, 1539-1544.
- Jinek, M., Chylinski, K., Fonfara, I., Hauer, M., Doudna, J.A. & Charpentier, E. (2012) A programmable dual-RNA-guided DNA endonuclease in adaptive bacterial immunity. *Science*, 337, 816-821.
- K.B., F. & G, P. (2007) *The Mouse Brain in Stereotaxic Coordinates* Elsevier, New York, NY.
- Karnan S., O.A., Konishi Y., Wahiduzzaman M., Hosokawa Y., Konishi H. (2016) Improved methods of AAV-mediated gene targeting for human cell lines using ribosome-skipping 2A peptide *Nucleic Acids Res.*, 44, e54.
- Kiani, S., Beal, J., Ebrahimkhani, M.R., Huh, J., Hall, R.N., Xie, Z., Li, Y. & Weiss, R. (2014) CRISPR transcriptional repression devices and layered circuits in mammalian cells. *Nat Methods.* , 11(7), 723-726.
- Laplante, M. & Sabatini, D.M. (2009) mTOR signaling at a glance. *Journal of cell science*, 122, 3589-3594.
- Larson, M.H., Gilbert, L.A., Wang, X., Lim, W.A., Weissman, J.S. & Qi, L.S. (2013) CRISPR interference (CRISPRi) for sequence-specific control of gene expression. *Nature protocols*, 8, 2180-2196.
- Li, X., Zhao, X., Fang, Y., Jiang, X., Duong, T., Fan, C., Huang, C.C. & Kain, S.R. (1998) Generation of destabilized green fluorescent protein as a transcription reporter. *The*

Journal of biological chemistry, 273, 34970-34975.

- Mali, P., Yang, L., Esvelt, K.M., Aach, J., Guell, M., DiCarlo, J.E., Norville, J.E. & Church, G.M. (2013) RNA-guided human genome engineering via Cas9. *Science*, 339, 823-826.
- McBride, J.L., Boudreau, R.L., Harper, S.Q., Staber, P.D., Monteys, A.M., Martins, I., Gilmore, B.L., Burstein, H., Peluso, R.W., Polisky, B., Carter, B.J. & Davidson, B.L. (2008) Artificial miRNAs mitigate shRNA-mediated toxicity in the brain: Implications for the therapeutic development of RNAi. *Proceedings of the National Academy of Sciences*, 105, 5868-5873.
- Nader, K., Schafe, G.E. & Le Doux, J.E. (2000) Fear memories require protein synthesis in the amygdala for reconsolidation after retrieval. *Nature*, 406, 722-726.
- Nihongaki, Y., Kawano, F., Nakajima, T. & Sato, M. (2015a) Photoactivatable CRISPR-Cas9 for optogenetic genome editing. *Nature biotechnology*, 33, 755-760.
- Nihongaki, Y., Kawano, F., Nakajima, T. & Sato, M. (2015b) Photoactivatable CRISPR-Cas9 for optogenetic genome editing. *Nat Biotech*, 33, 755-760.
- Piechota, M., Korostynski, M., Solecki, W., Gieryk, A., Slezak, M., Bilecki, W., Ziolkowska, B., Kostrzewa, E., Cymerman, I., Swiech, L., Jaworski, J. & Przewlocki, R. The dissection of transcriptional modules regulated by various drugs of abuse in the mouse striatum. *Genome Biol*, 11, R48.
- Platt, R.J., Chen, S., Zhou, Y., Yim, M.J., Swiech, L., Kempton, H.R., Dahlman, J.E., Parnas, O., Eisenhaure, T.M., Jovanovic, M., Graham, D.B., Jhunjhunwala, S., Heidenreich, M., Xavier, R.J., Langer, R., Anderson, D.G., Hacohen, N., Regev, A., Feng, G., Sharp, P.A. & Zhang, F. (2014) CRISPR-Cas9 Knockin Mice for Genome Editing and Cancer Modeling. *Cell*, 159, 440-455.
- Qi, L.S., Larson, M.H., Gilbert, L.A., Doudna, J.A., Weissman, J.S., Arkin, A.P. & Lim, W.A. (2013) Repurposing CRISPR as an RNA-guided platform for sequence-specific control of gene expression. *Cell*, 152, 1173-1183.
- Ran, F.A., Cong, L., Yan, W.X., Scott, D.A., Gootenberg, J.S., Kriz, A.J., Zetsche, B., Shalem, O., Wu, X., Makarova, K.S., Koonin, E.V., Sharp, P.A. & Zhang, F. (2015) In vivo genome editing using *Staphylococcus aureus* Cas9. *Nature*, 520, 186-191.
- Roukos, V., Voss, T.C., Schmidt, C.K., Lee, S., Wangsa, D. & Misteli, T. (2013) Spatial dynamics of chromosome translocations in living cells. *Science*, 341, 660-664.
- Sander, J.D. & Joung, J.K. (2014) CRISPR-Cas systems for editing, regulating and targeting genomes. *Nature biotechnology*, 32, 347-355.

- Smyth, J.W., Hong, T.T., Gao, D., Vogan, J.M., Jensen, B.C., Fong, T.S., Simpson, P.C., Stainier, D.Y., Chi, N.C. & Shaw, R.M. (2010) Limited forward trafficking of connexin 43 reduces cell-cell coupling in stressed human and mouse myocardium. *The Journal of clinical investigation*, 120, 266-279.
- Swiech, L., Heidenreich, M., Banerjee, A., Habib, N., Li, Y., Trombetta, J., Sur, M. & Zhang, F. (2014) In vivo interrogation of gene function in the mammalian brain using CRISPR-Cas9. *Nature biotechnology*.
- Tanenbaum, M.E., Gilbert, L.A., Qi, L.S., Weissman, J.S. & Vale, R.D. (2014) A protein-tagging system for signal amplification in gene expression and fluorescence imaging. *Cell*, 159, 635-646.
- Wang, D., Fischer, H., Zhang, L., Fan, P., Ding, R.X. & Dong, J. (1999) Efficient CFTR expression from AAV vectors packaged with promoters--the second generation. *Gene therapy*, 6, 667-675.
- Wang, H., Yang, H., Shivalila, C.S., Dawlaty, M.M., Cheng, A.W., Zhang, F. & Jaenisch, R. (2013) One-step generation of mice carrying mutations in multiple genes by CRISPR/Cas-mediated genome engineering. *Cell*, 153, 910-918.
- Yang, Y., Wang, L., Bell, P., McMenamin, D., He, Z., White, J., Yu, H., Xu, C., Morizono, H., Musunuru, K., Batshaw, M.L. & Wilson, J.M. (2016) A dual AAV system enables the Cas9-mediated correction of a metabolic liver disease in newborn mice. *Nat Biotechnol.*, 34(3), 334-338.
- Zetsche, B., Volz, S.E. & Zhang, F. (2015) A split-Cas9 architecture for inducible genome editing and transcription modulation. *Nature biotechnology*, 33, 139-142.

CHAPTER 4

ADENO-ASSOCIATED VIRAL SEROTYPES DIFFERENTIALLY TRANSDUCE

INHIBITORY NEURONS WITHIN THE RAT AMYGDALA

Authors: Christopher A. de Solis, Matthew P. Hosek, Roopashri Holehonnur, Anwesha Banerjee, Jonathan A. Luong, Lauren E. Jones, Dushyant Chaturvedi, Jonathan E. Ploski

School of Behavioral and Brain Sciences

The University of Texas at Dallas

800 West Campbell Road

Richardson, TX 75080-3021, USA

*Reprinted with permission from Elsevier: *Brain Research*, Volume 1672, October 2017.

Adeno-associated viral serotypes differentially transduce inhibitory neurons within the rat amygdala

Christopher A. de Solis, Matthew P. Hosek, Roopashri Holehonnur, Anwesha Banerjee, Jonathan A. Luong, Lauren E. Jones, Dushyant Chaturvedi, Jonathan E. Ploski

Brain Research, 2017; doi: <https://doi.org/10.1016/j.brainres.2017.07.023>

Abstract

Recombinant adeno-associated viruses (AAV) are frequently used to make localized genetic manipulations within the rodent brain. It is accepted that the different viral serotypes possess differing affinities for particular cell types, but it is not clear how these properties affect their ability to transduce specific neuronal cell sub-types. Here, we examined ten AAV serotypes for their ability to transduce neurons within the rat basal and lateral nuclei of the amygdala (BLA) and the central nucleus of the amygdala (CeA). AAV2 based viral genomes designed to express either green fluorescent protein (GFP) from a glutamate decarboxylase (GAD65) promoter or the far-red fluorescent protein (E2-Crimson) from a phosphate-activated glutaminase (PAG) promoter were created and pseudotyped as AAV2/1, AAV2/4, AAV2/5, AAV2/6, AAV2/7, AAV 2/8, AAV2/9, AAV2/rh10, AAV2/DJ and AAV2/DJ8. These viruses were infused into the BLA and CeA at equal titers and twenty-one days later tissue within the amygdala was examined for viral transduction efficiency. These serotypes transduced neurons with similar efficiency, except for AAV4 and AAV5, which exhibited significantly less efficient neuronal transduction. Notably AAV4 and AAV5 possess the most divergent capsid protein sequences compared to the other commonly available serotypes. We found that the Gad65-GFP virus did not exclusively express GFP within inhibitory neurons, as assessed by fluorescent *in situ* hybridization (FISH), but when this virus was used to transduce CeA neurons, the majority of the neurons that expressed GFP were in fact inhibitory neurons and this was likely due to the fact that this nucleus contains a very high percentage of inhibitory neurons.

Introduction

Within the field of neuroscience, it has become increasingly desirable to genetically manipulate specific subsets of cells within the rodent brain for the study of nervous system function (Josselyn et al., 2001; Ressler et al., 2002; Flint, 2003; Stork et al., 2003). One common method to genetically manipulate specific cells within the brain is to inject recombinant viruses directly into the brain region of interest, to deliver a desired transgene to cells within the targeted region (Koostra & Verma, 2003). Adeno-associated viruses (AAV) are the preferred virus to use for this purpose due to their transduction efficiency, relative ease to produce AAV at high titers suitable for *in vivo* use and the fact that AAV is well tolerated *in vivo*, producing little to no immune response or toxicity (Flotte et al., 1993; Kessler et al., 1996; Peel et al., 1997; Snyder et al., 1997; Lewin et al., 1998; Klein et al., 1999; Buning et al., 2003; Koostra & Verma, 2003; Wright et al., 2003; Daya & Berns, 2008). Different serotypes of AAV exist that possess unique capsid protein sequences, which can influence each serotypes ability to transduce particular types of cells. Notably, it has been discovered that serotypes of AAV vary in their ability to transduce particular cell types within and across differing brain regions. Because of this, there has been interest to identify serotypes of AAV that efficiently transduce specific cell types within brain regions of interest (Chao et al., 2000; Rabinowitz et al., 2002; Wu et al., 2006; Van Vliet et al., 2008), since it is highly desirable to utilize viruses that can target a high percentage of the desired cells within the targeted region.

In this study, we sought to examine whether specific serotypes of AAV transduced neurons within the basal and lateral nuclei of the amygdala (BLA) and the central nucleus of the amygdala (CeA) more efficiently than others. In particular, we were interested in identifying

serotypes of AAV that transduced inhibitory neurons more efficiently than others. This was, in part, due to the fact that the amygdala possesses a complex network of inhibitory neurons that controls amygdala function (Spampanato et al., 2011) and therefore it would be desirable to ascertain which serotypes of AAV transduce this population of cells most efficiently.

The amygdaloid nuclei are highly interconnected to each other but differ greatly in their populations of excitatory and inhibitory neurons and in the genetic expression profiles of their constituent cells, where the greatest differences exist between the BLA and the CeA (Spampanato et al., 2011). The BLA arises from cortical embryological tissues and contains a high concentration of excitatory neurons. The CeA, in contrast, arises from striatal tissues, and contains a relatively high percentage of inhibitory interneurons (Sah et al., 2003; Spampanato et al., 2011). These nuclei work together to regulate emotional learning and expression of emotion (LeDoux, 2000; Maren & Quirk, 2004; McGaugh, 2004; Johansen et al., 2011).

We examined ten AAV serotypes, eight naturally occurring (AAV2/1; AAV2/4; AAV2/5; AAV2/6; AAV2/7; AAV2/8; AAV2/9; AAV2/rh10) (Atchison et al., 1965; Hoggan et al., 1966; Blacklow et al., 1968; Bantel-Schaal & zur Hausen, 1984; Gao et al., 2004), and two created through directed evolution (AAV2/DJ; AAV2/DJ8)(Maheshri et al., 2006; Grimm et al., 2008; Koerber et al., 2008) for their ability to transduce neurons within the rat BLA and CeA. To assess viral transduction of inhibitory neurons we utilized an AAV2 based viral transgene designed to express green fluorescent protein from a glutamate decarboxylase (GAD65) promoter. GAD65 is the product of the GAD2 gene, which is exclusively expressed in inhibitory neurons and catalyzes an intermediary product of glutamate into GABA (Jiang et al., 2009; Marik et al., 2010). In addition, we generated an AAV2 based viral transgene designed to

express a far red fluorescent protein (E2-Crimson) from a phosphate-activated glutaminase (PAG) promoter. PAG is encoded by the GLS2 gene and is required for the conversion of glutamine into glutamate (Chung-Bok et al., 1997; Botman et al., 2014). PAG is expressed within neurons, but it is not exclusively expressed within inhibitory neurons (Van der Gucht et al., 2003). These AAV2 viral transgenes were pseudotyped as AAV2/1; AAV2/4; AAV2/5; AAV2/6; AAV2/7; AAV 2/8; AAV2/9, AAV2/rh10; AAV2/DJ; AAV2/DJ8 and co-infused into the rat BLA and CeA and the degree of viral transduction was examined. For clarity, these pseudotyped viruses will simply be referred to as AAV1, AAV2, AAV4 etc., in the text and the figures.

Materials and Methods

Subjects Adult male Sprague Dawley rats (Charles River Laboratories) weighing 300-400 g were housed individually and maintained on a 12 hr light / dark cycle. Food and water were provided ad libitum throughout the experiment. Animal use procedures were in accordance with the National Institutes of Health Guide for the Care and Use of laboratory animals and were approved by the University of Texas at Dallas Animal Care and Use Committee.

Viral Plasmids The AAV2-PAG-E2-Crimson-3xNLS plasmid was created using standard recombinant DNA techniques. First, the a 3XNLS was PCR amplified from the pDsRed2-Nuc plasmid (Clontech) utilizing the following PCR primers (dsRed2SexAI FP CCCTGAAGCTGAAGGACGGC; dsRed2BsiWI RP acgCGTACGttatctagatccggtggatc) and this PCR product was ligated into the SexAI and BsiWI sites of the AAV2 genome plasmid

harboring a red fluorescent protein gene (dsRed-Express) controlled by a mouse α CaMKII promoter (Addgene plasmid 22908)(Nathanson et al., 2009b), resulting in pAAV2- α CaMKII-dsRed-Express-3XNLS. Subsequently, the dsRed Express coding region was excised via the SpeI and XhoI sites and replaced with the E2-Crimson coding region that had been PCR amplified from pCMV-E2-Crimson (Clontech) utilizing the following PCR primers (Crimson FP SpeICACactagtGCCGCCACCCatggatagcactgagaacgtcatc; Crimson RP XhoI no stop aaaCTCGAGActggaacaggtggtggcgggcctc) to create pAAV2- α CaMKII-E2-Crimson-3XNLS. The α CaMKII promoter was excised from this plasmid by digesting with HindIII, the DNA was blunt ended and then digested with AscI. The 2.4 kb rat PAG promoter was PCR amplified from 2281GALuc 3 plasmid (a generous gift of Norm Curthoys (Rasmussen et al., 2007)), utilizing the following PCR primers (PAG FP2 agcACGCGTCCTCTACCCACTGAGCCATGTCCTAAGTTCCTAATTG; PAG RP2 AscI atcGGCGCGCCagatcctcggggcgtgggcgtc), and ligated into the prepared vector to create pAAV2-PAG-E2-Crimson-3XNLS. The AAV2-GAD65-GFP plasmid was a generous gift from Charles Gilbert and has been previously described (Marik et al., 2010). This plasmid contains a GAD65 promoter spanning -1132 to -90 with respect to the transcriptional start site of the endogenous Gad2 gene. AAV packaging plasmids (pRC) for different serotypes were obtained from: AAV1, AAV5 (Nicholas Muzyczka, University of Florida), AAV2, AAV4, AAV6, AAVDJ and AAVDJ8 (Cell BioLabs, Inc), AAV7, AAV8, AAV9, and AAVrh10 (Penn Vector Core, University of Pennsylvania).

Sequence analysis To produce the phylogenetic tree and sequence similarity/divergence table for the AAV serotype VP1 capsid proteins, the VP1 amino acid sequences for each serotype were imported into Lasergene/MegAlign Software (DNASTAR, Inc.) and aligned using the Clustal method and the pair-wise sequence distances were computed using the Clustal method with a PAM250 residue weight table, as described in a previous study (Holehonnur et al., 2014).

Virus production, purification and titering AAV2 viral genomes harboring a PAG-E2-Crimson (RFP) and GAD65-eGFP transgenes were pseudotyped as either AAV2/1, AAV2/4, AAV2/5, AAV2/6, AAV2/7, AAV 2/8, AAV2/9, AAV2/rh10, AAV2/DJ, and AAV2/DJ8 using a triple-transfection, helper-free method, in 293FT cells via a calcium – phosphate mediated transfection method, as previously described (Holehonnur et al., 2014). The resultant viruses were purified on an iodixanol step gradient and filtered/concentrated using Amicon Ultra-15 Centrifugal Filter Units (Millipore) resulting in viruses suspended in PBS-MK (1×PBS without calcium or magnesium, 1 mM MgCl₂, 2.5 mM KCl) (Hommel et al., 2003). DNase resistant viral titers were determined using a quantitative-PCR based method and the final viral titers were computed based on the standard curve and reported as genome copies (GC)/mL as previously described (Holehonnur et al., 2014). Quantitative-PCR for the AAV2-Gad65-GFP viral genome was performed with GFP Primer/Probe (ID# Mr04329676_mr, Invitrogen). The AAV2-PAG-E2-Crimson viral genome qRTPCR was performed with the following DNA primers, (FP AGCGCGTGATGAACTTCGA; RP GCCGATGAACTTCACGTGGTAGAT; 6FAM-ACCCAGGACTCCTCC Probe). A subset of these viruses were examined via western blot for appropriate VP1, VP2, and VP3 protein (Figure 4.1).

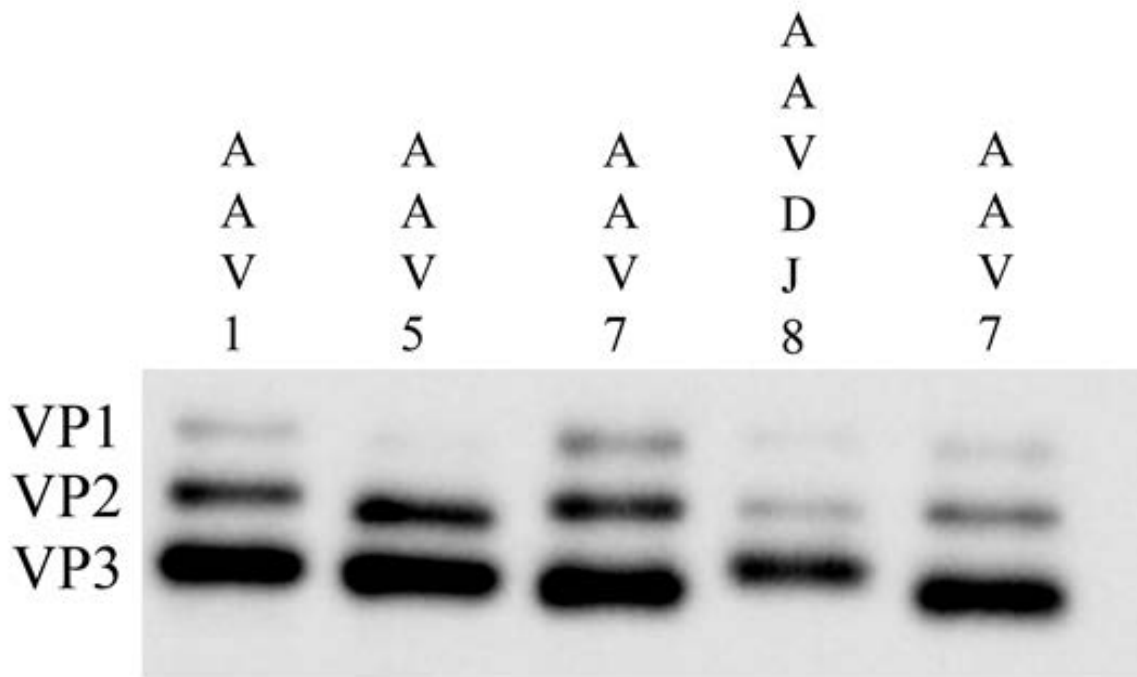


Figure 4.1 Western blot detection of VP1, VP2 and VP3.

1.0E+10 viral particles of AAV1, AAV5, AAV7 and AAVDJ8 were resolved on an SDS-PAGE gel and transferred to an immobilon PVDF membrane. An additional AAV7 sample was included from a separate viral preparation. The membrane was blocked with 4% Non-fat milk for 1 hr at RT. The membrane was then incubated with a primary antibody designed to detect VP1, VP2 and VP3 (ARP, #03-65158; 1:500) in 1% BSA in TBST overnight at 4C. The membrane was then incubated with an anti-mouse HRP secondary (Cell Signaling, #7076; 1:20000) in 5% non-fat milk in TBST for 1 hr at RT.

Viral infusion Twenty-eight gauge custom infusion cannulas (C315G, PlasticsOne) were inserted into polyethylene tubing (I.D. 0.0150 in, O.D. 0.043 in, wall thickness 0.0140 in)(A-M systems, Inc.) that were ~50 cm in length. These tubes were first backfilled with 1 x phosphate buffered saline, pH 7.4 (PBS), followed by sesame oil so that the ~5 cm closest to the infusion needle contained PBS and the rest of the infusion line was filled with sesame oil. These lines were then connected to 2 µl, 23-gauge (88500) stainless steel Hamilton syringes (Hamilton Company). Under a mixture of ketamine (100 mg/kg) and xylazine (10.0 mg/kg) anesthesia, rats

were stereotaxically implanted bilaterally, targeting the BLA [AP -2.9, ML \pm 4.7, DV - 8.6] or CeA [AP -2, ML \pm 4, DV -8.3]. The Gad65-GFP and PAG-RFP viruses were mixed using the appropriate volumes/concentrations so that the final titers of each virus would be 1.6E+12 GC/mL and 0.7 μ L was infused into the BLA and 0.4 μ L was infused into the CeA over a period of 10 minutes. Needles remained inside the target area for an additional ten minutes to allow diffusion of the virus away from the infusion site. Needles were then slowly withdrawn and the incision was closed using 9 mm wound clips (Mikron Precision, Inc.). Animals were allowed one-week recovery before clips were removed using a wound clip remover (Mikron Precision, Inc.). Three weeks post infusion, the rats were anesthetized with an overdose of chloral hydrate (250 mg/kg) and then perfused with a solution of phosphate-buffered saline (1 \times Phosphate buffer, 150 mM NaCl) and 10% buffered Formalin (Fisher Scientific). The brains were fixed in 10% formalin for 4-5 hours followed by cryoprotection in 1 \times PBS pH 7.4 and 30% sucrose for 4-6 days. Some of the animals were perfused with 4% paraformaldehyde, so immunohistochemistry could be performed on the tissue and these were distinct animals that were not utilized for quantification of AAV viral transduction efficiency.

Imaging and quantification of viral transduction Imaging and quantification was essentially performed as previously described (Holehonnur *et al.*, 2014). Following cryoprotection, the brains were frozen and 40 μ m coronal sections were obtained using a cryostat. Collected tissues included the entire amygdala (Bregma -4.16 to -1.50). Approximately 50-60 sections were taken per amygdala. Every alternate section was placed on Superfrost slides (Fisherbrand). Of these sections, every section that contained transduced cells was used for imaging and quantification of

viral transduction where optical density (OD), viral spread and viral transduced cell count was determined. The sections on superfrost slides were imaged using an Olympus IX51 inverted fluorescent microscope under GFP, RFP, and bright field filters at 40x magnification. All images were acquired using an Olympus DP72 Digital Camera and Cellsens software (Olympus) and images that were used for quantitation of GFP or RFP were all taken under the same exposure conditions respectively. Specifically, 40x GFP/RFP images were captured using the following settings: camera lens magnification: 2x, microscope objective: 4x, 2500 ms exposure time, ISO 400, CellSens Image Capture: 4140x3096 tiff, 8-bit RGB color, CCD Enhancements: Gamma +1, Sharpness +2, Contrast +2, no enhancements to white balance. Quantification was carried out using ImageJ software (<http://imagej.nih.gov>) to record the optical density (OD) and viral spread of transduced areas (μm^2), as well as a count of cells transduced above a minimum threshold level. OD was calculated by subtracting the background mean optical density (OD) from the mean OD of the total area transduced in each slice to create the OD of transduction per slice. OD of total transduction was calculated for every slice and averaged across all slices per amygdala to yield total OD of transduction per amygdala and this value was averaged among all amygdala that were infused with a particular serotype exhibiting transduction to yield Mean OD of viral transduction per serotype. The spread of transduction per amygdala was recorded as the sum of total area transduced in all slices per transduced amygdala and this value was averaged among all amygdala infused with a particular serotype exhibiting transduction to yield Mean Viral Spread per serotype. The mean viral transduction (Area*OD) per slice was calculated by subtracting the background mean optical density (OD) from the mean OD of the total area transduced in each slice to create the OD of transduction per slice. This value was multiplied by the total area

transduced within each slice, measured in μm^2 to yield a measure of total viral transduction per slice. The total viral transduction per amygdala was recorded as the sum of all measures of total viral transduction per slice per amygdala and the total viral transduction per serotype was reported as the mean total viral transduction of all amygdala that were infused with a particular serotype exhibiting transduction. Cell counts were obtained by first converting images to grayscale 8 bit and applying background subtraction function with a rolling ball radius of 50 pixels. Next, the threshold was set to 27 for the lower level and 255(max) for the higher level. The watershed function was applied and the cells within each image were counted. To determine the best ImageJ settings for counting transduced cells, the threshold for brightness, or intensity of fluorescence, was first reduced from the maximum value until the transduced cells in the images with the highest intensity and density were capable of being distinguished as individual units both by human and software analysis following the binary conversion. This was then checked against manual cell counts of the unaltered images to ensure that all visibly transduced cells were being counted accurately. This was considered to be the maximum usable threshold value. This value was then lowered incrementally until the minimum threshold value was reached, below which some cells that exhibited only minimal transduction began to disappear from the binary-converted images. The minimum value was then checked against other serotypes, including those of AAV4 and AAV5, many of which did not visibly fluoresce at the exposure times used to capture serotypes with higher-efficiency transduction. This method for determining threshold is the same one used in a previous study carried out by our lab, (Holehonnur *et al.*, 2014). The threshold value, therefore, can be considered as being standardized to the samples that exhibited the highest intensity of expressed fluorescent reporter protein. This value was used across all

samples and was found to be similarly accurate between cell counting analysis of both eGFP and E2Crimson.

OD, viral spread and transduced cell counts were collected both from the entirety of transduced tissue for each slice and referred to as “Total” and within the boundaries of the targeted BLA or CeA nuclei only and referred to “BLA Only” or “CeA only”. This was necessary since in these types of experiments, one will never exclusively target neurons in such small nuclei such as the BLA or CeA and therefore to assess viral transduction accurately one must take into account all viral transduction per coronal slice across the anterior-posterior axis (i.e., total).

Immunohistochemistry AAV2-Gad65-GFP and AAV2-PAG-E2-Crimson3xNLS were co-infused into the CeA at a titer of $1.6E + 12$ GC/mL as described above. Twenty-one days post infusion, the animals were anesthetized and perfused with 4 % paraformaldehyde in $1 \times$ PBS (pH = 7.4), the brains were extracted and fixed in 4% paraformaldehyde in $1 \times$ PBS (pH = 7.4) for 4-5 hrs and cryoprotected in $1 \times$ PBS pH7.4, 30% sucrose for 4-6 days. Following cryoprotection, 40 μ m coronal sections containing the CeA were blocked for 30 mins in blocking buffer ($1 \times$ PBS, 3% normal donkey serum, 0.3% Triton X-100) and incubated overnight 4°C with NeuN Antibody (1:500; MAB377 Millipore, Billerica, MA), diluted in blocking buffer. For secondary antibody staining 1:200 dilution of Alexa Fluor 350 conjugated anti-Mouse IgG (A20149; Thermofisher Scientific) was used and the slices were incubated for 2 hr at room temperature. Following this, the slides were cover-slipped with Vectashield HardSet Mounting Medium (Vector Laboratories) and IHC images were captured at 100 \times magnification using an Olympus

BX51 upright fluorescence microscope with an Olympus DP71 Digital Camera and DP manager software. For quantification, the number of GFP or E2 crimson cells that also co-localized with the NeuN Alexa Fluor 350 signal within an area of 135173.56 μm^2 from within the CeA of each slice was examined. The area within each slice quantified typically contained ~ 40 GFP/E2 crimson positive cells and a total of three slices were counted per serotype. Cells were manually quantified using Adobe Photoshop CS5 software and the colocalization results were reported as a percentage of total GFP/E2 crimson cells counted. Variability in co-localization results between slices was reported as standard error of the mean.

Double fluorescence in situ hybridization (FISH) Probe design: The entire rat GAD65 coding region (1966bps) was PCR amplified from rat cDNA utilizing the following DNA primers (FP GCTCTGGGGACTCTGAGAACCCGG; RP GTTGCTGCAGGGTTTGAGATGACCATGC), and cloned into the pCR4 TOPO vector using a TA cloning kit (Invitrogen, #450030). The full length GFP sequence (714 bps) was PCR amplified from plasmid DNA utilizing the following DNA primers (FP aaaactagtACCATGGTGAGCAAGGGCGAGGAG; RP atccCTCGAGttactgtacagctcgccatgccg), and cloned into the pCR4 TOPO vector using the same kit as above. Antisense-RNA probes, of the GAD65 and GFP sequences were prepared from these plasmids utilizing a MAXIscript T7/T3 transcription kit (Ambion, #AM1324). The GAD65 probe was labeled with UTP-digoxigenin (Roche, # 11209256910). The GFP probe was labeled with UTP-biotin (Roche, #11388908910). Tissue preparation: rats were infused bilaterally with AAV-Gad65-GFP (AAV2/1, AAV2/7 or AAV2/DJ8) into the BLA (0.7 μl) and the CeA (0.4 μl) at a titer of

1.60E+12 GC/mL. Twenty-one days post-infusion, brains were rapidly flash frozen using powdered dry ice. Twenty-micron coronal sections containing the amygdala containing GFP signal within the BLA (n = 3/serotype) and CeA (n = 3/serotype) were taken on slides (Fisher, #1255015) from 6 individual brains. Fluorescent in situ hybridization and detection: prior to hybridization, sections were fixed in 4% PFA (in 1 x PBS, pH 7.4) for 5 min, rinsed in 2 x SSC (AmericanBio, #AB13156) for 2 min, acetylated in 0.50% acetic anhydride (Sigma, #320102) in 1.5% triethanolamine (Sigma, #90276) for 10 min and then treated with 1:1 acetone (Sigma, #270725) : methanol (Fisher, #A412) for 5 min. Pre-hybridization was performed at 56 C for 1 hr in hybridization buffer ((50% formamide (AmericanBio, #AB00600), 5 x SSC, 1.25 x denhardt's solution (AmericanBio, #AB03075), 250 µg/mL (Sigma, #D1626), E. coli tRNA (Sigma, #R1753), 500 µg/mL salmon sperm and 5% dextran sulfate (AmericanBio, #AB00426)). Sections were hybridized overnight (12-14 hr) in hybridization buffer containing 100 ng of GAD65 probe and 100 ng of GFP probe. Post-hybridization washes (2 x SSC 5 min, 2 x SSC 10 min) were followed by treatment with RNAse (10 µg/mL; Fisher, #BP2539) for 15 min at 37 C. Following 2 x 5 min washes in 2 x SSC, sections were placed in 0.5 x SSC for 10 min, followed by a 30 min incubation in 0.5 x SSC at 56 C. After 2 x 5 min washes in RT 0.5 x SSC, sections were incubated in 2 x SSC containing 3% hydrogen peroxide to inhibit endogenous peroxidases and eliminate endogenous GFP signal. Sections were then washed twice in 2 x SSC for 5 min before being placed into TBS (0.01 M Tris-HCL, 0.1 M NaCl, pH 7.5) for 5 min. Sections were blocked with 2 % blocking buffer (Roche, #11096176001) in TBS, containing 5 % goat serum for 30 min, followed by a 2 hr incubation in anti-DIG-HRP (1:200, Perkin, NEF832001EA). Sections were then washed 3 x in TBS-T (TBS containing 0.05 %

Tween 20, pH 7.5) for 5 min, followed by a 30 min incubation with Cy3 in 1 x amplification buffer (1:50; TSA Plus Cyanine 3 System, Perkin Elmer, # NEL744001KT). After 3 x wash in TBS-T for 5 min each, samples were quenched in 3 % H2O2 in TBS for 30 min. After 2 x 5 min washes in TBS, sections were incubated in streptavidin-HRP (TSA kit #22, Life Technologies, #T20932), 1:100 in blocking buffer for 1 hr, followed by 3 x wash in TBS-T for 5 min each. Sections were then incubated with alexa-fluor 488 in amplification buffer containing 0.0015% H2O2 (1:50; TSA kit #22, Life Technologies, #T20932) for 30 min, followed by 3 x wash in TBS-T for 5 min each. Slides were then cover-slipped with Vectashield HardSet Mounting Medium (Vector Laboratories). Quantification: individual samples consisted of three 20 μM sections spaced a considerable distance apart within the same amygdala. Images were taken at 100 x magnification (Olympus BX51 microscope, Olympus DP71 Digital Camera and DP manager software). Quantification of overlapping signal of GAD65 mRNA and GFP mRNA was done with Adobe Photoshop CS5. The number of GAD65 positive cells and GFP positive cells were manually counted within an area of 135173.56 μm^2 of the BLA or CeA and the number reported is the percent overlap. For determining the percentage of Gad65 positive cells within a specified region of the BLA or CeA, all DAPI positive and Gad65 mRNA positive cells were counted within an area of 95236 μm^2 and were used to determine the percentage of inhibitory neurons within the region. For quantification for GFP positive cells within the BLA or CeA, all DAPI and GFP mRNA positive cells were counted within an area of 95236 μm^2 and this data was used to determine of percentage of cells that were transduced and expressing GFP from a GAD65 promoter within the BLA or CeA.

Statistics A One-Way ANOVA was used to compare differences between serotypes in spread, total viral transduction, and cell count. Post hoc analysis was performed using Fisher's PLSD.

Results

AAV serotypes exhibit differential transduction efficiency of rat BLA neurons

Serotypes of AAV possess differing capsid proteins, which determine each serotype's ability to transduce particular cell types (i.e., tropism). The AAV capsid is composed of three different proteins: Virion Proteins 1, 2, 3 (VP1, VP2 and VP3). Of these, VP1 is the largest capsid protein of the three, while VP2 and VP3 are produced through differences in splicing and translation initiation (Van Vliet et al., 2008) (Wu et al., 2006). Among the most commonly used AAV serotypes utilized in biomedical science, AAV4 and AAV5 possess the most divergent capsid proteins (Figure 4.2A, 4.2B), indicating that these serotypes might exhibit significantly differing tropism compared to the other serotypes.

To determine whether different AAV serotypes transduce neurons within amygdala nuclei (Figure 4.2C), in a differential manner, viruses were created that were designed to harbor either a transgene intended to express eGFP from a GAD65 promoter or a transgene intended to express E2-Crimson (far-red fluorescent protein) from a PAG promoter. The Gad65-eGFP virus was chosen because it should primarily express eGFP within GAD65 positive inhibitory neurons (Marik et al., 2010). The second virus containing the PAG-E2-Crimson transgene should express E2-Crimson (RFP) in inhibitory and excitatory neurons. The E2-Crimson was chosen to avoid the RFP signal from being detected in the GFP channel during fluorescence microscopy (Strack

et al., 2009). To further enhance the distinction between RFP- and GFP- signals, a nuclear localization sequence (NLS) was added to the E2-Crimson transgene.

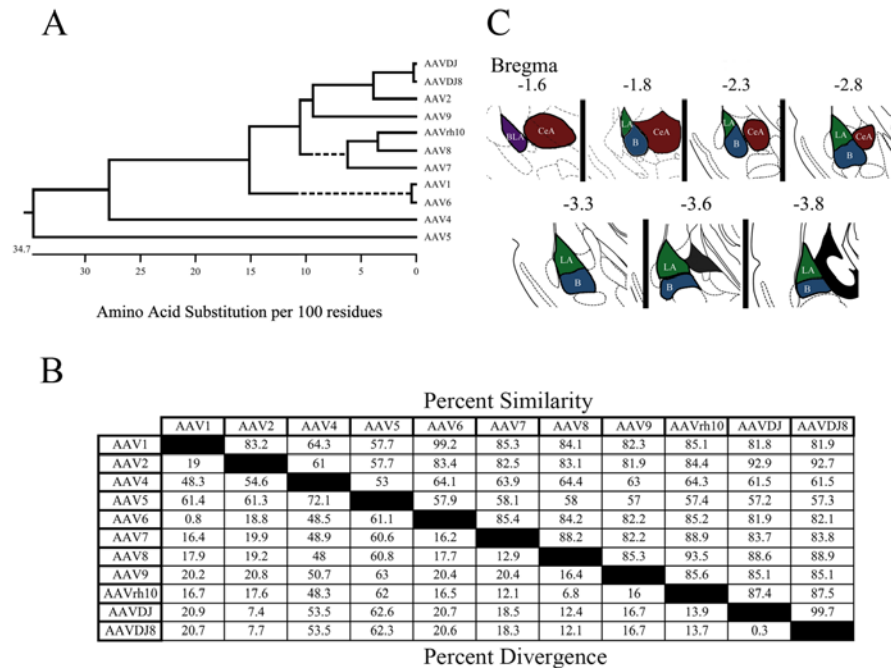


Figure 4.2. AAV VP1 capsid proteins exhibit divergent sequences.

(A) Phylogenetic tree detailing evolutionary divergence of VP1 capsid proteins of commonly used AAV serotypes. (B) Table outlining percentage similarity and divergence among AAV VP1 capsid protein sequences. (C) Anatomy of amygdaloid nuclei targeted within this study. Basal and lateral Amygdala complex (BLA; Purple), Basal Nucleus (B; Blue), Lateral Nucleus (LA; Green), Central Nucleus (CeA; Red).

In our first experiment, AAV2 based Gad65-eGFP and PAG-E2-Crimson viral genomes were pseudotyped as AAV1, AAV4, AAV5, AAV6, AAV7, AAV8, AAV9, AAVrh10, AAVDJ, and AAVDJ8. Each GAD65-eGFP and PAG-E2-Crimson virus of a particular pseudotype were mixed so each virus was at a titer of 1.60×10^{12} GC/mL and 0.7 microliters of virus was infused into the BLA (number of amygdala included in the analyses = $n = \text{AAV4} = 4$; AAV6, AAV7, AAV8 = 5; AAVrh10 = 6; AAV1, AAV5 = 7, AAV9 and AAVDJ = 8; AAVDJ8 = 10).

Twenty-one days later, the animals were perfused, the brains were dissected and coronal brain sections were taken and examined via fluorescence microscopy. Representative images depicting brightfield, RFP and GFP expression within the BLA from viral transduced tissue for each serotype are depicted in Figure 4.3. Most of the serotypes exhibit similar levels of expression/transduction for both the GFP and RFP viruses, however, AAV4 and AAV5 exhibit strikingly obvious reduced expression/transduction compared to the other serotypes for both the GAD65-GFP and PAG-E2-Crimson viruses. The transduction efficiency of each virus was evaluated by quantifying the spread and intensity of fluorescence (OD), as well as the number of cells transduced above a threshold brightness level for RFP and GFP. A measure of efficiency of transduction was calculated by multiplying the mean optical density (OD) of transduced tissue by the area over which viral transduction was observed, and this was reported as Mean Viral Transduction. Because viral infusions into the rodent brain do not typically entirely localize viral transduction to the intended target region, we specifically report these measurements that were obtained by quantifying expression in the entire transduced region in each examined amygdala-containing coronal slice (see Methods) and we refer to these measurements as “Total”. We also report these measurements that were obtained from viral transduction that occurred solely within the boundaries of the BLA and we refer to these measurements as “BLA Only”. The Total and BLA only measurements are graphed side-by-side in the figures (see Figure 4.4).

The different serotypes of AAV harboring the GAD65-GFP transgene exhibited differing levels of transduction compared to one other, but most did not significantly vary. AAV5-Gad65-GFP exhibited significantly lower “total” spread and OD compared to all other serotypes examined ($p < 0.05$). AAV5-Gad65-GFP exhibited significantly lower mean transduction

compared to all other serotypes except AAV1 ($p = 0.0686$) and AAV9 ($p = 0.0611$), but there was a trend toward significance. AAV5-Gad65-GFP exhibited significantly lower cell count than AAV6, AAV7, AAVrh10 and AAVDJ8 ($p < 0.05$), and there was a trend toward significance for AAVDJ ($p = 0.0539$). AAV7-Gad65-GFP exhibited significantly greater “total” cell count than all other serotypes ($p < 0.05$). AAV7-Gad65-GFP exhibited significantly greater “total” mean transduction compared to all other serotypes ($p < 0.05$), except for AAV8 ($p = 0.1332$).

For measures taken solely within the boundaries of the BLA, AAV5-Gad65-GFP exhibited significantly lower “BLA” spread compared to AAV7, AAV8, AAVrh10, AAVDJ, and AAVDJ8 ($p < 0.05$). AAV5-Gad65-GFP exhibited significantly lower “BLA” OD compared to all serotypes ($p < 0.05$), except AAV1, but there was a strong trend towards significance ($p = 0.0579$). AAV5-Gad65-GFP exhibited significantly lower “BLA” mean transduction compared to all other serotypes ($p < 0.05$), except AAV9 ($p = 0.1445$). AAV5-Gad65-GFP exhibited significantly lower “BLA” cell count compared to all other serotypes ($p < 0.05$), except AAV1, AAV8, and AAV9.

The AAV viruses harboring the PAG-E2-Crimson transgene exhibited a similar trend for transduction as compared to the AAV-GAD65-GFP viruses. Notably, AAV4 and AAV5-PAG-E2-Crimson viruses transduced BLA neurons less efficiently compared to the other serotypes and this was strikingly obvious. AAV5-PAG-E2-Crimson exhibited significantly lower “total” viral spread than AAV7, AAV8, AAV9, AAVrh10 and AAVDJ8 ($p < 0.05$), and there was a trend for lower spread for AAV1 ($p = 0.0713$) and AAV6 ($p = 0.0725$). AAV5-PAG-E2-Crimson exhibited significantly lower “total” OD for AAV8, AAVDJ and AAVDJ8 ($p < 0.05$), and there was a trend for lower OD for AAV9 ($p = 0.0524$). AAV5-PAG-E2-Crimson did not significantly

vary from the other serotypes for measures of “total” mean viral transduction ($p > 0.05$), however, it did exhibit significantly less total cell count compared to all other serotypes examined ($p < 0.05$), except for AAVDJ ($p = 0.1456$). For measures taken solely within the boundaries of the BLA, AAV5-PAG-E2-Crimson did not significantly differ from all other serotypes for BLA only mean transduction or BLA only viral spread ($p > 0.05$). AAV5-PAG-E2-Crimson did exhibit significantly lower BLA only OD, as compared to AAV8, AAVDJ and AAVDJ8 ($p < 0.05$) and significantly lower BLA only cell count as compared to AAV6, AAV7, AAV8 and AAVDJ ($p < 0.05$). We suspect that some of these measures were not statistically significant, because the nuclear localized E2-Crimson, was overall more difficult to detect than the Gad65-GFP using these methods resulting in measurements that were lower in magnitude.

While AAV4-GAD65-GFP and AAV4-PAG-E2-Crimson did exhibit some viral transduction as shown in Figure 4.5, at the titers and volumes infused, fluorescence was below the detectable threshold of the software parameters used to quantify transduction. Revising parameters to detect lower levels of fluorescence produced by AAV4 as well as increasing exposure times for images were implemented but resulted in erroneous data when applied to the other serotypes that exhibited more robust transduction at the same titers and volumes. Therefore, while it was obvious that AAV4-GAD65-GFP and AAV4-PAG-E2-Crimson viruses exhibited lower transduction to the other serotypes examined (similar to AAV5), AAV4 was not quantified and therefore it was not included in the statistical analysis.

Magnification of merged BLA images for viral expressed GFP and E2-Crimson, clearly depict partially overlapping expression of the Gad65-GFP and PAG-E2-Crimson transgenes. The E2-Crimson can clearly be seen as being localized to the nucleus (Figure 4.5). To further validate

that AAV5 exhibited lower transduction efficiency compared to the other serotypes, another batch of virus was produced for AAV5-Gad65-GFP and AA7-Gad65-GFP viruses and 0.7 microliters of virus was infused into the BLA at a titer of $1.60e + 12$ GC/mL or at a high titer of $1.0e + 13$ GC/mL ($n = 3$ per condition). Twenty-one days later, the animals were perfused and coronal brain slices containing the BLA were examined for viral transduction via fluorescence microscopy. Representative images are shown in Figure 4.6. AAV5-Gad65 exhibited obvious reduced GFP expression/viral transduction as compared to AAV7-Gad65-GFP which is consistent with our first experiment.

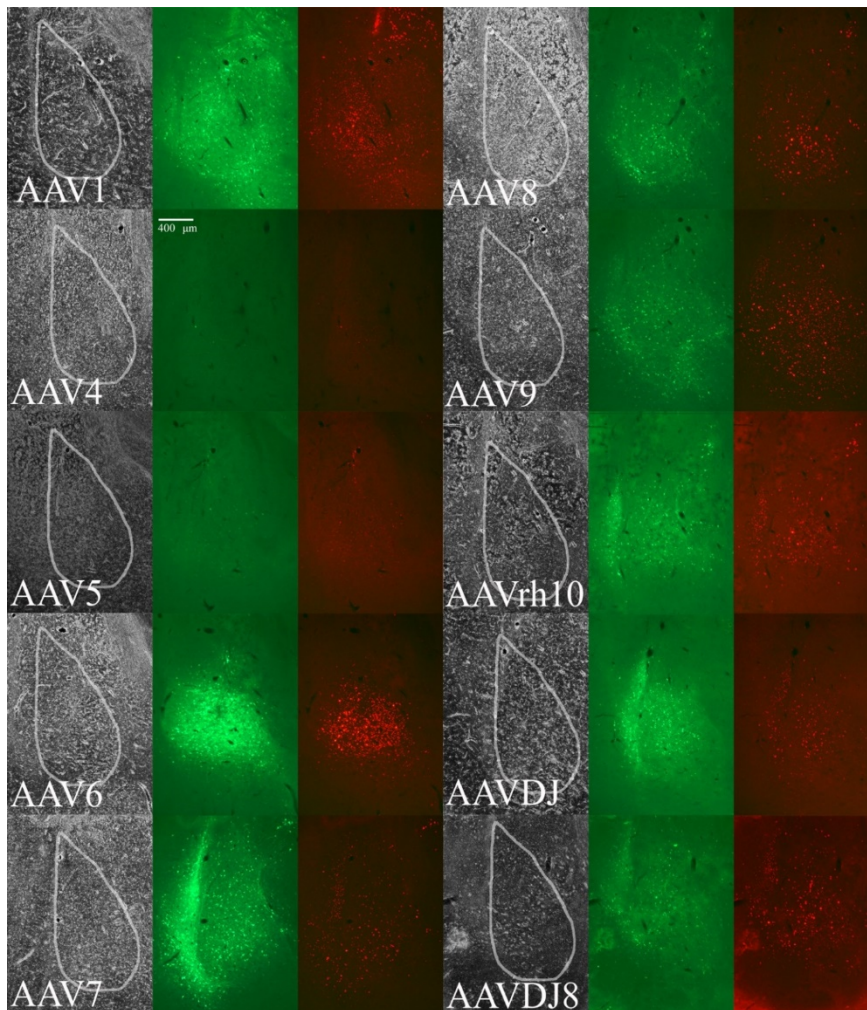


Figure 4.3 Representative images of BLA viral transduction of AAV serotypes using AAV-Gad65-GFP and AAV-PAG-RFP.

Rats were infused with a mixture of both AAV-Gad65-GFP and AAV-PAG-RFP into the BLA at the same titer (1.60E 12 GC/mL). Representative images depicting BLA viral transduction for each serotype. From left to right: bright field image of the BLA, AAV-Gad65-GFP, AAV-PAG-RFP. The location of the BLA is outlined in the brightfield image. The scale bar = 400 μ m.

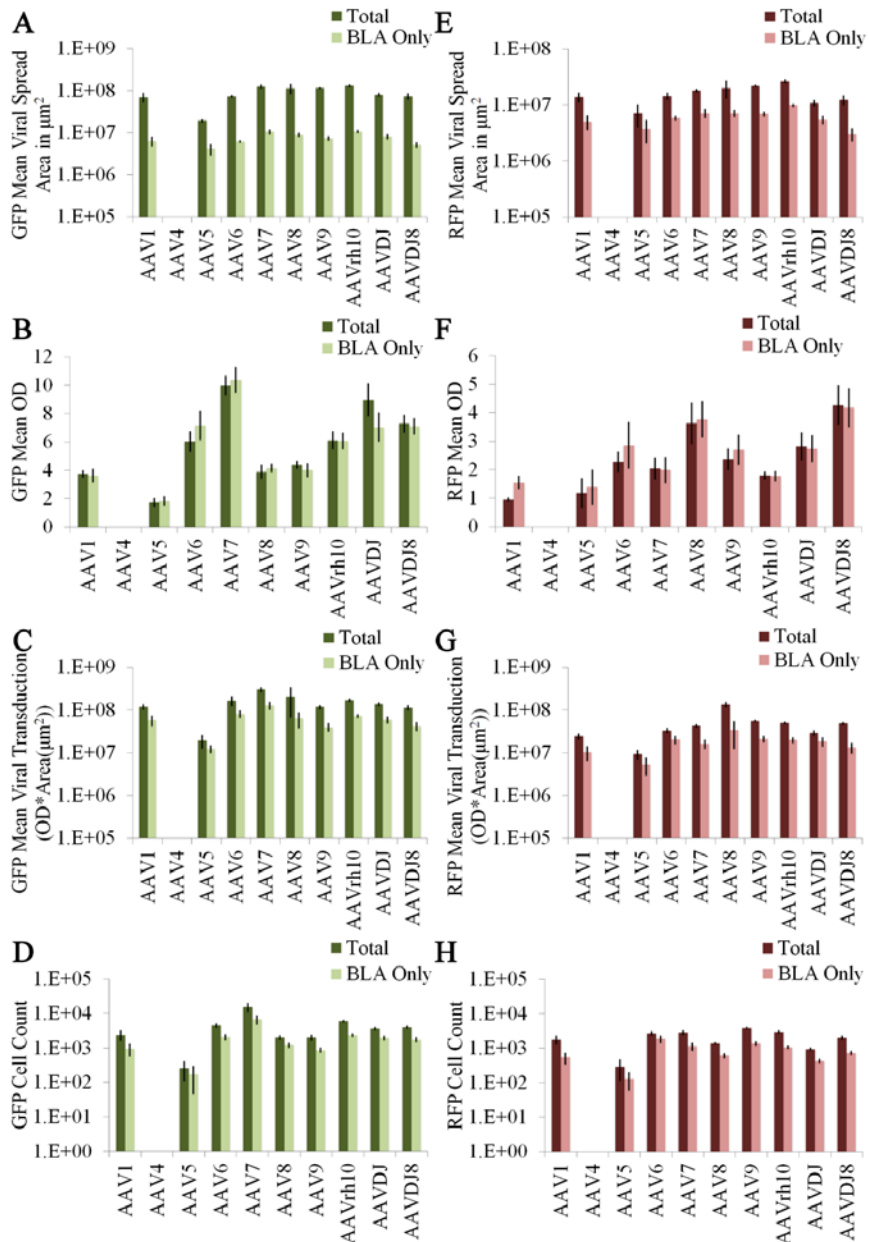


Figure 4.4 AAV serotypes exhibit differential transduction of BLA neurons.

Rats were infused with both AAV-Gad65-GFP and AAV-PAG-RFP into the BLA at a titer of $1.60E12$ GC/mL. Total viral spread, brightness of GFP and RFP and total count of cells transduced was quantitated and groups means were graphed for Total and BLA only measurements. (A) GFP Total Viral Spread, Area (μm^2). (B) GFP Mean Optical Density, Mean OD. (C) GFP Mean Viral Transduction, (OD*Area (μm^2)). (D) GFP Positive Cell Count. (E) RFP Total Viral Spread Area (μm^2). (F) RFP Mean OD. (G) RFP Mean Viral transduction (OD*Area (μm^2)). (H) RFP Positive Cell Count.

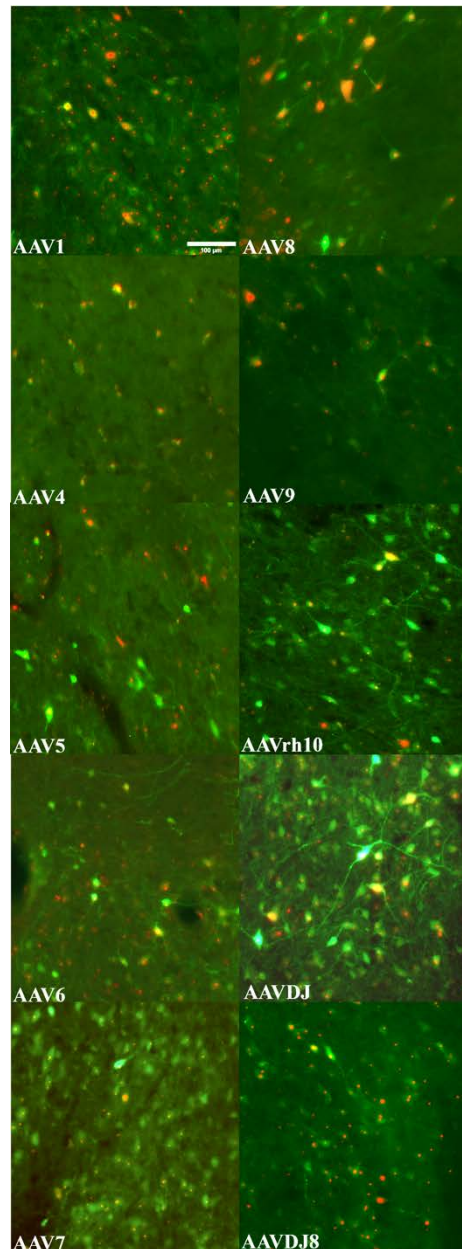


Figure 4.5 Magnified merged images depicting BLA cells positive for GFP (AAV-Gad65-GFP) and cells that are positive for RFP (AAV-PAG-RFP).

BLA cells co-expressing eGFP under the GAD65 promoter and E2 crimson under the control of the PAG promoter. 100x magnification of red- and green-fluorescence microscopy in the BLA merged into a single, overlaid image. Exposure times were not kept constant across the images. Scale bar = 100 μ m.

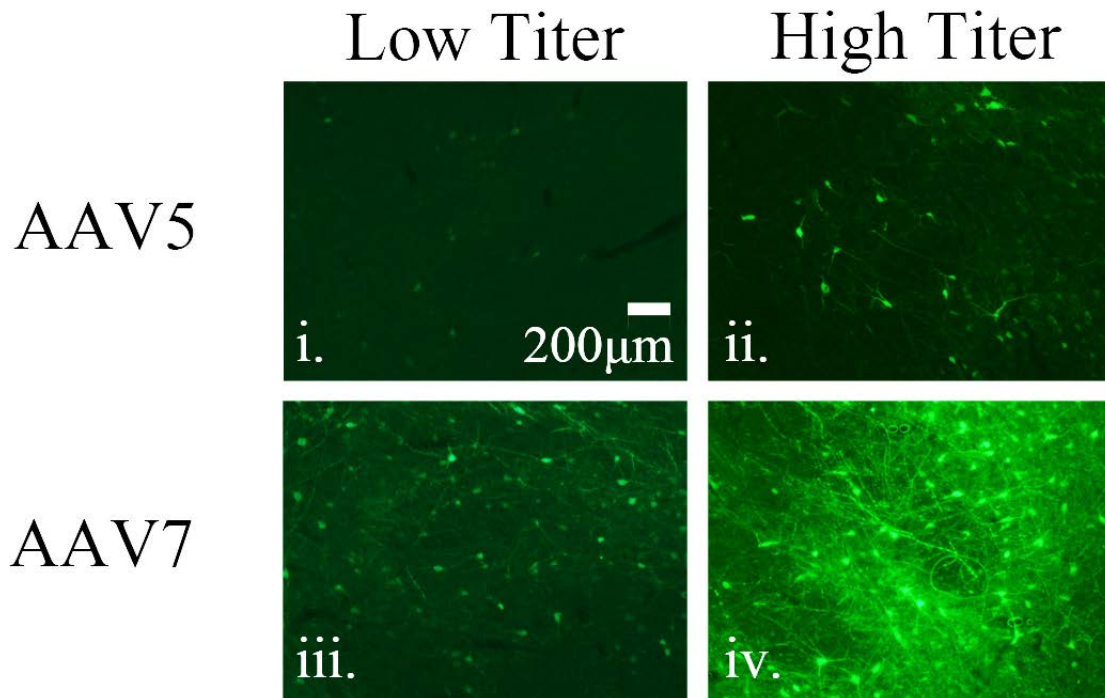


Figure 4.6. Representative images indicate that AAV5 serotype displays poor transduction efficiency at a low and high titer, compared to AAV7.

AAV-Gad65-GFP was pseudotyped as AAV5 and AAV7 and these were infused into the BLA and evaluated qualitatively 21 days later for viral transduction (i.) Low titer AAV5 ($1.6E+12$ GC/mL) (ii.) High titer AAV5 ($1.0E+13$ GC/mL). (iii.) Low titer AAV7 ($1.60E+12$ GC/mL). (iv.) AAV7 high titer ($1.0E+13$ GC/mL). Scale bar = 200 μ m.

AAV serotypes exhibit differential transduction efficiency of rat CeA neurons

In our next experiment, we sought to determine the transduction efficiency of the AAV-GAD65-eGFP and AAV-PAG-E2-Crimson viruses in CeA neurons. The CeA is heavily interconnected with the BLA, but the nuclei differ in their embryological origin and in their

proportions of glutamatergic and GABAergic neurons. AAV2 based Gad65-eGFP and PAG-E2-Crimson viral genomes were pseudotyped as AAV1, AAV4, AAV5, AAV6, AAV7, AAV8, AAV9, AAVrh10, AAVDJ, and AAVDJ8. Each Gad65-eGFP and PAG-E2-Crimson virus of a particular pseudotype were mixed so each virus was at a titer of 1.60×10^{12} GC/mL and 0.4 microliters of virus was infused into the CeA (number of amygdala included in the analyses = n = AAV5 = 3; AAV7 = 5; AAV4, AAV8 AAVDJ and AAVDJ8 = 6; AAV6 and AAV9 = 7; AAV1 and AAVrh10 = 8). Twenty-one days later the animals were perfused and the brains were dissected and coronal brain sections were taken and examined via fluorescence microscopy as described above. Representative images and associated quantification are depicted in Figures 4.7 and 4.8, respectively.

Similar to the results obtained from the above described BLA experiments, AAV4 and AAV5 exhibited lower viral transduction within the CeA for both the Gad65-GFP and PAG-E2-Crimson viruses. AAV7 tended to exhibit higher viral transduction. AAV5-Gad65-GFP exhibited significantly lower “total” spread compared to AAV1, AAV7, AAV9, AAVrh10 and AAVDJ8 ($p < 0.05$), and there was a trend for AAVDJ ($p = 0.0698$). AAV5-Gad65-GFP exhibited significantly lower “total” OD as compared to AAV1, AAV6, AAV7, AAVrh10, and AAVDJ ($p < 0.05$). AAV5-Gad65-GFP exhibited significantly lower “total” mean transduction, as compared to AAV7, AAV8, AAV9 and AAVrh10 ($p < 0.05$), and AAV1 and AAVDJ exhibited a trend, ($p = 0.0655$ and 0.0741 , respectively). AAV5-Gad65-GFP exhibited significantly lower “total” cell count compared to AAV7, AAVrh10 and AAVDJ ($p < 0.05$). AAV7-Gad65-GFP exhibited significantly higher “total” cell count, “total” spread, and “total” mean transduction compared to all other serotypes examined ($p < 0.05$). AAV7-Gad65-

GFP exhibited significantly higher “total” OD compared to all serotypes, except AAV6 ($p = 0.0599$).

For measures taken solely within the boundaries of the BLA, AAV5-Gad65-GFP exhibited significantly lower “BLA” spread compared to AAV7, AAV10 and AAVDJ ($p < 0.05$) with a trend for AAVDJ8 ($p = 0.0748$). AAV5-Gad65-GFP exhibited significantly lower “BLA” OD as compared to AAV6, AAV7, AAVrh10 and AAVDJ. AAV5-Gad65-GFP exhibited significantly lower “BLA” mean transduction compared to AAV6, AAV7 and AAVDJ ($p < 0.05$). AAV5-Gad65-GFP exhibited significantly lower “BLA” cell count compared to AAV7 ($p < 0.05$), and there was a trend for AAVDJ ($p = 0.0537$). AAV7-Gad65-GFP exhibited significantly higher “BLA” cell count, OD, spread and mean transduction compared to all other serotypes examined ($p < 0.05$).

The AAV viruses harboring the PAG-E2-Crimson transgene exhibited a similar trend for transduction as compared to the AAV-GAD65-GFP viruses within the CeA. Notably, AAV4 and AAV5-PAG-E2-Crimson viruses transduced CeA neurons less efficiently compared to the other serotypes, and this was obvious. AAV5-PAG-E2-Crimson exhibited significantly lower “total” spread compared to all serotypes ($p < 0.05$), except AAV8 and AAVDJ. AAV5-PAG-E2-Crimson exhibited significantly lower “total” OD compared to AAV6, AAV7 and AAVDJ8 ($p < 0.05$). AAV5-PAG-E2-Crimson exhibited significantly lower “total” mean transduction compared to AAV6, AAV7, AAV9 and AAVDJ8 ($p < 0.05$). AAV5-PAG-E2-Crimson exhibited significantly lower “total” cell count compared to all other serotypes ($p < 0.05$), except AAV8 ($p = 0.2761$) – there was a trend for AAVDJ ($p = 0.0704$). AAV7-PAG-E2-Crimson exhibited significantly higher “total” OD compared to all other serotypes ($p < 0.05$). AAV7-PAG-E2-

Crimson exhibited significantly higher “total” spread compared to all serotypes ($p < 0.05$), except AAV9 and AAVDJ8. AAV7-PAG-E2-Crimson exhibited significantly higher “total” mean transduction compared to AAV5, AAV8, AAVrh10 and AAVDJ ($p < 0.05$). AAV7-PAG-E2-Crimson exhibited significantly higher “total” cell count compared to AAV1, AAV5, AAV8 and AAVDJ ($p < 0.05$).

For measures taken solely within the boundaries of the CeA, AAV5-PAG-E2-Crimson exhibited significantly lower “CeA” spread compared to AAV6, AAV7 and AAVrh10 ($p < 0.05$), and there was a trend for AAV9 ($p = 0.0584$). AAV5-PAG-E2-Crimson exhibited significantly lower “CeA” OD compared to AAV6, AAV7, AAV9 and AAVDJ8. AAV5-PAG-E2-Crimson exhibited significantly lower “CeA” mean transduction compared to AAV6 and AAV7 ($p < 0.05$), with a trend for AAVDJ8 ($p = 0.0517$). AAV5-PAG-E2-Crimson exhibited significantly lower “CeA” cell count compared to AAV6, AAV7, AAV9, AAVrh10 and AAVDJ8. AAV7-PAG-E2-Crimson exhibited significantly higher “CeA” spread compared to AAV1, AAV5, AAV8 and AAVDJ. AAV7-PAG-E2-Crimson exhibited significantly higher “CeA” OD compared to AAV1, AAV5, AAV8, AAVrh10 and AAVDJ. AAV7-PAG-E2-Crimson exhibited significantly higher “CeA” mean transduction compared to AAV1, AAV5, AAV8, AAVrh10 and AAVDJ ($p < 0.05$), with a trend for AAV9 ($p = 0.0600$). AAV7-PAG-E2-Crimson exhibited significantly higher “CeA” cell count compared to AAV1, AAV5, AAV8, AAVDJ and AAVDJ8 ($p < 0.05$) with a trend for AAV9 ($p = 0.0513$).

Similar to our findings within the BLA, AAV4-Gad65-GFP and AAV4-PAG-E2-Crimson exhibited low transduction within the CeA. The AAV4 viral transduction was not quantified and therefore it was not included in the statistical analysis.

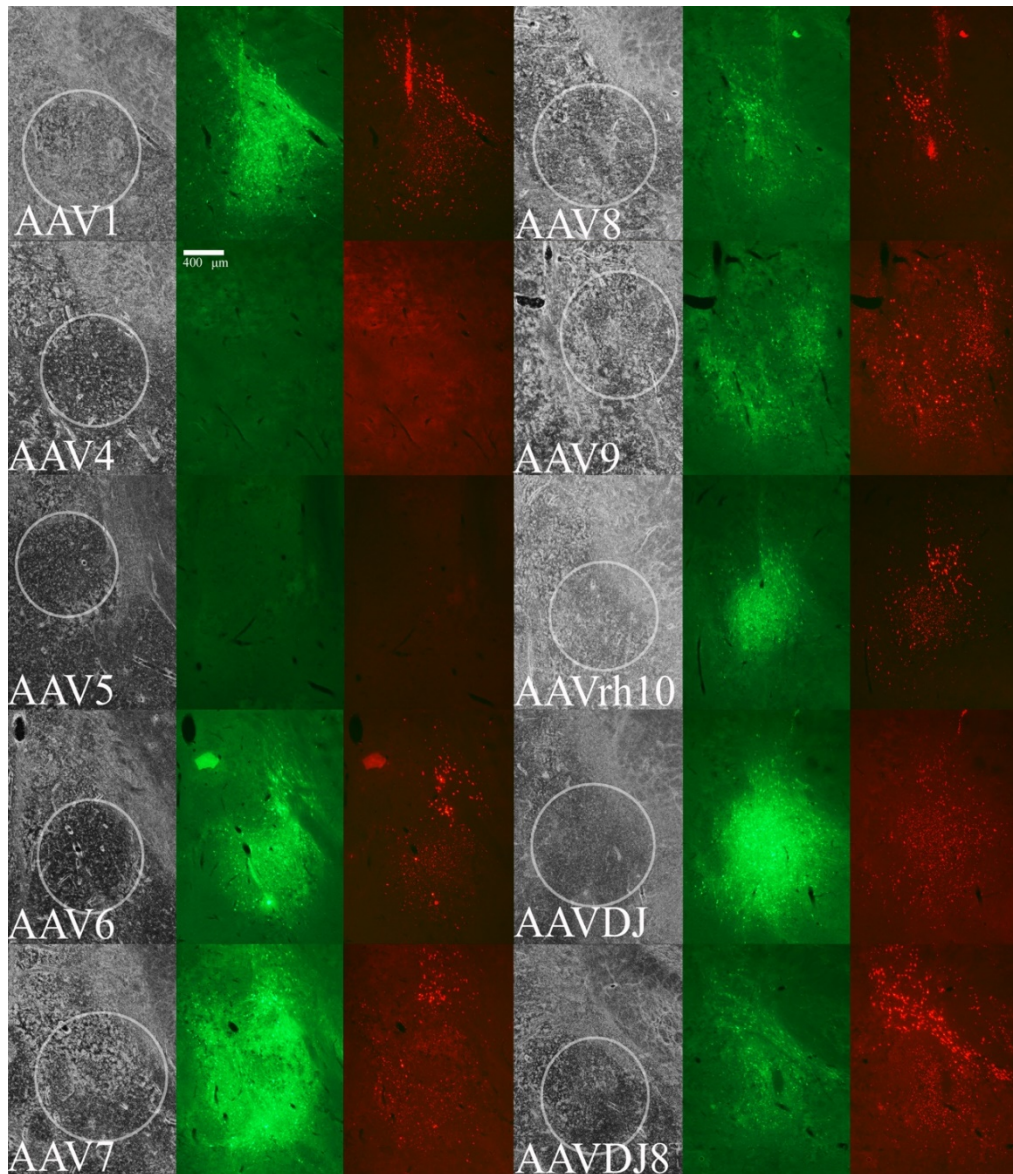


Figure 4.7 Representative images depicting differential neuronal transduction of AAV serotypes within the CeA.

Rats were infused with both AAV-Gad65-GFP and AAV-PAG-RFP into the CeA at the same titer of (1.60×10^{12} GC/mL). Representative images depicting CeA viral transduction for each serotype. From left to right: brightfield image of the CeA, AAV-Gad65-GFP, AAV-PAG-RFP. The location of the CeA is outlined in the brightfield image. Scale bar = 400 μ m.

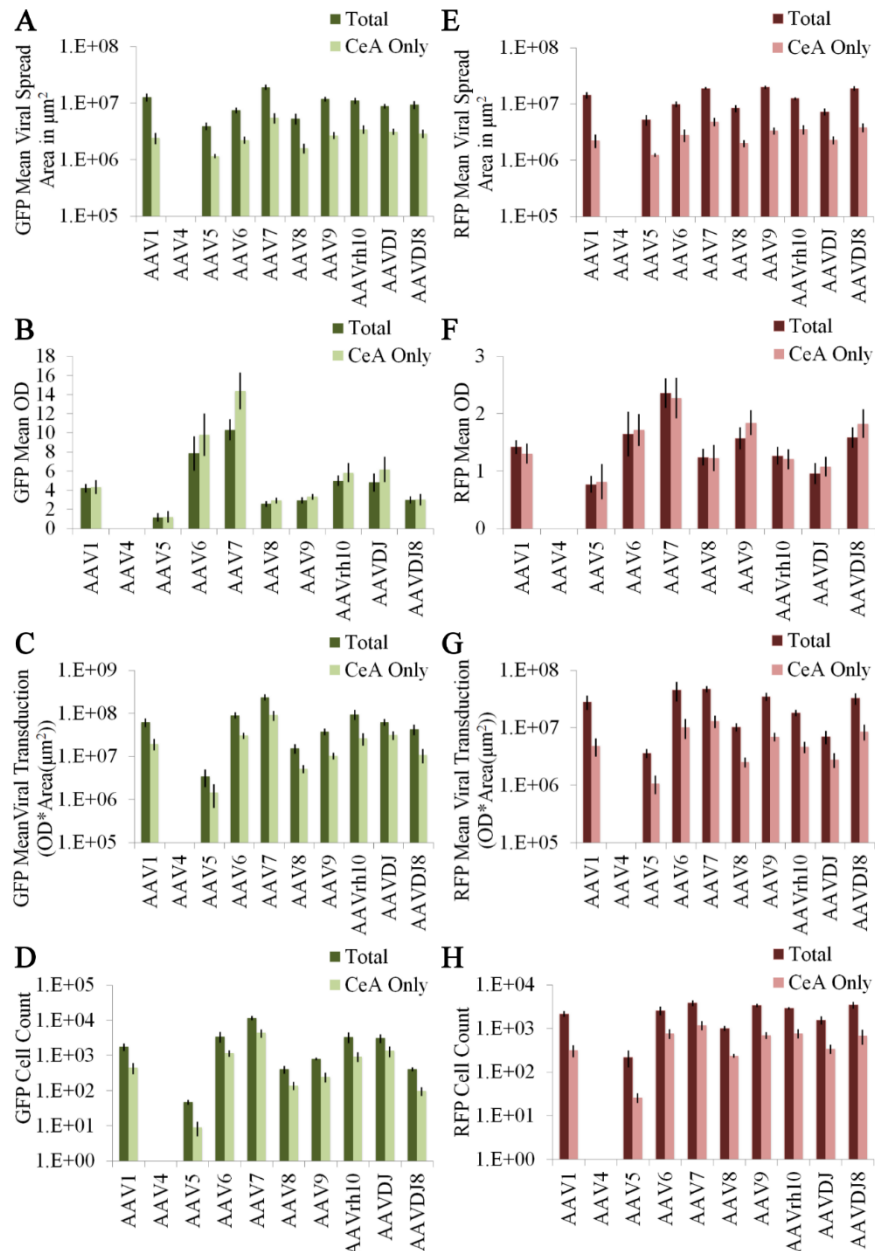


Figure 4.8 AAV serotypes exhibit differential transduction of CeA neurons.

Rats were infused with both AAV-Gad65-GFP and AAV-PAG-RFP into the CeA at the same titer of (1.60E+12 GC/mL). Total viral spread, brightness of GFP and RFP and total count of cells transduced was quantitated and groups means were graphed for Total and BLA only measurements. (A) GFP Total Viral Spread, Area (µm²). (B) GFP Mean Optical Density, Mean OD. (C) GFP Mean Viral Transduction, (OD*Area (µm²)). (D) GFP Positive Cell Count. (E) RFP Total Viral Spread Area (µm²). (F) RFP Mean OD. (G) RFP Mean Viral transduction (OD*Area (µm²)). (H) RFP Positive Cell Count.

AAV-Gad65-GFP virus does not exclusively express GFP in Gad65 positive neurons, but due to the high inhibitory neuron content of the CeA, GFP expression within this structure is predominantly isolated to inhibitory neurons

Previously, the AAV-Gad65-GFP virus was shown to selectively express GFP in inhibitory neurons within the forebrain (Marik *et al.*, 2010). However, to verify that this is indeed the case, we sought to determine if AAV-Gad65-GFP expression is localized specifically to inhibitory neurons. Because Gad65 protein localizes to axon terminals, it makes it very difficult to assess cellular co-localization of endogenous Gad65 protein with ectopically expressed GFP using standard immuno-histological methods. In some cases, Gad67 has been used as a marker for inhibitory neurons in place of Gad65 since these two proteins can serve as markers for inhibitory neurons and have shown to have a high degree of cellular overlap (Zhao *et al.*, 2013). However, we found that it was very difficult to accurately quantify the number of cells co-expressing GAD67 and GFP because of a low signal-to-noise ratio in part due to the fact that Gad67 protein localizes to neuronal fibers, which obscures one's ability to accurately detect cell body expression. For these reasons, to assess the degree of overlap from viral mediated Gad65-GFP expression and endogenous Gad65 expression, we used double Fluorescence *In Situ* Hybridization (FISH) designed to detect viral mediated GFP mRNA expression and endogenous Gad65 mRNA expression. This approach produced far clearer identification of the soma and nuclei of GAD65-expressing neurons. Animals were infused into the BLA and CeA with 0.7 or 0.4 microliters of AAV1-Gad65-GFP, AAV7-Gad65-GFP, and AAVDJ8-Gad65-GFP at a titer of 1.60×10^{12} GC/mL, respectively. Twenty-one days later, the animals were perfused and coronal brain sections containing the BLA and CeA were examined by FISH for viral mediated

GFP mRNA expression and endogenous Gad65 mRNA expression (n = 3 per nuclei). FISH revealed that for Gad65-GFP virus infused into the CeA, viral mediated GFP expression was predominantly localized to Gad65 positive neurons, indicating that the AAV-Gad65-GFP virus could be used as a marker for inhibitory neurons within this structure. However, for Gad65-GFP virus infused into the BLA, only ~ 50% of the GFP expressing cells were Gad65 positive neurons, indicating that the AAV-Gad65-GFP does not exclusively express GFP in Gad65 positive inhibitory neurons (Figure 4.9A, 4.9B). This discrepancy between these two structures is most likely explained by the fact that the CeA contains a significantly higher proportion of inhibitory neurons compared to the BLA and this is illustrated by Gad65 FISH (Figure 4.9C). To emphasize this point, we quantified the total number of cells within a given area of the CeA and the BLA as determined by DAPI staining, and additionally quantified the total number of Gad65 positive cells and the number of GFP expressing cells within this same region for the CeA and BLA (Figure 4.9D-F). For an area of 95236 micrometers² within either the CeA or BLA there were ~306 DAPI stained cells. Within this area in the CeA, ~60 % of the cells were positive for Gad65 mRNA. In contrast for the BLA, only ~15 % cells were positive for Gad65 mRNA, which highlights the difference in the number of inhibitory neurons across these structures. However, both of these areas within the BLA and CeA contained and ~ equal number of GFP expressing cells per total number of cells. Collectively, these data indicate that GFP expression is not selectively localized to Gad65 neurons, but since most of the neurons in the CeA are inhibitory, we can make inferences about the ability of these serotypes to transduce inhibitory neurons.

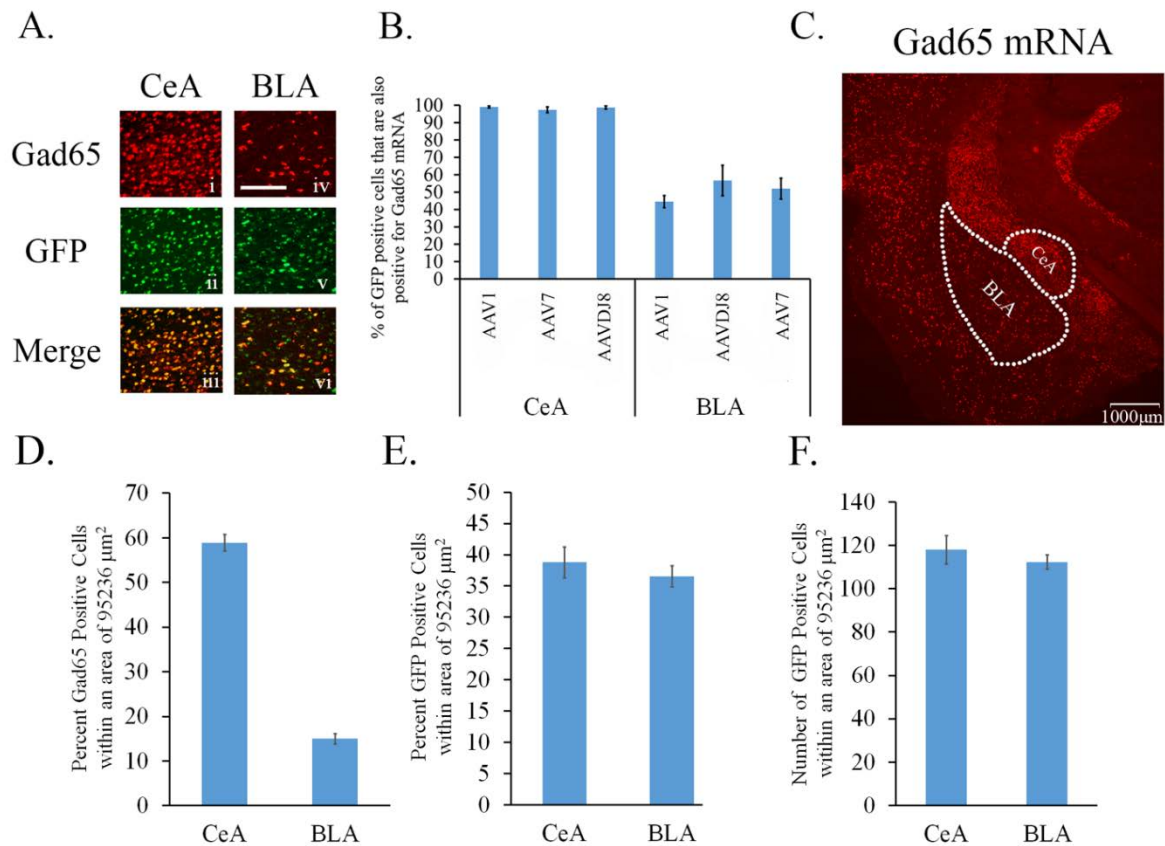


Figure 4.9 Double FISH was performed to determine the specificity of AAV-Gad65-GFP expression for Gad65 positive cells.

Rats were infused with Gad65-GFP into either the CeA or the BLA at a titer of $1.6\text{E}+12$ GC/mL. Twenty-one days later the brains were dissected and double FISH was performed for endogenous Gad65 mRNA (red) and viral GFP mRNA (green). **(A)** Representative images of FISH within the CeA or BLA. (i) FISH for Gad65 mRNA within the CeA. (ii) FISH for GFP mRNA within the CeA. (iii) Merge of Gad65 mRNA and GFP mRNA within the CeA. (iv) FISH for Gad65 mRNA within the BLA. (v) FISH for GFP mRNA within the BLA. (vi) Merge of Gad65 mRNA and GFP mRNA within the BLA. The scale bar = 100 μm . **(B)** Quantification of GFP mRNA positive cells that are also positive for Gad65 mRNA. **(C)** FISH for endogenous Gad65 mRNA depicting the density of Gad65 positive neurons in the BLA vs. the CeA. The scale bar = 1000 μm . **(D)** Quantification of FISH for Gad65 mRNA positive cells within the BLA compared to the CeA. Data shown as percent of DAPI positive cells that are also positive for Gad65 mRNA. **(E)** Quantification of FISH for GFP mRNA positive cells in the BLA compared to the CeA. Data shown as percent of DAPI positive cells that are also positive for GFP mRNA. **(F)** Number of GFP mRNA positive cells within a given area of the BLA compared to the CeA.

AAV-Gad65-GFP and AAV-PAG-E2-Crimson viruses predominantly express their transgenes within neurons

In our final experiment, we sought to determine to what degree the AAV-Gad65-GFP and AAV-PAG-E2-Crimson viruses were specifically expressing their transgenes within neurons (Figure 4.9). Therefore, the AAV2 based Gad65-eGFP and PAG-E2-Crimson viral genomes were pseudotyped as AAV1, AAV6, AAV7, AAV8, AAV9, AAVrh10, AAVDJ, and AAVDJ8. Each Gad65-eGFP and PAG-E2-Crimson virus of a particular pseudotype were mixed so each virus was at a titer of 1.60×10^{12} GC/mL and 0.4 microliters of virus was infused into the CeA (n = 3). Twenty-one days later, the animals were perfused and coronal brain sections containing the CeA were processed for NeuN immunohistochemistry to determine if the GFP and E2-Crimson expression was localized to neurons. Quantitation revealed that ~ 90% of the GFP or E2-Crimson expressing cells were also expressing NeuN, indicating that these viruses are predominantly expressing their transgenes within neurons.

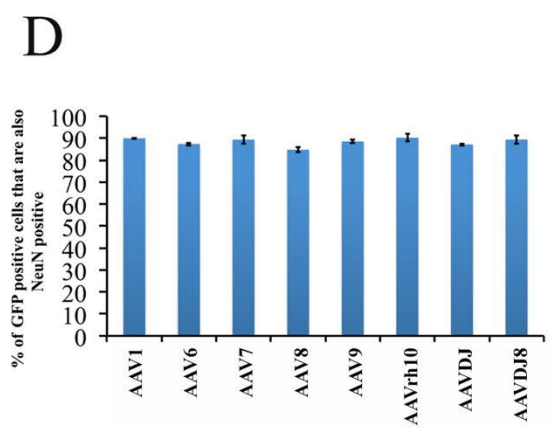
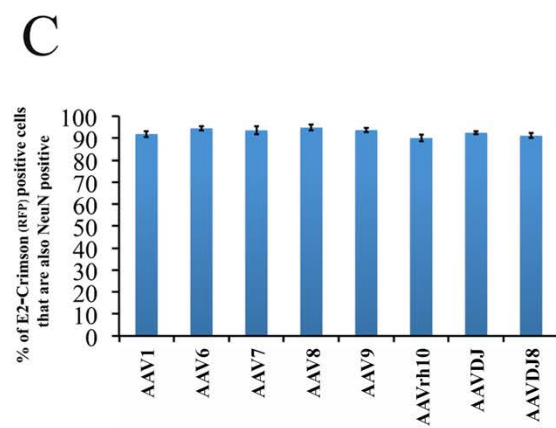
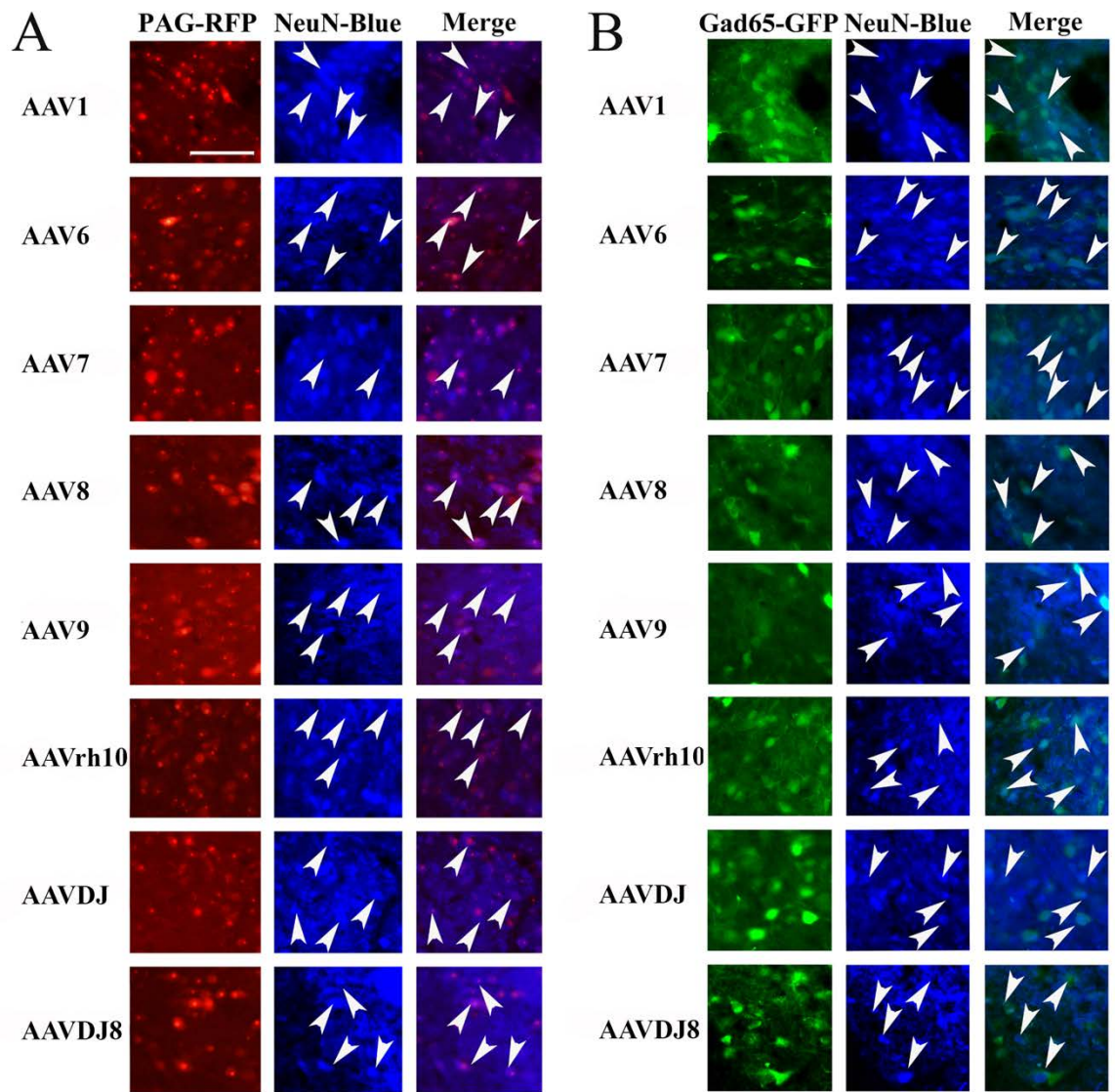


Figure 4.10 NeuN immunohistochemistry within CeA neurons transduced with either AAV-PAG-RFP or AAV-Gad65-GFP.

Animals were infused into the CeA with either AAV-PAG-RFP or AAV-Gad65-GFP at a titer of 1.6×10^{12} GC/mL, then processed for immunohistochemistry to detect amount of NeuN positive neurons that are also positive for GFP or RFP reporter signal. **(A)** (left) RFP reporter signal from AAV-PAG-RFP within the CeA (middle) Immunohistochemistry for NeuN within the CeA. (right) Merge of NeuN and RFP signal to determine overlap. Scale bar = 100 μ m **(B)** (left) GFP reporter signal from AAV-Gad65-GFP within the CeA. (middle) Immunohistochemistry for NeuN within the CeA. (right) Merge of NeuN and GFP signal to determine overlap. **(C)** Quantification of cells that are RFP positive that are also positive for NeuN indicate that ~90-95% of AAV-PAG-RFP expressing cells are neurons (NeuN positive). **(D)** Quantification of cells that are GFP positive that are also positive for NeuN indicate that ~85-90% of AAV-Gad-GFP expressing cells are neurons (NeuN positive).

Discussion

In this study, we evaluated 10 commonly available AAV serotypes for their ability to transduce neurons within the rat BLA and CeA nuclei. In particular, we were interested in assessing how efficiently these serotypes of AAV transduced inhibitory neurons. To accomplish this, an AAV2 based viral genome that harbored a transgene designed to express GFP from a Gad65 promoter, was pseudotyped as either AAV1, AAV4, AAV5, AAV6, AAV7, AAV8, AAV9, AAVrh10, AAVDJ, and AAVDJ8 and subsequently these viruses were infused into the rat BLA and CeA. The expression of GFP was quantified from coronal brain slices utilizing fluorescence microscopy and imageJ software. Our experiments indicated that the GFP expression was predominately localized to Gad65 positive cells (i.e., inhibitory neurons) within the CeA as assessed by co-localization of the viral expressed GFP mRNA and endogenously expressed Gad65 mRNA utilizing double FISH. We found that while most of these serotypes transduced these populations of neurons with similar efficiency, AAV4 and AAV5 transduced these neurons significantly less efficiently than the other serotypes examined, which correlates with the fact that these two serotypes possess significantly different capsid protein sequences compared to the

other serotypes examined. Notably, AAV4 and AAV5 exhibit the most different capsid sequences compared to all commonly available AAV serotypes. We also examined the transduction efficiency of AAV pseudotyped as the above-mentioned serotypes that were designed to express E2-Crimson (RFP) from a phosphate-activated glutaminase (PAG) promoter. PAG is expressed in glutamatergic neurons and subsets of GABAergic neurons (Van der Gucht et al., 2003). Our data indicate that AAV serotypes AAV4 and AAV5 transduce neurons less efficiently than the other serotypes examined as measured by reduced E2-Crimson (RFP) expression. The viruses examined predominantly expressed their transgene (i.e., GFP or RFP) within neurons as measured by anti-NeuN immunohistochemistry.

Gad65 gene expression is a reliable marker for inhibitory neurons (Sloviter & Nilaver, 1987; Zhao et al., 2013). However, we found that in our hands the AAV-Gad65-GFP virus did not express GFP exclusively in inhibitory Gad65 positive neurons when the virus was infused into the BLA. When the same virus was infused into the CeA, a region of the brain with a very dense population of inhibitory neurons, ~90% of the cells that expressed GFP were also Gad65 positive. Therefore, for this brain region, we could utilize GFP expression to be a marker for viral transduction of inhibitory neurons. The most likely explanation for these differences between these two different nuclei, is likely the fact that the AAV-Gad65-GFP virus exhibits leaky GFP expression in non-inhibitory neurons and when this virus is infused into the BLA, a region of the brain with significantly less inhibitory neurons as compared to the CeA, the virus is more likely to transduce non-inhibitory neurons which makes it more apparent the virus exhibits leaky GFP expression. In contrast, viral mediated GFP expression appears to be predominantly confined to inhibitory neurons within the CeA, and this is likely due to the fact that since the

CeA inhibitory neuron content is so high, most of the AAV-Gad65-GFP virus transduced inhibitory neurons. We chose to use the AAV-Gad65-GFP virus because a previous study had demonstrated that it could be used to label inhibitory neurons (Marik et al., 2010). However, the fact that this was not the case in our hands, is not entirely surprising since another study had shown that a variety of inhibitory neuron specific promoters, when utilized in AAV, did not direct transgene expression exclusively within inhibitory neurons (Nathanson et al., 2009a). Although this previous study did not examine the Gad65 promoter. Very recently a study was published describing the Dlx enhancer as a genetic element that could be used to direct AAV mediated transgene expression exclusively within inhibitory neurons. As of now, the Dlx enhancer appears to be the best choice for those that desire to restrict AAV mediated transgene expression to inhibitory neurons (Dimidschstein et al., 2016).

Our data indicate that AAV4 and AAV5 transduce inhibitory neurons less efficiently than the other serotypes we examined; however, the reduced transduction ability of these serotypes is likely not specific to inhibitory neurons per se, but rather to neurons in general. This is because we also observed reduced AAV 4 and 5 viral transduction within the BLA, a region where only 50% of the transduced neurons were inhibitory, and in addition we observed a similar phenomenon with the viruses designed to express RFP from a PAG promoter – a promoter that is not specific to inhibitory neurons. Furthermore, in a previous study from our laboratory, we demonstrated that neuronal BLA transduction efficiency of AAV5 viruses designed to express RFP from an α CamKII promoter was significantly lower compared to a number of other serotypes we examined (Holehonnur et al., 2014). This previous study did not examine AAV4.

To some it might seem surprising that AAV5 appears to transduce neurons significantly worse than many other serotypes, considering how frequently AAV5 has been reported to be used within the literature to study neural function in vivo. However, utilizing the methods described within this study and our previous study, these findings are highly reproducible. Notably, the one other serotype that also exhibited poor neural transduction was AAV4, which possesses viral capsid sequences most similar to AAV5's. Both of these serotypes did transduce neurons within the amygdala, but when the degree of viral transduction was directly compared to the other serotypes examined, it became obvious that they do not transduce amygdala neurons as well. It is worth noting that we utilized a common AAV purification method that includes an iodixanol step gradient and this method is widely utilized to purify AAV (Zolotukhin et al., 1999). However, cesium chloride purification methods are also widely used to purify AAV and it remains possible that different purification methods for AAV might yield AAVs with differing transduction abilities, but we currently do not have evidence to support this notion. Other factors to consider that may explain our results, include the time point we evaluated the viral transduction, the limitations of the viral titering method that was used and the potential for viral retrograde transport. In this study, we evaluated viral transduction twenty-one days following viral infusion. It remains possible that if we had examined earlier or later time points we may have observed different results. For the current study, each virus was titered by determining the number of dnase resistant viral genomes (GC/mL). This is the best way to determine the viral titers when making comparisons among differing AAV serotypes, which relies on detecting viral genomes that have been packaged into a viral capsid and thus, in theory, should allow for the quantitation of only functional virus. However, it remains possible that if the viral genomes were

protected from the dnase treatment by incorrectly formed capsids, it could lead to an inflated titer estimate. It is difficult to assess this possibly, but each of the viruses in this study were produced using the same exact procedures and treated the same way throughout the duration of this study, so even if this was the case for some of the AAV serotypes, it likely would be a problem inherent to the particular serotype when utilizing the procedures we followed. Lastly, some AAV serotypes have been reported to exhibit retrograde transport within neurons, where the viral particle can transduce axons and then travel in a retrograde manner to the cell body and eventually the viral genome can enter the nucleus of the neuron and begin to express the transgene it harbors (Kaspar et al., 2002; Kaspar et al., 2003; Taymans et al., 2007; Hollis et al., 2008). This ability allows the virus to essentially transduce neurons that have their cell bodies distal to the site of viral infusion if these neurons project axons to this viral infusion target site. Therefore, it's possible that when we infused the AAVs into the BLA or CeA, some of the virus may have transduced axons within these nuclei and traveled to distal sites within the brain or between these nuclei. However, despite the fact that some AAV serotypes have been reported to exhibit retrograde transport, they do so very inefficiently. AAV's ability for retrograde transport has generally been regarded as too inefficient to be useful, motivating neuroscientists to identify other viruses that exhibit more efficient retrograde transport such as canine adenovirus (CAV) (Bru et al., 2010), and more recently the creation of a synthetically created AAV serotype, AAV-Retro, that was created via directed evolution to possess superior retrograde transport (Tervo et al., 2016). Thus, it is highly unlikely that AAV retrograde transport adversely influenced our findings. Had there been AAV retrograde transport between the amygdala nuclei, the viral transduction would have been accounted for in our "Total" measurements, and thus it would not

have influenced our main findings. If there was retrograde transport to distal areas within the brain, our analyses would not have accounted for this viral transduction. But given that AAV retrograde transport is very inefficient, it is unlikely to have occurred at an appreciable extent to have adversely influenced our findings.

In conclusion, we report that iodixanol purified AAV4 and AAV5 transduce neurons within the CeA and BLA significantly less efficiently than many other commonly available serotypes. In cases where high levels of neuronal AAV mediated gene expression are desired, AAV4 and AAV5 are likely a poor choice, given other serotypes exhibit significantly greater neuronal transduction. In cases where it is desired to virally deliver transgenes to neurons at a lower copy number, possibly to limit toxicity, AAV4 and AAV5 could be a good choice.

References

- Atchison, R.W., Casto, B.C. & Hammon, W.M. (1965) Adenovirus-Associated Defective Virus Particles. *Science*, 149, 754-756.
- Bantel-Schaal, U. & zur Hausen, H. (1984) Characterization of the DNA of a defective human parvovirus isolated from a genital site. *Virology*, 134, 52-63.
- Blacklow, N.R., Hoggan, M.D. & Rowe, W.P. (1968) Serologic evidence for human infection with adenovirus-associated viruses. *Journal of the National Cancer Institute*, 40, 319-327.
- Botman, D., Tigchelaar, W. & Van Noorden, C.J. (2014) Determination of phosphate-activated glutaminase activity and its kinetics in mouse tissues using metabolic mapping (quantitative enzyme histochemistry). *The journal of histochemistry and cytochemistry : official journal of the Histochemistry Society*, 62, 813-826.
- Bru, T., Salinas, S. & Kremer, E.J. (2010) An update on canine adenovirus type 2 and its vectors. *Viruses*, 2, 2134-2153.
- Buning, H., Nicklin, S.A., Perabo, L., Hallek, M. & Baker, A.H. (2003) AAV-based gene transfer. *Current opinion in molecular therapeutics*, 5, 367-375.
- Chao, H., Liu, Y., Rabinowitz, J., Li, C., Samulski, R.J. & Walsh, C.E. (2000) Several log increase in therapeutic transgene delivery by distinct adeno-associated viral serotype vectors. *Molecular therapy : the journal of the American Society of Gene Therapy*, 2, 619-623.
- Chung-Bok, M.I., Vincent, N., Jhala, U. & Watford, M. (1997) Rat hepatic glutaminase: identification of the full coding sequence and characterization of a functional promoter. *Biochem J*, 324 (Pt 1), 193-200.
- Daya, S. & Berns, K.I. (2008) Gene therapy using adeno-associated virus vectors. *Clin Microbiol Rev*, 21, 583-593.
- Dimidschstein, J., Chen, Q., Tremblay, R., Rogers, S.L., Saldi, G.A., Guo, L., Xu, Q., Liu, R., Lu, C., Chu, J., Grimley, J.S., Krostag, A.R., Kaykas, A., Avery, M.C., Rashid, M.S., Baek, M., Jacob, A.L., Smith, G.B., Wilson, D.E., Kosche, G., Kruglikov, I., Rusielewicz, T., Kotak, V.C., Mowery, T.M., Anderson, S.A., Callaway, E.M., Dasen, J.S., Fitzpatrick, D., Fossati, V., Long, M.A., Noggle, S., Reynolds, J.H., Sanes, D.H., Rudy, B., Feng, G. & Fishell, G. (2016) A viral strategy for targeting and manipulating interneurons across vertebrate species. *Nat Neurosci*, 19, 1743-1749.
- Flint, J. (2003) Animal models of anxiety and their molecular dissection. *Seminars in Cell & Developmental Biology*, 14, 37-42.

- Flotte, T.R., Afione, S.A., Conrad, C., McGrath, S.A., Solow, R., Oka, H., Zeitlin, P.L., Guggino, W.B. & Carter, B.J. (1993) Stable in vivo expression of the cystic fibrosis transmembrane conductance regulator with an adeno-associated virus vector. *Proceedings of the National Academy of Sciences of the United States of America*, 90, 10613-10617.
- Gao, G., Vandenberghe, L.H., Alvira, M.R., Lu, Y., Calcedo, R., Zhou, X. & Wilson, J.M. (2004) Clades of Adeno-associated viruses are widely disseminated in human tissues. *Journal of virology*, 78, 6381-6388.
- Grimm, D., Lee, J.S., Wang, L., Desai, T., Akache, B., Storm, T.A. & Kay, M.A. (2008) In vitro and in vivo gene therapy vector evolution via multispecies interbreeding and retargeting of adeno-associated viruses. *Journal of virology*, 82, 5887-5911.
- Hoggan, M.D., Blacklow, N.R. & Rowe, W.P. (1966) Studies of small DNA viruses found in various adenovirus preparations: physical, biological, and immunological characteristics. *Proceedings of the National Academy of Sciences of the United States of America*, 55, 1467-1474.
- Holehonnur, R., Luong, J.A., Chaturvedi, D., Ho, A., Lella, S.K., Hosek, M.P. & Ploski, J.E. (2014) Adeno-associated viral serotypes produce differing titers and differentially transduce neurons within the rat basal and lateral amygdala. *BMC Neurosci*, 15, 28.
- Hollis, E.R., 2nd, Kadoya, K., Hirsch, M., Samulski, R.J. & Tuszynski, M.H. (2008) Efficient retrograde neuronal transduction utilizing self-complementary AAV1. *Mol Ther*, 16, 296-301.
- Hommel, J.D., Sears, R.M., Georgescu, D., Simmons, D.L. & DiLeone, R.J. (2003) Local gene knockdown in the brain using viral-mediated RNA interference. *Nat Med*, 9, 1539-1544.
- Jiang, N., Shi, P., Li, H., Lu, S., Braseth, L., Cuadra, A.E., Raizada, M.K. & Sumners, C. (2009) Phosphate-Activated Glutaminase-Containing Neurons in the Rat Paraventricular Nucleus Express Angiotensin Type 1 Receptors. *Hypertension*, 54, 845-851.
- Johansen, J.P., Cain, C.K., Ostroff, L.E. & LeDoux, J.E. (2011) Molecular mechanisms of fear learning and memory. *Cell*, 147, 509-524.
- Josselyn, S.A., Shi, C., Carlezon, W.A., Jr., Neve, R.L., Nestler, E.J. & Davis, M. (2001) Long-term memory is facilitated by cAMP response element-binding protein overexpression in the amygdala. *J Neurosci*, 21, 2404-2412.
- Kaspar, B.K., Erickson, D., Schaffer, D., Hinh, L., Gage, F.H. & Peterson, D.A. (2002) Targeted retrograde gene delivery for neuronal protection. *Mol Ther*, 5, 50-56.
- Kaspar, B.K., Llado, J., Sherkat, N., Rothstein, J.D. & Gage, F.H. (2003) Retrograde viral delivery of IGF-1 prolongs survival in a mouse ALS model. *Science*, 301, 839-842.

- Kessler, P.D., Podsakoff, G.M., Chen, X., McQuiston, S.A., Colosi, P.C., Matelis, L.A., Kurtzman, G.J. & Byrne, B.J. (1996) Gene delivery to skeletal muscle results in sustained expression and systemic delivery of a therapeutic protein. *Proceedings of the National Academy of Sciences of the United States of America*, 93, 14082-14087.
- Klein, R.L., Muir, D., King, M.A., Peel, A.L., Zolotukhin, S., Moller, J.C., Kruttgen, A., Heymach, J.V., Jr., Muzyczka, N. & Meyer, E.M. (1999) Long-term actions of vector-derived nerve growth factor or brain-derived neurotrophic factor on choline acetyltransferase and Trk receptor levels in the adult rat basal forebrain. *Neuroscience*, 90, 815-821.
- Koerber, J.T., Jang, J.H. & Schaffer, D.V. (2008) DNA shuffling of adeno-associated virus yields functionally diverse viral progeny. *Molecular therapy : the journal of the American Society of Gene Therapy*, 16, 1703-1709.
- Koostra, N.A. & Verma, I.M. (2003) Gene therapy with viral vectors. *Annual Review of Pharmacology and Toxicology*, 43, 413-439.
- LeDoux, J.E. (2000) Emotion circuits in the brain. *Annu Rev Neurosci*, 23, 155-184.
- Lewin, A.S., Drenser, K.A., Hauswirth, W.W., Nishikawa, S., Yasumura, D., Flannery, J.G. & LaVail, M.M. (1998) Ribozyme rescue of photoreceptor cells in a transgenic rat model of autosomal dominant retinitis pigmentosa. *Nature medicine*, 4, 967-971.
- Maheshri, N., Koerber, J.T., Kaspar, B.K. & Schaffer, D.V. (2006) Directed evolution of adeno-associated virus yields enhanced gene delivery vectors. *Nat Biotechnol*, 24, 198-204.
- Maren, S. & Quirk, G.J. (2004) Neuronal signalling of fear memory. *Nat Rev Neurosci*, 5, 844-852.
- Marik, S.A., Yamahachi, H., McManus, J.N., Szabo, G. & Gilbert, C.D. (2010) Axonal dynamics of excitatory and inhibitory neurons in somatosensory cortex. *PLoS Biol*, 8, e1000395.
- McGaugh, J.L. (2004) The amygdala modulates the consolidation of memories of emotionally arousing experiences. *Annu Rev Neurosci*, 27, 1-28.
- Nathanson, J.L., Jappelli, R., Scheeff, E.D., Manning, G., Obata, K., Brenner, S. & Callaway, E.M. (2009a) Short Promoters in Viral Vectors Drive Selective Expression in Mammalian Inhibitory Neurons, but do not Restrict Activity to Specific Inhibitory Cell-Types. *Front Neural Circuits*, 3, 19.
- Nathanson, J.L., Yanagawa, Y., Obata, K. & Callaway, E.M. (2009b) Preferential labeling of inhibitory and excitatory cortical neurons by endogenous tropism of adeno-associated virus and lentivirus vectors. *Neuroscience*, 161, 441-450.

- Peel, A.L., Zolotukhin, S., Schrimsher, G.W., Muzyczka, N. & Reier, P.J. (1997) Efficient transduction of green fluorescent protein in spinal cord neurons using adeno-associated virus vectors containing cell type-specific promoters. *Gene therapy*, 4, 16-24.
- Rabinowitz, J.E., Rolling, F., Li, C., Conrath, H., Xiao, W., Xiao, X. & Samulski, R.J. (2002) Cross-packaging of a single adeno-associated virus (AAV) type 2 vector genome into multiple AAV serotypes enables transduction with broad specificity. *Journal of virology*, 76, 791-801.
- Rasmussen, M., Kong, L., Zhang, G.-r., Liu, M., Wang, X., Szabo, G., Curthoys, N.P. & Geller, A.I. (2007) Glutamatergic or GABAergic neuron-specific, long-term expression in neocortical neurons from helper virus-free HSV-1 vectors containing the phosphate-activated glutaminase, vesicular glutamate transporter-1, or glutamic acid decarboxylase promoter. *Brain research*, 1144, 19-32.
- Ressler, K.J., Paschall, G., Zhou, X.L. & Davis, M. (2002) Regulation of synaptic plasticity genes during consolidation of fear conditioning. *J Neurosci*, 22, 7892-7902.
- Sah, P., Faber, E.S., Lopez De Armentia, M. & Power, J. (2003) The amygdaloid complex: anatomy and physiology. *Physiological reviews*, 83, 803-834.
- Sloviter, R.S. & Nilaver, G. (1987) Immunocytochemical localization of GABA-, cholecystokinin-, vasoactive intestinal polypeptide-, and somatostatin-like immunoreactivity in the area dentata and hippocampus of the rat. *J Comp Neurol*, 256, 42-60.
- Snyder, R.O., Miao, C.H., Patijn, G.A., Spratt, S.K., Danos, O., Nagy, D., Gown, A.M., Winther, B., Meuse, L., Cohen, L.K., Thompson, A.R. & Kay, M.A. (1997) Persistent and therapeutic concentrations of human factor IX in mice after hepatic gene transfer of recombinant AAV vectors. *Nature genetics*, 16, 270-276.
- Spampanato, J., Polepalli, J. & Sah, P. (2011) Interneurons in the basolateral amygdala. *Neuropharmacology*, 60, 765-773.
- Stork, O., Yamanaka, H., Stork, S., Kume, N. & Obata, K. (2003) Altered conditioned fear behavior in glutamate decarboxylase 65 null mutant mice. *Genes, Brain and Behavior*, 2, 65-70.
- Strack, R.L., Bhattacharyya, D., Glick, B.S. & Keenan, R.J. (2009) Noncytotoxic orange and red/green derivatives of DsRed-Express2 for whole-cell labeling. *BMC Biotechnology*, 9, 32.
- Taymans, J.M., Vandenberghe, L.H., Haute, C.V., Thiry, I., Deroose, C.M., Mortelmans, L., Wilson, J.M., Debyser, Z. & Baekelandt, V. (2007) Comparative analysis of adeno-associated viral vector serotypes 1, 2, 5, 7, and 8 in mouse brain. *Hum Gene Ther*, 18, 195-206.

Tervo, D.G., Hwang, B.Y., Viswanathan, S., Gaj, T., Lavzin, M., Ritola, K.D., Lindo, S., Michael, S., Kuleshova, E., Ojala, D., Huang, C.C., Gerfen, C.R., Schiller, J., Dudman, J.T., Hantman, A.W., Looger, L.L., Schaffer, D.V. & Karpova, A.Y. (2016) A Designer AAV Variant Permits Efficient Retrograde Access to Projection Neurons. *Neuron*, 92, 372-382.

Van der Gucht, E., Jacobs, S., Kaneko, T., Vandesande, F. & Arckens, L. (2003) Distribution and morphological characterization of phosphate-activated glutaminase-immunoreactive neurons in cat visual cortex. *Brain Res*, 988, 29-42.

Van Vliet, K.M., Blouin, V., Brument, N., Agbandje-McKenna, M. & Snyder, R.O. (2008) The Role of the Adeno-Associated Virus Capsid in Gene Transfer. In Jain, K.K. (ed) *Drug Delivery Systems*. Humana Press, Totowa, NJ, pp. 51-91.

Wright, J.F., Qu, G., Tang, C. & Sommer, J.M. (2003) Recombinant adeno-associated virus: formulation challenges and strategies for a gene therapy vector. *Current opinion in drug discovery & development*, 6, 174-178.

Wu, Z., Asokan, A. & Samulski, R.J. (2006) Adeno-associated virus serotypes: vector toolkit for human gene therapy. *Mol Ther*, 14, 316-327.

Zhao, C., Eisinger, B. & Gammie, S.C. (2013) Characterization of GABAergic Neurons in the Mouse Lateral Septum: A Double Fluorescence In Situ Hybridization and Immunohistochemical Study Using Tyramide Signal Amplification. *PLOS ONE*, 8, e73750.

Zolotukhin, S., Byrne, B.J., Mason, E., Zolotukhin, I., Potter, M., Chesnut, K., Summerford, C., Samulski, R.J. & Muzyczka, N. (1999) Recombinant adeno-associated virus purification using novel methods improves infectious titer and yield. *Gene Ther*, 6, 973-985.

CHAPTER 5

IS ARC MRNA LOCALIZATION UNIQUE: A SEARCH FOR MRNAS THAT LOCALIZE TO THE DISTAL DENDRITES OF DENTATE GYRUS GRANULE CELLS FOLLOWING NEURAL ACTIVITY

Authors: Christopher A. de Solis, Anna A Morales, Matthew P. Hosek, Alex Partin, Jonathan E. Ploski

School of Behavioral and Brain Sciences

The University of Texas at Dallas

800 West Campbell Road

Richardson, TX 75080-3021, USA

*Reprinted with permission from Frontiers: *Frontiers in Molecular Neuroscience*, October 2017.
Is Arc mRNA Unique: A Search for mRNAs That Localize to the Distal Dendrites of Dentate Gyrus Granule Cells Following Neural Activity
Christopher A. de Solis, Anna A Morales, Matthew P. Hosek, Alex Partin, Jonathan E. Ploski
Frontiers in Molecular Neuroscience, 2017; doi: <https://doi.org/10.3389/fnmol.2017.00314>

Abstract

There have been several attempts to identify which RNAs are localized to dendrites; however, no study has determined which RNAs localize to the dendrites following the induction of synaptic activity. We sought to identify all RNA transcripts that localize to the distal dendrites of dentate gyrus granule cells following unilateral high frequency stimulation of the perforant pathway (pp-HFS) using Sprague Dawley rats. We then utilized laser microdissection (LMD) to very accurately dissect out the distal 2/3rds of the molecular layer (ML), which contains these dendrites, without contamination from the granule cell layer (GCL), 2 and 4 hrs post pp-HFS. Next, we purified and amplified RNA from the ML and performed an unbiased screen for 27,000 RNA transcripts using Affymetrix microarrays. We determined that Activity Regulated Cytoskeletal Protein (Arc/Arg3.1) mRNA, exhibited the greatest fold increase in the ML at both timepoints (2 hr and 4 hr). In total, we identified 31 transcripts that increased their levels within the ML following pp-HFS across the two timepoints. Of particular interest is that one of these identified transcripts was an unprocessed micro-RNA (pri-miR132). Fluorescent in situ hybridization (FISH) and qRT-PCR were used to confirm some of these candidate transcripts. Our data indicates Arc is a unique activity dependent gene, due to the magnitude that its activity dependent transcript localizes to the dendrites. Our study determined other activity dependent transcripts likely localize to the dendrites following neural activity, but do so with lower efficiency compared to Arc.

Introduction

Changes that lead to lasting alterations in synaptic strength are believed to require de novo protein synthesis (Stanton & Sarvey, 1984; Deadwyler et al., 1987). This observation raises

an intriguing question: How does one nucleus that globally controls transcription for each individual neuron effectively subserve thousands of synapses that can be modified in a spatially and temporally restricted manner? Accumulating evidence suggests one possibility is to target specific mRNAs to dendritic spines, where these mRNAs can be locally translated in a spatially and temporally restricted manner following synaptic activity, leading to synapse specific modifications (Crino & Eberwine, 1996; Tiedge & Brosius, 1996; Weiler et al., 1997; Steward et al., 1998; Huber et al., 2000; Kacharina et al., 2000). Currently, there is strong support for this model, and numerous studies have reported the existence of mRNAs within dendrites (Miyashiro et al., 1994; Tian et al., 1999; Eberwine et al., 2002; Sung et al., 2004; Poon et al., 2006; Zhong et al., 2006; Cajigas et al., 2012). These studies vary on the methodology utilized to detect dendritically localized mRNAs and the number of mRNAs detected, with some studies only identifying tens of mRNAs whereas others identify thousands. These previous studies; however, were not designed to identify transcripts which localize to dendrites following synaptic activity.

Currently, only a few transcripts have been identified to be dendritically localized following synaptic activity, all of which were identified serendipitously (Link et al., 1995; Lyford et al., 1995; Tongiorgi et al., 1997; Mori et al., 2000; Havik et al., 2003; Tiruchinapalli et al., 2003). The most note-worthy transcript to exhibit this is the Activity Regulated Cytoskeletal protein (Arc/Arg3.1) mRNA. Arc mRNA is undoubtedly, thus far, the one RNA that exhibits the most convincing and robust localization to dendrites following neural activity and this has been elegantly, and unambiguously, demonstrated in vivo within the hippocampus following high frequency stimulation of the perforant path (Link et al., 1995; Lyford et al., 1995; Farris et al.,

2014). Brain Derived Neurotrophic Factor (BDNF) is another mRNA thought to be transported to the dendrites following neural activity; however, newer data has questioned this notion (Will et al., 2013). This potential reversal is, in part, due to the difficulty of reliably detecting dendritically localized mRNAs.

Over the last decade it has become apparent that there are hundreds of genes that are induced transcriptionally following synaptic activity (i.e., neural activity dependent genes) (Lin et al., 2008; Ploski et al., 2010). It currently remains unknown how many of these genes might have their mRNAs transported to dendrites following synaptic activity. Because some activity-induced transcripts transported to the dendrites may degrade quickly, it is necessary to design an experiment to identify which activity-dependent transcripts localize to the dendrites following synaptic activity [23]. For this reason, it is not surprising that most of the aforementioned studies did not identify Arc in their screens (Miyashiro et al., 1994; Tian et al., 1999; Eberwine et al., 2002; Sung et al., 2004; Zhong et al., 2006), and this is likely, in part, due to the limited time Arc resides within this compartment. Therefore, we sought to determine which activity dependent genes have their RNAs transported to the dendrites following neural activity.

To this end, we developed a unique method to identify transcripts that are transported to distal dendrites following synaptic activity using a combination of in vivo induction of long term potentiation (LTP) within the rat dentate gyrus followed by laser microdissection of the dentate gyrus molecular layer, and whole genome gene expression analysis.

Materials and Methods

Subjects: Adult male Sprague Dawley rats (Charles Rivers Laboratories) weighing 300-350 grams were housed in pairs in plastic cages and maintained on a 12 hr light/dark cycle. Food and

water were provided *ad libitum* throughout the experiment. Animal use procedures were in strict accordance with the National Institutes of Health Guide for the Care and Use of Laboratory Animals and were approved by the University of Texas at Dallas Animal Care and Use Committee.

Electrical stimulation experiments were performed as previously described (Ploski *et al.*, 2008; Ploski *et al.*, 2010). For LTP stimulation experiments, Sprague Dawley rats (300-350 g) were anesthetized with urethane (2 i.p. injections at 10 min intervals; total of 1.6 mg/kg) and placed in a stereotaxic frame. The skull was exposed and the rats were implanted with a concentric bipolar stimulating electrode (Kopf Instruments model #NEX-100) into the angular bundle of the perforant path (-7.8 AP, 4 ML, -3.4 DV). One-half hour following implantation of the stimulating electrode, rats were given LTP-inducing high-frequency stimulation (HFS), which consisted of six trains of pulses (400 Hz, 20 msec/pulse), delivered at a 10 second interval and repeated six times at an interval of 2 mins with a stimulation intensity of 500 μ Amps, 100 μ s. This protocol has been widely used in the perforant-dentate pathway to produce reliable and robust potentiation of perforant path synapses (Davis *et al.*, 2000; Messaoudi *et al.*, 2007; Ploski *et al.*, 2010). In all stimulation experiments current was applied such that it traveled from the tip to the tube of the bipolar stimulation electrode. The rats were sacrificed at either 2 or 4 hours following HFS and the brain was dissected and immediately frozen on powdered dry ice and stored at -80 °C until further processing.

Immunohistochemistry of Arc for confirmation of electrical stimulation of the perforant pathway:

At the appropriate time point, the brains were rapidly dissected and promptly frozen with powdered dry ice and stored at -80°C until further processing. Twenty-micron coronal sections containing the anterior dorsal hippocampus were obtained and rapidly frozen immediately after being mounted on Fisher Superfrost slides. Sections were fixed in 4 % PFA in PB Buffer (2 M sodium phosphate; AmericanBio, #3818-05) for 10 min. Sections were then washed 3 x for 10 min in PBS-A (NaCl 150 mM, NaOH 96 mM, NaH_2PO_4 125 mM), followed by a 1 hr incubation in blocking solution 1 % bovine serum albumin (1 % BSA, Sigma, Cat #A-3059; 0.1 % Triton X-100, AmericanBio, #AB02025), slices were incubated overnight at room temperature in anti-Arc/Arg3.1 antibody (1:500; Santa Cruz, #17839) in blocking solution, at room temperature in a humid chamber. On the following day sections were washed 3 x with PBS-B (NaCl 150 mM, NaOH 10 mM, NaH_2PO_4 12.5 mM) followed by a 2 hr incubation in Texas Red secondary antibody (1:1000, Life Technologies, #T6390). Sections were then washed 3 x with PBS-B and mounted (VectaShield, H-1000). IHC images were captured at $100\times$ magnification using an Olympus BX51 upright fluorescence microscope with an Olympus DP71 Digital Camera and DP manager software. Only samples exhibiting robust and uniform expression of Arc in the granule and molecular layers for the stimulated side of the brain were selected for further study. We attempted to deliver pp-HFS to 43 animals of which we found that 23 exhibited robust Arc IHC signal within the dentate gyrus and these were the animals used for further study.

Laser Microdissection and RNA Purification: Dissection and purification procedures were performed as previously described in (Partin *et al.*, 2013). Ten-micron sections containing the dorsal hippocampus were taken and placed onto MMI Laser Microdissection (LMD) slides (MMI, #50102) and stored at -80 °C until further processing. Immediately prior to microdissection, the slides were subjected to ethanol dehydration (75 % 45 secs, 95 % 45 secs, 100 % 15 secs, 100 % 45 secs, xylene 5 mins) using Histogen LCM Frozen Section Staining Kit (Arcturus, Mountain View, California). Microdissection was performed via laser microdissection on a SmartCut Laser Microdissection System, which was mounted on an Olympus CKX41 inverted microscope. For samples that were used in microarray analysis, one-hundred and twenty sections were dissected per sample (Control, n = 3; 2 hr, n = 3; 4 hr, n = 3) from the anterior-medial dentate gyrus, in which the distal 2/3rds of the molecular layer was collected. For samples utilized in qRT-PCR analysis, another set of animals were stimulated, dissected and subjected to qRT-PCR analysis. These animals had the distal half of the molecular layer collected, as well as the granule layer across twenty-one 10 micron sections per sample (control, n = 5; 2 hr, n = 4; 4 hr, n = 4). Control samples consisted of the contralateral, non-stimulated molecular and granule layers, respectively. Samples were collected in 25 µL of cell lysis buffer and purified using RNeasy-Micro Kit (Ambion, #AM1931). Samples were re-purified via precipitation using Pellet Paint NF (Novagen) and resuspended in a 10 µL volume. All steps were carried out according to manufacturers' instructions. Purified RNA was converted to cDNA (SuperScript II; Invitrogen, #18064014) for qRT-PCR analysis or amplified for microarray analysis.

RNA amplification: RNA in a 10 μ L volume was amplified using MessageAmp II aRNA Amplification Kit (Ambion) according to the manufacturer's instructions. The amplified RNA from this first round of RNA amplification was subjected to a second round of RNA amplification using MessageAmp II-Biotin Enhanced aRNA Amplification Kit and was performed according to the manufacturer's instructions to yield Biotin labeled aRNA suitable for Affymetrix microarray analysis. RNA from second round amplification was also converted to cDNA for qRT-PCR analysis.

DNA Microarray: Was essentially performed as previously described (Ploski *et al.*, 2006; Ploski *et al.*, 2010; Partin *et al.*, 2013). A total of 9 microarray hybridizations were performed at the UTSW microarray facility using Affymetrix single channel Rat Genome 230 2.0 Arrays, $n = 3$ per group, (3 x unstimulated, 3 x 2 hrs post stimulation and 3 x 4 hrs post stimulation). Gene lists were created based on the relatively stringent criteria that the gene must exhibit an average fold difference of 3-fold or greater in pair wise comparisons between the unstimulated and stimulated samples, with a t-test p-value of $p < 0.05$. Importantly, the Microarray Quality Control (MAQC) Consortium has reported that this approach can be successful in identifying reproducible gene lists (Shi *et al.*, 2006).

Quantitative real-time PCR (qRT-PCR) was performed using the $\Delta\Delta$ Ct method as we have described previously (Ploski *et al.*, 2006; Ploski *et al.*, 2008; Ploski *et al.*, 2010; de Solis *et al.*, 2015) using a CFX96 Real-Time System thermocycler (BioRad, #1845096) and QuantiTect SYBR Green PCR Kit (Qiagen, #204143) with custom designed primers at a concentration of

300 nM. For qRT-PCR experiments, all samples were performed in duplicate and relative gene concentrations were normalized against GAPDH levels. qRT-PCR was performed with the following conditions [(95 °C for 15 min) ((94 °C for 30 sec, 55 °C for 30 sec, 72 °C for 30 sec) x (35 cycles))] in a standard 20 µL reaction. PCR primers utilized for qRT-PCR were examined for their efficiency of PCR amplification and were found to be ~99% efficient.

PCR amplification of the RM2 locus: Standard PCR was performed using Titanium Taq (Clontech Laboratories, #639208) in a 20 µL volume from rat cDNA from the molecular layer using the following conditions [(95 °C for 60 sec), ((95 °C for 30 sec, 68 °C for 60 sec, 72 °C for 30 sec) x (35 cycles))].

PCR reactions were performed with the following primer sets: (miR-212 FP TAACAGTCTCCAGTCACGGCCACCGACGCC; RM2 RP GGTCTCACTGTAGTTCTGGCTAGCCTTGAAC TCACAGAAACCC), (miR-132 FP CAGGGCAACCGTGGCTTTCGATTGTTACTGTGGGAACCGG; RM2 RP). PCR products of 1.5 kb and ~.6 kb were obtained for the PCR amplification using the miR-132 FP and RM2 RP primers. No PCR products were obtained using the miR-212 FP and RM2 RP. The PCR products were cloned into the pCR4-Topo vector via a TA cloning kit (Invitrogen, #450030) and sequenced (Retrogen Inc.).

RNA in situ probe production: The probe template for Arc was a generous gift from Oswald Steward and it was designed to target the entire Arc coding region (Guzowski *et al.*, 1999; Farris *et al.*, 2014). The probe template for Homer1a was designed to target the Homer1a 3'

untranslated region and was a generous gift from John Guzowski (Guzowski *et al.*, 1999; Vazdarjanova *et al.*, 2002). The DNA templates to produce FISH RNA probes for Egr3, Egr4, Sox11, Ptgs2, pri-miR132 were PCR amplified from rat cDNA and these PCR products were cloned into the pCR4-TOPO vector using a TA cloning kit (Invitrogen, #450030). FISH Probes were prepared using MAXIscript T7/T3 Transcription Kit (Ambion, #AM1324) and were labeled with UTP-Digoxigenin (Roche, #11209256910). These probes were purified using mini Quick Spin RNA Columns (Roche, #11814427001). RNA probes that were labeled with radioactivity was performed as previously described (Ploski *et al.*, 2010; Partin *et al.*, 2013). DNA templates for Arc and Nurr1 were PCR amplified and used to produce a radiolabeled probe using a T7-based *in vitro* transcription kit (Megashortscript; Ambion) using [³⁵S]CTP (1.5 μCi) (PerkinElmer). Removal of unincorporated nucleotides after the *in vitro* transcription reaction was performed using sepharose spin columns (Roche).

In Situ Hybridization and Fluorescent In Situ Hybridization (FISH): *In Situ Hybridization* was performed as previously described (Ploski *et al.*, 2010; Partin *et al.*, 2013). FISH was performed as previously described (Farris *et al.*, 2014). For FISH, Prior to hybridization, sections were fixed in 4 % PFA in PBS (pH 7.4) for 5 min, rinsed in 2x SSC (AmericanBio, #AB13156) for 2 min, incubated in 0.50 % acetic anhydride (Sigma, #320102) in 1.5 % triethanolamine (Sigma, #90276) for 10 min and then treated with 1:1 acetone (Sigma, #270725) : methanol (Fisher, #A412) for 5 min. Pre-hybridization was performed at 56 °C for 1 hr in hybridization buffer ((50% formamide (AmericanBio, #AB00600), 5x SSC, 1.25 x denhardt's solution (AmericanBio, #AB03075), 250 μg/mL, E. coli tRNA (Sigma, #R1753), 500 μg/mL salmon

sperm (Sigma, #D7656) and 5 % dextran sulfate (AmericanBio, # AB00426)). Sections were hybridized overnight (12-14 hr) in hybridization buffer containing 100 ng of probe. Post-hybridization washes (1 x 2x SSC 5 min, 1 x 2x SSC 10 min) were followed by treatment with RNase (10 µg/mL; Fisher, #BP2539) for 15 min at 37 °C. Following 2 x 5 min washes in 2 x SSC, sections were placed in 0.5x SSC for 10 min, followed by a 30 min incubation in 0.5x SSC at 56 °C. After 2 x 5 min washes at RT in 0.5x SSC, sections were incubated in 2x SSC containing 3 % hydrogen peroxide to inhibit endogenous peroxidases. Sections were then washed 2 x 2x SSC for 5 min before being placed into TBS (0.01 M Tris-HCL, 0.1 M NaCl, pH 7.5) for 5 min. Sections were blocked with 2 % blocking buffer (Roche, #11096176001) in TBS, containing 5 % goat serum for 30 min, followed by a 2 hr incubation in anti-DIG-HRP (1:200; Perkin Elmer, #NEF832001EA) in blocking buffer. Sections were then washed 3 x in TBS-T (TBS containing 0.05 % Tween 20, pH 7.5) for 5 min, followed by a 30 min incubation with Cy3 in 1 x amplification buffer (1:50; TSA Plus Cyanine 3 System, Perkin Elmer, #NEL744001KT). After 3 x wash in TBS-T for 5 min each, slides were then coverslipped with Vectashield HardSet Mounting Medium (Vector Laboratories). Images were taken at 100x and 400x magnification (Olympus BX51 microscope, Olympus DP71 Digital Camera and DP manager software). Images for each gene were captured at the optimal exposure for each magnification. Images for Pri-miR132 were captured at the same exposure for both the 2 hr and 4 hr time points. Quantification was performed on three individual animals across 3 slices each, spaced 80 µM apart. ImageJ (U.S. National Institutes of Health, Bethesda, Maryland, USA, <http://imagej.nih.gov/ij/>) was used to obtain the mean optical density (mean OD) of 400x images. The mean OD of the GCL or ML were compared to the region immediately below the ML (lateral posterior thalamic nucleus). The

values for the stimulated and control side were then compared. The values were displayed as the fold change from the control side.

NeuN IHC: Rats were perfused with 4 % PFA in 1 x PBS. The NeuN IHC was performed on free-floating coronal rat sections (40 μ m). Sections were blocked in donkey serum in 1x PBS for 1 hr at RT. They were then incubated overnight in an anti-NeuN antibody (1:500; Millipore #MAB377). Sections were washed with PBS for 10 min, 3x before being incubated with the secondary for 2 hr at RT (1:200; Invitrogen #T6390). There were 3, 10 min final washes with PBS before being mounted onto superfrost slides (Fisher) and a florescent mounting media containing DAPI (Vectashield).

Statistical Analysis: Statistics for the image quantification, microarray and qRT-PCR analysis data were done using two-tailed t-test assuming equal variances.

Results

Genome wide DNA microarray screen reveals Arc to be the most prominent mRNA within the molecular layer post-pp-HFS, compared to unstimulated controls

One of the best methods for determining if specific mRNAs localize to dendrites is by *in situ* hybridization. *In situ* hybridization on hippocampal coronal tissue sections is especially ideal because of the unique neuroanatomical organization of the hippocampus: neuronal cells bodies are localized to discrete layers wherein the dendrites from these cell bodies project uniformly away from the soma and, therefore, spatially separating the cell body from the dendrites. These

features of the hippocampus allowed for the serendipitous discovery that Arc mRNA localizes to dendrites (Link *et al.*, 1995; Lyford *et al.*, 1995) following neural activity of dentate gyrus neurons. Stimulating the angular bundle of the perforant pathway with high frequency stimulation (pp-HFS) is one way to induce neural activity within the hippocampus, and specifically the dentate gyrus. This treatment initiates neural activity that induces long term potentiation (LTP) of dentate gyrus granule neurons on the stimulated side of the brain. This method of inducing neural activity is ideal because it utilizes a pattern of stimulation that produces highly reliable and robust alterations in synaptic plasticity (Bliss & Lomo, 1973; Malenka & Nicoll, 1999; Schafe *et al.*, 2001; Rodrigues *et al.*, 2004), and leads to robust gene expression within dentate gyrus granule cells. To illustrate this, we applied pp-HFS to urethane-anesthetized rats. One hour later, the brains were dissected and *in situ* hybridization was performed on coronal brain sections containing the dorsal hippocampus with radiolabeled riboprobes for Arc mRNA and Nurr1 mRNA – two immediate early genes. As expected, both Arc mRNA and Nurr1 mRNA are robustly increased within the granule cell layer (GCL) of the dentate gyrus on the ipsilateral side of stimulation. In contrast, the contralateral side exhibits very low levels of these mRNAs. However, Arc mRNA is also detected in the molecular layer (ML) of the dentate gyrus on the ipsilateral side of stimulation, indicating that this mRNA is transported to the dendrites contained within the ML (Figure 5.1A). Notably, the ML consists of primarily dendrites, neuropil and traversing axons, but is virtually devoid of neuronal cell bodies. We performed immunohistochemistry for the neuronal marker NeuN, on coronal brain sections containing the dorsal hippocampus to demonstrate this. NeuN signal was very

prominent in the neuronal cell bodies within the GCL of the dentate gyrus. However, there was a clear lack of NeuN stained cells within the ML. (Figure 5.1B).

Next, we sought to identify all known transcripts within the rat dentate gyrus that are transported to the distal dendrites following synaptic activity induced by pp-HFS. Synaptic activity within the dentate gyrus of urethane-anesthetized rats induced by pp-HFS should lead to a robust increase in gene transcription of 100's of genes within GCL neurons, and we hypothesized that some of these mRNAs might be transported to the dendrites contained within the molecular layer of the dentate gyrus. However, to successfully achieve our goal of detecting mRNAs within the ML, we would need to be able to dissect the ML away from the GCL and other surrounding structures. These structures are so small, that accurate manual dissection would likely be impossible. Therefore, we utilized laser microdissection to dissect out the distal 2/3rds of the ML so we could ensure that we would avoid GCL contamination during the isolation of the ML (Figure 5.1C).

We stimulated the ipsilateral side (side of stimulation) with pp-HFS and then sacrificed the animals at 2 and 4 hrs post stimulation. Cryocut coronal sections containing the anterior dorsal hippocampus were collected and subjected to Arc immunohistochemistry to verify Arc gene expression was induced within the ipsilateral dentate gyrus (Figure 5.1D). We used this approach as an indirect way to verify the stimulation procedure was successful at inducing neural activity within the dentate gyrus for each animal that received pp-HFS. Next, additional cryocut sections were obtained from the dorsal hippocampus of animals that successfully received the pp-HFS. The ipsilateral and contralateral (unstimulated) distal 2/3rds of the molecular layer of the dentate gyrus was microdissected. Purification of the RNA followed by two rounds of RNA

amplification was completed in preparation for DNA microarray analysis. We chose to analyze mRNA levels at 2 and 4 hours post stimulation compared to unstimulated controls because these are time points at which mRNAs would likely localize to dendrites following stimulation. For example, it has been previously demonstrated that Arc mRNA can be detected within the dendrites after only 30 minutes following stimulation and continues to accumulate within the dendrites for at least 2 hours post stimulation (Steward *et al.*, 1998). During this period, numerous transcription factors are transcriptionally induced and promote transcription of a multitude of genes during additional waves of transcription. Two and four hours post stimulation should be ideal time points to allow pp-HFS-induced genes to be transcribed and also allow enough time for dendrite-destined transcripts to accumulate within this compartment.

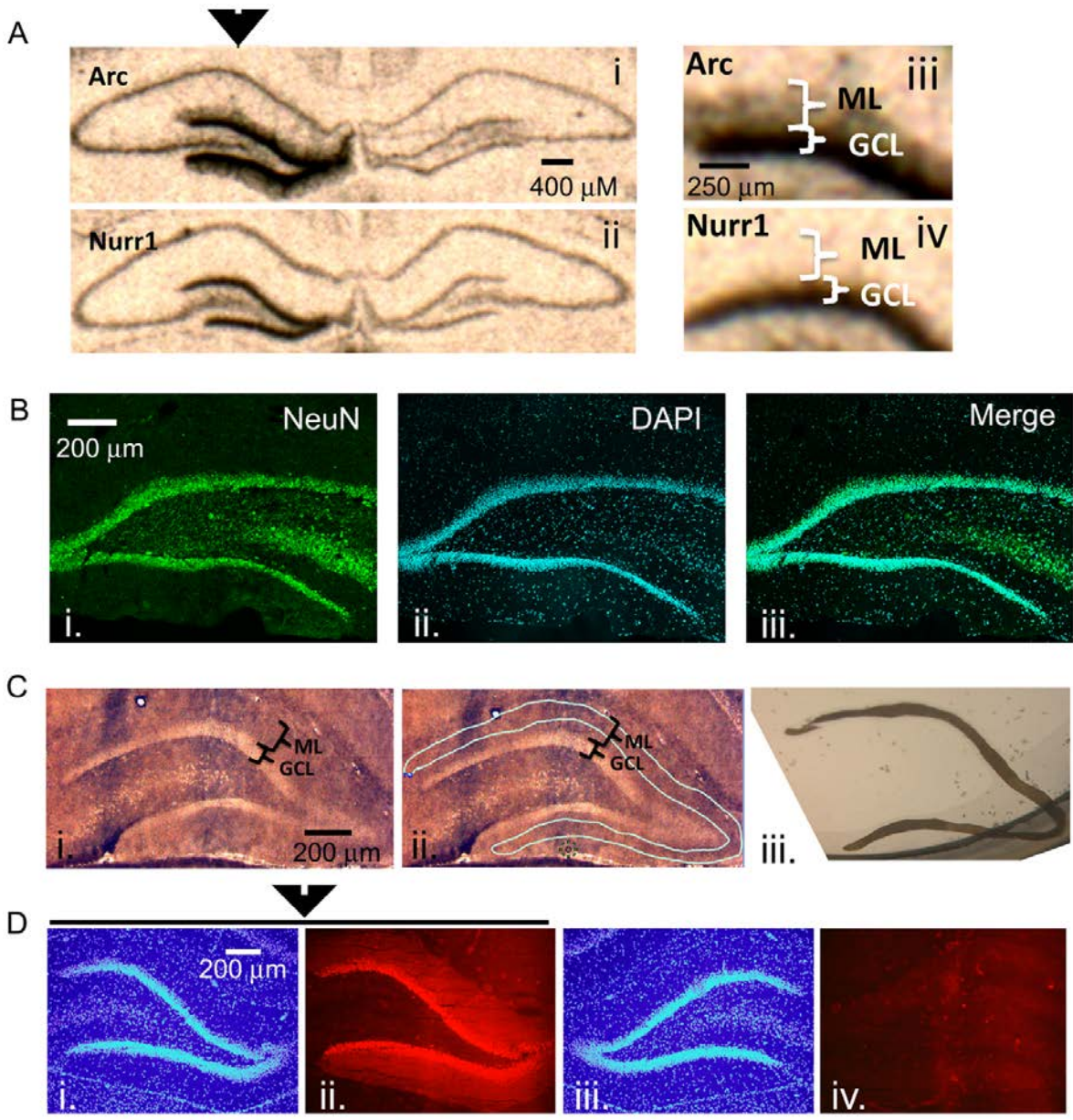


Figure 5.1 The dendrites of dentate gyrus granule neurons are suitable to screen to RNA transcripts in distal dendrites.

(A). Radioactive *In situ* hybridization of the immediate early genes (IEGs) Arc (i., ii.) and Nurr1 (ii., iv.) following unilateral pp-HFS to demonstrate robust presence of Arc mRNA in the ML 1 hr following stimulation. Arrow indicates the side of the brain that received pp-HFS prior to sacrificing the rat. (B). A NeuN stain was performed to show the abundance of neuronal cell bodies in the GCL and their absence in the ML. A coronal section was stained for (i.) NeuN and (ii.) Dapi. (iii.) A merge of NeuN and DAPI depicts the lack of NeuN positive cell bodies within the ML. (C) (i.) A section containing the DG that was prepared for LMD. (ii.) The same section is traced for the desired tissue sample of the ML prior to dissection. (iii.) An image of the dissected ML tissue following LMD. (D) Confirmation of successful pp-HFS via Arc IHC. Staining of (i.) DAPI and (ii.) Arc protein on the stimulated side depicts robust localization of Arc to the ML compared to the contralateral/non-stimulated hemisphere (iii., iv.), respectively.

Our genome-wide screen, using Affymetrix DNA microarrays examined the expression levels of over 27,000 unique transcripts. After filtering data for changes of 3-fold or more, 31 transcripts were identified that were higher within the ML of the stimulated side ($p < 0.05$); one RNA exhibited a greater than 3-fold decrease in levels. Twenty-two of the 31 transcripts that were identified to be upregulated within the ML following pp-HFS, have been previously identified to be regulated via pp-HFS (Matsuo *et al.*, 2000; Yamazaki *et al.*, 2001; Ploski *et al.*, 2010; Ryan *et al.*, 2011; Ryan *et al.*, 2012). Eighteen of these 31 transcripts were also previously identified to be differentially regulated in neurons grown in culture following KCl-mediated induction of neural activity (Lin *et al.*, 2008). The one transcript we identified to be decreased within the ML following pp-HFS, (coiled-coil domain containing 177; *Ccdc177*), to our knowledge has not been previously identified to be regulated by pp-HFS, or KCl-mediated induction of neural activity. These types of studies have consistently identified a good number of genes that exhibit greater mRNA fold changes than Arc, so the fact that our screen identified Arc as the transcript with the highest increase in mRNA fold change within the ML 2 and 4 hrs

following pp-HFS, is a good indication that the screen successfully identified mRNAs which have become enriched within the ML following pp-HFS (Figure 5.2).

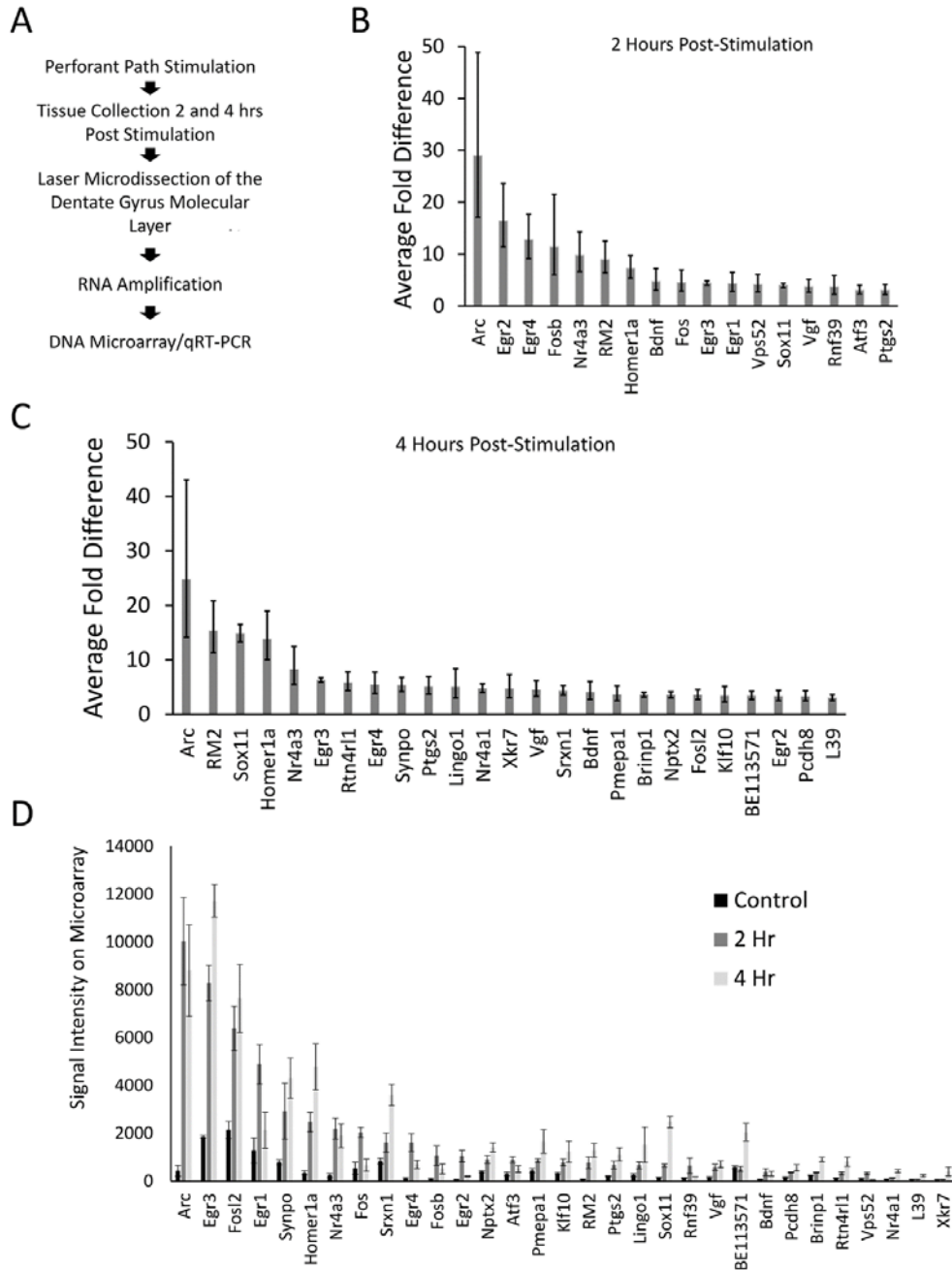


Figure 5.2 Microarray of distal dendrites of granule cell 2hr and 4hr post stimulation

(A) Stepwise outline of experiment from surgery to DNA microarray. (B) Microarray results for 2 hr post-pp-HFS, compared to controls, depicted as fold change. Error bars represent Standard Deviation (SD), n = 3 per group. (C) Microarray results for 4 hr post pp-HFS, compared to controls, depicted as fold change. Error bars represent Standard Deviation (SD), n = 3 per group. (C) Raw signal intensity from DNA microarray for control, 2 hr and 4 hr samples. Error bars represent Standard Error of the Mean (SEM), n = 3 per group.

Another way to examine the microarray data is to view each gene's signal intensity on the microarray comparing the control, 2 hr, and 4 hr samples (Figure 5.2D). Most of these genes exhibit fairly low signals on the microarray, which could indicate their overall levels are low in the ML. In contrast, Arc mRNA exhibits the highest signal intensity with only a few other mRNAs exhibiting similar levels. The first round RNA amplification was converted to cDNA and analyzed via qRT-PCR to confirm the results from the microarray (Figure 5.3).

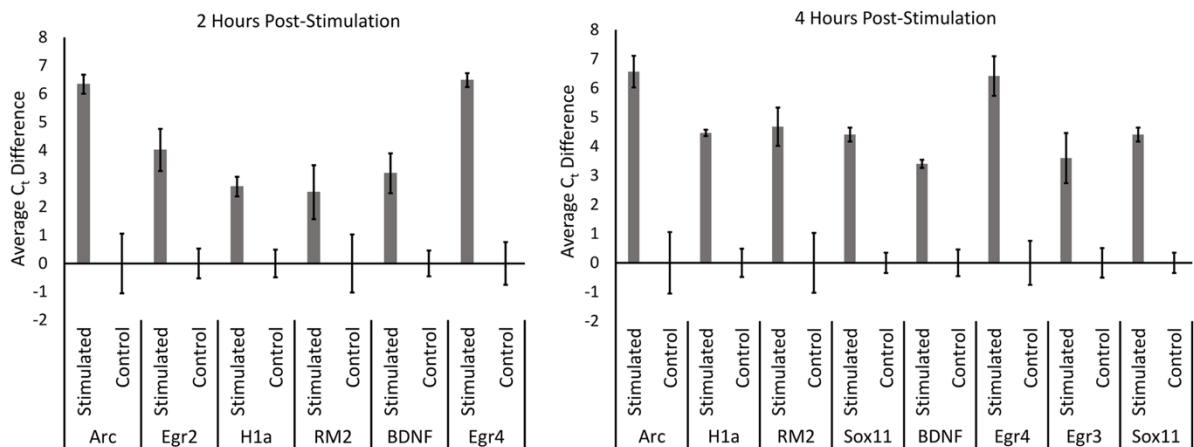


Figure 5.3 Confirmation of microarray via qRT-PCR

qRT-PCR was performed for control, 2 hr and 4 hr samples from the microarray experiment. aRNA that was generated for the microarray was converted into cDNA and used to confirm results from the microarray via qRT-PCR. All genes tested exhibited significantly higher levels in stimulated samples compared to controls in both 2 hr and 4 hr time points ($p < 0.05$), (with the exception of pri-miR132 2 hr). Error bars represent SEM, n = 3 per group.

RM2 is a non-coding transcript containing pri-miRNA132

The second most robustly upregulated transcript at 4 hrs post stimulation was a partially characterized transcript referred to as RM2. This transcript was identified in NCBI Genbank as a partial transcript (GenBank: AB032083.1), and it had reportedly been previously identified to be induced within the hippocampus following LTP inducing stimulation (Matsuo *et al.*, 2000). There was no evidence that RM2 contained a reading frame to code for a protein. We reasoned that this transcript could be part of a larger, as of yet, unidentified transcript. Therefore, we examined the rat genome upstream from the RM2 genomic locus and we determined that a CREB dependent non-protein coding transcript that codes for the miRNAs, miRNA-212 and miRNA-132 (Vo *et al.*, 2005) was directly adjacent to the RM2 locus. We hypothesized that the RM2 sequence might be part of a contiguous RNA that contains miRNA 212 and 132. To test this hypothesis, we subjected cDNA generated from RNA obtained from the distal molecular layer, 4 hrs post HFS (similar material that was used for the microarray analysis), to PCR with PCR primers specific for the RM2 microarray probe and the miRNA-212 or miRNA-132 loci. The PCR did not amplify a DNA product using the miRNA212 primer and RM2 primer, but it did amplify two PCR products that were ~1.6 kb and ~660 bps utilizing the miRNA132 and RM2 primers. These PCR products were cloned and subjected to DNA sequencing for verification. We determined that indeed RM2 was contiguous with an RNA transcript that contained miRNA132 (Figure 5.4). The ~660 bps transcript was shorter than the ~1.6 kb transcript because it was lacking a region intervening between miR132 and RM2, most likely due to the presence of an intron that was spliced out. These data are consistent with findings published while this work was ongoing (Takebayashi *et al.*, 2014). Collectively, these findings

are intriguing because miRNA132 is believed to localize to dendrites (Edbauer *et al.*, 2010; Bicker *et al.*, 2014), but it is currently unknown how it gets there (Tai & Schuman, 2006). Conventional wisdom dictates miRNAs are expressed within the nucleus as part of larger RNA polymerase II transcripts (pri-miRNAs), and these are cleaved within the nucleus by Drosha and DGCR8 to create pre-miRNAs, which are then exported to the cytoplasm for further processing by DICER to convert pre-miRNAs to mature miRNAs (Corbin *et al.*, 2009; Bicker *et al.*, 2014). However, our data indicates there is a large upregulation of pri-miRNA132/RM2 within the molecular layer (dendrites) following synaptic activity, indicating that pri-miRNA132 may leave the nucleus unprocessed. This possibility makes it plausible that miRNA132 is transported to the dendrites as a pri-miR-132. Recent reports lend credibility to this model. For example, pri-miRNAs, Drosha and DGCR8 have recently been reported to be present within the post synaptic density (Lugli *et al.*, 2012). These data indicate that miRNA132, might be transported to the dendrites following synaptic activity as a longer unprocessed transcript which is then likely processed to a mature miRNA when it reaches its destination. We will refer to RM2 as pri-miR132.

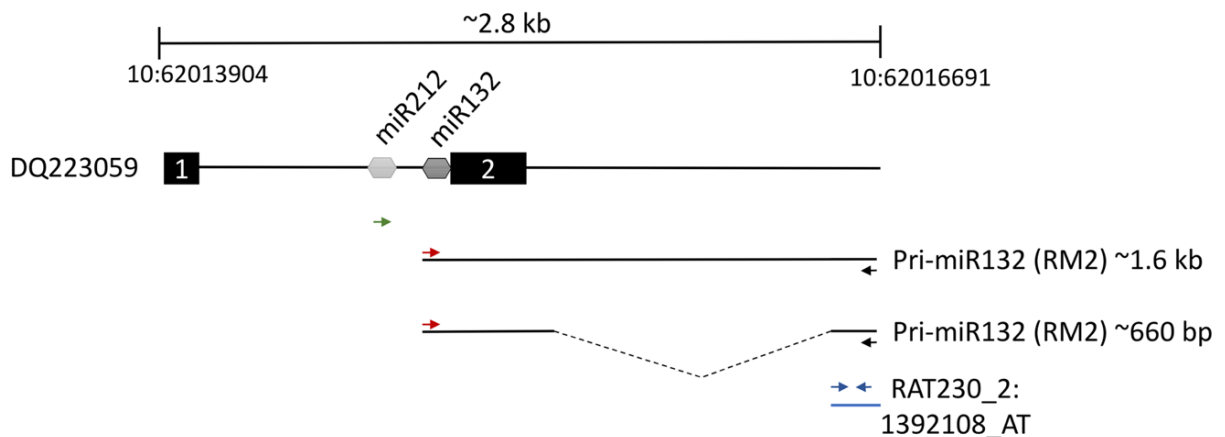


Figure 5.4 Unpossessed miR132 present in the dendrites

Two thousand eight hundred base pair region of rat chromosome 10 between nucleotides 62013904 and 62016691 containing the pri-miR132/RM2 gene loci. Dq223059 transcript contains both miR212 and miR132 between putative exon 1 and exon 2. We discovered a ~1.6 kb and a ~660 bps transcript that was present within ML samples that were collected 4 hr post-pp-HFS. These transcripts contained the miR132 coding sequences to be contiguous with RNA sequences represented by the Affymetrix RM2 probe, RAT230_2:1392108_AT. The red and black arrows indicate the positions of the forward and reverse PCR primers, respectively, used to amplify the ~1.6 kb and ~660 bps transcripts. The green arrow represents the forward PCR primer intended to amplify the miR212 sequence when coupled with the RM2 reverse primer (black arrow); however, this primer pair did not yield a PCR product. Blue arrows indicate the locations of the PCR primers used for qRT-PCR of the pri-miR132/RM2 transcript. Dotted line within the ~660 bps transcript indicates the location of a likely intron.

Fluorescent *in situ* hybridization and qRT-PCR indicate that multiple transcripts localize to the ML post-pp-HFS

We then stimulated another group of animals with pp-HFS and 2 and 4 hours later, the brains were dissected and coronal sections containing the dorsal hippocampus were taken. We performed secondary confirmation on a subset of candidate genes, which were identified utilizing fluorescent *in situ* hybridization (FISH) using gene specific riboprobes (Figure 5.5). We chose to examine mRNA expression for the selected genes for the 4 hr time point following pp-HFS, since this was the time point these genes exhibited the highest expression within the ML, according to the microarray data. For pri-miR132, we also examined expression at the 2 hr time point. As expected, FISH performed for Arc yielded a robust and very convincing signal for Arc within the GCL and ML on the stimulated side of the brain. In contrast, the unstimulated, control side exhibited very little signal within these regions. We also examined the expression pattern for Egr3, Egr4, H1a, pri-miR132, Sox11, and Ptgs2 (n = 3). In all of these cases, these genes exhibited a significantly elevated expression signal within the GCL on the stimulated side of the

brain as compared to the unstimulated hemisphere. Sox11, a known neurogenesis marker (Bergsland *et al.*, 2006), is seen expressed in small subsets of cells within the subgranular zone within the GCL of the unstimulated side, but the stimulated side appears to express Sox11 in all of the GCL cells similar to the other mRNAs we examined. In contrast, there was generally little

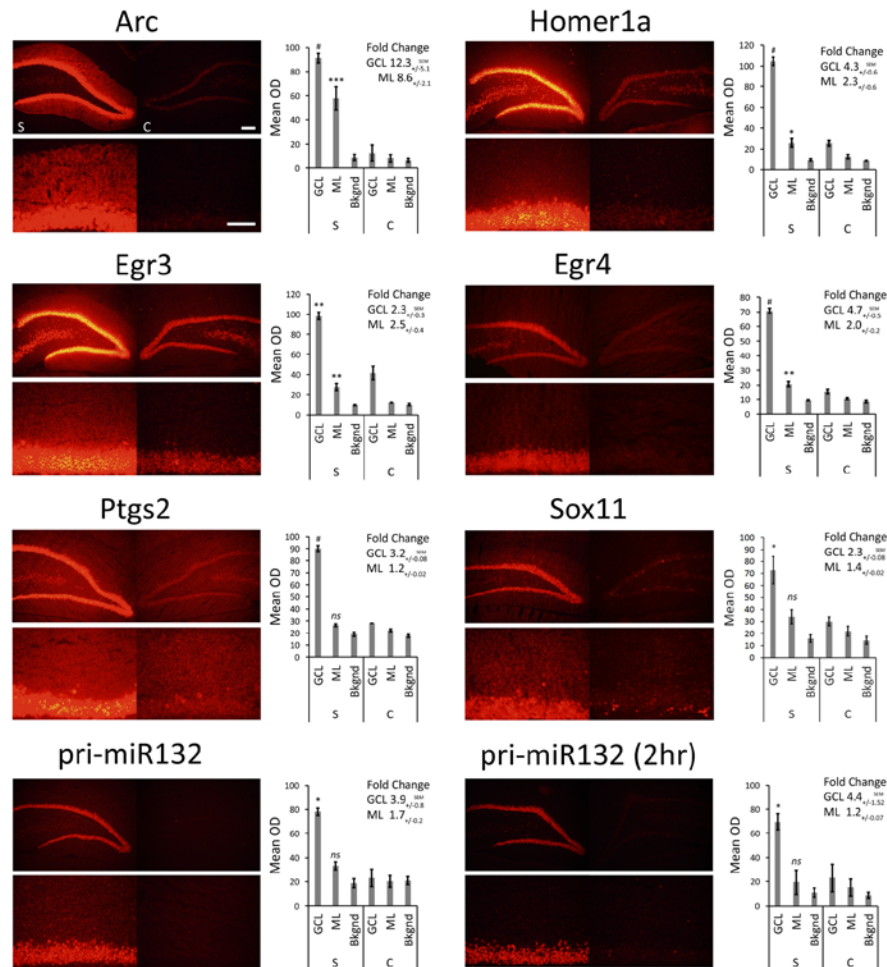


Figure 5.5 FISH for genes upregulated 4hr post induction of LTP

(A) FISH for Arc, Egr3, Egr4, H1a, pri-miR132, Sox11 and Ptgs2. Rats were stimulated with pp-HFS and tissue was taken at the 4 hr time point followed by FISH with transcript specific riboprobes. A 2 hr time point is included for pri-miR132. Each slice was imaged at two different magnifications; zoom-out (top) and zoom-in (bottom). Control DG (right; c = control) and the stimulated DG (left; s = stimulated). (B) The mean optical density of the *in situ* signal from the

ML, GCL and background was quantified. (* = $p < 0.05$, ** = $p < 0.005$, # $p = <0.001$) *ns* = not significant. Error bars represent SEM. $n = 3$ per group. Zoom-out Scale Bar- 200um. Zoom-in Scale Bar 100um.

or no signal detected within the ML for these genes. *Egr3*, *Egr4* and *H1a* exhibited a modest, but statistically significant signal within the ML on the stimulated side. These three mRNAs also appeared to be expressed within the hilus on the stimulated side. None of the genes appeared to be expressed by specific cells localized within the ML (i.e., glia). If the mRNAs for *pri-miR132*, *Sox11*, and *Ptgs2* do indeed localize to dendrites within the ML, they likely do so at much lower levels than *Arc* mRNA, considering that our ability to detect them within the ML using FISH is limited. Statistical data for these FISH experiments and intensity curves are provided in figure 5.6.

In our final set of experiments, we sought to determine if utilizing a more sensitive approach could detect pp-HFS-induced mRNAs within the ML. We stimulated another group of animals with pp-HFS and then 2 and 4 hours later, the brains were dissected and coronal sections containing the dorsal hippocampus were prepared for laser microdissection. This time we dissected tissue from the GCL from both the stimulated and unstimulated sides of the brain. We also dissected tissue from the distal most 1/3rd of the ML from both the stimulated and unstimulated sides of the brain. The RNA was isolated from this tissue and converted to cDNA and subsequently analyzed via qRT-PCR with gene specific primers (Figure 5.7). At two hours post pp-HFS, *Arc* mRNA was detected in the GCL and ML on the stimulated sides compared to the unstimulated sides, as expected ($p < 0.05$; $n = 4$ for 2 hrs, $n = 5$ for control). *H1a*, *pri-miR-132*, *Sox11*, *BDNF*,

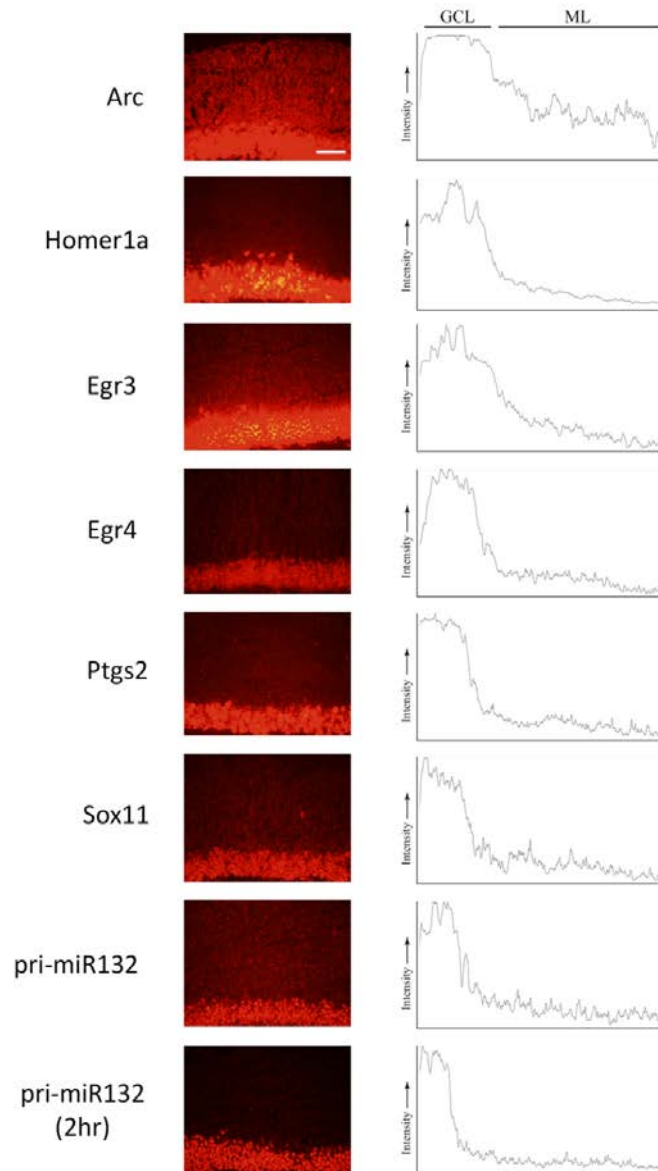


Figure 5.6 Signal intensity from FISH plotted across granule cells and dendrites

ImageJ was used to plot the intensity of the RNA from the GCL and ML to visualize the signal across the two regions. Images were taken at the 4 hr (and pri-miR132 2hr) time point at an optimal exposure for each gene. Plots are representative of the image displayed in this figure. Scale bar = 100um.

Egr2 and Egr4 all exhibited an increase in the GCL on the stimulated side compared to the unstimulated side ($p < 0.05$; $n = 4$ for 2 hrs, $n = 5$ for control). However, for this time point, none of these targets exhibited an increase in the ML on the stimulated side compared to the unstimulated side ($p > 0.05$; $n = 4$ for 2 hrs, $n = 5$ for control), except for pri-miR-132 and Egr4 ($p < 0.05$; $n = 4$ for 2 hrs, $n = 5$ for control). Notably, Egr4 exhibited a large increase in the ML, with a C_t difference of ~ 4 or ~ 16 fold. At four hours post pp-HFS, Arc mRNA was detected in the GCL and ML on the stimulated sides compared to the unstimulated sides, as expected ($p < 0.05$; $n = 4$ for 4 hrs, $n = 5$ for control). H1a, pri-miR-132, Sox11, BDNF, Egr3 and Egr4 all exhibited an increase in the GCL on the stimulated side compared to the unstimulated side for this time point ($p < 0.05$; $n = 4$ for 4 hrs, $n = 5$ for control). The qRT-PCR also detected an increase for H1a, pri-miR-132, Sox11, Egr3 and Egr4 within the ML on the stimulated side compared the unstimulated side for the 4 hour time point ($p < 0.05$; $n = 4$ for 4 hrs, $n = 5$ for control). Interestingly, there wasn't an appreciable increase in BDNF in the ML on the stimulated side compared to the non-stimulated side of the brain. PCR primers used to generate DNA templates for RNA probe production are listed in figure 5.8. Primer sequences can be found in figure 5.9. Statistical data for these qRT-PCR experiments are provided in figure 5.10.

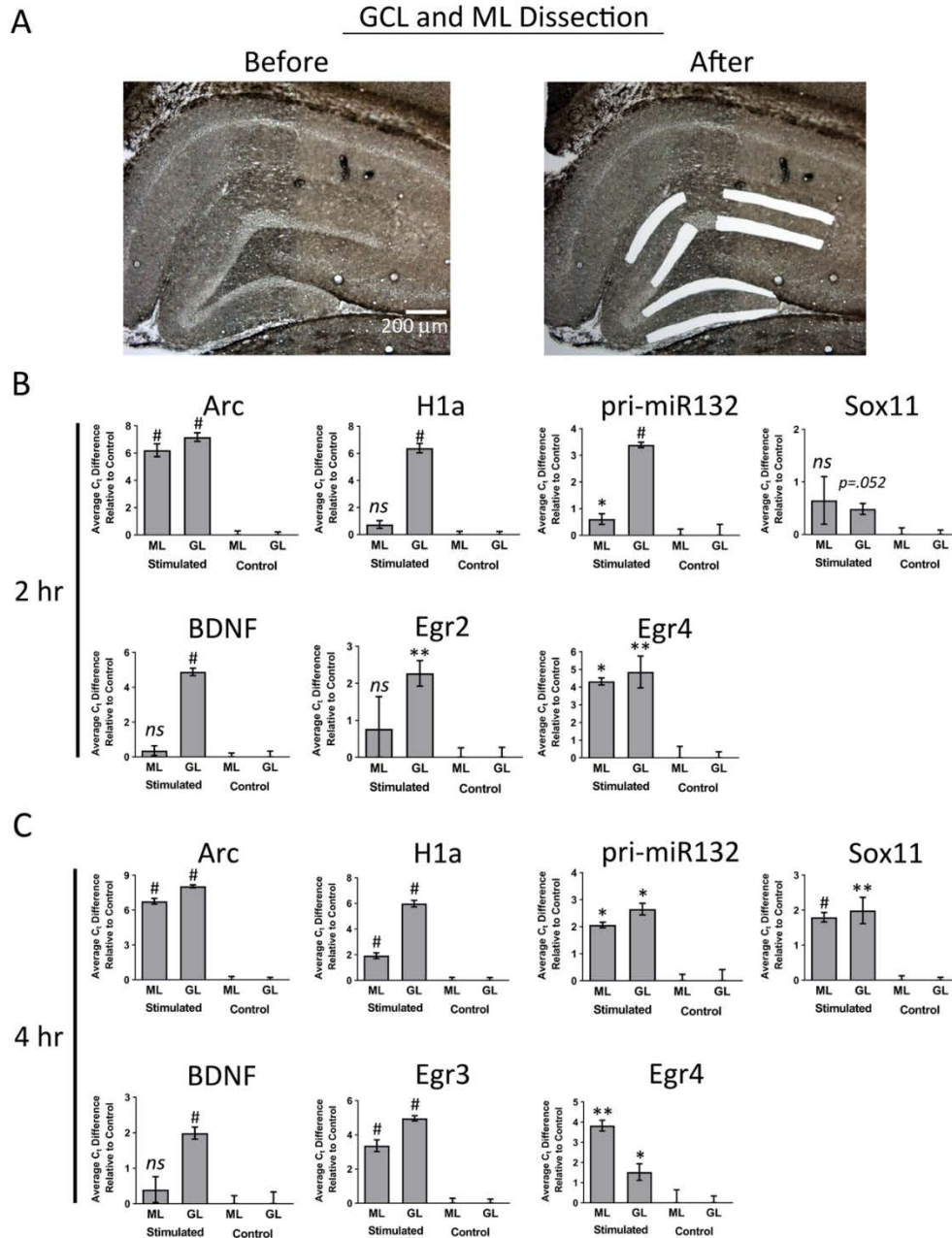


Figure 5.7 qRT-PCR of sample from the ML and GCL 2 hr and 4 hr post induction of LTP
(A) Example images depicting tissue Before LMD and After LMD of GCL and ML tissue from coronal hippocampal sections. Note only the distal 1/3^d of the of the ML was dissected. **(B)** qRT-PCR was performed on these samples for Arc, H1a, pri-miR132, Sox11, BDNF, Egr2 (2 hr only), Egr3 (4 hr only) and Egr4, 2 hrs and 4 hrs post-pp-HFS. (* = $p < 0.05$, ** = $p < 0.005$, # $p < 0.001$) *ns* = not significant. $n = 5$ for control, $n = 4$ for 2 hr and 4 hr samples. Error bars represent SEM.

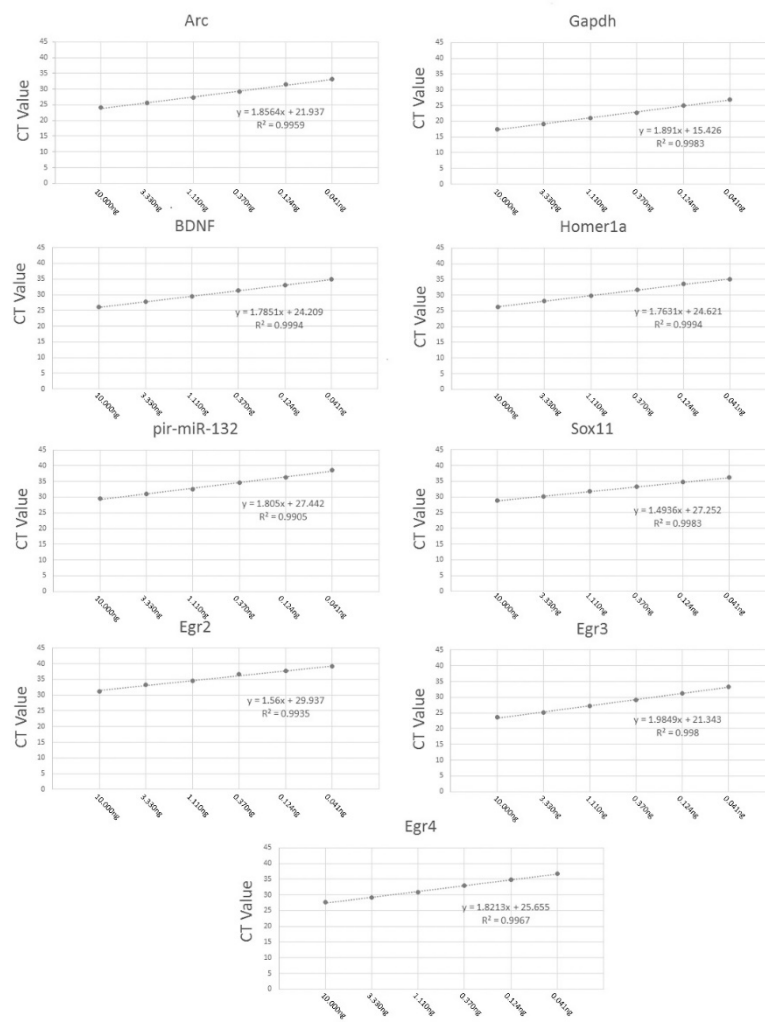


Figure 5.8 Standard curves for qRT-PCR primers

Confirmation of qRT-PCR primers. A defined amount of RNA, extracted from rat hippocampus, was converted to cDNA using Superscript Reverse Transcriptase II. Six samples, in duplicate were subjected to qRT-PCR, each a 1:3 dilution of the previous sample (10ng, 3.33ng, 1.11ng, 0.037ng, 0.124ng and 0.041ng). The scatter plot, slope and R² are provided for each gene.

Primers used for qRT-PCR

Arc	FP	CCCTGCAGCCCAAGTTCAAG
	RP	GAAGGCTCGCTGCCTGCTC
pri-miR-132	FP	TCCTGGCACCAGAAATAAACG
	RP	ACAAAAGCATGCCCCAGCAC
BDNF	FP	AAGGCTGCAGGGGCATAGAC
	RP	TGAACCGCCAGCCAATTCTC
Sox11	FP	CTCCTCGGGAGGCAGTCG
	RP	TCTGCGCCACATCTCTGACC
Homer1a	FP	CTGCTCCAAGGAAAGCCTTGC
	RP	AAACAACCTTCAATGCTGACGG
Egr2	FP	GAAGCGCCACACCAAGATCC
	RP	CCTCCAATGGCGCTGTTACC
Egr3	FP	GCGCTCAGTACGCAGACGAC
	RP	GTCGCCGCAGTTGGAATAGG
Egr4	FP	CTGCCCGTGGAGAGCTG
	RP	TGAAGTTGCGCAGGCAGATG
Gapdh	FP	GCATCCTGCACCACCAACTG
	RP	ACGCCACAGCTTTCAGAGG

Primers used to generate in situ Probes

pri-miR132	FP	CAGGGCAACCGTGGCTTTCGATTGTTACTGTGGGAACCGG
	RP	GGTCTCACTGTAGTTCTGGCTAGCCTTGAACCTCACAGAAACCC
Sox11	FP	CTCCTCTGAGCTGCTCGATC
	RP	CGGCTTGGCAAACAAGCCTTAC
Egr3	FP	CCTCGAGATGACCGGCAAACTCGCCGAG
	RP	AATACGACTCACTATAGGGAGAGGGCGCAGGTGGTGACCACAGG
Cox2	FP	CGCTCAGCCATGCAGCAAATCC
	RP	GGGTTAATGTCATCTAGTCTGGAGTGGG
Egr4	FP	CCTCGAGATGCTCCACCTGAGCGACTTC
	RP	CAGCGCGCGAAAGAGAGGCCACG

Figure 5.9 qRT-PCR Primer Sequences

A list of primers used for qRT-PCR and primers used to amplify sequences for *in situ* probe templates.

qRTPCR of Microarray Samples (Figure 3)

		<i>p</i>	Tstat
2 Hr	Arc	0.005235384	5.527
4 Hr	Arc	0.006010528	5.319
2 Hr	BDNF	0.019112599	3.799
4 Hr	BDNF	0.002055996	7.121
2 Hr	Homer1a	0.010397923	4.552
4 Hr	Homer1a	0.000865502	8.941
2 Hr	Egr3	0.011763453	4.392
4 Hr	Egr3	0.022871237	3.594
2 Hr	Egr4	0.001226428	8.162
4 Hr	Egr4	0.003228142	6.309
4 Hr	Sox11	0.000473963	10.449
2 Hr	pri-miR132	0.146500796	1.798
4 Hr	pri-miR132	0.018554421	3.834

Control n=3; 4 Hr n=3; 2 Hr n=3

in situ Quantification (Figure 5)

GCL: Stimulated vs Control

	<i>p</i>	Tstat
Arc	0.0004622	10.517
Homer1a	0.0000499	18.530
Egr3	0.0018237	7.351
Egr4	0.0000150	25.099
Ptgs2	0.0000026	38.827
Sox11	0.0119573	4.371
pri-miR132	0.0055121	5.448
pri-miR132 (2 Hr)	0.0092211	4.713

Control n=3; Stimulated n=3

in situ Quantification (Figure 5)

ML: Stimulated vs Control

	<i>p</i>	Tstat
Arc	0.0025699	6.708
Homer1a	0.0418832	2.952
Egr3	0.0088150	4.774
Egr4	0.0075926	4.981
Ptgs2	0.1199903	1.971
Sox11	0.47322114	0.791
pri-miR132	0.1765127	1.639
pri-miR132 (2 Hr)	0.7825205	0.295

Control n=3; Stimulated n=3

qRTPCR of GCL and ML (Figure 6)
ML: Stimulated vs Control

		<i>p</i>	Tstat
2 Hr	Arc	0.0000854	11.724
4 Hr	Arc	0.0000005	17.096
2 Hr	BDNF	0.4270680	0.815
4 Hr	BDNF	0.3672717	0.922
2 Hr	Homer1a	0.0871780	2.038
4 Hr	Homer1a	0.0006023	5.809
2 Hr	Egr2	0.4532284	0.934
4 Hr	Egr2	<i>nd</i>	<i>nd</i>
2 Hr	Egr3	<i>nd</i>	<i>nd</i>
4 Hr	Egr3	0.0002308	7.550
2 Hr	Egr4	0.0017489	5.713
4 Hr	Egr4	0.0023898	4.949
2 Hr	Sox11	0.2493412	1.536
4 Hr	Sox11	0.0000322	9.693
2 Hr	pri-miR132	0.0458440	3.004
4 Hr	pri-miR132	0.0024867	8.031

Control n=5; 4 Hr n=4; 2 Hr n=4

qRTPCR of GCL and ML (Figure 6)
GCL: Stimulated vs Control

		<i>p</i>	Tstat
2 Hr	Arc	0.0000027	20.057
4 Hr	Arc	0.0000001	27.586
2 Hr	BDNF	0.0000024	19.356
4 Hr	BDNF	0.0007550	10.134
2 Hr	Homer1a	0.0000118	16.139
4 Hr	Homer1a	0.0000008	17.793
2 Hr	Egr2	0.0019791	5.277
4 Hr	Egr2	<i>nd</i>	<i>nd</i>
2 Hr	Egr3	<i>nd</i>	<i>nd</i>
4 Hr	Egr3	0.0000013	16.066
2 Hr	Egr4	0.0080544	5.506
4 Hr	Egr4	0.0273757	2.887
2 Hr	Sox11	0.0526621	3.282
4 Hr	Sox11	0.0028880	8.948
2 Hr	pri-miR132	0.0000056	14.265
4 Hr	pri-miR132	0.0058658	5.741

Control n=5; 4 Hr n=4; 2 Hr n=4

qRTPCR of GCL and ML (Figure 6)
ML: 2 Hr vs 4 Hr

		<i>p</i>	Tstat
Arc		0.3542154	1.030
BDNF		0.9259294	0.097
Homer1a		0.0175692	3.302
Egr2		<i>nd</i>	<i>nd</i>
Egr3		<i>nd</i>	<i>nd</i>
Egr4		0.1937313	1.480
Sox11		0.0798914	2.440
pri-miR132		0.0057621	4.502

Control n=5; 4 Hr n=4; 2 Hr n=4

qRTPCR of GCL and ML (Figure 6)
GCL: 2 Hr vs 4 Hr

		<i>p</i>	Tstat
Arc		0.8903248	0.147
BDNF		0.0453306	2.694
Homer1a		0.3868788	0.940
Egr2		<i>nd</i>	<i>nd</i>
Egr3		<i>nd</i>	<i>nd</i>
Egr4		0.0264433	3.354
Sox11		0.0069674	4.037
pri-miR132		0.2083755	1.562

Control n=5; 4 Hr n=4; 2 Hr n=4

qRTPCR of GCL and ML (Figure 6)
GCL vs ML

		<i>p</i>	Tstat
2 Hr	Arc	0.2917397	1.172
4 Hr	Arc	0.0086008	4.530
2 Hr	BDNF	0.0000076	15.651
4 Hr	BDNF	0.0001623	9.517
2 Hr	Homer1a	0.0000278	11.942
4 Hr	Homer1a	0.0000349	11.083
2 Hr	Egr2	0.4385327	0.861
4 Hr	Egr3	0.0036289	5.927
2 Hr	Egr4	0.2813487	1.287
4 Hr	Egr4	0.0195007	3.343
2 Hr	Sox11	0.5916628	0.569
4 Hr	Sox11	0.0414128	3.050
2 Hr	pri-miR132	0.0000503	12.658
4 Hr	pri-miR132	0.0673866	2.353

Control n=5; 4 Hr n=4; 2 Hr n=4

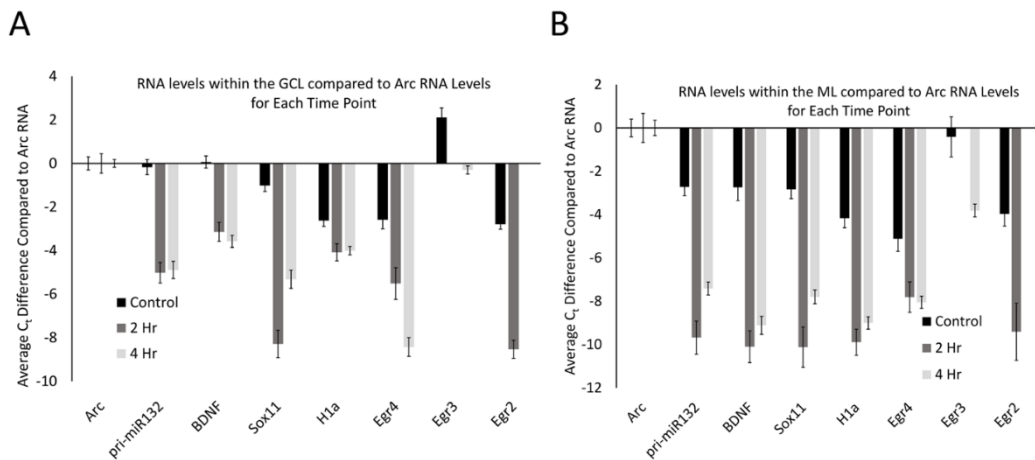
Figure 5.10 Statistics for qRTPCR experimets

P-values and T statistic (Tstat) for all statistics presented in figure 5.7. All statistics were done using a Two-sample, Two-tailed t-test assuming equal variances, where a *p* of <0.05 is considered significant. *nd* = not determined.

Arc mRNA is relatively abundant within the GCL and ML compared to other mRNAs examined

The qRT-PCR data allowed us to examine the relative levels of these mRNAs within the dentate gyrus, which could provide some insight into how these differing mRNAs compare to the levels of Arc mRNA. To do this, we first normalized the levels of each RNA to the levels of GAPDH mRNA. We then compared the control GCL sample Arc mRNA levels to the other control GCL mRNA samples examined, (i.e., Egr2, Egr3, etc.). We found that Arc mRNA levels were modestly higher than the other mRNAs examined except for Egr3 (Figure 5.11A); however, when we compared Arc GCL mRNA levels at the 2 and 4 hr timepoints to the other GCL mRNAs examined at these time points, we found that Arc levels were much higher than the other mRNAs for these time points. We then compared the control sample's Arc mRNA levels within the ML to the other control ML mRNAs. We found that Arc ML mRNA levels were higher than the other ML mRNAs examined, except for Egr3 (Figure 5.11B). When we compared the 2 and 4 hr time point Arc mRNA levels within the ML to the other mRNAs examined for the 2 and 4 hr time points, we found that Arc ML levels were significantly higher than the other mRNAs. We report the relative fold differences of Arc mRNA compared to the other mRNAs examined in the GCL and ML (Figure 5.11C-D). Arc mRNA generally is more abundant than the other mRNAs examined. Within the ML compartment, Arc levels can exceed the levels of some of these other mRNAs 100 - 1000-fold. In our last analysis, we compared the GCL versus ML levels of each mRNA (Figure 5.12A-B). We found that Arc mRNA levels were consistently higher within the ML compared to the GCL across all samples (control, 2 hr, and 4 hr). In contrast, virtually all the other mRNAs examined exhibited much higher GCL levels

compared to ML levels. An important exception was Egr4 at the 4 hr time point. Collectively, these mRNA level findings corroborate the DNA microarray findings indicating that Arc mRNA levels are much higher within the ML compared to most of the other mRNAs we examined. Additionally, these data support the notion that while some of these mRNAs do increase their levels within the ML following pp-HFS, their relative levels compared to Arc mRNA are exceedingly low and this is likely the main reason why FISH analysis was unable to convincingly detect these candidate mRNAs within the ML.



C Relative Fold Differences in Arc mRNA levels within the GCL compared to mRNA levels of each gene

	Arc	pri-miR132	BDNF	Sox11	H1a	Egr4	Egr3	Egr2
Control	1.00	1.13	0.96	2.02	6.16	6.00	0.23	6.90
2 Hr	1.00	32.33	8.85	311.91	16.91	45.57	nd	369.65
4 Hr	1.00	29.65	11.94	39.91	16.07	344.29	1.23	nd

Note: Comparisons are for each time point; Numbers reflect the relative amount of Arc mRNA

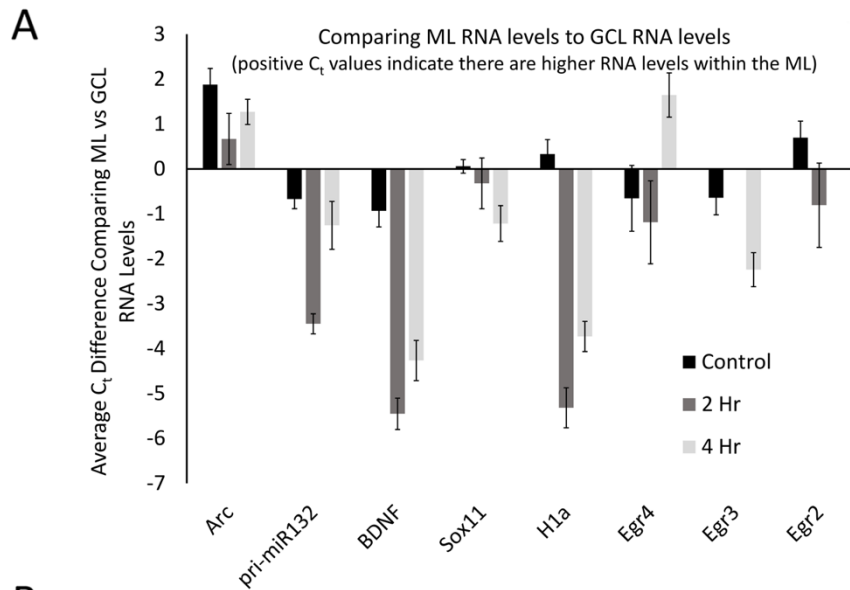
D Relative Fold Differences in Arc mRNA levels within the ML compared to mRNA levels of each gene

	Arc	pri-miR132	BDNF	Sox11	H1a	Egr4	Egr3	Egr2
Control	1.00	6.59	6.72	7.15	18.04	34.73	1.33	15.67
2 Hr	1.00	820.30	1097.50	1116.68	952.12	224.41	nd	682.06
4 Hr	1.00	170.81	554.00	223.44	514.22	265.49	14.06	nd

Note: Comparisons are for each time point; Numbers reflect the relative amount of Arc mRNA

Figure 5.11 qRTPCR results normalized to Arc

Arc mRNA levels at each time point (control, 2 hr, 4 hr), are much higher than other candidate gene transcripts examined. **(A)** mRNA levels in reference to Arc mRNA levels within the GCL. Comparisons are between each mRNA examined compared to Arc mRNA for each time point. Negative C_t values indicate lower mRNA levels. (n = 5 for control, n = 4 for 2 hr and 4 hr samples). Error bars represent SEM. **(B)** Comparison of mRNA levels in reference to Arc mRNA levels within the ML. Comparisons are between each mRNA examined compared to Arc mRNA for each time point. Negative C_t values indicate lower mRNA levels. (n = 5 for control, n = 4 for 2 hr and 4 hr samples). Error bars represent SEM. **(C)** Relative fold differences of Arc compared to the other mRNAs examined for each time point within the GCL. Numbers reflect the relative amount of Arc mRNA. In most comparisons presented, Arc exhibits higher levels of mRNA than the other genes analyzed at each time point. Numbers above one indicates higher levels of Arc mRNA. *nd* = not determined. **(D)** Relative fold differences of Arc compared to the other mRNAs examined for each time point within the ML. Numbers reflect the relative amount of Arc mRNA. Numbers above one indicates higher levels of Arc mRNA. In most comparisons presented, Arc exhibits higher levels of mRNA than the other genes analyzed at each time point. *nd* = not determined.



B

ML vs GCL Fold Differences in RNA

	Arc	pri-miR132	BDNF	Sox11	H1a	Egr4	Egr3	Egr2
Control	3.68	0.63	0.52	1.04	1.26	0.64	0.64	1.62
2 Hr	1.59	0.09	0.02	0.80	0.03	0.44	<i>nd</i>	0.57
4 Hr	2.41	0.42	0.05	0.43	0.08	3.13	0.21	<i>nd</i>

Note: Numbers above 1 indicate higher ML RNA levels

Figure 5.12 qRT-PCR result comparison of ML and GCL levels

Arc mRNA levels are proportionally higher within the ML compared to the GCL. **(A)** Levels of each mRNA in the ML compared to their levels in the GCL for each time point. Positive C_t values indicate higher levels within the ML. (n = 5 for control, n = 4 for 2 hr and 4 hr samples). Error bars represent SEM. **(B)** Fold differences of RNA levels in the ML, compared to the GCL for each time point. Numbers above 1 indicate higher mRNA levels within the ML. (n = 5 for control, n = 4 for 2 hr and 4 hr samples). *nd* = not determined.

Discussion

Decades ago, Arc was serendipitously identified to localize to dendrites of granule cell neurons within the hippocampus following neural activity (Link *et al.*, 1995; Lyford *et al.*, 1995). Besides this being an intriguing phenomenon, arguably, the most noteworthy aspect of this phenomenon was how robust it is and how easy it is to detect using *in situ* hybridization. To date, no other activity dependent transcript has been shown with such unambiguity to localize to dendrites. Considering this fact, one may wonder if Arc mRNA is unique among activity dependent transcripts for its ability to accumulate within the dendrites with such robustness and efficiency. Because of this, we sought to identify all known transcripts within the GCL of the rat dentate gyrus which are transported to the distal dendrites following synaptic activity induced by pp-HFS. Our genome wide screen revealed that out of 27,000 unique transcripts represented on the Affymetrix DNA microarray, Arc exhibited the greatest accumulation within the dendrites following pp-HFS. Subsequent experiments utilizing FISH and qRT-PCR generated data consistent with this observation. Our study also revealed other activity dependent transcripts likely localize to granule cell dendrites following pp-HFS, but do so with much less robustness and efficiency. In particular, we report that Homer1A, Egr3, and Egr4 transcripts localize to the dendrites of granule cell neurons following pp-HFS. We also identified pri-miR132 RNA as

being localized to granule cell dendrites; however, our FISH experiments were not able to confirm this finding, and this may be due technical limitations of the FISH technique not being capable of detecting low levels of this transcript. Additional analysis of the qRT-PCR data revealed that Arc is generally a much more abundant mRNA within the GCL and ML compared to the other RNAs examined and it possesses proportionally more mRNA within the ML compared to the GCL for all samples tested (i.e., control, 2 hr, and 4 hr). Arc mRNA appears to be a very abundant activity dependent transcript, and it is this abundance that likely contributes to the ability to detect Arc mRNA within the dendrites of the ML with impressive ease and unambiguity when utilizing FISH.

The design of our study benefits from the fact that pp-HFS leads to robust induction of gene expression within the dentate gyrus and associated molecular layer and this dramatically increases the signal to noise ratio that is required for optimal gene discovery. Additionally, the dentate gyrus ML can be easily identified allowing for highly accurate laser microdissection, eliminating gene dilution/negation effects due to contamination from surrounding structures, such as the GCL. Furthermore, the use of the *in vivo* anesthetized LTP preparation has the additional advantage of avoiding gene dilution effects which may be inherent in either awake-behaving models, due to variability in the baseline expression of activity-dependent genes (Cirelli *et al.*, 2004), or *in vitro* slice methods, in which cutting the brain slice alone may result in significant changes in gene expression (Taubenfeld *et al.*, 2002). So, in theory our study design should provide a unique method to detect transcripts that accumulate in the dendrites contained within the ML following pp-HFS, with a few caveats. The ML is composed primarily of dendrites from GCL neurons, but glial cells are present too. So, it is a possibility that some of the

31 genes we identified in our microarray screen to be increased within the ML following pp-HFS could be due to an increase in expression within glial cells contained within the ML. However, for this to be the case it would mean that pp-HFS would have had to induce ML glial gene expression on the side of stimulation and glial cells contained within the ML of the unstimulated side did not exhibit a commensurate increase in gene expression. While we cannot rule out this possibility for every candidate gene we identified, there are a number of reasons this would be unlikely and/or would not significantly influence our main findings.

Most of the transcripts we identified, have previously been identified to be increased due to pp-HFS or KCl-mediated neuronal depolarization (Matsuo *et al.*, 2000; Yamazaki *et al.*, 2001; Ploski *et al.*, 2010; Ryan *et al.*, 2011; Ryan *et al.*, 2012) and are; therefore, generally believed to be of neuronal origin. While this doesn't rule out that the expression could be also originating from glial cells, *in situ* hybridization experiments from our study and others (Ploski *et al.*, 2010), have determined that expression of many of these genes are clearly of neuronal origin and, if there is glial expression, is it below the detectable level utilizing *in situ* hybridization. For example, if gene expression within glia was changing due to pp-HFS, we should have detected it within cellular nuclei within the ML following pp-HFS during our FISH experiments. Instead, every gene that we examined for gene expression using FISH following pp-HFS, exhibited a clear GCL signal indicating neuronal origin and there was no indication that gene expression was being induced within specific cellular nuclei within the ML, indicating that expression from glial cells was an unlikely source for the origin of these transcripts. FISH revealed that Egr3, Homer1A, and Egr4 exhibited a diffuse signal within the confines of the ML on the stimulated side of the brain, consistent with dendritic localization of these transcripts. The induction of glial

gene expression within the ML due to pp-HFS has never been reported, but even if some of transcripts that we identified in our screen are of glial origin, the fact remains that there is no evidence of any other activity dependent transcript is comparable to Arc, in its ability to locate to the dendrites with such efficiency or magnitude.

It also remains possible that our microarray screen might have identified transcripts that increase their levels within the ML due to pp-HFS, that are not activity dependent transcripts. For example some transcripts such as alpha Ca²⁺/calmodulin-dependent protein kinases II, (α CaMKII), are constitutively expressed and localize to the dendrites, but synaptic activity has been shown to enhance their trafficking to the dendrites (Mori *et al.*, 2000; Havik *et al.*, 2003). We did not identify α CaMKII transcripts in our microarray screen, quite possibly due to the fact that the enhanced trafficking that α CaMKII might have undergone, was not significant enough to reach the threshold set by our filtering of the microarray data. Most of the genes identified in our screen have been previously identified to be activity dependent genes (Lin *et al.*, 2008; Ploski *et al.*, 2010).

In our study, we chose to analyze mRNA levels at 2 and 4 hours post stimulation compared to unstimulated controls utilizing DNA microarray technology; however, we could have utilized RNAseq technology instead. We opted to utilize DNA microarrays in part because we suspected that the transcripts of interest (i.e., RNAs that localize to dendrites following pp-HFS), would likely be relatively rare transcripts compared to the total cellular RNAs that might be present within the ML. Since DNA microarray is a probe-based technology, by design, as long as the transcripts for a particular probe produce a signal above a threshold level, we would be able to collect data regarding the specific transcript/gene, and easily filter out all of the genes

that did not differ in their expression between the stimulated and unstimulated sides. In contrast, RNAseq relies on the chance event of sequencing each transcript within the sample; therefore, transcripts of low abundance might never be sequenced and therefore no data would be collected regarding those transcripts. This issue can be overcome by increasing the sequencing depth for each sample. Since next generation DNA sequencing costs have dropped dramatically over the years, this is less of a concern, since it is no longer cost prohibitive to perform extensive next generation sequencing to ensure an adequate sequencing depth. When we performed the DNA microarray experiment; however, we opted to take a more cautious approach as it remained uncertain what sequencing depth would be required to adequately analyze our samples.

The time periods we examined RNA expression were based on three factors: the time period pp-HFS induced gene expression would likely occur, the amount of time it might take for transcribed RNA to accumulate within the dendrites, and keeping the number of samples within a manageable range. Previous studies have indicated that Arc mRNA is transcribed relatively rapidly following pp-HFS and it accumulates within the dendrites over many minutes and hours, where 2 hrs post-pp-HFS appears to have a stronger Arc mRNA signal within the dendrites compared to earlier time points(Steward *et al.*, 1998). Based on this phenomenon, we reasoned that if there were other immediate early genes expressed due to pp-HFS and transported to the dendrites, 2 hrs pp-HFS would likely be a good time point to capture them. Because pp-HFS also induces the expression of numerous transcription factors that create additional waves of transcription, if some of these transcripts are transported to the dendrites, we thought we might be able to capture them at the 4 hr time point, when they might have had enough time to accumulate within the dendrites. However, the fact remains that we might have missed

transcripts if they had a relatively short half-life within the dendrites, or if their accumulation within the dendrites didn't occur until after the 4 hr time point. Interestingly, Arc mRNA expression has been shown to express for up to eight hours within GCL neurons due to exploratory behavior indicating that gene expression might continue on for hours post-stimulation (Ramirez-Amaya *et al.*, 2005). Consistent with this view, one study identified gene expression changes 5 and 24 hrs after pp-HFS, but in most cases the gene expression changes were modest at these time points indicating the robust transcription changes seen shortly after pp-HFS were ending or over (Ryan *et al.*, 2012).

Numerous attempts have been made to identify the mRNAs that localize to dendrites. Some of these attempts have used a candidate gene approach, while others have utilized an unbiased screening approach. For example, some studies have isolated mRNA selectively from dendrites by dissecting out portions of dendrites from sparsely populated neuronal cultures followed by RNA amplification to generate enough RNA suitable for differential display or DNA microarray screens (Miyashiro *et al.*, 1994; Eberwine *et al.*, 2002). One study used a similar approach but grew the neurons on a porous filter that allowed neuronal processes to pass through the pores of the filter to physically separate the neuronal processes from the cell bodies. The neuronal processes were then mechanically sheared from the neuronal cell bodies, the RNA was isolated, amplified and subjected to DNA microarray, resulting in many candidate genes (Poon *et al.*, 2006). Other notable approaches for identifying mRNAs which localize to dendrites have included biochemical fractionation of synaptoneuroosomes (Sung *et al.*, 2004) or post synaptic density (PSD) (Tian *et al.*, 1999) fractions followed by the isolation and examination of the RNA contained within these fractions. RNA has been isolated from manually dissected

dendrites and cell bodies from the CA1 region of the hippocampus followed by DNA microarray analysis to compare differential abundance of RNAs between these two regions (Zhong *et al.*, 2006). A more recent study (Cajigas *et al.*, 2012) manually dissected dendrites and cell bodies from the CA1 region of the hippocampus and subjected normalized cDNA libraries generated from the dissected material to 454 Deep Sequencing and identified over 8000 genes (~ a third of the genome). The authors of this study then used bioinformatics to remove genes that might have been detected due to contamination from glia, cell bodies and interneurons to reduce the list to ~ 2500 genes. In the discussion of this paper the authors claim that half of all genes expressed within CA1 neurons contain their mRNAs within the dendrites of CA1 neurons. Similar studies have been conducted to detect micro-RNAs (miRNAs) within dendrites (Kye *et al.*, 2007; Lugli *et al.*, 2008; Siegel *et al.*, 2009). Collectively, all of these studies are technically demanding and noteworthy; however, there is little consistency among the genes identified between these above-mentioned studies and some are lacking specific information regarding which transcripts were identified due to a lack of bioinformatic information available at the time these studies were conducted.

Our data indicates multiple genes might increase their mRNAs within the distal dendrites of the ML following pp-HFS; however, these genes do so at much lower levels than Arc. Some of these mRNAs code for transcription factors (Sox11, Egr2, Egr3 and Egr4). This is an intriguing finding, but it is of course difficult to explain why nuclear localized proteins would have their mRNAs present within the dendrites. One possibility is that these transcription factors are locally translated following synaptic activity and then the proteins localize to the nucleus to regulate gene expression. This model provides an elegant mechanism for synapse to nucleus

signaling. However, one obvious flaw with this view, is that our data indicates these RNAs localize to dendrites hours after the synaptic activity and it remains uncertain if they would remain within this compartment long enough to effectively serve as a link between future synaptic activity and the nucleus. Alternatively, maybe most of these RNAs are present within the dendrites simply due to diffusion and there is no physiological significance for their existence within the dendrites. For example findings from Cajigas *et al.* (Cajigas *et al.*, 2012), indicate that many RNAs from many different genes, (possibly thousands), have RNAs that localize to the dendrites. We suspect that in many of these cases there likely isn't a physiological reason why these RNAs are within the dendrites. Notably, even for highly studied mRNAs like Arc, where high levels of Arc mRNAs are present within the dendrites of the ML, it still remains undetermined what the true significance of localizing Arc mRNA to the dendrites is, because no such studies have been performed to answer this question. It is generally accepted that Arc mRNA is locally translated at activated synapses. But would there be a physiological consequence if Arc mRNA was restricted to the cell body region? More research is needed to determine this.

In conclusion, our data indicates Arc is a unique activity dependent gene, due to the magnitude and efficiency which its activity dependent transcript localizes to the dendrites. Our study determined other activity dependent transcripts likely localize their transcripts to the dendrites following neural activity, but do so with significantly less magnitude compared to Arc.

References

- Bergsland, M., Werme, M., Malewicz, M., Perlmann, T. & Muhr, J. (2006) The establishment of neuronal properties is controlled by Sox4 and Sox11. *Genes & development*, 20, 3475-3486.
- Bicker, S., Lackinger, M., Weiss, K. & Schratt, G. (2014) MicroRNA-132, -134, and -138: a microRNA troika rules in neuronal dendrites. *Cell Mol Life Sci*, 71, 3987-4005.
- Bliss, T.V. & Lomo, T. (1973) Long-lasting potentiation of synaptic transmission in the dentate area of the anaesthetized rabbit following stimulation of the perforant path. *J Physiol*, 232, 331-356.
- Cajigas, I.J., Tushev, G., Dieck, S., Fuerst, N. & Schuman, E.M. (2012) The Local Transcriptome in the Synaptic Neuropil Revealed by Deep Sequencing and High-Resolution Imaging. *Neuron*, 74, 453-466.
- Cirelli, C., Gutierrez, C.M. & Tononi, G. (2004) Extensive and divergent effects of sleep and wakefulness on brain gene expression. *Neuron*, 41, 35-43.
- Corbin, R., Olsson-Carter, K. & Slack, F. (2009) The role of microRNAs in synaptic development and function. *BMB reports*, 42, 131-135.
- Crino, P.B. & Eberwine, J. (1996) Molecular characterization of the dendritic growth cone: regulated mRNA transport and local protein synthesis. *Neuron*, 17, 1173-1187.
- Davis, S., Vanhoutte, P., Pages, C., Caboche, J. & Laroche, S. (2000) The MAPK/ERK cascade targets both Elk-1 and cAMP response element-binding protein to control long-term potentiation-dependent gene expression in the dentate gyrus in vivo. *J Neurosci*, 20, 4563-4572.
- de Solis, C.A., Holehonnur, R., Banerjee, A., Luong, J.A., Lella, S.K., Ho, A., Pahlavan, B. & Ploski, J.E. (2015) Viral delivery of shRNA to amygdala neurons leads to neurotoxicity and deficits in Pavlovian fear conditioning. *Neurobiol Learn Mem*, 124, 34-47.
- Deadwyler, S.A., Dunwiddie, T. & Lynch, G. (1987) A critical level of protein synthesis is required for long-term potentiation. *Synapse*, 1, 90-95.
- Eberwine, J., Belt, B., Kacharina, J.E. & Miyashiro, K. (2002) Analysis of subcellularly localized mRNAs using in situ hybridization, mRNA amplification, and expression profiling. *Neurochem Res*, 27, 1065-1077.
- Edbauer, D., Neilson, J.R., Foster, K.A., Wang, C.F., Seeburg, D.P., Battersby, M.N., Tada, T., Dolan, B.M., Sharp, P.A. & Sheng, M. (2010) Regulation of synaptic structure and function by FMRP-associated microRNAs miR-125b and miR-132. *Neuron*, 65, 373-384.

- Farris, S., Lewandowski, G., Cox, C.D. & Steward, O. (2014) Selective localization of arc mRNA in dendrites involves activity- and translation-dependent mRNA degradation. *J Neurosci*, 34, 4481-4493.
- Guzowski, J.F., McNaughton, B.L., Barnes, C.A. & Worley, P.F. (1999) Environment-specific expression of the immediate-early gene Arc in hippocampal neuronal ensembles. *Nat Neurosci*, 2, 1120-1124.
- Havik, B., Rokke, H., Bardsen, K., Davanger, S. & Bramham, C.R. (2003) Bursts of high-frequency stimulation trigger rapid delivery of pre-existing alpha-CaMKII mRNA to synapses: a mechanism in dendritic protein synthesis during long-term potentiation in adult awake rats. *Eur J Neurosci*, 17, 2679-2689.
- Huber, K.M., Kayser, M.S. & Bear, M.F. (2000) Role for rapid dendritic protein synthesis in hippocampal mGluR-dependent long-term depression. *Science*, 288, 1254-1257.
- Kacharina, J.E., Job, C., Crino, P. & Eberwine, J. (2000) Stimulation of glutamate receptor protein synthesis and membrane insertion within isolated neuronal dendrites. *Proc Natl Acad Sci U S A*, 97, 11545-11550.
- Kye, M.J., Liu, T., Levy, S.F., Xu, N.L., Groves, B.B., Bonneau, R., Lao, K. & Kosik, K.S. (2007) Somatodendritic microRNAs identified by laser capture and multiplex RT-PCR. *RNA*, 13, 1224-1234.
- Lin, Y., Bloodgood, B.L., Hauser, J.L., Lapan, A.D., Koon, A.C., Kim, T.K., Hu, L.S., Malik, A.N. & Greenberg, M.E. (2008) Activity-dependent regulation of inhibitory synapse development by Npas4. *Nature*, 455, 1198-1204.
- Link, W., Konietzko, U., Kauselmann, G., Krug, M., Schwanke, B., Frey, U. & Kuhl, D. (1995) Somatodendritic expression of an immediate early gene is regulated by synaptic activity. *Proc Natl Acad Sci U S A*, 92, 5734-5738.
- Lugli, G., Larson, J., Demars, M.P. & Smalheiser, N.R. (2012) Primary microRNA precursor transcripts are localized at post-synaptic densities in adult mouse forebrain. *J Neurochem*, 123, 459-466.
- Lugli, G., Torvik, V.I., Larson, J. & Smalheiser, N.R. (2008) Expression of microRNAs and their precursors in synaptic fractions of adult mouse forebrain. *J Neurochem*, 106, 650-661.
- Lyford, G.L., Yamagata, K., Kaufmann, W.E., Barnes, C.A., Sanders, L.K., Copeland, N.G., Gilbert, D.J., Jenkins, N.A., Lanahan, A.A. & Worley, P.F. (1995) Arc, a growth factor and activity-regulated gene, encodes a novel cytoskeleton-associated protein that is enriched in neuronal dendrites. *Neuron*, 14, 433-445.

- Malenka, R.C. & Nicoll, R.A. (1999) Long-term potentiation--a decade of progress? *Science*, 285, 1870-1874.
- Matsuo, R., Murayama, A., Saitoh, Y., Sakaki, Y. & Inokuchi, K. (2000) Identification and cataloging of genes induced by long-lasting long-term potentiation in awake rats. *J Neurochem*, 74, 2239-2249.
- Messaoudi, E., Kanhema, T., Soule, J., Tiron, A., Dageyte, G., da Silva, B. & Bramham, C.R. (2007) Sustained Arc/Arg3.1 synthesis controls long-term potentiation consolidation through regulation of local actin polymerization in the dentate gyrus in vivo. *J Neurosci*, 27, 10445-10455.
- Miyashiro, K., Dichter, M. & Eberwine, J. (1994) On the nature and differential distribution of mRNAs in hippocampal neurites: implications for neuronal functioning. *Proc Natl Acad Sci U S A*, 91, 10800-10804.
- Mori, Y., Imaizumi, K., Katayama, T., Yoneda, T. & Tohyama, M. (2000) Two cis-acting elements in the 3' untranslated region of alpha-CaMKII regulate its dendritic targeting. *Nat Neurosci*, 3, 1079-1084.
- Partin, A.C., Hosek, M.P., Luong, J.A., Lella, S.K., Sharma, S.A. & Ploski, J.E. (2013) Amygdala nuclei critical for emotional learning exhibit unique gene expression patterns. *Neurobiol Learn Mem*, 104, 110-121.
- Ploski, J.E., Newton, S.S. & Duman, R.S. (2006) Electroconvulsive seizure-induced gene expression profile of the hippocampus dentate gyrus granule cell layer. *J Neurochem*, 99, 1122-1132.
- Ploski, J.E., Park, K.W., Ping, J., Monsey, M.S. & Schafe, G.E. (2010) Identification of plasticity-associated genes regulated by Pavlovian fear conditioning in the lateral amygdala. *J Neurochem*, 112, 636-650.
- Ploski, J.E., Pierre, V.J., Smucny, J., Park, K., Monsey, M.S., Overeem, K.A. & Schafe, G.E. (2008) The activity-regulated cytoskeletal-associated protein (Arc/Arg3.1) is required for memory consolidation of pavlovian fear conditioning in the lateral amygdala. *J Neurosci*, 28, 12383-12395.
- Poon, M.M., Choi, S.H., Jamieson, C.A., Geschwind, D.H. & Martin, K.C. (2006) Identification of process-localized mRNAs from cultured rodent hippocampal neurons. *J Neurosci*, 26, 13390-13399.

- Ramirez-Amaya, V., Vazdarjanova, A., Mikhael, D., Rosi, S., Worley, P.F. & Barnes, C.A. (2005) Spatial exploration-induced Arc mRNA and protein expression: evidence for selective, network-specific reactivation. *J Neurosci*, 25, 1761-1768.
- Rodrigues, S.M., Farb, C.R., Bauer, E.P., LeDoux, J.E. & Schafe, G.E. (2004) Pavlovian fear conditioning regulates Thr286 autophosphorylation of Ca²⁺/calmodulin-dependent protein kinase II at lateral amygdala synapses. *J Neurosci*, 24, 3281-3288.
- Ryan, M.M., Mason-Parker, S.E., Tate, W.P., Abraham, W.C. & Williams, J.M. (2011) Rapidly induced gene networks following induction of long-term potentiation at perforant path synapses in vivo. *Hippocampus*, 21, 541-553.
- Ryan, M.M., Ryan, B., Kyrke-Smith, M., Logan, B., Tate, W.P., Abraham, W.C. & Williams, J.M. (2012) Temporal profiling of gene networks associated with the late phase of long-term potentiation in vivo. *PLoS One*, 7, e40538.
- Schafe, G.E., Nader, K., Blair, H.T. & LeDoux, J.E. (2001) Memory consolidation of Pavlovian fear conditioning: a cellular and molecular perspective. *Trends Neurosci*, 24, 540-546.
- Shi, L. & Reid, L.H. & Jones, W.D. & Shippy, R. & Warrington, J.A. & Baker, S.C. & Collins, P.J. & de Longueville, F. & Kawasaki, E.S. & Lee, K.Y. & Luo, Y. & Sun, Y.A. & Willey, J.C. & Setterquist, R.A. & Fischer, G.M. & Tong, W. & Dragan, Y.P. & Dix, D.J. & Frueh, F.W. & Goodsaid, F.M. & Herman, D. & Jensen, R.V. & Johnson, C.D. & Lobenhofer, E.K. & Puri, R.K. & Schrf, U. & Thierry-Mieg, J. & Wang, C. & Wilson, M. & Wolber, P.K. & Zhang, L. & Amur, S. & Bao, W. & Barbacioru, C.C. & Lucas, A.B. & Bertholet, V. & Boysen, C. & Bromley, B. & Brown, D. & Brunner, A. & Canales, R. & Cao, X.M. & Cebula, T.A. & Chen, J.J. & Cheng, J. & Chu, T.M. & Chudin, E. & Corson, J. & Corton, J.C. & Croner, L.J. & Davies, C. & Davison, T.S. & Delenstarr, G. & Deng, X. & Dorris, D. & Eklund, A.C. & Fan, X.H. & Fang, H. & Fulmer-Smentek, S. & Fuscoe, J.C. & Gallagher, K. & Ge, W. & Guo, L. & Guo, X. & Hager, J. & Haje, P.K. & Han, J. & Han, T. & Harbottle, H.C. & Harris, S.C. & Hatchwell, E. & Hauser, C.A. & Hester, S. & Hong, H. & Hurban, P. & Jackson, S.A. & Ji, H. & Knight, C.R. & Kuo, W.P. & LeClerc, J.E. & Levy, S. & Li, Q.Z. & Liu, C. & Liu, Y. & Lombardi, M.J. & Ma, Y. & Magnuson, S.R. & Maqsodi, B. & McDaniel, T. & Mei, N. & Myklebost, O. & Ning, B. & Novoradovskaya, N. & Orr, M.S. & Osborn, T.W. & Papallo, A. & Patterson, T.A. & Perkins, R.G. & Peters, E.H. & Peterson, R. & Phillips, K.L. & Pine, P.S. & Pusztai, L. & Qian, F. & Ren, H. & Rosen, M. & Rosenzweig, B.A. & Samaha, R.R. & Schena, M. & Schroth, G.P. & Shchegrova, S. & Smith, D.D. & Staedtler, F. & Su, Z. & Sun, H. & Szallasi, Z. & Tezak, Z. & Thierry-Mieg, D. & Thompson, K.L. & Tikhonova, I. & Turpaz, Y. & Vallanat, B. & Van, C. & Walker, S.J. & Wang, S.J. & Wang, Y. & Wolfinger, R. & Wong, A. & Wu, J. & Xiao, C. & Xie, Q. & Xu, J. & Yang, W. & Zhong, S. & Zong, Y. & Slikker, W., Jr. (2006) The MicroArray Quality Control (MAQC) project shows inter- and intraplatform reproducibility of gene expression measurements. *Nat Biotechnol*, 24, 1151-1161.

- Siegel, G., Obernosterer, G., Fiore, R., Oehmen, M., Bicker, S., Christensen, M., Khudayberdiev, S., Leuschner, P.F., Busch, C.J., Kane, C., Hubel, K., Dekker, F., Hedberg, C., Rengarajan, B., Drepper, C., Waldmann, H., Kauppinen, S., Greenberg, M.E., Draguhn, A., Rehmsmeier, M., Martinez, J. & Schratt, G.M. (2009) A functional screen implicates microRNA-138-dependent regulation of the deacetylase enzyme APT1 in dendritic spine morphogenesis. *Nature cell biology*, 11, 705-716.
- Stanton, P.K. & Sarvey, J.M. (1984) Blockade of long-term potentiation in rat hippocampal CA1 region by inhibitors of protein synthesis. *J Neurosci*, 4, 3080-3088.
- Steward, O., Wallace, C.S., Lyford, G.L. & Worley, P.F. (1998) Synaptic activation causes the mRNA for the IEG Arc to localize selectively near activated postsynaptic sites on dendrites. *Neuron*, 21, 741-751.
- Sung, Y.J., Weiler, I.J., Greenough, W.T. & Denman, R.B. (2004) Selectively enriched mRNAs in rat synaptoneuroosomes. *Brain Res Mol Brain Res*, 126, 81-87.
- Tai, H.C. & Schuman, E.M. (2006) MicroRNA: microRNAs reach out into dendrites. *Curr Biol*, 16, R121-123.
- Takebayashi, H., Yamamoto, N., Umino, A. & Nishikawa, T. (2014) Identification of developmentally regulated PCP-responsive non-coding RNA, *prt6*, in the rat thalamus. *PLoS One*, 9, e97955.
- Taubenfeld, S.M., Stevens, K.A., Pollonini, G., Ruggiero, J. & Alberini, C.M. (2002) Profound molecular changes following hippocampal slice preparation: loss of AMPA receptor subunits and uncoupled mRNA/protein expression. *J Neurochem*, 81, 1348-1360.
- Tian, Q.B., Nakayama, K., Okano, A. & Suzuki, T. (1999) Identification of mRNAs localizing in the postsynaptic region. *Brain Res Mol Brain Res*, 72, 147-157.
- Tiedge, H. & Brosius, J. (1996) Translational machinery in dendrites of hippocampal neurons in culture. *J Neurosci*, 16, 7171-7181.
- Tiruchinapalli, D.M., Oleynikov, Y., Kelic, S., Shenoy, S.M., Hartley, A., Stanton, P.K., Singer, R.H. & Bassell, G.J. (2003) Activity-dependent trafficking and dynamic localization of zipcode binding protein 1 and beta-actin mRNA in dendrites and spines of hippocampal neurons. *J Neurosci*, 23, 3251-3261.
- Tongiorgi, E., Righi, M. & Cattaneo, A. (1997) Activity-dependent dendritic targeting of BDNF and TrkB mRNAs in hippocampal neurons. *J Neurosci*, 17, 9492-9505.

- Vazdarjanova, A., McNaughton, B.L., Barnes, C.A., Worley, P.F. & Guzowski, J.F. (2002) Experience-dependent coincident expression of the effector immediate-early genes *arc* and *Homer 1a* in hippocampal and neocortical neuronal networks. *J Neurosci*, 22, 10067-10071.
- Vo, N., Klein, M.E., Varlamova, O., Keller, D.M., Yamamoto, T., Goodman, R.H. & Impey, S. (2005) A cAMP-response element binding protein-induced microRNA regulates neuronal morphogenesis. *Proc Natl Acad Sci U S A*, 102, 16426-16431.
- Weiler, I.J., Irwin, S.A., Klintsova, A.Y., Spencer, C.M., Brazelton, A.D., Miyashiro, K., Comery, T.A., Patel, B., Eberwine, J. & Greenough, W.T. (1997) Fragile X mental retardation protein is translated near synapses in response to neurotransmitter activation. *Proc Natl Acad Sci U S A*, 94, 5395-5400.
- Will, T.J., Tushev, G., Kochen, L., Nassim-Assir, B., Cajigas, I.J., Tom Dieck, S. & Schuman, E.M. (2013) Deep sequencing and high-resolution imaging reveal compartment-specific localization of *Bdnf* mRNA in hippocampal neurons. *Sci Signal*, 6, rs16.
- Yamazaki, M., Matsuo, R., Fukazawa, Y., Ozawa, F. & Inokuchi, K. (2001) Regulated expression of an actin-associated protein, synaptopodin, during long-term potentiation. *J Neurochem*, 79, 192-199.
- Zhong, J., Zhang, T. & Bloch, L.M. (2006) Dendritic mRNAs encode diversified functionalities in hippocampal pyramidal neurons. *BMC Neurosci*, 7, 17.

CHAPTER 6

INCREASING GLUN2B VIA GLUN2B(E1479Q) ENABLES MODIFICATION OF A STRONG FEAR MEMORY TRACE VIA RECONSOLIDATION UPDATING

Authors: Christopher A. de Solis, Mario A. Galdamez, Cuauhtémoc U. Gonzalez, Samuel W. Woodard, Roopa Holehonnur, Carlos E. Salinas, Joel N. Miller, John M. Perish, Ozzy H. Pineda, Alfredo Sandoval Jr., Jonathan E. Ploski

School of Behavioral and Brain Sciences

The University of Texas at Dallas

800 West Campbell Road

Richardson, TX 75080-3021, USA

Abstract

Memory retrieval does not initiate the reconsolidation process for some memories rendering pharmacotherapies designed to disrupt reconsolidation ineffective (Wang *et al.*, 2009b; Winters *et al.*, 2009), in particular, strong memories have been shown to be difficult to disrupt via reconsolidation blockade and this is likely due to the inability of these memories to destabilize upon retrieval. In an effort to understand the molecular basis for why weak and strong fear memories differ in their requirements to initiate reconsolidation, we recently determined that training-dependent changes in the N-methyl D-aspartate receptor (NMDAR) subunit composition occur at basal and lateral amygdala (BLA) synapses that correlate with a strong memory's inability to be modified upon retrieval. We then demonstrated that genetically increasing the NMDAR GluN2A/GluN2B ratio is sufficient to block retrieval-induced memory destabilization and this prevents an existing memory trace from being modified via reconsolidation updating. Now we would like to determine if increasing the GluN2B/GluN2A ratio via overexpression of GluN2B or GluN2B(E1479Q) mutant might enhance the initiation of reconsolidation. GluN2B(E1479Q) contains a point mutation in the PDZ domain of GluN2B which leads to higher surface levels of the subunit by inhibiting phosphorylation-driven endocytosis (Sanz-Clemente *et al.*, 2010). In order to examine these questions, we generated lentiviruses designed to express these subunits from a TRE3G promoter. Injecting these viruses into the BLA of α -CaMKII-tTA mice allows us to restrict expression of the GluN2B transgenes to excitatory neurons and also enables expression of the transgene to be selectively expressed before or after fear conditioning training using doxycycline (Dox) (Holehonnur *et al.*, 2016).

Here, we examine how the overexpression of GluN2B and GluN2B(E1479Q) influences the consolidation, extinction and the initiation of reconsolidation of weak and strong Pavlovian auditory fear memories. We found that overexpression of GluN2B(E1479Q) within BLA neurons prior to fear conditioning led to an increase in LTM freezing levels. STM was not affected. Extinction was not affected due to overexpression of GluN2B(E1479Q) or GluN2B(WT) at the time of extinction learning. Increasing GluN2B at the time of reconsolidation with GluN2B(E1479Q), but not GluN2B(WT), allowed for pharmacologically induced amnesia of a strong fear memory. This amnesia was found to be dependent on retrieval. Increasing GluN2B(E1479Q) at the time of reactivation did not affect the initiation of reconsolidation for a weak fear memory.

Introduction

Extensive data indicate that reactivation of weak fear memories induces a period of vulnerability during which they are susceptible to modification or erasure. If these memories are not re-stabilized via the protein synthesis-dependent mechanism of reconsolidation, the memories are lost (Nader et al., 2000a; Nader et al., 2000b; Tronson & Taylor, 2007; Alberini, 2011). It is thought that this transient labialization functions to allow new information to be integrated into the existing memory trace (Przybylski & Sara, 1997; McKenzie & Eichenbaum, 2011) - these alterations may weaken, strengthen, or modify the original memory (Tronson et al., 2006). Pharmacologically blocking the reconsolidation process is a potentially powerful treatment for attenuating memories associated with pathologies, such as PTSD and drug addiction (Taylor et al., 2009; Milton & Everitt, 2010; Pitman, 2011; Suris et al., 2013).

Recent clinical evidence, however, indicates that the effectiveness of this approach may be limited because some memories can be resistant to retrieval-dependent memory destabilization (Wood et al., 2015). That is, retrieval does not initiate the reconsolidation process for some memories, rendering pharmacotherapies designed to disrupt reconsolidation ineffective (Wang et al., 2009b; Winters et al., 2009). This indicates that there are two phases of reconsolidation. The first phase, initiation (or induction) of reconsolidation, is the cellular and molecular events during memory retrieval that produce lability or instability in the memory trace. The second phase of reconsolidation is the re-stabilization (or re-storage), phase of reconsolidation that is generally targeted by blockers of reconsolidation (i.e., anisomycin, propranolol, mifepristone, etc.). It is now known that a number of variables including age of the memory, the strength of a memory and the conditions under which memory retrieval occurs, have been identified as important factors that may contribute to how effective memory retrieval is at initiating the destabilization of the memory and the induction of reconsolidation updating (Suzuki et al., 2004; Wang et al., 2009b; Winters et al., 2009; Holehonnur et al., 2016). Typically, old or strong memories have been shown to be difficult to disrupt via reconsolidation blockade. This is likely due to the inability of these memories to destabilize upon retrieval.

Memories that do not destabilize following memory retrieval can be created artificially by infusing inhibitors of memory destabilization immediately prior to memory retrieval. Utilizing this methodology, it was discovered that activation of the GluN2B subunit containing NMDA receptor is critical for an auditory fear memory to destabilize following retrieval (Ben Mamou et al., 2006; Milton et al., 2013). Published data currently indicate that there are at least three major cellular events that are critical for retrieval induced memory destabilization of

auditory fear memories: NMDAR activation (Ben Mamou et al., 2006; Milton et al., 2013), ubiquitin proteasome dependent protein degradation (Jarome et al., 2011), and alterations in AMPA receptor subunit trafficking/endocytosis (Hong et al., 2013). NMDAR activation is critical to initiate ubiquitin proteasome dependent protein degradation and alterations in AMPA receptor subunit trafficking/endocytosis.

In an effort to understand the molecular basis for why weak and strong fear memories differ in their requirements to initiate reconsolidation updating, our lab determined that training-dependent changes in the N-methyl D-aspartate receptor (NMDAR) subunit composition occur at basal and lateral amygdala (BLA) synapses that correlate with a strong memory's inability to be modified upon retrieval. We then demonstrated that genetically increasing the NMDAR GluN2A/GluN2B ratio was sufficient to block retrieval-induced memory destabilization and this prevents an existing memory trace from being modified via reconsolidation updating (Holehonnur et al., 2016). These experiments provided the first causal evidence that alterations in the GluN2A/GluN2B ratio are sufficient to gate the induction of reconsolidation. Here, we intend to extend these exciting findings by identifying mechanisms that could enhance the induction of reconsolidation so strong pathological memories can be therapeutically modified via reconsolidation updating.

In these experiments we attempt to determine if increasing the GluN2B/GluN2A ratio influences consolidation, extinction, and the initiation of reconsolidation updating of strong and weak Pavlovian auditory fear memories. In order to answer these questions, we have developed doxycycline (Dox)-dependent lentiviruses designed to express GFP, GluN2B(WT), or GluN2B(E1479Q). GluN2B(E1479Q) contains a mutation that leads to higher surface levels of

the subunit by inhibiting phosphorylation-driven endocytosis, leading to a greater increase in the GluN2B/GluN2A ratio.

Material and Methods

Subjects 2-3 month male and female C57B/6J mice (containing a α Camkii-tTA transgene) were individually housed in polycarbonate cages on a 12 hour light/dark cycle. Food and water were provided *ad libitum*. Animal use procedures were in accordance with the National Institutes of Health Guide for the Care and Use of laboratory animals and were approved by the University of Texas at Dallas Animal Care and Use Committee.

Fear Conditioning Fear conditioning training and testing was essentially completed as previously performed (Holehonnur *et al.*, 2016). **Handling:** Two days post-viral infusion, mice were handled for 2-3 mins for 2 days. In tandem, mice were habituated to both the training context and retrieval context for 10 min a day for 4 days. For reconsolidation experiments, two days before training, mice were habituated to the infusers. **Training:** Weak fear conditioning (3TSP) consisted of a 2 min acclimation period, followed by exposure to a single tone (30 sec, 5 kHz, 75 dB), which co-terminated with a 2 sec, 0.75 mA foot shock. The mice received 2 more tone-shock pairings at an inter trial interval (ITI) of 60 sec. For strong memories (10TSP), animals were given a 2 min acclimation period and received similar TSPs, however, the ITI of the 10TSP was random (5-7min ITI over 45 min). Short-term memory (STM) was examined 3 hours after training by exposing the mice to 3 tones (2 min intertrial interval; 30 sec, 5 kHz, 75 dB) in an altered context (a modified chamber and the absence of light, with distinct olfactory and tactile

cues). Long-term memory (LTM) and post-reactivation LTM (PR-LTM) was examined 24 hours post-training or reactivation (presentation of a single 30 sec tone) in a similar context as the STM test. Freezing behavior of each animal was hand scored from a video by individuals blinded to the experimental conditions. A Coulbourn Instruments fear conditioning system with computer-controlled shockers, USB cameras for video monitoring / video capture and FreezeFrame Software (Actimetrics) for unbiased behavioral analysis was used to auditory fear condition mice and to test for conditioned fear responses.

Drug Administration/ Infusion

Following reactivation of the fear memory via exposure to a 30 sec tone, mice were immediately taken out of the behavior chambers and infused in the BLA with either anisomycin or vehicle (0.9% saline) at a rate of 0.15 ul/min, a total of 0.3 ul per side. The Anisomycin concentration was 125 ug/uL and was prepared similarly to Holehonnur *et al.* (2016).

Immunocytochemistry (ICC) Glass coverslips were placed in 24 well cell culture plates and treated with poly-l-lysine (0.1 mg/mL; Sigma) overnight. The following day, the poly-l-lysine was removed and the coverslips were washed 3 x with phosphate buffered saline pH 7.4 (PBS). 293FT cells were seeded at 65% confluency on these glass coverslips. Twenty-four hours later, the cells were transfected with AAV viral plasmids designed to express tTa from a CMV promoter (CloneTech), using Lipofetamine 2000 (Invitrogen). Six hours post transfection, media was replaced with fresh media containing lentivirus, and in some cases, the media contained 10 ug/mL of Dox to suppress expression of the lentiviral transgene. The ICC procedure was carried

out 40 hr post addition of the lentivirus, as previously described (Holehonnur *et al.*, 2015) using an anti-Flag antibody (1:200; Sigma, M2) and TxRed secondary antibody (1:000; Life Technologies). The ICCs were imaged at 200X magnification using a fluorescence microscope (Olympus, BX51). The on and off Dox pictures were taken at the same exposure conditions.

Immunohistochemistry (IHC) Mice were perfused with 4 % PFA in 1 x PBS. The Flag IHC was performed on coronal mouse sections (40 μ m) that contained GFP reporter signal. Sections were blocked in goat serum (5%) in 1 x PBS for 1 hr at RT. They were then incubated overnight in an anti-Flag antibody (1:800; Cell signaling) in 1% BSA at 4 C. Sections were washed with PBS for 10 min, 3x before being incubated with the secondary for 2 hr at RT (1:200; Invitrogen #T6390). There were 3, 10 min final washes with PBS before being mounted onto superfrost slides (Fisher) and a fluorescent mounting media containing DAPI (VectaShield).

Viral production, purification, and titering Procedures were carried out as previously described (Holehonnur *et al.*, 2014). The ViraPower (Thermo Scientific Method) was used to produce all lentivirus. Viruses were produced using a quadruple-transfection method into 293FT cells (Invitrogen) using lipofectamine (Invitrogen) following the manufacturer's instructions for lentivirus production. A total of 3 x 15 cm cell culture plates were transfected per virus. Viruses were purified using a high-speed centrifugation method. The serum free media (Optimem; Invitrogen) containing the lentivirus was collected and was centrifuged (15 min x 3500 g) to remove debris. The supernatant was then filtered through a sterile 0.45 μ m vacuum-filter (Millipore). The flow through was then collected and centrifuged for 1.5 hr x 26,000 g to pellet

the lentivirus. The supernatant was removed and the pellet containing the lentivirus was resuspended in 40 ul of sterile 1 x PBS. For titering, 2 ul of the virus was put on 293FT cells at 50% confluency. To guarantee successful transduction we added the lentivirus along with TransDux (SBI Bioscience). Cells were then harvested and DNA purified. Five microliters of the purified DNA was used for titering using the SybrGreen method.

Viral infusion and Cannula Implantation Viral infusions targeting the BLA of α Camkii-tTA mice were performed similarly as described (Holehonnur *et al.*, 2014). Briefly, mice were rendered unconscious with an intra-peritoneal injection of ketamine (100 mg/kg) and xylazine (10 mg/kg) prior to stereotaxic surgery. Thirty-one gauge custom infusion cannulas (C315G, PlasticsOne) were very securely inserted into polyethylene tubing (I.D. 0.0150in. O.D. 0.043 in., wall thickness 0.0140 in; A-M systems, Inc.) that were 50 cm in length. These tubes were first backfilled with 1 x phosphate buffered saline, pH 7.4 (PBS), followed by sesame oil, where only 1 x PBS was present in the ~5 cm region closest to the infusers to avoid getting sesame oil in the brain. Syringes (2 uL, 23-gauge (88500); Hamilton Company)) were used for the viral infusion. The viral cocktail was drawn up into the infusion cannula. Infusers were bilaterally lowered into the BLA of mice [AP +1.6, ML \pm 3.3, -DV \pm 4.97] and infused (1 uL/side) at a rate of 0.07 uL/min for 15 min using an infusion pump (New Era Pump Systems Inc., NE-300). For reconsolidation experiments, cannula (PlasticsOne; infuser projection, 1mm; Dummy cannula projection, 0.5mm) targeting the mouse amygdala were implanted at the same time as viral infusion using dental acrylic (Ketac; Henry Schein Animal Health). To suppress expression of the lentiviral transgene, animals were placed on a diet of 200 mg/kg dox feed (BioServ).

Results

Strong fear memories have an impaired ability to be modified via extinction training and reconsolidation updating. Animals that are auditory fear conditioned with 1-3 tone-shock pairings (TSP) produce relatively weak fear memories that destabilize upon retrieval and undergo reconsolidation updating. In contrast, animals that receive 10TSPs produce strong memories that do not destabilize upon retrieval and are, thus, not modifiable via reconsolidation updating. This has been recently demonstrated in mice in a recent paper from our laboratory (Holehonnur et al., 2016) (see Figure 6.1A-E from this publication). Here, we demonstrate this phenomenon in rats (Figure 6.1). Animals that received 1TSP create weaker fear memories compared to animals that received 10TSPs (Figure 6.1B). Additionally, the strength of the memory correlates with the ability of the fear memory to destabilize upon retrieval (Figure 6.1D). When animals possessing strong auditory fear memories are exposed to the CS (i.e., tone) and subsequently administered anisomycin bilaterally to the BLA, their memories do not destabilize upon memory reactivation and remain intact during PR-LTM testing as indicated by normal freezing levels similar to controls. In contrast, animals possessing weak memories exhibit amnesia 24 hr after receiving anisomycin, indicating that their memories were disrupted.

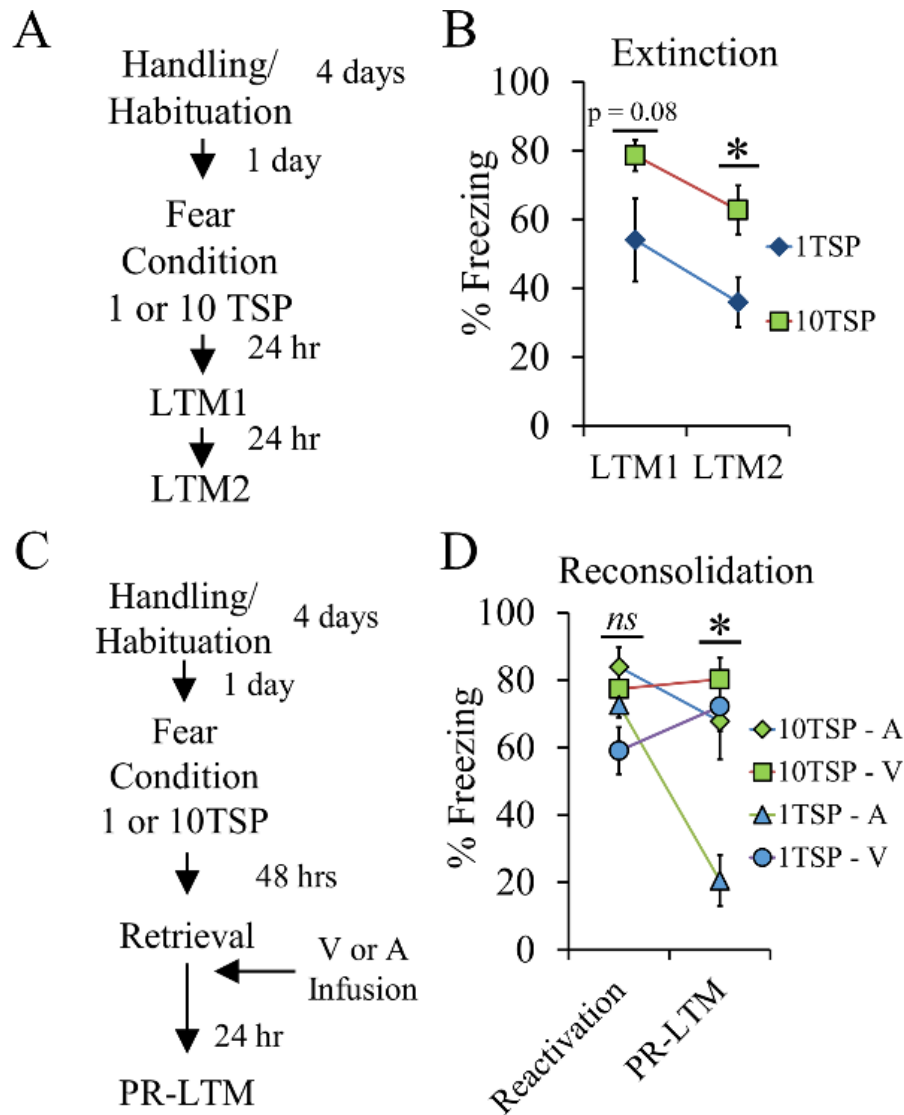


Figure 6.1 Strong fear memories are resistant to typical extinction and reconsolidation.

When rodents are conditioned with 10 tone-shock pairings (TSP), they exhibit significantly higher freezing levels across 10 tones of retrieval, compared to animals conditioned with 1 TSP, across multiple days of retrieval. In addition, we demonstrate that strong memories (10 TSP) are resistant to the initiation of reconsolidation and thus are resistant to the amnesic effects of post-reactivation treatment with anisomycin, compared to animals that received the same post-retrieval treatment, but were conditioned with only 1 TSP (weak memories). a). Timeline of extinction experiment. b). LTM tone average data for two days of LTM tests, spaced 24 hr apart. One-way repeated measures ANOVA for LTM 1, $F(1,10) = 3.631, p = 0.0858$. One-way repeated measures ANOVA for LTM 2, $F(1,10) = 6.899, p < 0.05.$, $n = 6$ animals per group. c).

Timeline of reconsolidation experiment d). Tone averaged data for the reactivation next to tone averaged data for post-reactivation-LTM (PRLTM) 24 hr later. Reactivation: Two-way ANOVA, $ns = F(1,29) = 0.335, p > 0.05$. PR-LTM: Two-way repeated measures ANOVA revealed a training by drug treatment interaction $F(1,29) = 6.838, p < 0.05$., Post-hoc analysis revealed 1TSP/A group significantly different than other groups $p < 0.05$. $n = 7-10$ animals per group. A = anisomycin, V = vehicle. ns = not significant. * = $p < 0.05$.

Increasing GluN2B(E1479Q), but not GluN2B(WT) leads to enhanced consolidation of fear memories.

NMDAR subunit composition alters the properties of the NMDAR due to inherent differences between GluN2A and GluN2B. GluN1:GluN2A receptors have a higher open probability, faster decay times and lower sensitivity to glutamate and glycine than GluN1:GluN2B containing receptors (Lau & Zukin, 2007; Paoletti *et al.*, 2013). GluN2A and GluN2B differ considerably in their cytoplasmic tails which confer subunit specific abilities to bind to postsynaptic scaffolding proteins and various signaling proteins regulating the strength of synaptic transmission and induction of plasticity (Gardoni *et al.*, 1998; Strack & Colbran, 1998). For example, the alpha calcium/calmodulin-dependent kinase II (α -CaMKII) binds to GluN2B with much higher affinity than to GluN2A. This interaction is a major determinant of the magnitude of hippocampal long-term potentiation (LTP) (Barria & Malinow, 2005).

Because of the differing properties of GluN2A and GluN2B, we reasoned that a shift from GluN2B to GluN2A could likely be a mechanism by which the induction of reconsolidation could be inhibited. We then determined that auditory fear memories created with 10TSPs are resistant to retrieval-dependent memory destabilization and is associated with an increase in the synaptic GluN2A/GluN2B ratio in neurons of the basal and lateral complex of the amygdala (BLA) when compared to weaker fear memories created via 1 or 3 tone-shock pairings. We then found that genetically increasing the NMDAR GluN2A/GluN2B ratio is sufficient to block

retrieval induced memory destabilization, thus, preventing an existing fear memory trace from being modified via reconsolidation updating (Holehonnur *et al.*, 2016). These experiments provided the first causal evidence that alterations in the GluN2A/GluN2B ratio are sufficient to gate the induction of reconsolidation. Here we will focus on attempting to enhance the induction of reconsolidation by overexpression of wild type GluN2B and a mutant form of GluN2B [GluN2B(E1479Q)] which exhibits higher surface levels due to a mutation in its C-terminal tail (Figure 6.2).

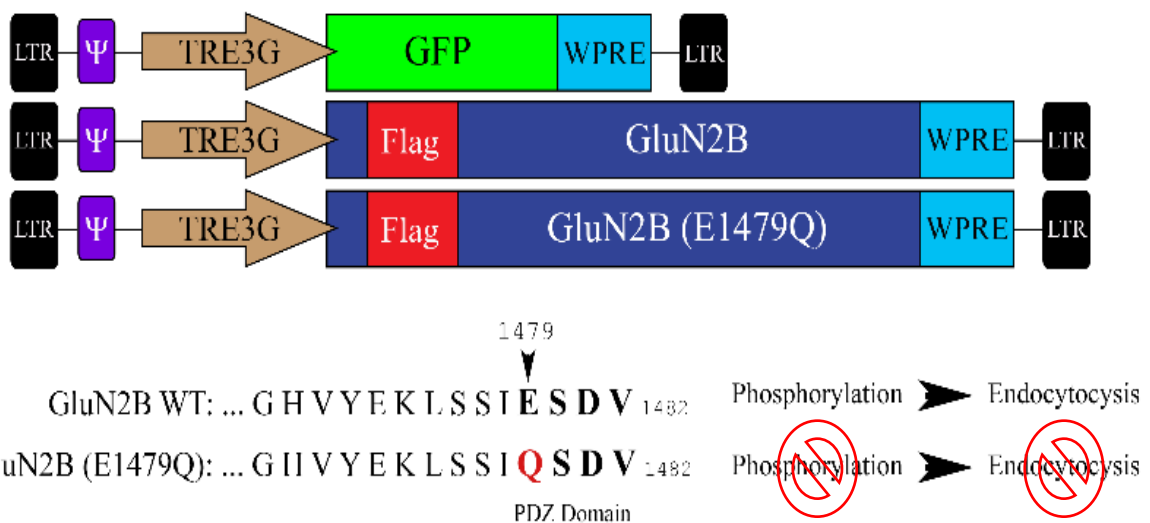


Figure 6.2 Lentiviral maps

Lentiviral maps for GluN2b constructs. Lentiviral genomes designed to express GFP, GluN2B(wildtype) and GluN2B(E1479Q) from a TRE3G promoter that allows for Dox dependent expression. GluN2B(WT) and GluN2B(E1479Q) contain a flag tag so expression can be confirmed *in vitro* and *in vivo*. GluN2B(E1479Q) contains a mutation in the coding region of the PDZ domain that prevents the subunit from being endocytosed from the membrane. When these viruses are used in combination with α -CaMKII mice, we can restrict expression to excitatory neurons and temporally control transcription of the lentiviral transgene using doxycycline (Dox).

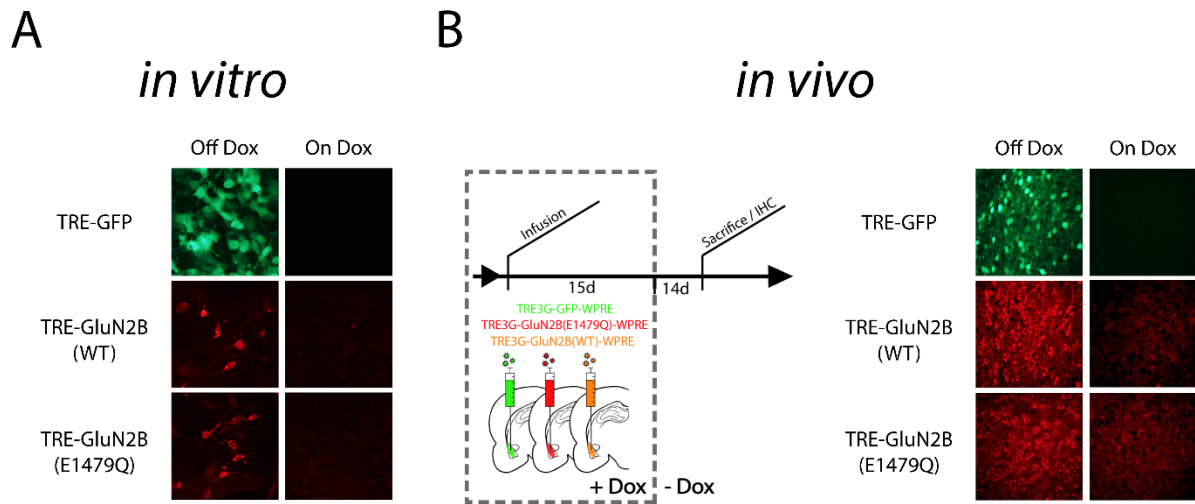


Figure 6.3 Functionality of GFP and GluN2B lentiviruses *in vitro* and *in vivo*.

A). Lentivirus was generated and applied to 293FT cells in media with or without Dox (Left). ICC was performed for the flag tag to detect GluN2B levels. All constructs (TRE-GFP, TRE-GluN2B and TRE-GluN2B(E1479Q)) were tightly regulated by Dox and displayed no expression on Dox. **B).** Lentivirus was generated and infused into the BLA (1.0 ul/side) of α Camkii-tTA mice while on Dox. Mice were then either taken off Dox or left on Dox for 8 days before Flag IHC was performed. All viruses were shown to be tightly regulated via Dox.

Consolidation of Pavlovian auditory fear memory can be enhanced by increasing the synaptic GluN2B/GluN2A ratio in the BLA at the time of acquisition.

We examined how over-expression of wild-type GluN2B within mouse α -CaMKII positive BLA excitatory neurons influence acquisition and consolidation of an auditory fear memory. GluN2B levels were increased within α -CaMKII positive BLA excitatory neurons by the infusion of lentiviruses into the BLA of α -CaMKII-tTA mice. These viruses are designed to express GluN2B from a TRE3g promoter, which restricts expression to α -CaMKII positive BLA excitatory neurons (when used within α -CaMKII-tTA mice), allows sufficiently strong expression of the transgene and allows the transgene expression to be suppressed by feeding the

animals doxycycline (Dox) containing chow (Holehonnur *et al.*, 2015), allowing us to control when the transgenes are expressed.

We hypothesized that animals overexpressing either GluN2B(WT) or GluN2B(E1479Q) within BLA excitatory neurons prior to and during auditory fear conditioning will have normal STM but enhanced LTM, indicating normal acquisition of fear but enhanced consolidation of fear memory compared to animals that receive a control virus (GFP). To do this, we infused viruses designed to express either GFP, GluN2B(WT), or GluN2B(E1479Q) into the BLA of α -CaMKII-tTA mice to overexpress the lentiviral transgenes exclusively in excitatory neurons within the BLA. Dox dependent expression of the GluN2B transgene was confirmed by staining for the flag tag following addition of the lentivirs onto 293FT cells (**Figure 6.3A**) or in vivo within the BLA of α -CaMKII-tTA mice (**Figure 6.3B**) In addition, Dox dependency of GFP expression from our control virus was also confirmed (**Figure 6.3A-B**). Fifteen days following infusion, animals were fear conditioned (3 TSP), tested for STM 3 hours later and LTM 21 hours later (**Figure 6.4A**). We determined that viral mediated overexpression of GluN2B(E1479Q) or GluN2B(WT) prior to and during fear conditioning had no influence on STM (**Figure 6.4B**), but did significantly enhance LTM compared to animals that overexpressed GFP in the case of animals that received infusions of GluN2B(E1479Q) (B 6.3C), however, we saw no enhancement at LTM for GluN2B(WT). Although we saw no enhancement in the GluN2B(WT) group, there are findings using GluN2B(WT) in experiments that overexpressed GluN2B in forebrain neurons in mice (Tang *et al.*, 1999) and rats (Wang *et al.*, 2009a).

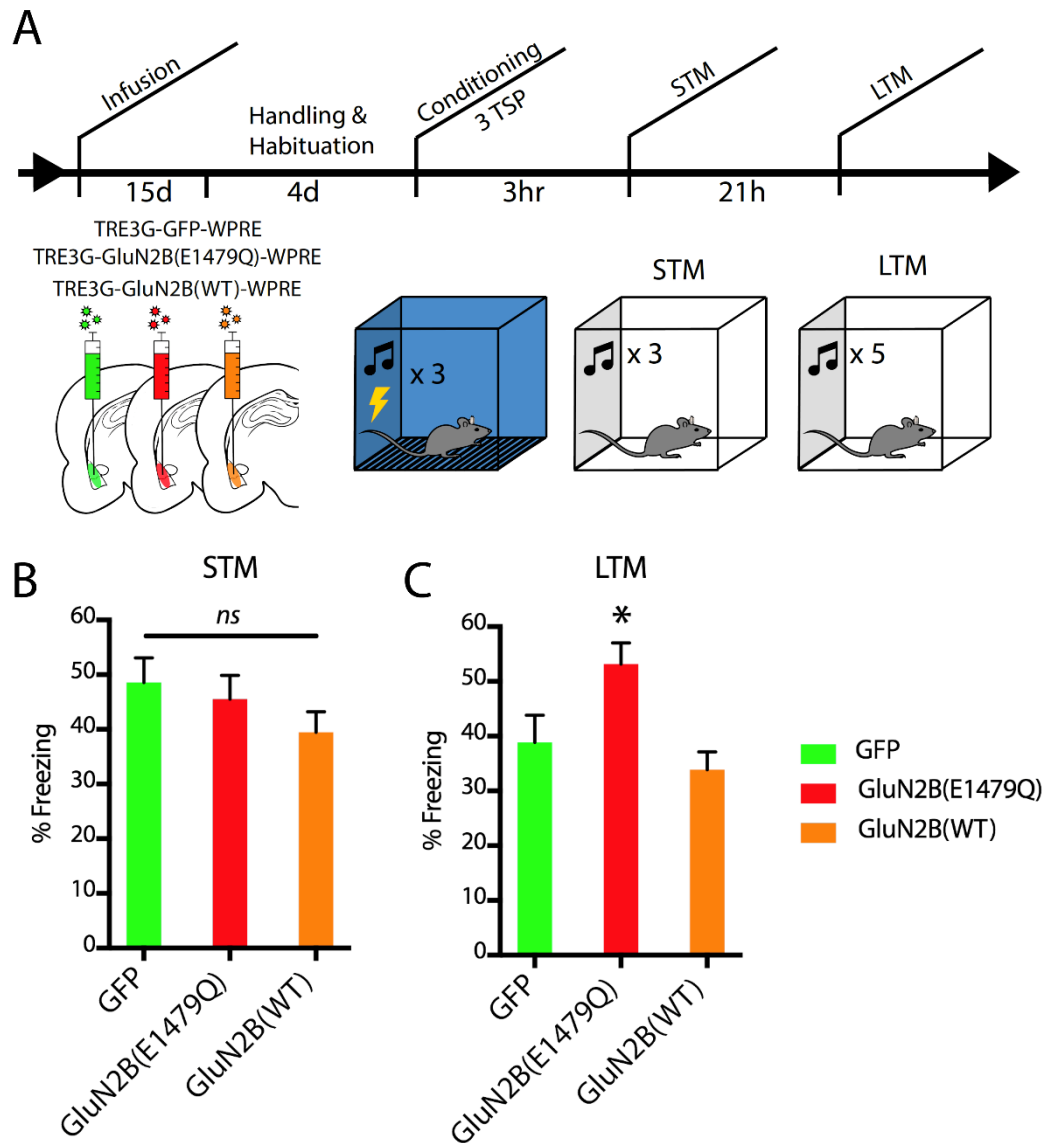


Figure 6.4 Increasing GluN2B levels with GluN2B(E1479Q) leads to enhanced consolidation of a fear memory.

Either wildtype GluN2B or GluN2B(E1479Q) were infused into α -CaMKII-tTA mice prior to and during consolidation of fear memories (3 tone-shock pairings (TSP)). Animals that were infused with GluN2B(E1479Q) exhibited enhanced fear learning. **A**). Timeline of consolidation experiments. **B**). STM tone average data. One-way repeated measures ANOVA, $ns = F(2,25) = 1.215$, $p = 0.3125$. **c**). LTM tone averaged data. One-way repeated measures ANOVA, $F(2,25) = 6.166$, $p = 0.006$. Consolidation experiment group sizes: $n = 8-9$ per group.

Increasing GluN2B at the time of extinction does not lead to enhanced extinction learning

GluN2B has been implicated in having a role in extinction learning. It has been shown that blocking activity of GluN2B containing NMDARs with ifenprodil within the BLA at the time of extinction, will block the animals' ability to extinguish a fear memory. However, it remains unknown how overexpression of GluN2B at the time of extinction learning within BLA neurons will influence extinction learning. We hypothesized that animals overexpressing GluN2B(E1479Q) within BLA excitatory neurons only after an auditory fear memory has fully consolidated will have normal STM, indicating normal acquisition of the fear memory, but enhanced extinction compared to animals that receive the control virus (GFP). To do this, we infused into the BLA of α -CaMKII-tTA mice either GFP, GluN2B(WT) or GluN2B(E1479Q). From the time of surgery, all animals were placed on Dox to suppress expression of the GluN2B or GFP transgene. Forty-eight hours following the formation of a auditory fear memory (3TSP), animals were taken off Dox for 14 days to initiate the expression of GFP, GluN2B(WT), or GluN2B(E1479Q) (Figure 6.5A). Animals will then be exposed to 3 days of LTM (10 tones/day). A test of STM 3 hr following training showed no differences in any of the group's ability to acquire the memory $F(2,27) = 2.084$, $p = 0.1440$. After being off Dox for 14 days, the animals were subjected to 3 extinction sessions that revealed there was no effect on extinction across sessions between any of the groups (Figure 6.5B). Data is displayed as the 10-tone average for each session.

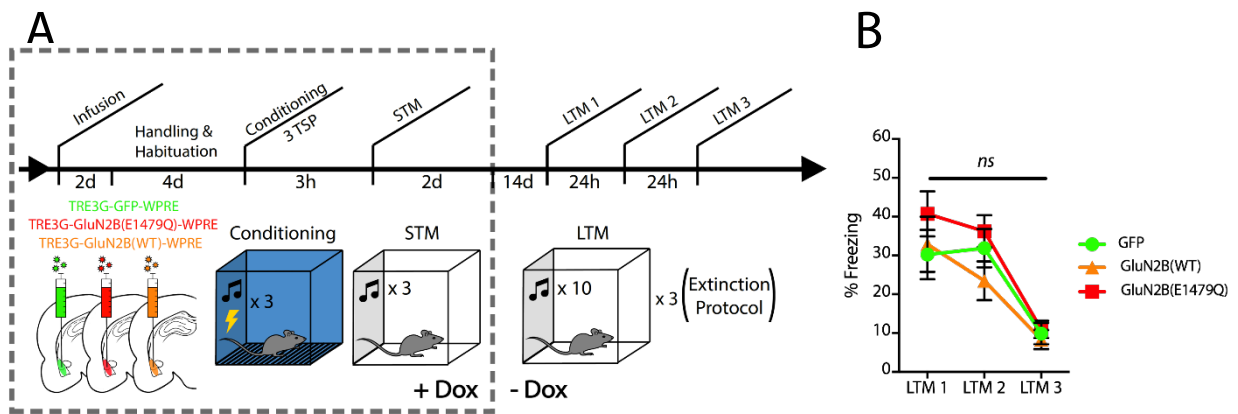


Figure 6.5 Increasing GluN2B at the time of extinction learning does not lead to enhanced extinction.

A). Experiment timeline. **B).** Tone averaged data (10 tones/day) for 3 days of LTM. A One-way repeated measures ANOVA revealed no change in freezing in groups across LTMs, $ns = F(2,27) = 0.948, p > 0.05$. Experiment group sizes: $n = 9-10$ per group. $ns =$ not significant. STM (not shown) was not significant across groups $F(2,27) = 0.948, p < 0.05$.

Initiation of reconsolidation of a strong Pavlovian auditory fear memory is enabled by increasing the synaptic GluN2B/GluN2A ratio in BLA neurons

It has yet to be determined if increasing the GluN2B/GluN2A ratio within BLA excitatory neurons is sufficient to initiate reconsolidation for a strong memory and render it susceptible to modification via reconsolidation updating. Below we propose experiments that will determine if overexpression of GluN2B(WT) or GluN2B(E1479Q) within BLA excitatory neurons enhances the induction of reconsolidation updating of a strong memory. We hypothesized that increasing the GluN2B/GluN2A ratio will enhance the induction of reconsolidation of a strong fear memory. To test this, we infused α -CaMKII-tTA mice with viruses designed to express either GFP, GluN2B(WT) or GluN2B(E1479Q) into the BLA and fear condition these animals using strong fear conditioning (i.e., 10TSP) while on Dox to suppress the overexpression of the viral

transgene. Forty-eight hours later (i.e., following consolidation) we removed Dox from their diet of all animals. After 8 days off Dox, we reactivated the memory by exposing the animals to a single CS (reactivation), immediately followed by infusion with either vehicle or anisomycin. Twenty-four hours later, we administered an LTM test (PR-LTM) to determine if animals that received the GluN2B virus and anisomycin are amnesic (**Figure 6.6A**). The GluN2B(WT) and GluN2B(E1479Q) were tested in separate experiments. This is due to the large amount of animals needed for these experiments. Our results show that overexpression of GluN2B(E1479Q) (**Figure 6.6C**), but not GluN2B(WT) (**Figure 6.6B**), enhances the induction of reconsolidation of a strong fear memory. We suspect the reason overexpression of wild-type GluN2B does not lead to enhancement of the initiation of reconsolidation is that it does not sufficiently increase the GluN2B/GluN2A ratio. For example, some studies have found that overexpression of wild-type GluN2B does not increase the GluN2B/GluN2A ratio (Barria & Malinow, 2002; Foster et al., 2010). This is in contrast to GluN2A, in which overexpression of GluN2A does lead to a significant increase in the synaptic GluN2A/GluN2B ratio (9). We hypothesized that GluN2B(E1479Q)'s ability to render a strong memory capable of initiating reconsolidation would be dependent on the retrieval of the fear memory. To test this, we repeated the experiment but also included 'no retrieval groups' that do not receive a reactivation session, but rather just the infusion of anisomycin or vehicle. In addition, all animals were infused into the BLA with GluN2B(E1479Q) (**Figure 6.7A**). Upon retrieval, the two retrieval groups had similar freezing levels ($p > 0.05$). All no reactivation and reactivation groups received infusion of anisomycin or saline in the same environment. Upon PR-LTM, only the animals that received anisomycin and reactivation showed amnesia compared to the previous exposure to the tone 24

hr earlier ($p < 0.05$) (**Figure 6.7B**), showing memory retrieval is necessary for this amnesic effect. For one final reconsolidation experiment, we sought to test whether or not increasing GluN2B at the synapse affected reconsolidation of a weak memory. We also tested the animals 1 week after the PRLTM session to look for return of fear and found that the amnesic effect was lasting 1 week out ($p < 0.05$). We repeated the reconsolidation experiments similarly, but instead of using 10TSP, we used 3TSP to train the animals so only a weak fear memory is created (**Figure 6.8A**). Upon reactivation, all animals displayed similar freezing behavior to the tone ($p > 0.05$), and then were infused into the BLA immediately with either saline or anisomycin. During PR-LTM, animals that received anisomycin, whether or not they received infusion of GluN2B(E1479Q) or GFP control, showed an attenuated fear response to the tone ($p < 0.05$) (**Figure 6.8B**), indicating that increasing GluN2B at the time of reconsolidation of a weak fear memory does not interfere with initiation or restabilization phases of reconsolidation.

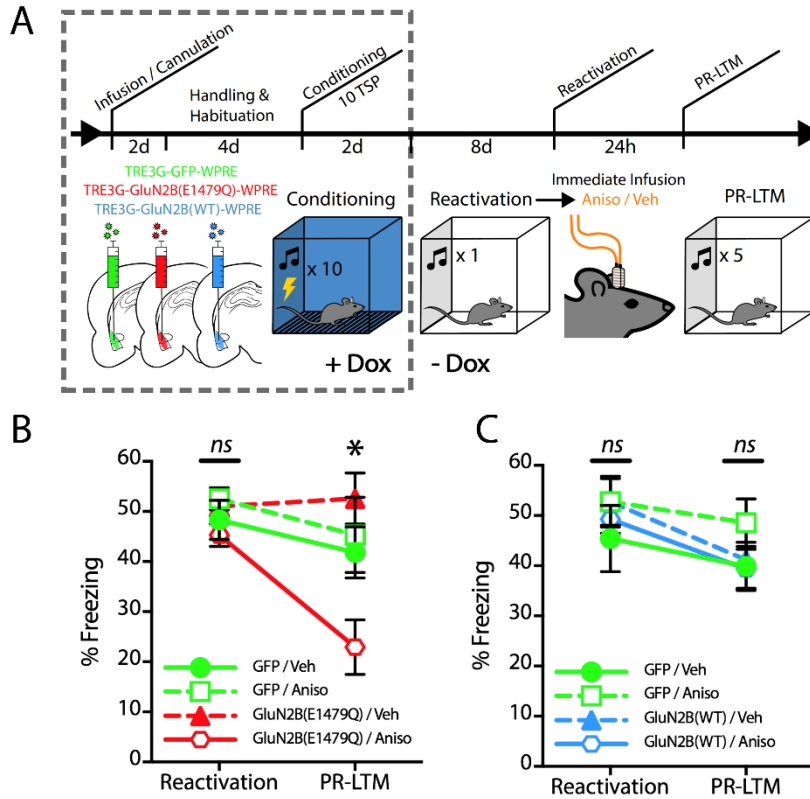


Figure 6.6 Overexpression of GluN2B(E1479Q) enables reconsolidation of a strong fear memory.

Overexpression of wildtype GluN2B at the time of reactivation of a strong fear memory created with 10 TSP, did not lead to enhancement in the initiation of reconsolidation. However, overexpression of GluN2B(E1479Q) allowed for the initiation of reconsolidation to occur. **a**). Timeline of reconsolidation experiment. **b**). GluN2B(WT): Tone averaged data for the reactivation of the strong memory next to tone averaged data for post reconsolidation-LTM (PR-LTM) 24 hr later. Reactivation: Two-way ANOVA, $ns = F(1,24) = 0.004, p > 0.05$. PR-LTM: Two-way repeated measures ANOVA, $ns = F(1,124) = 0.540, p > 0.05$. Reconsolidation experiment group sizes: $n = 7$ per group. ns = not significant. **c**). GluN2B(E1479Q): Tone averaged data for the reactivation of the strong memory next to tone averaged data for PRLTM 24 hr later. Reactivation: Two-way ANOVA, $ns = F(1,25) = 0.576, p > 0.05$. PR-LTM: Two-way repeated measures ANOVA, $F(1,25) = 0.6161, p = 0.0201$ revealed a virus by drug interaction where the GluN2B(E1479Q)/anisomycin group was significantly different than the other groups, $p < 0.05$. Reconsolidation experiment group sizes: $n = 7-8$ per group. ns = not significant. * = $p < 0.05$. Aniso=anisomycin.

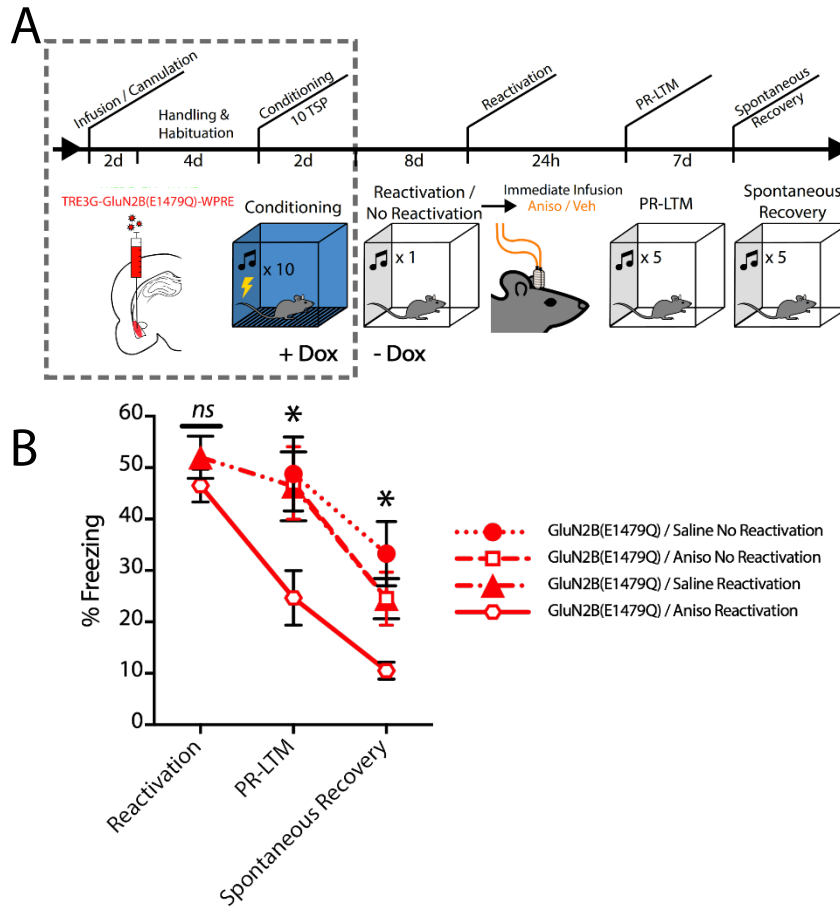


Figure 6.7 Enabling of initiation of reconsolidation of strong fear memories enabled by overexpression of GluN2B(E1479Q) is retrieval dependent.

A). Timeline for experiment. **B).** Tone averaged data for the reactivation of the strong memory next to tone averaged data for post reconsolidation-LTM (PR-LTM) 24 hr later. Reactivation: Two-way ANOVA, $ns = F(1,30) = 0.004, p < 0.05$. PR-LTM: Two-way repeated measures ANOVA, $F(1,30) = 2.303, p < 0.05$. Spontaneous recovery of fear was tested 1 week after PR-LTM and show a lasting amnesic effect ($p < 0.05$). Group sizes: $n = 7$ per group. ns = not significant. ns = not significant. $*$ = $p < 0.05$. Aniso=anisomycin.

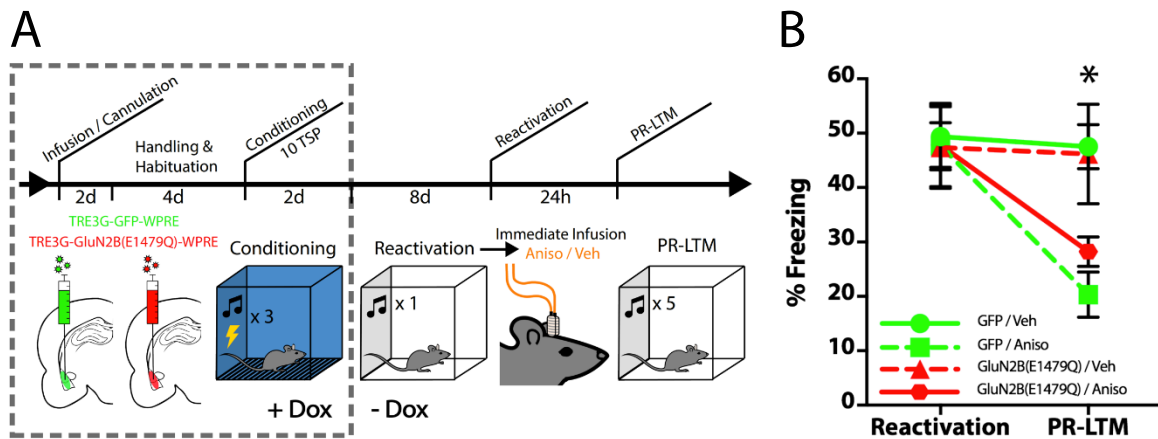


Figure 6.8 Increasing the GluN2B/GluN2A ratio does not enhance or interfere with the initiation or restabilization phases of reconsolidation of a weak fear memory.

When excitatory BLA neurons overexpress the mutant GluN2B(E1479Q) following conditioning and during reconsolidation of weak fear memories (3 tone-shock pairing (TSP)), there is no inhibition or enhancement of reconsolidation, compared to a GFP control **a**). Experiment timeline. **b**). Reactivation tone averaged data next to tone averaged data for post-reactivation-LTM (PR-LTM). Reactivation: One-way repeated measures ANOVA, $ns = F(1,26) = 0.0071$, $p > 0.05$. PR-LTM: Two-way ANOVA for effect of Drug, $F(1,26) = 0.576$, $p > 0.05$. PR-LTM: Two-way repeated measures ANOVA, $F(1,26) = 0.885$, $p > 0.05$. Experiment group sizes: $n = 7-10$ per group. $ns =$ not significant. $*$ = $p < 0.05$.

Discussion

Our data indicate that overexpression of GluN2B and GluN2B(E1479Q) *does not* influence the acquisition of fear memory (i.e., STM) but GluN2B(E1479Q) does enhance the consolidation of fear memory (i.e., freezing levels during LTM). These findings are consistent with studies that overexpress GluN2B in forebrain neurons in mice (Tang *et al.*, 1999) and rats (Wang *et al.*, 2009a). Importantly, these data indicate that overexpression of GluN2B and GluN2B(E1479Q) does not interfere with the expression of fear or sensory perception because STM is intact. The inability of the overexpression of GluN2B and GluN2B(E1479Q) to enhance extinction learning may due to the fact that NMDARs on BLA excitatory neurons are not

necessary or do not contribute significantly to auditory fear memory extinction. However, given that pharmacological agents that manipulate NMDARs, when infused into the BLA influence auditory fear memory extinction, it could mean that NMDARs on BLA interneurons are necessary for auditory fear memory extinction.

Overexpression of GluN2B(E1479Q), but not GluN2B(WT), enables the induction of reconsolidation of a strong fear memory and is specific to memory retrieval. We suspect the reason overexpression of wild-type GluN2B does not lead to enhancement of the initiation of reconsolidation is that it does not sufficiently increase the GluN2B/GluN2A ratio enough. For example, some studies have found that overexpression of wild-type GluN2B does not increase the GluN2B/GluN2A ratio (Barria & Malinow, 2002; Foster *et al.*, 2010). This is in contrast to GluN2A, in which overexpression of GluN2A does lead to a significant increase in the synaptic GluN2A/GluN2B ratio (9).

An interesting set of experiments would further validate that we are enabling the initiation of reconsolidation of strong fear memories, would be to detect molecular markers of reconsolidation in strong trained animals that have been infused with GluN2B(E1479Q). If the presence of GluN2B(E1479Q) at BLA synapses during the time of memory reactivation of a strong fear memory led to increased pGluR1 levels, mimicking what typically occurs following the reactivation of a weak memory, this would further indicate that we are indeed initiating reconsolidation of a strong memory. In addition to examining levels of pGluR1, other markers could also be examined, such as ubiquitination of SHANK and/or GKAP.

References

- Alberini, C.M. (2011) The role of reconsolidation and the dynamic process of long-term memory formation and storage. *Front Behav Neurosci*, **5**, 12.
- Barria, A. & Malinow, R. (2002) Subunit-specific NMDA receptor trafficking to synapses. *Neuron*, **35**, 345-353.
- Barria, A. & Malinow, R. (2005) NMDA receptor subunit composition controls synaptic plasticity by regulating binding to CaMKII. *Neuron*, **48**, 289-301.
- Ben Mamou, C., Gamache, K. & Nader, K. (2006) NMDA receptors are critical for unleashing consolidated auditory fear memories. *Nat Neurosci*, **9**, 1237-1239.
- Foster, K.A., McLaughlin, N., Edbauer, D., Phillips, M., Bolton, A., Constantine-Paton, M. & Sheng, M. (2010) Distinct roles of NR2A and NR2B cytoplasmic tails in long-term potentiation. *J Neurosci*, **30**, 2676-2685.
- Gardoni, F., Caputi, A., Cimino, M., Pastorino, L., Cattabeni, F. & Di Luca, M. (1998) Calcium/calmodulin-dependent protein kinase II is associated with NR2A/B subunits of NMDA receptor in postsynaptic densities. *J Neurochem*, **71**, 1733-1741.
- Holehonnur, R., Lella, S.K., Ho, A., Luong, J.A. & Ploski, J.E. (2015) The production of viral vectors designed to express large and difficult to express transgenes within neurons. *Molecular brain*, **8**, 12.
- Holehonnur, R., Luong, J.A., Chaturvedi, D., Ho, A., Lella, S.K., Hosek, M.P. & Ploski, J.E. (2014) Adeno-associated viral serotypes produce differing titers and differentially transduce neurons within the rat basal and lateral amygdala. *BMC neuroscience*, **15**, 28.
- Holehonnur, R., Phensy, A.J., Kim, L.J., Milivojevic, M., Vuong, D., Daison, D.K., Alex, S., Tiner, M., Jones, L.E., Kroener, S. & Ploski, J.E. (2016) Increasing the GluN2A/GluN2B Ratio in Neurons of the Mouse Basal and Lateral Amygdala Inhibits the Modification of an Existing Fear Memory Trace. *The Journal of neuroscience : the official journal of the Society for Neuroscience*, **36**, 9490-9504.
- Hong, I., Kim, J., Kim, J., Lee, S., Ko, H.G., Nader, K., Kaang, B.K., Tsien, R.W. & Choi, S. (2013) AMPA receptor exchange underlies transient memory destabilization on retrieval. *Proc Natl Acad Sci U S A*, **110**, 8218-8223.
- Jarome, T.J., Werner, C.T., Kwapis, J.L. & Helmstetter, F.J. (2011) Activity dependent protein degradation is critical for the formation and stability of fear memory in the amygdala. *PLoS One*, **6**, e24349.
- Lau, C.G. & Zukin, R.S. (2007) NMDA receptor trafficking in synaptic plasticity and neuropsychiatric disorders. *Nat Rev Neurosci*, **8**, 413-426.

- McKenzie, S. & Eichenbaum, H. (2011) Consolidation and reconsolidation: two lives of memories? *Neuron*, **71**, 224-233.
- Milton, A.L. & Everitt, B.J. (2010) The psychological and neurochemical mechanisms of drug memory reconsolidation: implications for the treatment of addiction. *The European journal of neuroscience*, **31**, 2308-2319.
- Milton, A.L., Merlo, E., Ratano, P., Gregory, B.L., Dumbreck, J.K. & Everitt, B.J. (2013) Double dissociation of the requirement for GluN2B- and GluN2A-containing NMDA receptors in the destabilization and restabilization of a reconsolidating memory. *J Neurosci*, **33**, 1109-1115.
- Nader, K., Schafe, G.E. & Le Doux, J.E. (2000a) Fear memories require protein synthesis in the amygdala for reconsolidation after retrieval. *Nature*, **406**, 722-726.
- Nader, K., Schafe, G.E. & LeDoux, J.E. (2000b) The labile nature of consolidation theory. *Nat Rev Neurosci*, **1**, 216-219.
- Paoletti, P., Bellone, C. & Zhou, Q. (2013) NMDA receptor subunit diversity: impact on receptor properties, synaptic plasticity and disease. *Nat Rev Neurosci*, **14**, 383-400.
- Pitman, R.K. (2011) Will reconsolidation blockade offer a novel treatment for posttraumatic stress disorder? *Frontiers in behavioral neuroscience*, **5**, 11.
- Przybylski, J. & Sara, S.J. (1997) Reconsolidation of memory after its reactivation. *Behav Brain Res*, **84**, 241-246.
- Sanz-Clemente, A., Matta, J.A., Isaac, J.T. & Roche, K.W. (2010) Casein kinase 2 regulates the NR2 subunit composition of synaptic NMDA receptors. *Neuron*, **67**, 984-996.
- Strack, S. & Colbran, R.J. (1998) Autophosphorylation-dependent targeting of calcium/calmodulin-dependent protein kinase II by the NR2B subunit of the N-methyl- D-aspartate receptor. *J Biol Chem*, **273**, 20689-20692.
- Suris, A., Smith, J., Powell, C. & North, C.S. (2013) Interfering with the reconsolidation of traumatic memory: sirolimus as a novel agent for treating veterans with posttraumatic stress disorder. *Annals of clinical psychiatry : official journal of the American Academy of Clinical Psychiatrists*, **25**, 33-40.
- Suzuki, A., Josselyn, S.A., Frankland, P.W., Masushige, S., Silva, A.J. & Kida, S. (2004) Memory reconsolidation and extinction have distinct temporal and biochemical signatures. *J Neurosci*, **24**, 4787-4795.
- Tang, Y.P., Shimizu, E., Dube, G.R., Rampon, C., Kerchner, G.A., Zhuo, M., Liu, G. & Tsien, J.Z. (1999) Genetic enhancement of learning and memory in mice. *Nature*, **401**, 63-69.

- Taylor, J.R., Olausson, P., Quinn, J.J. & Torregrossa, M.M. (2009) Targeting extinction and reconsolidation mechanisms to combat the impact of drug cues on addiction. *Neuropharmacology*, **56 Suppl 1**, 186-195.
- Tronson, N.C. & Taylor, J.R. (2007) Molecular mechanisms of memory reconsolidation. *Nat Rev Neurosci*, **8**, 262-275.
- Tronson, N.C., Wiseman, S.L., Olausson, P. & Taylor, J.R. (2006) Bidirectional behavioral plasticity of memory reconsolidation depends on amygdalar protein kinase A. *Nat Neurosci*, **9**, 167-169.
- Wang, D., Cui, Z., Zeng, Q., Kuang, H., Wang, L.P., Tsien, J.Z. & Cao, X. (2009a) Genetic enhancement of memory and long-term potentiation but not CA1 long-term depression in NR2B transgenic rats. *PLoS One*, **4**, e7486.
- Wang, S.H., de Oliveira Alvares, L. & Nader, K. (2009b) Cellular and systems mechanisms of memory strength as a constraint on auditory fear reconsolidation. *Nat Neurosci*, **12**, 905-912.
- Winters, B.D., Tucci, M.C. & DaCosta-Furtado, M. (2009) Older and stronger object memories are selectively destabilized by reactivation in the presence of new information. *Learn Mem*, **16**, 545-553.
- Wood, N.E., Rosasco, M.L., Suris, A.M., Spring, J.D., Marin, M.F., Lasko, N.B., Goetz, J.M., Fischer, A.M., Orr, S.P. & Pitman, R.K. (2015) Pharmacological blockade of memory reconsolidation in posttraumatic stress disorder: three negative psychophysiological studies. *Psychiatry research*, **225**, 31-39.

CHAPTER 7

CONCLUSIONS

It has been known that shRNAs can induce an inflammatory response and can lead to neurotoxicity (McBride et al., 2008; Martin et al., 2011). In chapter 2, I sought to use a viral system with shRNAs to knockdown genes associated with consolidation of Pavlovian auditory fear memories (de Solis et al., 2015), however, our attempts led us to the conclusion that because of the toxic nature of shRNAs, this technique for investigation of a particular gene's involvement in learning and memory is not optimal. We found that there is a dose dependent effect in the degree of memory impairment based on the amount of an shRNA expressing AAV infused into the brain. The presence of the shRNA at a level that causes adequate knockdown a target gene had deleterious effects on learning and memory. Lowering the dose of shRNA expressing AAV ~20 fold allowed some conclusions on the role of some genes involvement in learning and memory, however, was still displaying the memory impairing effects compared to a no-shRNA control. The toxic/memory impairing effect was seen to be the case across multiple genes involved in learning memory and also across multiple control shRNAs that do not target any RNA in the rodent genome (control shRNAs).

Despite numerous reports of the toxic nature of shRNAs, researchers continue to use the technology to study learning and memory (Gunduz-Cinar et al., 2018). In addition, experiments published in high profile journals continue to use shRNA without proper controls (Mews et al., 2017), comparing an shRNA targeting a specific gene for knockdown with a GFP control. There are also recently published studies that use the shRNA technology via different delivery

methods, such as lipofection of plasmids designed to express shRNAs to a target brain region that have been used to study learning and memory, but do not see the memory impairing effects of the RNA interference (RNAi) as we did using AAV as a delivery method (Cruz et al., 2015). This result may suggest that modifying the duration or method of delivery of shRNAs to cells may be an option for behavioral neuroscience experiments using shRNAs.

There are alternatives to shRNAs that utilize RNAi. One mechanism of the toxicity of the shRNA is thought to be aberrant off target effects that lead to dysregulation of miRNA expression patterns (Pan et al., 2011). Short-interfering RNAs (siRNAs), another method of RNAi that can be used in neurons using AAV, targets RNAs for degradation using similar mechanisms as shRNAs (Reynolds et al., 2004). However, siRNAs were once thought to produce more off target effects than shRNAs (Jackson & Linsley, 2010). Recent research on this subject, however, has determined that siRNAs actually dysregulate gene expression less than shRNAs (Boudreau et al., 2009). There are several other options to study genes using RNAi such as artificial miRNAs and newly modified shRNAs (shRNAmirs) (Fellmann et al., 2013). Although harnessing RNAi to knockdown genes is powerful tool, knockout of the gene is usually a more powerful option. Recent developments in research on the CRISPR/Cas systems have made gene knockout via AAV, which encode components of the system, as easy as delivering shRNAs to neurons in the brain for knockdown (Ran et al., 2015).

Having attempted to use shRNAs to study genes involved in learning and memory and discovering the system is not optimal, in chapter 3, I investigated the knockdown efficiency of an AAV based CRISPR/Cas9 system. In addition, I modified the system to make the expression of the gRNA dependent on the presence of Dox (de Solis et al., 2016). We initially developed an

AAV construct to express Cas9 and render the expression inducible via a TRE3G promoter. However, this system was found to be a leaky as there was editing of our target locus, Tet2, that occurred in the presence of Dox, but unfortunately, also in the absence of Dox. After attempts to fix the leaky system, the construct coding the gRNA was modified to render the gRNA inducible, where the presence of Dox promotes expression of the gRNA from an H1/TO promoter. This system functioned very well *in vitro* and *in vivo* and we also discovered that editing of the genome *in vivo* with this system could be achieved with as little as 24 hr of exposure to Dox.

This series of experiments was the first demonstration of an inducible CRISPR/Cas9 AAV system used to edit post-mitotic neurons in the mammalian brain. There do exist other systems that have been designed for inducible Cas9 expression, such as light inducible Cas9 (Nihongaki et al., 2015) and split Cas9 systems where editing is achieved by exposure to a drug (tamoxifen) (Davis et al., 2015), which would be interesting to see their effectiveness *in vivo*, but have only been demonstrated *in vitro*. There are reports of other CRISPR/Cas9 systems that had success with TRE3G driven Cas9 expression that did not show leaky expression, however, the success of these *in vitro* experiments may be due to using a low plasmid copy number (Gonzalez et al., 2014).

This system was designed to be inducible to study various learning and memory processes, such as acquisition, consolidation, reconsolidation memory updating, and extinction. The usefulness of this system has not been demonstrated in behavioral neuroscience research, rather, experimenters are continually using RNAi systems, such as AAV shRNA systems (Cruz et al., 2015; Mews et al., 2017; Gunduz-Cinar et al., 2018) to study a gene's role in a particular

behavior. The lack of use may be due to the novelty of the technology, but it also may be due to the low amount of gene knockdown the system currently produces and to the inability to produce a behavioral effect. The editing efficacy when we target neurons in the amygdala is ~40% loci edited. Hopefully, this can be improved upon. Factors that may be affecting the level of editing are the titer of the viruses being used, the promoter used to drive expression of the Cas endonuclease or gRNA, and the AAV serotype used to package the system's components and their delivery to neurons. If these factors can be optimized to edit the maximum number of alleles within a target brain region, this system may have even greater potential.

In chapter 4, I sought to determine which of the many AAV serotypes have the optimal expression patterns within the BLA and CeA, and specifically in inhibitory neurons (de Solis et al., 2017a). To do this, we used a viral plasmid designed to express GFP from a Gad65 promoter (AAV-Gad65-GFP) (Marik et al., 2010). We packaged this transgene into either AAV1, AAV4, AAV5, AAV6, AAV7, AAV8, AAV9, AAVrh10, AAVDJ or AAVDJ8 serotypes and infused them into the rat amygdala (BLA and CeA). Examining the various serotypes for a number of factors, such as the spread of the virus, intensity of the GFP signal and number of cells expressing GFP. AAV1, AAV7, and AAVDJ8 showed overall good transduction across both the BLA and CeA. It was determined that the expression in the BLA was leaky (expression in cells other than inhibitory neurons), however, the expression was localized to inhibitory neurons in the CeA, allowing us to make claims of their efficiency in inhibitory neurons.

A surprising result was the inability of the AAV construct, Gad65-GFP, to localize expression the GFP exclusively to inhibitory neurons, as this virus had been previously reported to tightly restricted to Gad65 positive cells (Marik et al., 2010). Another finding from this

experiment was the surprisingly low expression from AAV4 and AAV5. This low level of function has been recorded once before with AAV5 (Holehonnur et al., 2014). AAV5 is one of the most commonly used AAV serotypes in neuroscience, yet, in many serotype comparison experiments (Burger et al., 2004; Klein et al., 2008), it has not been reported as one of the 'higher functioning' AAV serotypes.

This comparison provides valuable information that can be applied to our findings with shRNAs in chapter 2, as those experiments used AAVDJ8. AAV4 or AAV5 may be a better choice for experiments using shRNAs, as the lower level of expression may decrease the neurotoxic and memory impairing effects of shRNAs.

Determining which genes are important for learning and memory and basic neuronal function is an ongoing and important area of research, in chapter 6, I explored what mRNAs are present in the dendrites following the induction of LTP (de Solis et al., 2017b). Determining what genes are robustly transported to the dendrites, and potentially translated locally, could help explain how a neuron maintains and modifies 1000s of connections with other cells. To determine what mRNAs are present in the dendrites, we used laser microdissection to remove the distal dendrites of the dentate gyrus of rats 2 hr or 4 hr following induction of LTP induced by high frequency stimulation of the perforant path. We then purified the RNA from the dendrites and subjected it to microarray for a screen of all 27,000 known transcripts in the rat genome. Many mRNAs were upregulated as a result of the HFS of the perforant path, but the most interesting and most upregulated transcripts were Arc mRNA and pri-miRNA-132, an unprocessed miRNA.

Arc mRNA is known to be robustly upregulated following HFS within the dendrites of dentate gyrus granule cells (Steward et al., 1998). However, until these experiments, there was no unbiased screening to discover other mRNAs transported to the dendrites as robustly as Arc mRNA following stimulation of LTP. Our screen ultimately showed that Arc mRNA is the most robustly transported to the dendrites following 2 hr or 4 hr following induction of LTP. Although there were no other RNAs found to be robust as Arc, pri-miRNA-132 was the second most present in the dendrites at the 4 hr time point. miR-132 is a miRNA involved in consolidation of memories in the hippocampus (Wang et al., 2013) and has been reported to be present in the dendrites (Bicker et al., 2014), however, to date there has been no report of an unprocessed miRNA being abundant in dendrites following neuronal activation. This finding is very interesting because it suggests that a mechanism of local pri-miRNA processing may exist in the dendrites following synaptic activation.

In chapter 6, I applied my knowledge of viral vector development to study the molecular mechanisms underlying strong memories and their inability to undergo reconsolidation. Particularly strong memories, such as traumatic memories that lead to the development of PTSD, are resistant to reconsolidation (Lee et al., 2017). The molecular mechanisms as to why strong fear memories are not able to undergo reconsolidation are poorly understood. In rodent models, it has been shown that strong memories are resistant to attenuation of fear by pharmacologically induced amnesia (Wang et al., 2009). One mechanism that could be gating the initiation of reconsolidation of strong memories in a rodent model of auditory fear conditioning is the increase of GluN2A/GluN2B ratio following consolidation of the fear memory (Holehonnur et al., 2015). Using an inducible transgenic mouse line, the authors were able to overexpress

GluN2A at the time of memory retrieval of a weak memory. This blocked the initiation of reconsolidation and made these weak trained animals resistant to the amnesic effects of a post-retrieval treatment of protein synthesis inhibitor infused into the BLA, which is typically a characteristic of a strong memory.

A high GluN2A/GluN2B ratio is known to decrease the chance of a neuron undergoing LTP. While high levels of another NMDA receptor subunit, GluN2B, make it more likely that LTP will occur upon activation (Barria & Malinow, 2005). Adding to the above-mentioned study, pharmacological investigation of these two receptors show a differential effect on the reconsolidation of auditory fear memories if their activity is blocked (Milton et al., 2013). But no one has attempted to overexpress GluN2B at the time of memory retrieval to observe the effects on reconsolidation of a strong memory, and to determine if the increase of the GluN2B/GluN2A ratio would allow for the initiation of reconsolidation of a strong memory, thus being susceptible to post-retrieval infusion of anisomycin into the BLA.

To do this, we generated lentivirus designed to overexpress GluN2B(WT) or GluN2B(E1479Q), which has been shown to increase surface levels of GluN2B by inhibiting endocytosis of the subunit, driven by a TRE3G promoter to render the expression inducible by presence or absence of Dox. Infusing the virus into the BLA of α CaMKII-tTA mice, it was possible to overexpress these transcripts at the time of various mnemonic processes including consolidation, extinction, and reconsolidation of strong and weak fear memories.

The overexpression of GluN2B(E1479Q), but not GluN2B(WT), led to an enhancement of consolidation. There have been prior reports of overexpression of GluN2B(WT) in the forebrain having consolidation enhancing effects. However, there are also prior reports of

GluN2B(WT) failing to show an increase GluN2B levels at the synapse. This may be the case with our GluN2B(WT) construct, thus why we do not see an enhancing effect of consolidation of fear memories. Neither of these two methods of increasing the GluN2B/GluN2A ratio had any enhancement on extinction learning. This may be due to the lack of overexpression of GluN2B within inhibitory neurons, as recent reports of involvement of GABAergic interneurons being primarily responsible for driving extinction learning within the BLA (Davis et al., 2017).

Interestingly, the overexpression of GluN2B(E1479Q), but not GluN2B(WT), at the time of retrieval of a strong memory allowed for the initiation of reconsolidation, thus allowing for the amnesic effects of post-retrieval infusion of anisomycin into the BLA. This is an important finding because it is the first demonstration of a genetic manipulation to influence reconsolidation of a strong memory. Furthermore, it is one of the few demonstrations of any manipulation that has allowed for the initiation of reconsolidation of a strong auditory fear memory, as the only other demonstration of this effect has been to trigger prediction error signaling in BLA neurons during the retrieval of strong memories (Diaz-Mataix et al., 2013).

An additional reconsolidation experiment was performed that determined whether the initiation of reconsolidation of a strong memory due to the expression of GluN2B(E1479Q) within the BLA at the time of memory reactivation is dependent upon retrieval of the memory. Animals overexpressing GluN2B(E1479Q) that were given a memory retrieval session and infusion of anisomycin into the BLA showed pharmacologically induced amnesia, as opposed to no retrieval controls. In addition, these animals were tested for lasting effects of pharmacologically induced amnesia one week later and displayed a lasting attenuation of fear. This is in contrast to prior studies claiming the fear attenuating effects of post-retrieval

anisomycin administration is reversed when animals are tested weeks after the post-retrieval administration of protein synthesis inhibitors (Lattal & Abel, 2004).

If this finding is to be translatable to humans suffering from PTSD and other fear related anxiety disorders, there should be treatments that could feasibly be used in reconsolidation-based therapy. One example of a potential treatment is strategic administration of the drug simvastatin. Simvastatin is an FDA approved drug designed to lower LDL cholesterol levels but has also been prescribed recently as a cognitive enhancer to patients with dementia (Huang et al., 2017). Originally, the drug was thought to be contributing to memory due to the effects the drug has on lowering oxidative stress associated with a disease state (Rasmussen et al., 2016), however, it has recently been shown that treatment of mice with simvastatin significantly increases the GluN2B/GluN2A ratio (Parent et al., 2014; Chen et al., 2016). The effects on reconsolidation have not yet been tested, but would be an interesting experiment to attempt reproduce the results we have seen with lentiviral mediated expression of GluN2B(E1479Q).

In conclusion, having the skills to design, create, and optimize viral tools for studying neuronal function can be a very useful tool in itself. Development of new viral tools specialized for neuroscience research are now being developed very rapidly and will hopefully continue to uncover how the brain functions.

References

- Barria, A. & Malinow, R. (2005) NMDA receptor subunit composition controls synaptic plasticity by regulating binding to CaMKII. *Neuron*, 48, 289-301.
- Bicker, S., Lackinger, M., Weiss, K. & Schratt, G. (2014) MicroRNA-132, -134, and -138: a microRNA troika rules in neuronal dendrites. *Cell Mol Life Sci*, 71, 3987-4005.
- Boudreau, R., Martins, I. & Davidson, B. (2009) Artificial microRNAs as siRNA shuttles: improved safety as compared to shRNAs in vitro and in vivo. *Molecular therapy : the journal of the American Society of Gene Therapy*, 17, 169 - 175.
- Burger, C., Gorbatyuk, O.S., Velardo, M.J., Peden, C.S., Williams, P., Zolotukhin, S., Reier, P.J., Mandel, R.J. & Muzyczka, N. (2004) Recombinant AAV viral vectors pseudotyped with viral capsids from serotypes 1, 2, and 5 display differential efficiency and cell tropism after delivery to different regions of the central nervous system. *Molecular therapy : the journal of the American Society of Gene Therapy*, 10, 302-317.
- Chen, T., Zhang, B., Li, G., Chen, L. & Chen, L. (2016) Simvastatin enhances NMDA receptor GluN2B expression and phosphorylation of GluN2B and GluN2A through increased histone acetylation and Src signaling in hippocampal CA1 neurons. *Neuropharmacology*, 107, 411-421.
- Cruz, E., Soler-Cedeno, O., Negron, G., Criado-Marrero, M., Chompre, G. & Porter, J.T. (2015) Infralimbic EphB2 Modulates Fear Extinction in Adolescent Rats. *The Journal of neuroscience : the official journal of the Society for Neuroscience*, 35, 12394-12403.
- Davis, K.M., Pattanayak, V., Thompson, D.B., Zuris, J.A. & Liu, D.R. (2015) Small molecule-triggered Cas9 protein with improved genome-editing specificity. *Nat Chem Biol*, 11, 316-318.
- Davis, P., Zaki, Y., Maguire, J. & Reijmers, L.G. (2017) Cellular and oscillatory substrates of fear extinction learning. *Nature neuroscience*, 20, 1624-1633.
- de Solis, C.A., Ho, A., Holehonnur, R. & Ploski, J.E. (2016) The Development of a Viral Mediated CRISPR/Cas9 System with Doxycycline Dependent gRNA Expression for Inducible In vitro and In vivo Genome Editing. *Frontiers in molecular neuroscience*, 9, 70.
- de Solis, C.A., Holehonnur, R., Banerjee, A., Luong, J.A., Lella, S.K., Ho, A., Pahlavan, B. & Ploski, J.E. (2015) Viral delivery of shRNA to amygdala neurons leads to neurotoxicity and deficits in Pavlovian fear conditioning. *Neurobiol Learn Mem*, 124, 34-47.
- de Solis, C.A., Hosek, M.P., Holehonnur, R., Ho, A., Banerjee, A., Luong, J.A., Jones, L.E., Chaturvedi, D. & Ploski, J.E. (2017a) Adeno-associated viral serotypes differentially transduce inhibitory neurons within the rat amygdala. *Brain research*, 1672, 148-162.

de Solis, C.A., Morales, A.A., Hosek, M.P., Partin, A.C. & Ploski, J.E. (2017b) Is Arc mRNA Unique: A Search for mRNAs That Localize to the Distal Dendrites of Dentate Gyrus Granule Cells Following Neural Activity. *Frontiers in molecular neuroscience*, 10, 314.

Diaz-Mataix, L., Ruiz Martinez, R.C., Schafe, G.E., LeDoux, J.E. & Doyere, V. (2013) Detection of a temporal error triggers reconsolidation of amygdala-dependent memories. *Curr Biol*, 23, 467-472.

Fellmann, C., Hoffmann, T., Sridhar, V., Hopfgartner, B., Muhar, M., Roth, M., Lai, D.Y., Barbosa, I.A., Kwon, J.S., Guan, Y., Sinha, N. & Zuber, J. (2013) An optimized microRNA backbone for effective single-copy RNAi. *Cell reports*, 5, 1704-1713.

Gonzalez, F., Zhu, Z., Shi, Z.D., Lelli, K., Verma, N., Li, Q.V. & Huangfu, D. (2014) An iCRISPR platform for rapid, multiplexable, and inducible genome editing in human pluripotent stem cells. *Cell Stem Cell*, 15, 215-226.

Gunduz-Cinar, O., Brockway, E., Lederle, L., Wilcox, T., Halladay, L.R., Ding, Y., Oh, H., Busch, E.F., Kaugars, K., Flynn, S., Limoges, A., Bukalo, O., MacPherson, K.P., Masneuf, S., Pinard, C., Sibille, E., Chesler, E.J. & Holmes, A. (2018) Identification of a novel gene regulating amygdala-mediated fear extinction. *Molecular psychiatry*.

Holehonnur, R., Kim, L.J., Jones, L.E., Daison, D.K., Vuong, D.T., Khakoo, S.F. & Ploski, J.E. (2015) Overexpression of GluN2A or GluN2B within neurons of the mouse basal and lateral amygdala alters amygdala dependent mnemonic processing. *Society for Neuroscience Abstract - Chicago*.

Holehonnur, R., Luong, J.A., Chaturvedi, D., Ho, A., Lella, S.K., Hosek, M.P. & Ploski, J.E. (2014) Adeno-associated viral serotypes produce differing titers and differentially transduce neurons within the rat basal and lateral amygdala. *BMC Neurosci*, 15, 28.

Huang, W., Li, Z., Zhao, L. & Zhao, W. (2017) Simvastatin ameliorate memory deficits and inflammation in clinical and mouse model of Alzheimer's disease via modulating the expression of miR-106b. *Biomedicine & pharmacotherapy = Biomedecine & pharmacotherapie*, 92, 46-57.

Jackson, A.L. & Linsley, P.S. (2010) Recognizing and avoiding siRNA off-target effects for target identification and therapeutic application. *Nature reviews. Drug discovery*, 9, 57-67.

Klein, R.L., Dayton, R.D., Tatom, J.B., Henderson, K.M. & Henning, P.P. (2008) AAV8, 9, Rh10, Rh43 vector gene transfer in the rat brain: effects of serotype, promoter and purification method. *Molecular therapy : the journal of the American Society of Gene Therapy*, 16, 89-96.

Lattal, K.M. & Abel, T. (2004) Behavioral impairments caused by injections of the protein synthesis inhibitor anisomycin after contextual retrieval reverse with time. *Proceedings of the National Academy of Sciences of the United States of America*, 101, 4667-4672.

Lee, J.L.C., Nader, K. & Schiller, D. (2017) An Update on Memory Reconsolidation Updating. *Trends in cognitive sciences*, 21, 531-545.

Marik, S.A., Yamahachi, H., McManus, J.N., Szabo, G. & Gilbert, C.D. (2010) Axonal dynamics of excitatory and inhibitory neurons in somatosensory cortex. *PLoS Biol*, 8, e1000395.

Martin, J., Wolken, N., Brown, T., Dauer, W., Ehrlich, M. & Gonzalez-Alegre, P. (2011) Lethal toxicity caused by expression of shRNA in the mouse striatum: implications for therapeutic design. *Gene Ther*, 18, 666 - 673.

McBride, J.L., Boudreau, R.L., Harper, S.Q., Staber, P.D., Monteys, A.M., Martins, I., Gilmore, B.L., Burstein, H., Peluso, R.W., Polisky, B., Carter, B.J. & Davidson, B.L. (2008) Artificial miRNAs mitigate shRNA-mediated toxicity in the brain: Implications for the therapeutic development of RNAi. *Proceedings of the National Academy of Sciences*, 105, 5868-5873.

Mews, P., Donahue, G., Drake, A.M., Luczak, V., Abel, T. & Berger, S.L. (2017) Acetyl-CoA synthetase regulates histone acetylation and hippocampal memory. *Nature*, 546, 381-386.

Milton, A.L., Merlo, E., Ratano, P., Gregory, B.L., Dumbreck, J.K. & Everitt, B.J. (2013) Double dissociation of the requirement for GluN2B- and GluN2A-containing NMDA receptors in the destabilization and restabilization of a reconsolidating memory. *The Journal of neuroscience : the official journal of the Society for Neuroscience*, 33, 1109-1115.

Nihongaki, Y., Yamamoto, S., Kawano, F., Suzuki, H. & Sato, M. (2015) CRISPR-Cas9-based photoactivatable transcription system. *Chem Biol*, 22, 169-174.

Pan, Q., de Ruiter, P., von Eije, K., Smits, R., Kwekkeboom, J., Tilanus, H., Berkhout, B., Janssen, H. & van der Laan, L. (2011) Disturbance of the microRNA pathway by commonly used lentiviral shRNA libraries limits the application for screening host factors involved in hepatitis C virus infection. *FEBS Lett*, 585, 1025 - 1030.

Parent, M.A., Hottman, D.A., Cheng, S., Zhang, W., McMahon, L.L., Yuan, L.L. & Li, L. (2014) Simvastatin treatment enhances NMDAR-mediated synaptic transmission by upregulating the surface distribution of the GluN2B subunit. *Cellular and molecular neurobiology*, 34, 693-705.

Ran, F.A., Cong, L., Yan, W.X., Scott, D.A., Gootenberg, J.S., Kriz, A.J., Zetsche, B., Shalem, O., Wu, X., Makarova, K.S., Koonin, E.V., Sharp, P.A. & Zhang, F. (2015) In vivo genome editing using *Staphylococcus aureus* Cas9. *Nature*, 520, 186-191.

Rasmussen, S.T., Andersen, J.T., Nielsen, T.K., Cejvanovic, V., Petersen, K.M., Henriksen, T., Weimann, A., Lykkesfeldt, J. & Poulsen, H.E. (2016) Simvastatin and oxidative stress in humans: A randomized, double-blinded, placebo-controlled clinical trial. *Redox biology*, 9, 32-38.

Reynolds, A., Leake, D., Boese, Q., Scaringe, S., Marshall, W.S. & Khvorova, A. (2004) Rational siRNA design for RNA interference. *Nat Biotechnol*, 22, 326-330.

Steward, O., Wallace, C.S., Lyford, G.L. & Worley, P.F. (1998) Synaptic activation causes the mRNA for the IEG Arc to localize selectively near activated postsynaptic sites on dendrites. *Neuron*, 21, 741-751.

Wang, R.Y., Phang, R.Z., Hsu, P.H., Wang, W.H., Huang, H.T. & Liu, I.Y. (2013) In vivo knockdown of hippocampal miR-132 expression impairs memory acquisition of trace fear conditioning. *Hippocampus*, 23, 625-633.

Wang, S.H., de Oliveira Alvares, L. & Nader, K. (2009) Cellular and systems mechanisms of memory strength as a constraint on auditory fear reconsolidation. *Nature neuroscience*, 12, 905-912.

BIOGRAPHICAL SKETCH

Christopher Andrew de Solis was born and grew up in “The Main Line” of Philadelphia, Pennsylvania. He attended K-12 in the Tredyfferrin Easttown school district, currently one of the top public school districts in the United States. After graduating from Conestoga High School, Christopher attended Kutztown University of Pennsylvania for voice and piano training, where he found his interests in neuroscience through learning about the neuronal correlates of psychoacoustics. Christopher then transferred to Temple University where he obtained a double major in Comparative Psychology and Neuroscience where he obtained his first laboratory experience doing research on stress and learning and memory with Diana S. Woodruff-Pak and research on nicotine addiction with Thomas J. Gould. After obtaining his bachelors in science, he continued his research path at The University of Pennsylvania in the Children’s Hospital of Philadelphia with Douglas C. Wallace researching the role of mitochondrial DNA (mtDNA) in neurodegenerative disorders. His Ph.D. was obtained at The University of Texas at Dallas, where he worked under the mentorship of Jonathan E. Ploski on development of viral vector tool kits for investigation of learning and memory phenomena, such as consolidation and reconsolidation. Following his Ph.D., he will join the lab of Eric Kandel at Columbia University as a Howard Hughes Medical Institute postdoctoral associate.

CURRICULUM VITAE

Christopher A. de Solis, Ph.D

U.S. Citizen | cad130330@utdallas.edu

The University of Texas at Dallas
School of Behavioral and Brain Sciences
800 W. Campbell Rd. Richardson Texas 75080

EDUCATION

Ph.D: Cognition and Neuroscience, 08/2013 – 08/2018.

The University of Texas at Dallas, Richardson, TX

BS: Dual Major in Neuroscience* and Psychology, 2007-2011. (*=graduated with distinction)
Temple University, Philadelphia, PA

RESEARCH EXPERIENCE

University of Texas at Dallas, Richardson, TX. 2013 – Present.

Doctoral Research, Cellular and Molecular Neuroscience Laboratory

Mentor: Jonathan E. Ploski, Ph.D

- Tool development for RNAi (shRNA) for *in vitro* and *in vivo* use.
- Viral vector development for CRISPR/Cas systems. Built several kits including doxycycline and cre-recombinase dependent genome editing systems for *in vitro* and *in vivo* use for multiple Cas endonucleases.
- Examined adeno-associated virus (AAV) serotypes for their ability to transduce and function within inhibitory neurons *in vivo*.
- Screened for RNAs present in distal dendrites following neural activity in the hippocampus.
- Dissertation research explores genetic overexpression of GluN2B effects on consolidation and induction of reconsolidation, with respect to weak versus strong fear memories.

Children's Hospital of Philadelphia/University of Pennsylvania, Philadelphia, PA. 2011 – 2013.

Research Technician, Center for Mitochondrial and Epigenomic Medicine (CMEM)

Mentor: Douglas C. Wallace, Ph.D

- Examined the implications of mtDNA and nDNA mutations in genes that code for mitochondrial proteins, aimed at developing models of Parkinson's disease, diabetes and cardiomyopathy.

Temple University, Philadelphia, PA. 2010 – 2011.

Undergraduate Research, Neurobiological Investigations of Learning and Addiction Laboratory

Mentor: Thomas J. Gould, Ph.D

- Investigated the effects of acute nicotine administration on contextual and auditory fear learning and memory.

Temple University, Philadelphia, PA. 2009 – 2011.

Undergraduate Research, Systems Neuroscience Laboratory

Mentor: Diana S. Woodruff-Pak, Ph.D

- Explored the effects of acute and chronic involuntary exercise stress on learning and memory.

PUBLICATIONS

de Solis CA, Morales AA, Hosek MP, Partin AC, Ploski JE. Is Arc mRNA Unique: A Search for mRNAs That Localize to the Distal Dendrites of Dentate Gyrus Granule Cells Following Neural Activity. *Front Mol Neurosci*. 2017 Oct 10; 10: 314. [PubMed ID: 29066948](#)

de Solis CA*, Hosek MP*, Holehonnur R, Ho A, Banerjee A, Luong JA, Jones LE, Chaturvedi D, Ploski JE. Adeno-associated viral serotypes differentially transduce inhibitory neurons within the rat amygdala. *Brain Res*. 2017 Oct 1; 1672: 148-162. [PubMed ID: 28764932](#)

de Solis CA, Ho A, Holehonnur R, Ploski JE. The Development of a Viral Mediated CRISPR/Cas9 System with Doxycycline Dependent gRNA Expression for Inducible *In vitro* and *In vivo* Genome Editing. *Front Mol Neurosci*. 2016 Aug 18; 9:70. [PubMed ID: 27587996](#), [F1000Prime Recommended](#)

de Solis CA, Holehonnur R, Banerjee A, Luong JA, Lella SK, Ho A, Pahlavan B, Ploski JE. Viral delivery of shRNA to amygdala neurons leads to neurotoxicity and deficits in Pavlovian fear conditioning. *Neurobiol Learn Mem*. 2015 Oct; 124:34-47. [Featured in special edition \(MCCS, 2015\) of the journal. PubMed ID: 26182988](#)

TEACHING EXPERIENCE

University of Texas at Dallas, Richardson, TX. 2013-Present

Teaching assistant for undergraduate neuroscience courses:

- Neuroscience Lab Methods (Animal behavior and drug administration, electrophysiology techniques).
- Cellular Neuroscience
- Neurophysiology
- Neuropharmacology
- Integrative Neuroscience

ACTIVITIES AND AWARDS

- Co-founder of the Undergraduate Neuroscience Society (UNS) at Temple University.
- Temple University Neuroscience Program Travel Award (\$500).

MEETINGS AND PRESENTATIONS

- Society for Neuroscience Meeting, Chicago, IL, 2009.
- Society for Neuroscience Meeting, San Diego, CA, 2010 (**Poster Presentation**).
- Society for Neuroscience Meeting, Washington DC, 2011 (**Poster Presentation**).
- Molecular and Cellular Cognition Society Meeting, New Orleans, LA, 2012 (**Poster Presentation**).
- Society for Neuroscience Meeting, New Orleans, LA, 2012 (**Poster Presentation**).
- Pavlovian Society Meeting, Austin, TX, 2013.
- Molecular and Cellular Cognition Society Meeting, San Diego, CA, 2013 (**Poster Presentation**).
- Society for Neuroscience Meeting, San Diego, CA, 2013 (**Poster Presentation**).
- Conference on Learning and Memory, Austin, TX, 2014 (**Poster Presentation**).
- Conference on Emotional Learning and Memory, Dallas, TX, 2014 (**Poster Presentation**).
- Molecular and Cellular Cognition Society Meeting, Washington DC, 2014 (**Poster Presentation**).
- Society for Neuroscience Meeting, Washington DC, 2014 (**Poster Presentation**).
- Pavlovian Society Meeting, Portland, OR, 2015 (**Poster Presentation**).
- Society for Neuroscience Meeting, Chicago, IL, 2015 (**Poster Presentation**).
- Conference on Learning and Memory, Austin, TX, 2016 (**Poster Presentation**).
- Pavlovian Society Meeting, Jersey City, NJ, 2016 (**Poster Presentation**).
- Molecular and Cellular Cognition Society Meeting, San Diego, CA, 2016 (**Poster Presentation**).
- Society for Neuroscience Meeting, San Diego, CA, 2016 (**Poster Presentation**).
- Pavlovian Society Meeting, Philadelphia, PA, 2017 (**Poster Presentation**).
- Molecular and Cellular Cognition Society Meeting, Washington DC, 2017 (**Poster Presentation**).
- Society for Neuroscience Meeting, Washington DC, 2017.
- International Conference on Learning & Memory, Huntington Beach, CA, 2018 (**Poster Presentation**).

PROFESSIONAL SOCIETIES

- Society for Neuroscience, 2009 – Present.
- Molecular and Cellular Neuroscience Society (MCCS), 2012 – Present.
- Pavlovian Society, 2013 – Present.

PLASMID BANK (Addgene Submissions)

CRISPR/Cas Plasmids

<https://www.addgene.org/browse/article/23805/>

MEDIA

genomeweb.org

[“Chemically Induced Guide RNAs Drive CRISPR/Cas9 System for Editing Mouse Neurons In Vivo”](#) by Andrew Han

Contribution: First authored paper featured the in article.

UTDallas News Center

[“Researcher Aims to Update Gene Editing System for Brain Studies”](#) by Phil Roth

Contribution: First authored paper featured in the article.